

CO₂ Sequestration through Deep Saline Injection and Photosynthetic Biological Fixation: System Design for Two Plausible CO₂ Sequestration Strategies

Dirk Van Essendelft, J. Taron, M. Fitzgerald, A. Abdel-Hafez, A. Sakti, O. Achimugu, I. Faoro,

Department of Energy and Geo-Environmental Engineering,

The Pennsylvania State University

Executive Summary

Two scenarios are developed for sequestration of CO₂ from a 500 MW coal-fired power plant operating on an integrated gasification combined cycle process. The proposed conceptual design examines both the photosynthetic biological fixation of CO₂ through a large scale reactor design and full scale operation of a CO₂ injection system into a deep saline reservoir. Analysis of saline aquifer sequestration capacity and potential is evaluated from the basis of well-documented information from the Viking aquifer in the Alberta basin in western Canada, where ten injection wells in a circular pattern are shown to effectively distribute the CO₂ within a competent structural trap. Hydrodynamic, solubility, and mineral trapping are quantified for the design period, and leakage of CO₂ through the shale caprock and local abandoned wells is shown to approach 0.05 percent of the total injected volume in a 20 year design scheme. Alternatively, photosynthetic fixation is found to be viable in the higher sunlit regions of the Southwestern United States should the market for algal biomass continue to expand. Energy production for either process scheme is examined for possible inputs from photovoltaic arrays and a cascading closed loop cycle (CCLC) for excess heat utilization. Characterization of saline aquifers in such a high sun intensity region in a manner such as that presented for Alberta would support development of a dual approach process scheme.

Table of Contents

Introduction.....	4
Introduction.....	4
1. Part I: Evaluation and Selection of Sequestration Methods.....	4
1.1. Geological Sequestration Methods.....	4
1.1.1. General Considerations.....	4
1.1.2. Deep Saline Aquifer Injection.....	7
1.1.3. Coalbed Injection.....	7
1.1.4. Oil and Gas Reservoir Injection.....	7
1.2. Additional Sequestration Methods.....	8
1.2.1. Ocean Fertilization.....	8
1.2.2. Deep Ocean Injection.....	8
1.2.3. Terrestrial Aforestation.....	8
1.2.4. Mineral Carbonization.....	9
1.2.5. Biological Sequestration: Industrial-Bioreactor.....	9
1.3. Selected Methods.....	9
2. Part II: The IGCC Power Plant.....	10
3. Part III: The Photosynthetic Biological Reactor.....	11
3.1. Thermal Pretreatment.....	11
3.2. Bio-Reactor Design.....	12
3.2.1. Principles and Theory.....	12
3.2.2. Design Summary.....	17
3.3. Light Separation and Transmission.....	22
3.3.1. Wavelength Requirements.....	23
3.3.2. Solar Irradiance.....	24
3.3.3. Solar Energy to Electrical Energy Conversion.....	25
3.3.4. Light Separation Equipment.....	29
3.3.5. Discussion of Fiber Optics.....	30
3.3.6. Design Summary using Photovoltaic Cells.....	30
3.3.7. Design Summary using Thermal Energy.....	31
3.4. Light Collection.....	32
3.4.1. Light/Energy Requirements.....	33
3.4.2. Types of Collectors.....	33
3.4.3. Parabolic Trough Collector.....	33
3.5. Linear Fresnel Collector.....	34
3.6. Parabolic Mini Dish.....	35
3.7. Heliostats.....	35
3.7.1. CONCEPT OF THE MTSA.....	35
3.7.2. Heliostat Design.....	36
3.8. Land Requirements.....	40
3.8.1. Design Summary.....	40
3.9. Cost and Feasibility Study – PBR System.....	41
3.9.1. Current and Future Market Conditions.....	41
3.9.2. Sequestration Using PBR and PV.....	43
3.9.3. Sequestration using PBR and CCLC.....	44
4. Recommended Sequestration System and Design.....	44

5. Part IV: Deep Saline Aquifer Injection.....	45
5.1. Test Case: Viking Aquifer	45
5.2. Trapping Mechanisms and Sequestration Capacity.....	46
5.2.1. Hydrodynamic Trapping.....	46
5.2.2. Solubility Trapping.....	47
5.2.3. Mineral Trapping and Capacity	48
5.3. Aquifer Integrity and Leakage.....	50
5.3.1. Caprock Integrity	50
5.3.2. Well Bore Integrity	52
5.4. Chemical Changes During Injection.....	54
5.5. Injection Modeling.....	55
5.5.1. Possible Injection Scenarios in Viking.....	56
5.5.2. Number of Required Injection Wells.....	56
5.5.3. State of Aquifer Stress and Maximum Injection Pressure	59
5.5.4. Numerical Modeling of Pressure Generation	60
5.5.5. Permeability Reduction.....	61
5.5.6. Number of Injection Wells.....	62
5.5.7. CO ₂ Transport Extent.....	63
5.6. Compression Modeling and design.....	64
5.7. General Well Design.....	65
5.8. Piping Corrosion	66
5.9. Drilling Costs	67
5.10. Monitoring and Verification	68
5.11. Economic Analysis	69
6. Part V: Energy Supply Study.....	69
6.1. Introduction.....	69
6.2. The Cascading Closed Loop Cycle.....	70
6.3. Availability	72
6.4. Design Considerations	73
6.5. Proposed application.....	74
6.6. Addition to the Steam Turbine Cycle in the IGCC.....	74
7. Summary and Conclusions	75
8. References.....	77

INTRODUCTION

Sequestration of anthropogenic CO₂ emissions remains an important and viable strategy in the worldwide effort to reduce the human contribution to climate change. From this basis, the viability of newly constructed power plants is now, and will be increasingly so in the future, largely dependent upon an available method of sequestering a significant portion of the CO₂ it will generate. The need for technologies capable of accomplishing this task is apparent. Due to such necessity, the purpose of this study is to examine possible methods to sequester the CO₂ emitted from a 500 MW power plant and to do so in the most efficient manner possible. To this end, several existing and proposed methods of sequestration were examined and compared on the basis of several controlling criteria including the location of the power plant, sustainability of the sequestration method, environmental health and safety issues, potential storage capacity, public acceptance of the method, and economic viability. The general sequestration areas that were examined include biological fixation, oceanic storage, geologic storage, and mineralization. From the examination, two plausible sequestration options emerged, namely biological fixation through the use of an industrial bioreactor and injection into a deep saline aquifer. Both options were continued to a conceptual process design in which deep saline aquifer injection is designed to support the full captured carbon dioxide stream from an IGCC power plant, and the industrial bioreactor was designed to handle half of the CO₂ flow stream. Presented below are the findings obtained during this study.

1. PART I: EVALUATION AND SELECTION OF SEQUESTRATION METHODS

CO₂ sequestration methods may be roughly divided into those that incorporate as the primary mechanism: 1) Injection and entrapment within pressure or structural boundaries, such as geologic storage and deep ocean storage, 2) those that seek chemical boundaries, such as mineral carbonization, and 3) those that utilize aerobic uptake through biological means, such as photosynthetic bioreactors, or herbaceous means, such as terrestrial afforestation and ocean farming. Geologic storage may be further divided into the type of reservoir to be utilized. Several sequestration methods were evaluated. A brief discussion and summary of findings, in addition to some general critical concerns, can be found in the following discussion. A comprehensive review can be found in Appendix A.

1.1. GEOLOGICAL SEQUESTRATION METHODS

Geologic methods of sequestration involve the capture of CO₂ emissions from the waste streams of fossil-fuel burning power plants, or other high volume CO₂ producing plants, and subsequent compression for transportation to a suitable disposal site for pressurized injection. In the geologic medium, suitable disposal sites include oil/natural gas wells that are either under producing or no longer in production, un-mineable coal seams, deep saline aquifers, and deep ocean injection, where pressure and temperature boundaries maintain CO₂ in its liquid phase. Each of these methods presents some unique benefits and challenges.

1.1.1. General Considerations

Physical Properties of CO₂

Physical properties of CO₂ are relevant to its storage underground because they define the density and viscosity of the stored gas, and thus its occupied volume and mobility. They are also relevant because large volume changes are associated with CO₂ phase changes, so it might be

desirable to store CO₂ under physical conditions that are not close to the phase boundary conditions, thus avoiding unexpected volume and mobility changes. Figure 1 shows the phase diagram of CO₂.

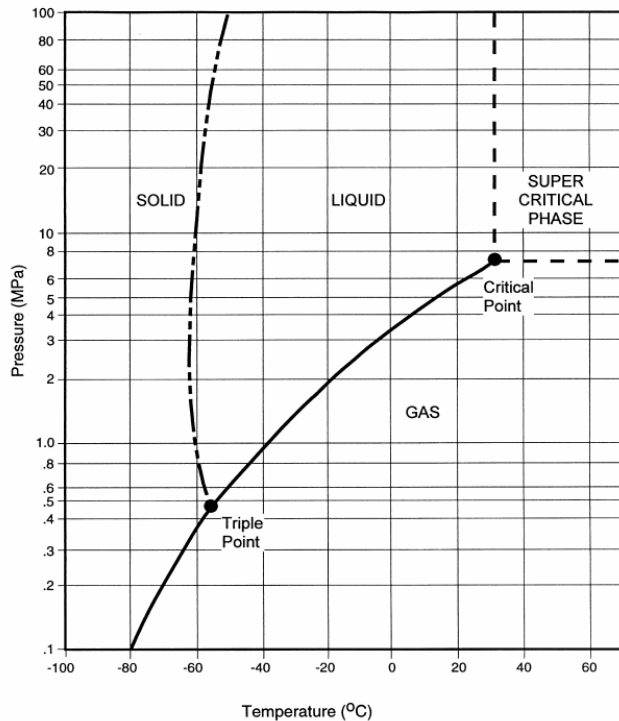


Figure 1
CO₂ Phase Diagram [1]

As is evident from the phase diagram, CO₂ occurs as a solid, a liquid, a gas, or a supercritical fluid. Above its critical temperature of 31.1°C and critical pressure of 7.38 MPa (73.8 bars), CO₂ exists in the so-called dense phase condition, i.e., as a supercritical fluid. A supercritical fluid is a gas-like compressible fluid in that it fills and takes the shape of its container, but it has liquid-like densities. It is desirable to store CO₂ as a supercritical fluid or a liquid because of higher phase density that will occupy much less space in the subsurface. For example, one tonne of CO₂ at a density of 785 kg/m³ (i.e. 22°C and 7 MPa or 50°C and 15MPa) occupies 1.27 m³, while at standard temperature and pressure, at the ground surface, one tonne of CO₂ occupies 512 m³.

Transportation

It is preferred to transport the CO₂ at a pressure beyond its supercritical pressure threshold so as to avoid any two phase mixtures. This enhances liquid phase transportation and enhances the economic benefits. The operating pressure and temperature lies in between 8619 kPa at 4°C and 15,300 kPa at 38°C. The upper and lower limits are set, respectively, by the ASME-ANSI 900# flange rating and ambient condition coupled with the phase behavior of CO₂ [2]. Literature suggests that the CO₂ emissions from a 500 MW coal power plant will be approximately 10,000 to 14,000 ton per day which is equivalent to 53 to 83 m³/s [3]. For this a 14 to 16 inch diameter pipeline will be required. A larger diameter pipeline gives a higher margin of safety for occasional higher CO₂ flows.

Safety, Health and Environmental Risks

The geologic storage sites should be selected to minimize the potential for leakage. Although CO₂ at low concentrations is not directly hazardous to human health, it may detrimentally alter environmental processes [4]. Leakages could occur over small areas from discrete point sources, such as abandoned wells. Uncontrolled leakages would have widespread implications for the environment. Leakages might damage crops, groundwater quality and/or human and animal health. Other concerns include acidification, changes in biological diversity and species composition and asphyxiation at high CO₂ concentrations. In addition, biogeochemical processes may be affected as increased CO₂ concentrations could change pH, microbial populations and nutrient supply [4, 5].

The risks of geologic sequestration fall in two categories: Global and local risks. Global risks arise from leaks that return stored CO₂ to the atmosphere. Additionally, global risks involve the release of CO₂ that may contribute significantly to climate change. Moreover, the global risk may alternatively be viewed as uncertainty in the effectiveness of CO₂ containment [6].

Local risks are classified as hazards for things like humans, ecosystems and groundwater [1]. Local risks arise from the elevated CO₂ concentrations associated with the flux of CO₂ through the shallow subsurface to the atmosphere. Additionally, local risks occur as a result of the chemical effects of dissolved CO₂ in the subsurface. Moreover, local effects could arise from the displacement of fluids by the injected CO₂ [6]. If leakage to the atmosphere were to occur in low-lying areas with little wind, or in sumps and basements overlying these diffuse leaks, humans and animals could be harmed [1].

Catastrophic releases could occur as a result of a blowout of an injection well or existing well in the vicinity, or as a result of seismic disturbance [7]. Groundwater can be affected by CO₂ leaking directly into an aquifer or by brines displacement into overlying aquifers, with concomitant potential to contaminate potable water supplies. There may also be acidification of soils and displacement of oxygen in soils [8].

Risks can be minimized by the avoidance of vulnerable areas, monitoring of the injection process and CO₂ plume delineation. Remote sensing techniques and water quality analyses also may be explored for near-surface monitoring of injection sites and for detection of leaks. Seismic monitoring must be conducted to avoid potential seismic catastrophes [9].

Public Perception

Public perception is an interesting issue and is of significant importance. As yet, little has been published on the question of whether people will find CO₂ sequestration underground to be acceptable. Some [10] state that CO₂ removal, as a dedicated single technology, is an option that does not enjoy enthusiastic public support and conclude that these barriers can only be overcome by research and design and effective demonstration of the technology. It will not be possible to overcome them by communication alone. The IPCC report of 2005 states that two conditions will have to be met before the CO₂ sequestration is considered as a credible technology namely anthropogenic global climate change has to be regarded as a relatively serious problem and there must be acceptance of the need for large reductions in CO₂ emissions to reduce the threat of global climate change. Also people in business, government, or NGO's must seek out and hear objections raised by skeptics and come out with answers to them for this technique to be

accepted [11, 12]. To further maximize by the advocacy community and the public, policymakers will need to convince those sectors that the storage option is needed, that it will not crowd out more desirable strategies, and that it will perform effectively and safely [11].

With regards to policy related issues, geologic CO₂ storage capacity need to be seen and understood to be an investment in a nation or regions future economic and environmental well being in the way that estimates of hydrocarbon resources/reserves are viewed today. The potential to store CO₂ should be treated as a natural resource [13].

1.1.2. Deep Saline Aquifer Injection

Deep saline injection refers to the injection of CO₂ into deep sedimentary basins, where pressure and temperature favor the existence of dense phase (liquid or supercritical) CO₂. Because the EPA classifies aquifers with greater than 10,000 mg/l salinity unfit as sources of drinking water [14], such aquifers serve as an effective resource for CO₂ storage. Physically, the CO₂ may be stored beneath an impermeable caprock, where buoyant forces maintain the pure phase atop the water saturated zone. Over time, CO₂ will dissolve into solution and, eventually, react to form mineral carbonates in the reservoir. Ultimately, solubility and mineral carbonization represent the most confident storage mechanisms, and physical trapping must persist for sufficient time to ensure efficient storage by these means.

Deep saline aquifers are wide spread and underlie many parts of the world, thereby reducing the costs of infrastructure associated with pipeline construction. The storage capacity accompanied with this option is high, with a global capacity estimated between 300 and 10,000 GtCO₂ [15]. Residence time in saline aquifers is long ranging from hundreds to several thousands years [2], depending on the local hydrologic gradients. Such aquifers are typically not suitable for irrigation and other uses, so injection of CO₂ has limited environmental impacts and less likely to present a problem for potential future use [8].

1.1.3. Coalbed Injection

Coalbed injection involves the injection of CO₂ into deep, unmineable coal seams, where the combined influence of physical trapping from low permeability surroundings and physical or chemical adsorption to the coal structure serves to contain the injected gas. As an additional benefit, the possibility of a recoverable reserve of methane presents an attractive economic solution. Conclusions of a DOE study [15] suggest approximately 90 Gt of national CO₂ sequestration capacity in unmineable coal seams, including 38 Gt in Alaska. Alternately, enhanced coalbed methane (ECBM) recovery potential was estimated at approximately 150 Tcf including 47 Tcf in Alaska. With approximately 2 Gt/year of CO₂ currently being emitted from U.S. power plants, the literature would thus suggest sufficient capacity exists for sequestration via ECBM-CO₂. However, design of a sequestration system under conditions of a specific power plant will require full analysis of the specific site. The study of Stevens *et al.* [16] concluded in the finale 225 GT of worldwide storage capacity.

1.1.4. Oil and Gas Reservoir Injection

Both depleted and active fossil fuel reservoirs are potential storage space for CO₂ in underground formations. CO₂ may be injected directly into a depleted or inactive reservoir without expectation of any further oil production, or the CO₂ injection may result in enhanced oil/gas

recovery and simultaneous CO₂ sequestration. CO₂ may also be injected into producing oil and gas reservoirs, where CO₂-enhanced oil recovery (EOR) and CO₂-enhanced gas recovery (EGR) will offer an economic benefit. Typically, oil reservoirs have undergone a variety of production and injection processes during primary and secondary recovery. As a tertiary recovery process, CO₂ can be injected into the reservoir to improve the mobility of the remaining oil thereby extending the production life of the reservoir. Also, significant quantities of natural gas can be produced by pressurization of the reservoir. This is a mature technology and is very viable as is elucidated in Appendix A.

1.2. ADDITIONAL SEQUESTRATION METHODS

1.2.1. Ocean Fertilization

Ocean fertilization is the process of seeding the shallow ocean waters with nutrients to stimulate the growth of marine photosynthetic organisms. The main concept underlying this sequestration method is that the shallow ocean organisms are capable of naturally sequestering atmospheric CO₂, but lack some key nutrients to make the rate of sequestration feasible as an actual sequestration strategy. Experiments have been performed to determine the key nutrients required, and also the impact that this method would have upon the oceans and the ecosystem as a whole. To date, there are still a lot of unknowns about using this method as a viable sequestration strategy, which must be determined before it should be utilized.

1.2.2. Deep Ocean Injection

Deep ocean injection, as a sequestration method, utilizes the ocean as a storage medium for containing either gaseous or liquefied CO₂. Injection of gaseous CO₂ to the ocean occurs at depths between 500 and 2,000 meters below the ocean surface and works on the principle that the injection gaseous CO₂ will diffuse into the seawater and react to form carbonates which will then settle to the bottom. The other form of deep ocean injection is to inject liquefied (compressed) CO₂ at a depth greater than 3,000 meters where the density difference between the ocean water and the liquefied CO₂ will cause the CO₂ to settle downward where it will form a pool on the ocean floor. Research is ongoing to determine the effects of sequestering CO₂ through this method. Currently it is predicted that diffusion of the CO₂ pool into the deep ocean waters will cause the oceans pH to decrease leading to an acidic ocean as well as the potential for an early release of the CO₂ back to the atmosphere.

1.2.3. Terrestrial Aforestation

Terrestrial sequestration is the net removal of CO₂ from the atmosphere or the prevention of CO₂ from leaving the terrestrial ecosystem. Since the terrestrial ecosystem includes soil and vegetation, various researches in this habitat focuses on means of improving land use management and soil texture in a way to enhance CO₂ sequestration. Therefore, CO₂ sequestration in the terrestrial ecosystem can be managed through various land use management. (1) Afforestation, reforestation and restoration of graded land (2) Agro forestry on Agricultural lands (3) Improving growth rate with the aid of required nutrients. A review of potential for terrestrial CO₂ sequestration based on various management practices inline with the required management practice (RMP). Analysis so far suggest that, there is potential for terrestrial CO₂ sequestration though with limitations (such as availability of land space), proper land and soil

management will to an extent sequester a reasonable amount of CO₂ in to the terrestrial biosphere why considering factors such as the environment and public acceptance.

1.2.4. Mineral Carbonization

Carbon dioxide sequestration by mineral carbonation mimics naturally occurring rock weathering which is known to have an important role in the historical reduction of the CO₂ concentration in the atmosphere after the creation of the earth [17]. The main advantage of the process is the formation of mineral carbonates which are the end products of geologic processes and are known to be stable over geological time periods (millions of years). The carbonation process energy required would be 30 to 50% of the capture plant output [18]. Considering the additional energy requirements for the capture of CO₂, a CO₂ capture system (CCS) with mineral carbonation would require 60 to 180% more energy input per kilowatt hour than a reference electricity plant without capture or mineral carbonation [18, 19]. These energy requirements raise the cost per ton of CO₂ avoided for the overall system significantly. The best case studied so far is the wet carbonation of ultramafic minerals [20-22]. The estimated cost of this process is approximately 50–100 US\$/tCO₂ net mineralized in addition to CO₂ capture and transport costs, but taking into account the additional energy requirements [23]. The mineral carbonation process would require 1.6 to 3.7 tons of silicates per ton of CO₂ to be mined, and produce 2.6 to 4.7 tons of materials to be disposed per ton of CO₂ stored as carbonates [18]. A number of issues still need to be clarified before any estimates of the storage potential of mineral carbonation can be given. The issues include assessments of the technical feasibility and corresponding energy requirements at large scales, but also the fraction of silicate reserves that can be technically and economically exploited for CO₂ storage. The environmental impact of mining, waste disposal and product storage could also limit potential.

1.2.5. Biological Sequestration: Industrial-Bioreactor

Sequestration by biological means in an industrial Photobioreactor (PBR) was investigated. In this method microalgae are grown in a controlled, indoor environment and fed light from a solar field, internal lighting, or a combination of both. A survey of existing technologies and microalgae was completed. In addition, fundamental, photosynthetic relationships and associations were identified (see Appendix A for detailed discussion). Further, a rate law and specific mathematical models were developed. These mathematical models were used to design and optimize the PBR. The PBR consists of a large vessel or set of vessels that are partitioned by parallel plates separated by a distance, *d*. The plates consist of frosted glass with fiber optic lamps arranged inside of them in such a way that uniform light intensity is created and distributed across the surface of the plates. The system is designed to provide a light at the saturation light intensity with high cellular concentration and maximum rate normalized by the plate area.

1.3. SELECTED METHODS

Because of the scope of the investigation, the field of options had to be reduced. Ocean sequestration was eliminated because it had quite negative public perception and the environmental impacts were not well known. Mineralization was eliminated because it was exorbitantly expensive. Terrestrial afforestation was eliminated because the land requirement was unreasonable. Oil/Natural Gas and coal bed injection were eliminated because they were quite location limited in comparison to saline injection. Deep saline aquifer injection and

sequestration by industrial photobioreactor were pursued. Sequestration by the industrial photobioreactor was pursued because there are very few adverse environmental impacts, the future market for algal biomass looks strong, it has the potential to make existing technologies green, and can be easily transferred to several locations. The deep saline aquifer injection was pursued because it is very common in location and would not require large transport distances from existing sites, has high storage capacity, has long retention times, does not present unreasonable environmental risks, and utilizes mature and well known technology.

2. PART II: THE IGCC POWER PLANT

The selected source for CO₂ is an integrated gasification combined cycle (IGCC) power plant. The IGCC combines gasification technology with combined cycle technology. The first step in the IGCC process is gasification. Gasification converts any hydrocarbon into a synthesis gas (or syngas) is comprised of mainly of hydrogen (H₂) and carbon monoxide (CO) at high temperature and pressure. In the case under consideration, the hydrocarbon source is coal. Gasification process produces fewer pollutants in the effluent than combustion and consequently fewer pollutants in the flue gas streams. Even though it produces fewer pollutants, the syngas must be cleaned-up to removing the acid gases (such as hydrogen sulfide), particulate matter, Hg and other undesirable components. This is done primarily to protect the catalysts and materials down stream from the gasification. With a CO₂ capture option, syngas passes through a Water Gas Shifter (WGS) reactor where steam is introduced to the syngas the CO is converted to CO₂ and more H₂.

A Pd membrane can be used to separate hydrogen from the effluent from the WGS and hydrogen is combusted in a combined cycle gas turbine that produces electricity. Both the syngas production process and the gas turbine combustion process generate steam that is utilized to generate electricity by a steam turbine. Advantages of IGCC include the reduction of CO₂ emissions, increased efficiency, and flexible fuel supply. Further, IGCC technology with CO₂ capture is beneficial for the environment because of the reduction of the emission of pollutants (e.g., SO₂, NO_x, particulate matter, and mercury). The collection of sulfur and gasification slag obtained from the process has byproduct value, which avoids the cost byproduct disposal, and easier CO₂ removal. The energy consumption for CO₂ capture is lower in comparison with conventional power plant. However, the capital cost for IGCC is higher. In addition, IGCC is a complex process that requires a high degree of component integration [24]. Figure 2 shows the schematic of IGCC process under consideration.

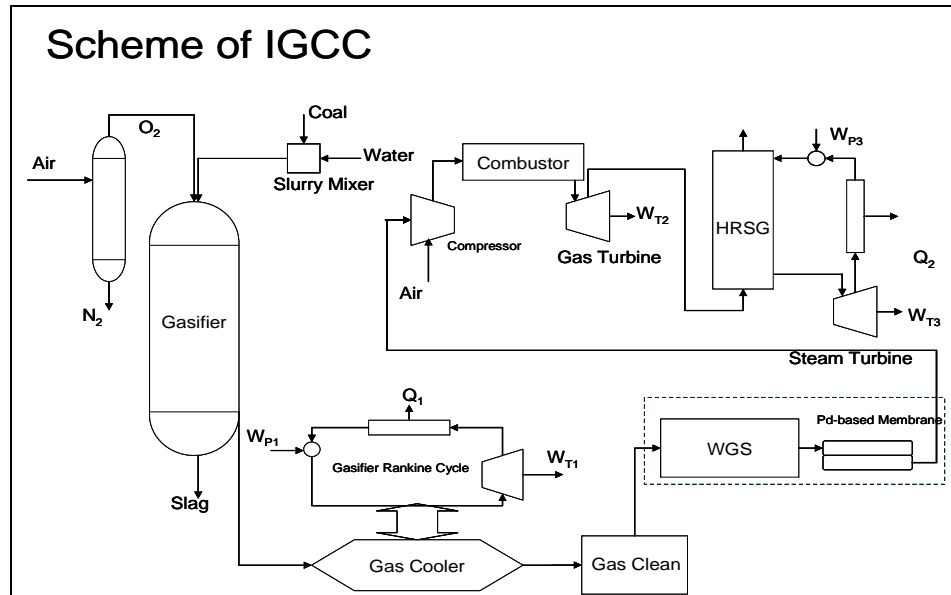


Figure 2
Schematic diagram of the IGCC power plant [24]

There are two output streams from the proposed plant design: a pre-combustion stream that comes from the palladium filter and a post combustion stream that comes from the heat recovery steam generation module (HSRG). The pre-combustion stream will have a molar composition close to: 68.3% CO_2 , 12.5% CO , 12.5% H_2O , and 6.7% N_2 and a total flow of 14,875 kmol/hr [24]. It is advantageous to oxidize the CO to CO_2 both for safety and energy considerations. Thus the composition that will be sequestered is 80.2% CO_2 , 12.4% H_2O , 6.6% N_2 , and 0.8% O_2 at a total flow rate of 14,994 kmol/hr. The second stream coming from the HSRG will have a molar composition of 14.6% H_2O , 12.2% O_2 , and 73.2% N_2 and a total flow rate of 94,248 kmol/hr [24].

3. PART III: THE PHOTOSYNTHETIC BIOLOGICAL REACTOR

3.1. THERMAL PRETREATMENT

The majority of waste heat generated by conventional coal power plants is generally discharged to the environment at 250°F to 800°F, and feeding the bioreactor using the CO_2 gas at those temperatures is not possible [25]. It is necessary for these gasses to be cooled before they can be used in sequestration. In particular, the flue gas from the IGCC process under consideration will have an output temperature of around 100°C from the palladium filter [24]. The maximum temperature tolerated by the microorganisms in the reactor is 95°F (preferably not exceeding 70°F) [26, 27]. The common cooling processes are air-to-air or air-to-water heat exchangers and the cooling water towers. It would be advantageous to find and employ a feasible option that can cool the gas, and at the same time, utilize the heat energy producing electric energy. A possible solution is the Cascading Closed Loop Cycle (CCLC).

3.2. BIO-REACTOR DESIGN

3.2.1. Principles and Theory

To effectively design a photobioreactor (PBR) for the purposes of CO₂ sequestration, it is paramount to understand the principles that govern photosynthesis and the parameters that control CO₂ fixation. A first principles model has been developed that allows for the optimization of reactor parameters such that the highest sequestration rate can be obtained. In addition the scale-up parameters have been identified.

Design Principles

The most important consideration in the utilization of light for photosynthesis is the saturation light intensity. The saturation light intensity is the light intensity at which the pigments within the photosynthetic organisms become overloaded with light and no longer efficiently use light. Figure 3 shows the light utilization efficiency and photosynthetic efficiency as a function of light intensity.

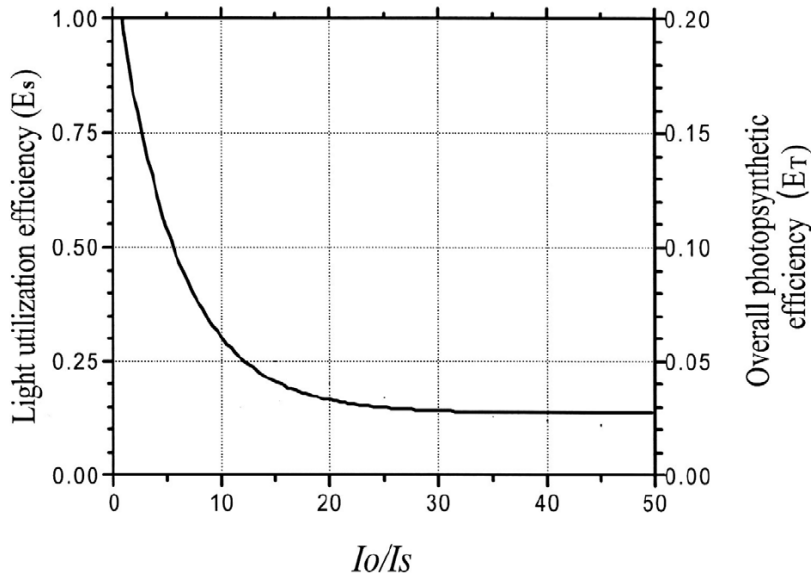


Figure 3
Photosynthetic Efficiency vs Light Intensity [28]

Here, I_o is the incident light intensity and I_s is the saturation light intensity. The light utilization efficiency is defined as the light used in photosynthesis over the incident photosynthetically active radiant (PAR) and given the symbol E_s . The overall photosynthetic efficiency is the biomass energy over the incident PAR and can generally be taken as $0.20 \cdot E_s$ [29]. At an incident light intensity below the saturation light intensity, the light utilization efficiency remains at 100%, and the photosynthetic efficiency remains at 20%. Above the saturation light intensity, both efficiencies drop off dramatically according to the following equation [29]. The following equation is valid for $I_s > I_o$. For $I_s < I_o$, $E_s=1$.

$$E_s = \frac{I_s}{I_o} \ln \left(\frac{I_s}{I_o} + 1 \right) \quad (1)$$

Because of the expense of the light collection system, it is important that the light be utilized as efficiently as possible. A loss of efficiency in utilization results in a larger and much more expensive light collection system. It is important, then, not to exceed the saturation light intensity within the PBR.

More importantly, photosynthesis is a photochemical reaction and the rate can then be determined from the utilization efficiency (Et) and the absorbed light [30, 31]. The absorbed light is governed by the Beer-Lambert law [32]. For a cylindrical system, the Beer-Lambert derivation yields Eq. (2), and for a cubic system it yields Eq. (3). Eq. (2) is used for radiant light intensity from a cylindrical lamp of radius r_0 at a distance r from the center of the lamp [33]. Eq. (3) is useful from the determining the light intensity from a distance x from a radiating plate.

$$I = \frac{r_0 I_0}{r} \exp(-a(r - r_0)) \quad (2)$$

$$I = I_0 \exp(-ax) \quad (3)$$

Here, I_0 is the incident light intensity and a is the extinction coefficient. If the light path is small and the concentration is low $a = \epsilon C$, where ϵ is the specific light absorption coefficient and C is the cellular concentration. However, this simple relation does not account for attenuation due to cellular reflection or light path length. A more accurate model for a is expressed in Eq. (4) [33].

$$a = \frac{\epsilon_m C}{(K_c + C)(K_x + x)} \quad (4)$$

If $C \ll K_c$ and $x \ll K_x$, Eq. (4) simplifies to $\epsilon_m C / (K_c K_x)$, thus $\epsilon_m = \epsilon (K_c K_x)$ [33]. The light absorbed by the cells can be calculated by Eq. (5) [33].

$$I_{util} = I_0 - I \quad (5)$$

I is calculated using Eqs (2)-(4). The cellular yield can be calculated using Eq. (6) [31].

$$Y = Et \cdot A \cdot K \cdot I_{util} - G \cdot R \cdot C \cdot V \quad (6)$$

Here, Y is the cellular yield (g dry weight/h), Et is the photosynthetic conversion efficiency taken as $0.2 \cdot E_s$, A is the illuminated area (m^2), K is the energy equivalent of the algae (g dry weight/W/h), I_{util} is the light utilized in Eq. (5) (W/m^2), G is the ratio of dry weight of cells to the weight of carbon within the cells, R is the respiration rate (g carbon/g dry weight/h), C is the cellular concentration (g dry weight/L), and V is the culture volume (L). Eq. (6) was derived by first principles from an energy and mass balance and has been shown to accurately model the productivity at light intensities under the saturation intensity [34].

The specific carbon dioxide fixation rate (g CO_2 /L/day) can then be calculated as:

$$R_{CO_2} = \frac{88 \cdot Y}{G \cdot V} \quad (7)$$

Scale-Up

Knowing how growth rates and energetic parameters are affected by scale up and developing a basis of comparison between reactor types is important when developing an industrial process. For a PBR, there are two important parameters in comparison between reactors and in scaleup: the light energy supplied per unit volume (I_0/V), and the light distribution coefficient (K_{iv}) [30]. It is obvious that the greater the light supplied per unit volume, the higher the rate will be. It should also be obvious that for constant illumination area, cellular concentration, and volume, that the growth rate will be linear below the saturation light intensity and will fall away from linear in proportion to E_s in Eq. (1) above the saturation intensity. However, it is also important how the light is distributed within the reactor. This is something that varies with reactor type. The light distribution coefficient is a measure of how the light is distributed and is defined as the cell concentration at which 50% of the PBR volume received enough light to have positive cellular yield [29]. The light intensity at which no net growth occurs can be found from Eq. (6) by setting Y equal to zero. The volume that is above that light intensity can be found using Eqs (2) and (3). The percentage can then be calculated from that volume. The concentration will have to be varied until the fraction is 0.5, this concentration is taken as K_{iv} . Figure 4 shows this concept for two different types of reactors.

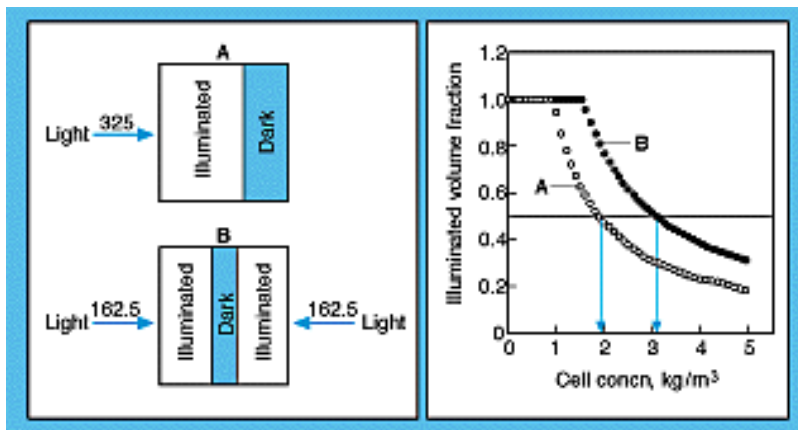


Figure 4
Light Distribution Coefficient, Conceptual Example [30]

Because K_{iv} is higher for the lower reactor type in Figure 4 even though the total light illumination is the same, the rate is higher because the sustained cellular concentration is higher. It was shown that the growth rate is linear with respect to both I_0/V and K_{iv} [30]. Thus a single coefficient, the light supply coefficient ($I_0/V * K_{iv}$), is a measure that can be used for comparison between reactor types and for scale up [30]. That is to say, if data is collected in one reactor type in the lab, it can be used to size and design a full scale reactor of any other type or size as long as the light supply coefficient is the same between them. This is shown in Figure 5. The linear portion of the growth rate vs light supply coefficient is linear because it falls below the saturation light intensity. Equation (1) will have to be incorporated into the growth rate above the saturation intensity. It is important to note that at high light intensities, E_t becomes constant with respect to light intensity at approximately 0.03 rather than 0.2 at low light intensities. It is because of this that two linear or nearly linear regions exist in Figure 5. A low light supply coefficient corresponds to low light intensity and vice versa. It would be expected that the rate would be linear with respect to light supply coefficient until the point of light saturation and that

the change in rate with respect to supplied light is proportional to the light utilization efficiency. Figure 5 is then consistent with Figure 3 in that there is a sharp change in the rate with respect to light supply coefficient at the saturation point and in that a linear (or near linear) relationship is established once again at high intensities but with reduced slope. However, a discontinuity would not be expected. Unfortunately the data just above the saturation point is missing in Figure 5. It is not possible to fully validate the data with the above predictions and expectations. However, the principles were validated in the literature review and by calculations which can be found in Appendix A

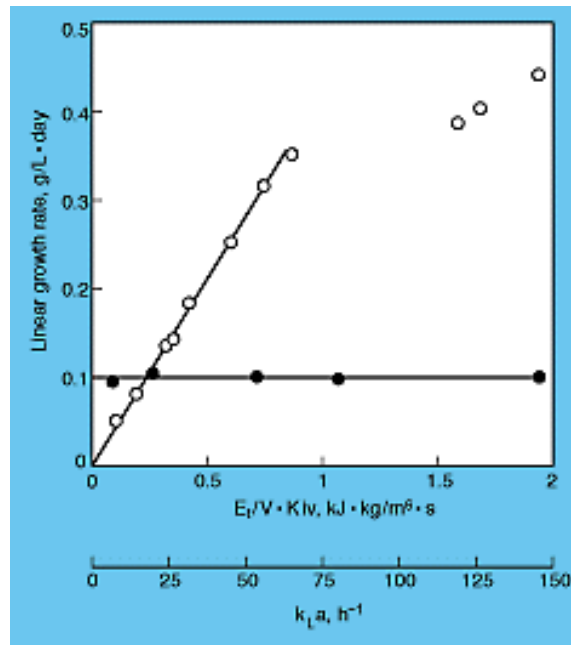


Figure 5
Growth Rate vs Light Supply Coefficient (open circles)
Growth Rate vs Volumetric Mass Transfer Coefficient (closed circles) [30]

Also shown in Figure 5 is the effect of the volumetric mass transfer coefficient (k_L) on rate. k_L is a measure of mixing within the reactor. It has been shown to be zero order in PBR's [30]. This is a result of the relatively low rate of photosynthesis in comparison to the diffusion rates of products and reagents. Thus a minimal amount of mixing is needed to sustain a given rate [30]. It is also advantageous to most photosynthetic organisms to avoid high fluid shear stress because most do not have strong cellular walls [30].

Data and Estimations

It was not possible to find all the data needed for one particular strain of photosynthetic micro-algae. Thus, the data used in this design is representative of micro-algae, but is not specific to any single micro organism. Laboratory experimentation would have to be done to determine the data needed for a selected micro-algae strain, which is not possible within the limits of this investigation. A review of probable microalgae can be found in Appendix A. The data and estimations for microalgae used in this design as well as the methods needed to obtain the data are discussed in brief in the following:

A good estimate for the saturation light intensity is 30 to 45 W/m² or 140 to 210 uE/m²/s [31, 35-37]. The saturation light intensity is a specific property of each individual photosynthetic organism and can be experimentally determined by collecting data of specific growth rate vs luminous intensity. The light intensity at which growth becomes non-linear with respect to luminous intensity is the saturation light intensity. A value of 45 W/m² was used in the design.

The energy equivalent of the algae will have to be determined experimentally by calorimetric experiments. A reasonable estimate is 23.1 kJ/g dry weight, resulting in K=0.156 g dry weight/h/W [31].

The ratio of g dry weight to g of carbon could be measured by combustion and GCMS. A typical composition is 49% carbon, which results in a G of 2.04 [31].

The respiration rate is a function of cellular concentration and would have to be carefully measured under the growth conditions. Figure 6 shows the respiration rate of *Scenedesmus obliquus* [31].

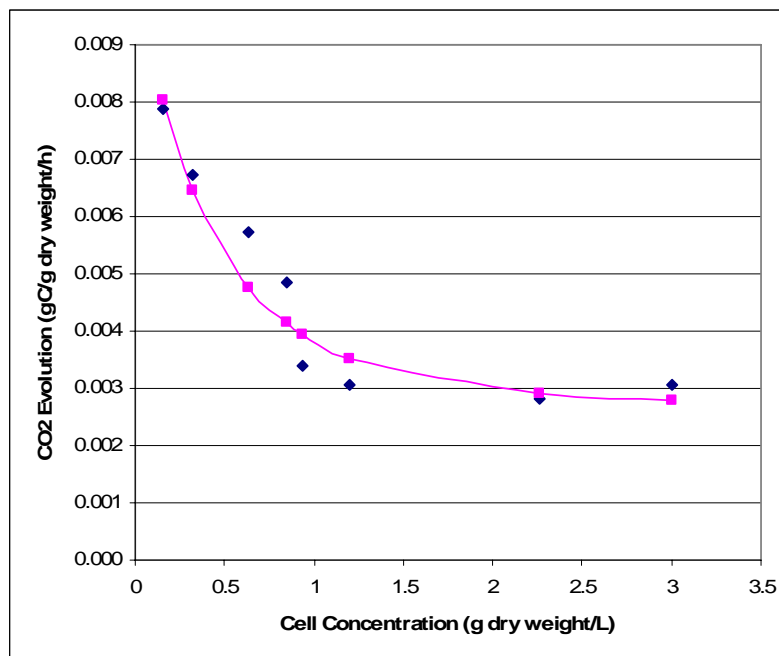


Figure 6
Respiration Rates as a function of Cellular Concentration [31]

The data from Figure 6 was entered into a spreadsheet program and a hyperbolic function of the form $a/(b+C)^d + e$ was used to fit the function using a minimization of sum of squared error method. The constants were found to be: a=1.854, b=2.582, d=5.819, e=0.002715. This function was used to calculate the respiration rate for the final design. The fit to the data is shown as the pink line in Figure 6.

Finally, the parameters used in the modified Beer-Lambert's law need to be measured. This can be done using a quantum sensor and a several optical cells of varying path lengths. These

measurements were performed for *Synechococcus* sp. PCC 6301 and the parameters were found to be: $\epsilon_m=50$, $K_c=2.7$ g dry weight/L, and $K_x=4.7$ cm [32].

3.2.2. Design Summary

Using flat plates that consist of fiber optics buried in frosted glass has been shown to produce uniform, controllable light intensity within the body of the reactor [38]. The design will then consist of several parallel frosted glass illumination plates separated by a distance, d , and will be evenly distributed within the reaction volume. The light intensity at the boundary of the plate will be held constant at the saturation light intensity to ensure the highest photosynthetic rate and the highest possible efficiency. The challenge is to find the optimal spacing and cellular concentration that will yield the highest rate per square meter of illuminated plate.

Light intensity is additive [33]. For example, if light is introduced into a space that is lined with perfectly reflecting surfaces and there is no material that absorbs the light within that body enclosed by the reflecting surfaces, the light will not dissipate. It is theoretically possible to continually introduce a low light intensity into a body of perfect reflection and no adsorption and have it build to infinite intensity as time approaches infinity. Even with adsorption and imperfect reflection, it is possible to have apparent light intensity greater than the source input intensity if the light at a given distance from the source is reflected back to the source and not all of the light is adsorbed in the body or by the reflective elements. Because light intensity is additive, the light intensity from a single illuminated plate can be considered apart from the adjoining plates. The final intensity states can be determined by summing up the independent contributions from each illumination and by using Beer-Lambert's law. Furthermore, reflection and transmission losses by and through the light source plates can be considered in the same manner if it is assumed that there are numerous plates in parallel. It is thus possible to lump the losses due to reflection and transmission efficiencies by the luminous plates into a single coefficient, pct . Light intensity between two adjoining and reflective plates can then be used to build a representative model for the rest of the reactor.

The light intensity from a single, representative plate considering reflection can be seen in Figure 7. For the purposes of illustration, the distance between plates was set 1cm with pct set to 0.8 and a cellular concentration of 5 g dry weight/L. The adsorption constants are the same as determined in the previous section. A single reflective, illuminating plate is at $x=0$ with an input intensity of 45 W/m^2 . A second non-illuminating, but reflective plate exists at $x=1$. Light leaves the illuminating plate at 45 W/m^2 . As it travels through the reactor volume, it is adsorbed according to Beer-Lambert's law and the intensity decreases to approximately 11.5 W/m^2 at $x=1$. At this point, it is reflected, but at a reduced intensity proportional to pct . Because of the reflection, a virtual light source with an apparent intensity of approximately 9 W/m^2 and a position of $x=1$ is considered. This light then travels back to the illuminating plate at $x=0$ and reaches with an intensity of approximately 2 W/m^2 . This is then reflected off of the surface of the illuminated plate in proportion to pct . Once again, a virtual light source with an intensity of 2 W/m^2 must be considered. Thus the total intensity at $x=0$ is then 47 W/m^2 rather than 45 W/m^2 .

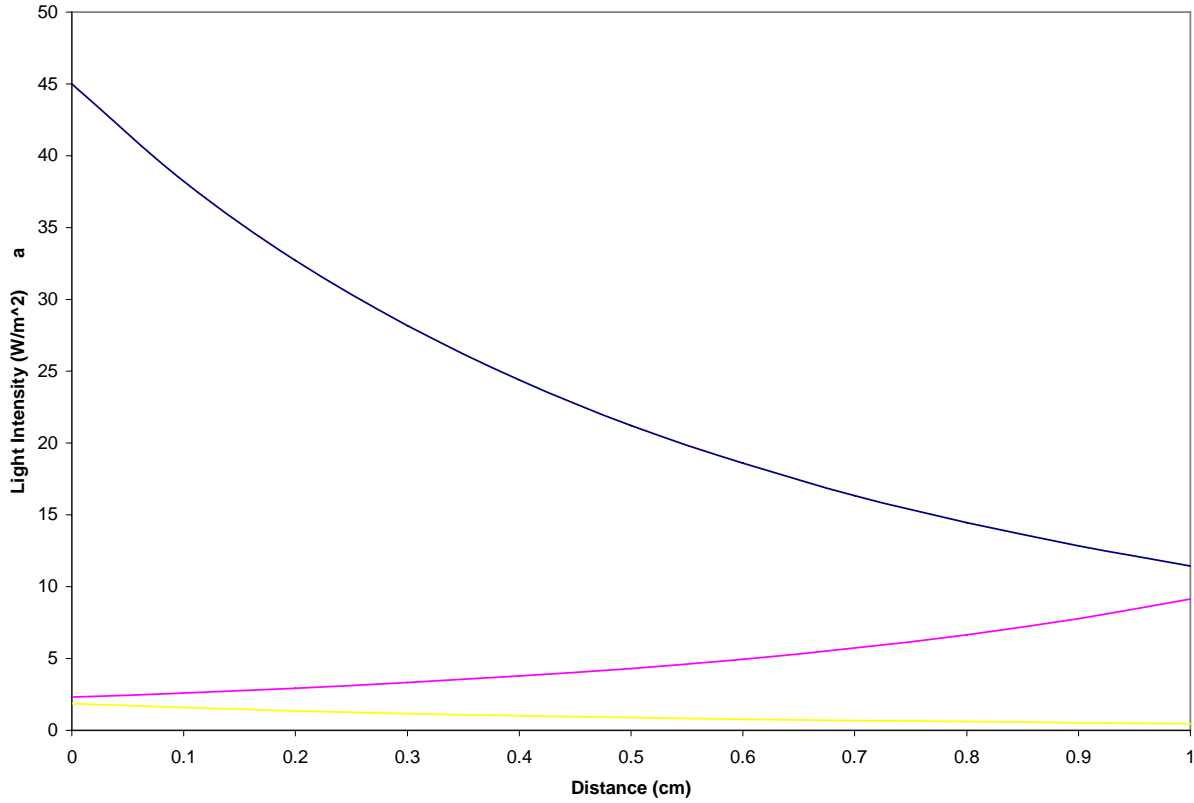


Figure 7
Light Intensity Distribution between Plates with Reflection Considered

Equation 8 can be used to iteratively calculate the apparent light intensity at $x=0$. Here, x is the position between plates, d is the distance between the parallel plates, and I_{app} denotes the apparent light intensity. The remaining parameters are the same as those in Eqs. (3) and (4). The light not utilized in photosynthesis can be calculated by keeping track of I_{app} with pct set to unity and subtracting I_{app} with the desired pct once the iteration is complete.

$$I_{appnew} = I_0 + pct^2 \cdot I_{app} \exp\left(\frac{-2\varepsilon_m Cd}{(K_c + C)(K_x + d)}\right) \quad (8)$$

The apparent light intensity calculated in the iteration is then used to calculate the light intensity at the boundary with illumination from both boundaries ($x=0$ and $x=d$). This can be calculated by adding the apparent light intensity to the transmitted light intensity using Eqs. (3) and (4) with x set to the spacing between the plates and I_0 set to the apparent light intensity found using Eq.(8). This is shown in Eq. (9). The input light intensity can then be adjusted until the light intensity at the boundaries is at the saturation light intensity.

$$I = I_{app} \left(\exp\left(\frac{-\varepsilon_m Cx}{(K_c + C)(K_x + x)}\right) + \exp\left(\frac{-\varepsilon_m C(d-x)}{(K_c + C)(K_x + (d-x))}\right) \right) \quad (9)$$

A model was developed to address the issues above. The computer program first calculates the luminous intensity at the plates as a function of cellular concentration, distance between the plates, pct, and light intensity introduced into the reactor. The light intensity fed into the reactor was adjusted a loop until there was no point between the plates that exceeded the saturation light intensity. The rate was then calculated under those conditions and the concentration and rate were saved as data points. The concentration was stepped up and the loop and rate was calculated again. A full set of these rates was calculated as a function of cellular concentration with the constraint that the light intensity not exceed the saturation light intensity. The maximum volumetric rate was calculated and the associated cellular concentration was identified. The sequestration rate normalized by the plate area (ASR) was calculated from the volumetric rate and d was adjusted manually until the ASR was maximized. A copy of the computer program can be found in Appendix B. Figure 8 shows the simplified logic diagram for the computer program.

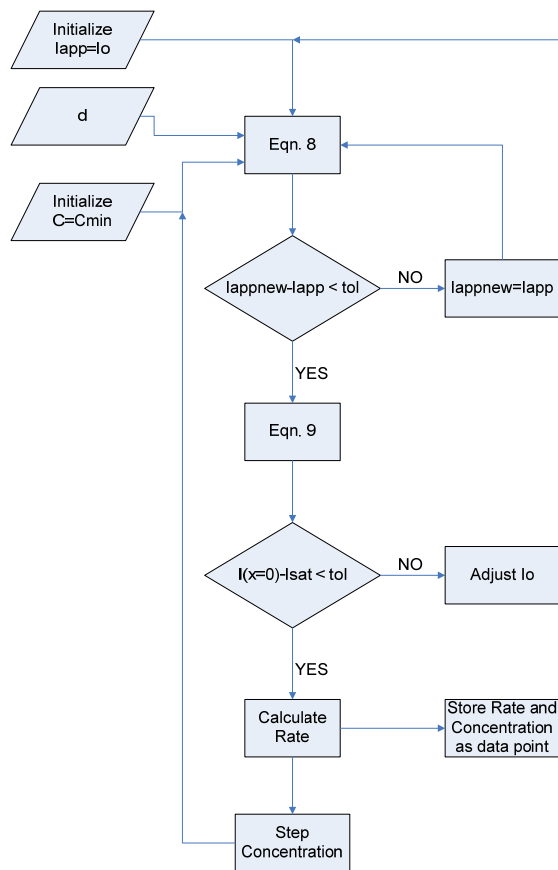


Figure 8
Computational Logic Diagram

Figure 9 shows the rate of CO_2 fixation as a function of cellular concentration under optimal conditions. Figure 10 shows the light intensity distribution between the luminous plates at the conditions of the maximum rate. It is important to note that the luminous intensity does not exceed the saturation intensity (45 W/m^2) within the reactor body, nor does the intensity between the plates drop far from the saturation intensity. This is important because it ensures that the entire volume of the reactor is operating at or close to maximum efficiency and rate.

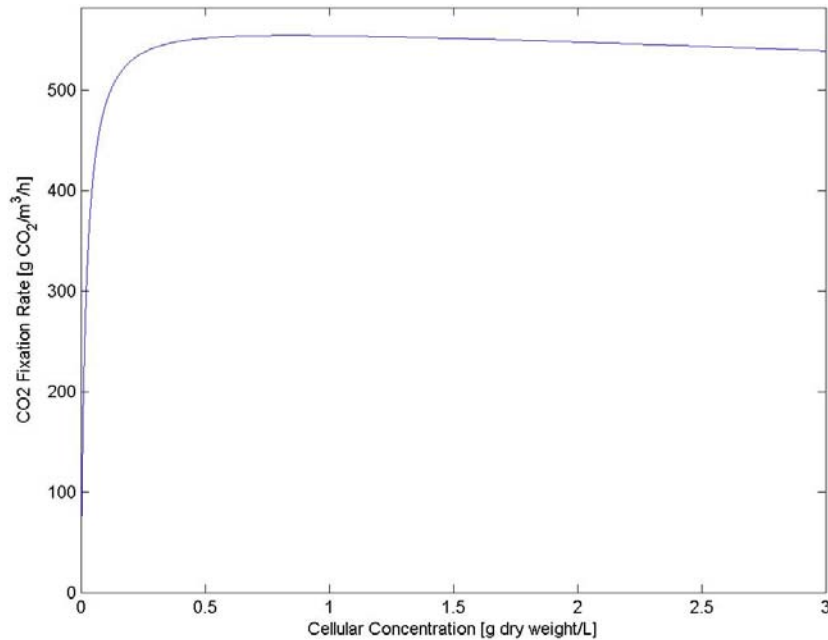


Figure 9
Fixation Rate vs Cellular Concentration Under Optimal Conditions

Using the estimated data in the previous section and the method discussed above, the optimal conditions were identified to be: $d=0.70$ cm, $C=0.844$ g dry weight/L, and a light intensity input of 35.56 W/m². This results in a volume specific rate of 13.30 g CO₂/L/day, an area specific rate of 93.11 g CO₂/m²/day, and a light utilization efficiency of 99.5%. A pct of 95% was used. At this rate, a total volume of 4.43×10^5 m³ and a luminous plate area of 6.20×10^7 m² is needed to sequester 2.325 MtCO₂/year (~half of the output from a 500MWe plant). A PAR light requirement of 4.41×10^6 kW is required which results in a total sunlight requirement of 8.82×10^6 kW. A greater amount of light will have to be collected due to transmission and collection losses. These will be discussed in following sections.

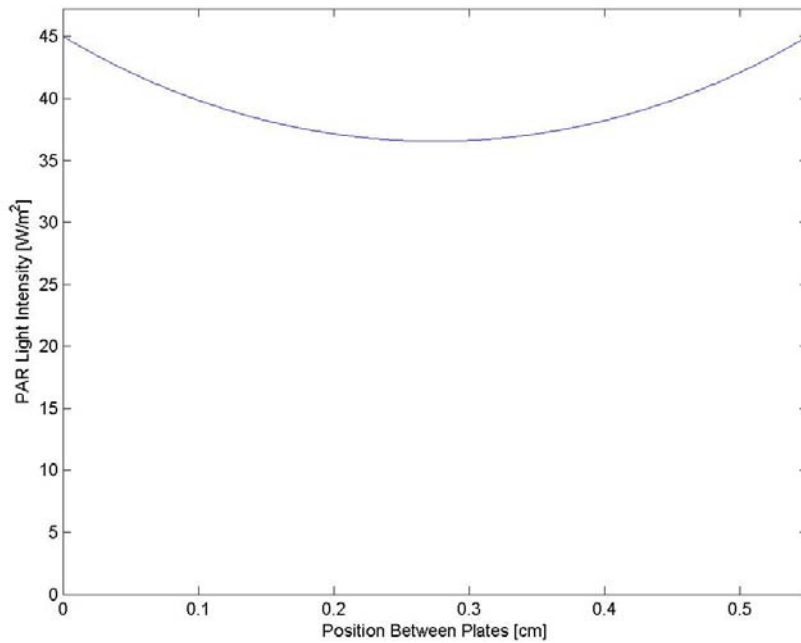


Figure 10
Light Intensity Distribution vs Position Between Plates

The reactor system will consist of several reactors (four for each light tower, with a total of 36), a filtration system, a CO₂ adsorption system, and a makeup and pH control system. Figure 11 shows a conceptual diagram for the proposed system.

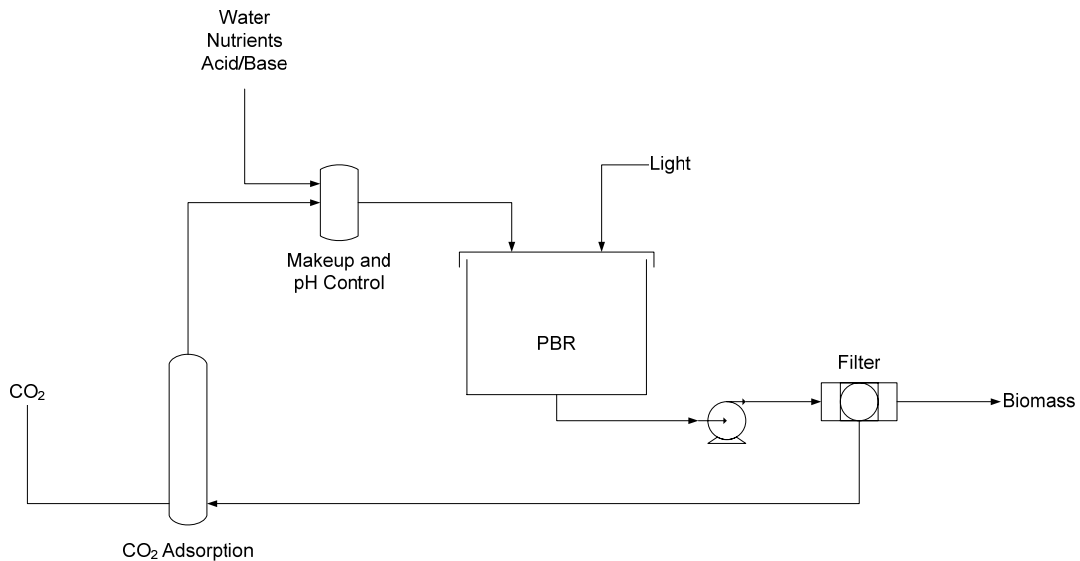


Figure 11
Conceptual Reactor System Diagram

Light, micro-algae, and growth media are fed into the PBR(s). The micro-algae consume water, carbon dioxide, and nutrients from the growth media as well as consuming light energy. The

depleted growth media and the grown micro-algae are removed from the bottom of the PBRs. The effluent is filtered to remove grown biomass. The biomass is sent to be dried and used elsewhere. The filtrate consists of growth media with depleted water, nutrients, and dissolved carbon dioxide. The depleted growth media is sent to be saturated with carbon dioxide, to have nutrients added back, and to be pH and temperature adjusted as needed. The CO₂ saturation occurs in a CO₂ adsorption system. The adsorption system will have to be designed such that a high percentage of the CO₂ is captured in solution. It will be beneficial to use a pre-combustion separated stream from an IGCC plant because of the high carbon dioxide content and the amount of water in the stream. The water from the gasification can be used to supply the water needed in the bioreactor after being cleaned and temperature and pH adjusted. Sulfur and Nitrogen compounds are generally not a problem with most microbes as they need a small amount in their growth media. The saturated solution is sent to a mixing vessel in which nutrients are added and an acid or base is added so that the solution going into the reactor(s) is the correct composition and pH.

Having several bioreactors running continuously is advantageous because several species of microbes can be grown and sold at the same time as the market or plant conditions dictate. There is also a possibility waste treatment if the microbes are not intended for human consumption. In addition, the microbes could be fed excess natural and regional fertilizers if available.

Other design considerations beyond the scope of this investigation include a cleaning system for the luminous plates as mineral deposits and microbial wastes could build up and block desired light. An automated system with a roller type brush that fits between the plates could be employed. A cellular concentration and control system will have to be developed to maintain optimal cellular concentration within the reactor as well as light intensity monitoring and feedback systems. One possibility for concentration control is a calibrated light sensor system on the output of the reactor and a bypass from the pump to the top of the reactor (not shown in Figure 11). In this way, the bypass can be increased if cellular concentration begins to fall and decreased if cell concentration rises. Light monitoring and feedback can be done by employing small, calibrated light sensors in between the luminous plates at various points in the reactor and employing computer control to adjust the light input into the system.

3.3. LIGHT SEPARATION AND TRANSMISSION

Efficient operation of the photosynthetic bioreactor (PBR) requires 4.41×10^6 kW of power supplied on a continuous basis. This amounts to an energy supply of 1.06×10^8 kWh per day. To supply the required power, energy from the sun in the form of visible light and infrared radiation are utilized, with both visible light and infrared radiation supplying the power in different ways. All the energy required for the algae to fix the CO₂ for growth is supplied by solar energy collected using the heliostat collectors located around central towers. The solar spectrum reflected to the central towers will undergo spectrum separation into the visible portion and the infrared portion using a spectrally selective cold mirrors. The cold mirrors are designed such that they will reflect the visible portion of the solar spectrum on to a bundle of fiber-optic lines located in the column of the tower which will transmit to the PBR as part of the energy requirement. The rest of the light, the infrared portion, will pass through the cold mirrors where it will be adsorbed either by photovoltaic cells (PV cells) or a heat exchanger for a cascading closed loop cycle (CCLC). This collected energy will then be used to generate electricity that

will be used to power light-emitting-diode (LED) grow lights in the PBR, which will provide the additional required power for the PBR during times when the light transmitted through the fiber optics is insufficient such as night, early morning, and late evening. The system was designed in such that the electricity generation equipment and the solar collector provide no more power than what is needed by the PBR. During the early morning or late evening hours the light transmitted to the fiber optics is less than is required by the PBR so additional power will need to be supplied by the grow lights during this time. As the power from the sun reaches and exceeds the required power inside the PBR, some of the computer-controlled heliostats will adjust and reflect towards the “electrical generation only” towers. This will ensure that the light intensity within the PBR does not exceed the saturation light intensity and that there is electrical power to supply light to the reactor during the night, early morning and early evening. Figure 12 shows the incident light, I_o , the light transmitted to the reactor by fiber optics, P_{solar} transmitted, the light supplied to the reactor by electricity, $P_{electric}$ light, and the total power supplied to the reactor by light, P_{total} . The integration of P_{total} throughout the 12 hour light period is that which is needed as energy in a full 24 hour operation period.

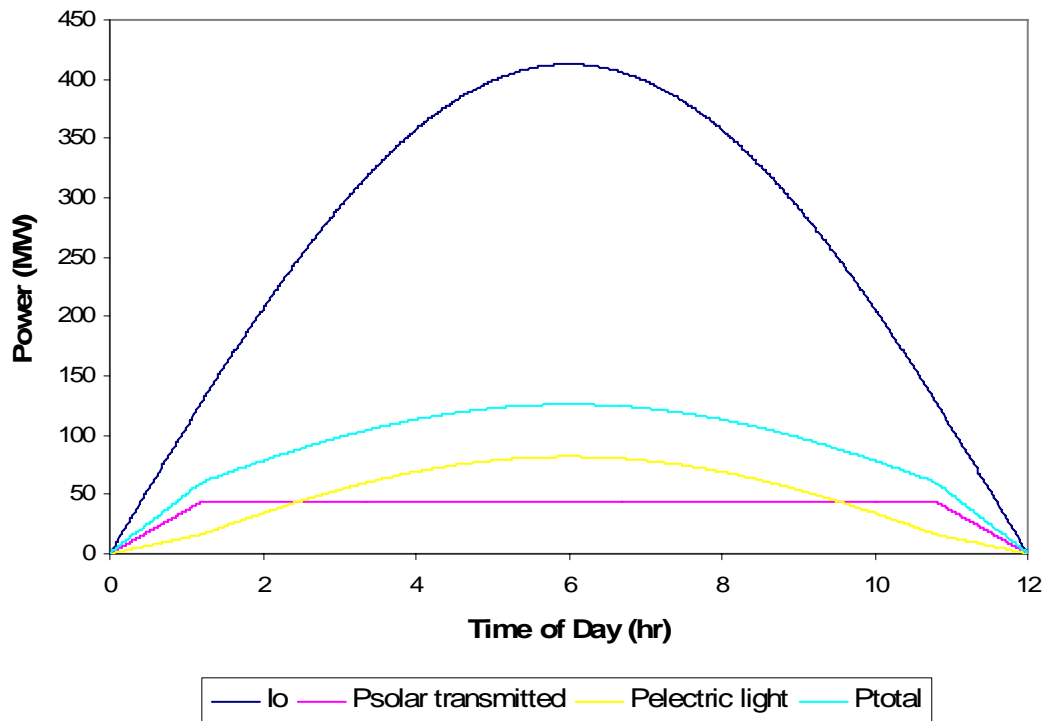


Figure 12
Incident Light and Light Utilization

3.3.1. Wavelength Requirements

Photosynthetic organisms use energy from sunlight in fixing CO_2 for cellular growth. The portion of the solar spectrum that is used in this process is the visible light portion, which has the characteristic wavelengths between 400 and 700 nm. To this end, it is useful to separate the light into grouped wavelengths so that more energy from the sunlight can be used. The solar spectrum can be divided into three distinct groupings, which are termed ultraviolet, visible light, and infrared. The ultraviolet plus x-ray spectra account for 1 percent of the energy coming from the

sun and have the characteristic wavelengths less than 300 nm. Visible light spectra account for 45 percent of the energy coming from the solar spectra and have the characteristic wavelengths from 300 to 700 nm. Infrared radiation is the heat component of the solar spectrum and accounts for 54 percent of the energy, with the characteristic wavelengths from 700 to 11,000 nm [39].

3.3.2. Solar Irradiance

The design of a solar collection and transmission system requires an estimation of how much energy is delivered by the sun to the location at which the system will be located. The rate at which solar energy reaches a unit area at the earth is called the solar irradiance and is typically measured in watts per square meter (W/m^2). This solar irradiance is not constant throughout the day. To design a solar collection system a designer must know the average solar energy density. The typical units of measure are watt-hours per square meter (Wh/m^2). The power released from the sun reaches the outer layer of the earth's atmosphere at $1367 \text{ W}/\text{m}^2$ (known as the extraterrestrial solar constant (SC)) where it then undergoes additional losses due to atmospheric particles such as water molecules, ozone, and dust. The actual amount of solar power received at the earth's surface can vary greatly depending on the amount of matter encountered in the atmosphere, and can range from 90 percent, of the SC on a very clear day to around 30 percent on a very cloudy day [33]. Since the actual solar irradiation can vary so much over the course of the year it is best to view the solar irradiation as an average over the course of the year. Figure 13 provides an average daily solar irradiation for the entire United States that can be used to estimate the solar irradiance at a particular location in the United States.

The location of the PBR is intended to be in the southwest United States and will have an average solar irradiance of $7.0 - 8.0 \text{ kWh}/\text{m}^2/\text{day}$. If the system were to be located in Alberta, Canada for example, then the average solar-irradiance would decrease to $3.0 - 4.0 \text{ kWh}/\text{m}^2/\text{day}$ [40]. In the later case, implementation of a solar collecting system does not make sense and was not considered. To design the solar collecting system for the PBR an average value of $8.0 \text{ kWh}/\text{m}^2/\text{day}$ was assumed in the calculations of required collector surface area, see Appendix C for detailed procedure of calculating collector surface area.

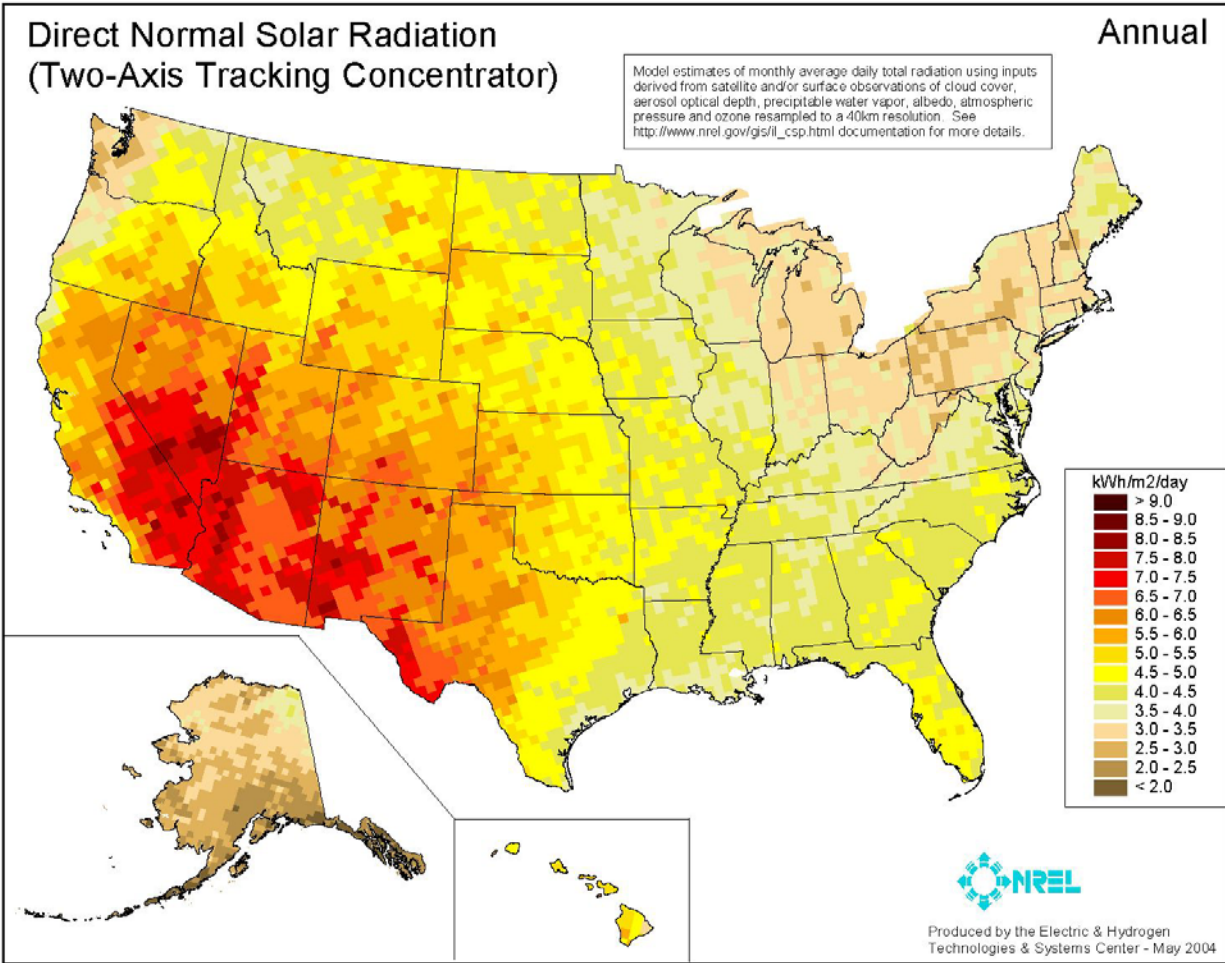


Figure 13
Average daily solar irradiation in kW/m²/day for 2004 [41]

3.3.3. Solar Energy to Electrical Energy Conversion

To convert sun energy into electrical energy two viable options were explored. The first was to use photovoltaic cells (solar cells) and the other was to use a CCLC. The use of solar energy to generate electricity is not a new idea but is one that is receiving a lot of attention as of late [39, 42]. It has been proposed that if better methods to harness the energy from the sun could be developed, fossil fuels could be eliminated for energy production all together [39].

Photovoltaic Cells

Photovoltaic cells (PV) use energy supplied by the sun to generate electricity through a process known as the photovoltaic effect, which was first recognized in 1839 by French physicist Alexandre-Edmond Becquerel [43]. A PV cell is a semiconductor device which utilizes energy of photons (light) to generate electricity using a rather simple mechanism. Photons from the sun are absorbed by a PV cell and excite electrons in the semiconductor material into a conduction band gap. The excited electrons can travel from atom to atom along the conduction band to produce direct current electricity [43].

There are a lot of materials that can be used as the semiconductor material, with each one having a unique conversion efficiency of sun energy to electrical energy. Each semiconductor material also utilizes a unique range of the solar spectrum. The main issue facing PV cell development is that the easily available and cheaper semiconductor materials tend to have lower conversion efficiencies. The previous development of PV cells has yielded efficiencies that range from 6 percent for amorphous silicon to greater than 30 percent for multiple-junction research lab cells [33]. Multiple-junction cells are essentially PV cells that utilize multiple semiconductors made with different materials so that more of the spectrum of energy is used in the conversion from solar power to electrical power. Silicon (amorphous, mono-crystalline, or poly-crystalline) is one of the most common materials that is being used in the production of PV cells today, and it has an approximate conversion efficiency of 6 – 21.5 percent. This means that if the sun was supplying 1000 W/m^2 of power to the PV cell, and the PV cell has a surface area of 1m^2 , that 60 – 215 W of useable electricity would be produced. Typically this electricity will need to be inverted to alternating current (AC) before it can be used in most electrical home appliances, this includes lights [39, 43].

A decision was made to use a particular brand of solar cells manufactured by Sun Power Corporation in the design of the PBR. This was due to the rated efficiency of the cells and the amount of information available about them. The “A-300 Solar Cell” is the chosen PV cell used in the design and it has the following characteristics:

- Dimensions: 125mm x 125mm with $270 \mu\text{m} \pm 40\mu\text{m}$ thickness
- Open Circuit Voltage: 0.670V
- Short Circuit Current: 5.9A
- Maximum Power Current: 5.54A
- Rated Power: 3.1W
- Efficiency: Up to 21.5%

These cells come combined in the “SPR-220” high efficiency PV module from Sun Power Corporation and has a peak power rating of 220W under the standard test conditions (AM 1.5) for PV cells. The efficiency of the module is 17.7 percent and this is due to losses occurred during the transmission of the electricity through the wiring of the module. To this end, the design of the electricity generation system used an efficiency of 15 percent to account for additional losses, which will be encountered during the transmission of the power to a central collection area [44].

In general, silicon based PV cells can utilize approximately 54 percent of the total energy coming from the sun, operating on the portion of the solar spectrum from 300 to 1200 nm, this represents the entire portion of the visible light and part of the infrared spectra, see Figure 14 below [39].

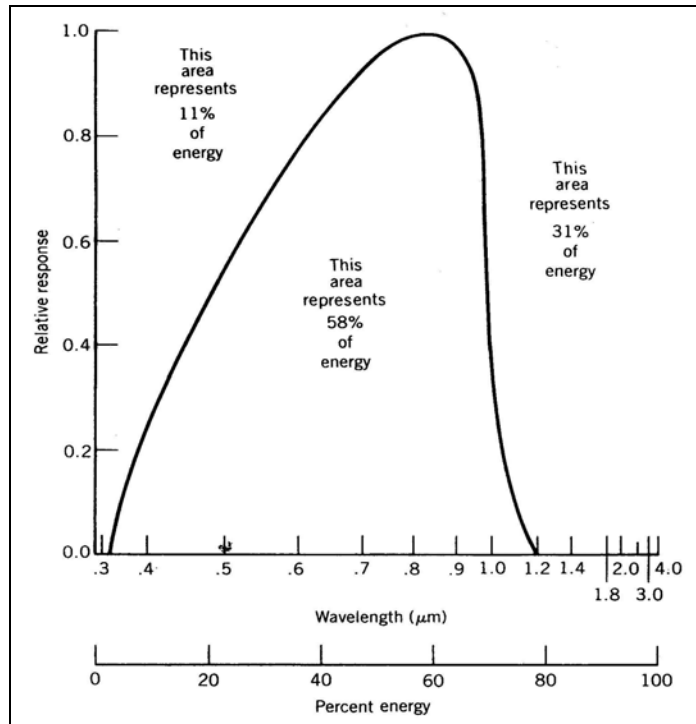


Figure 14

Schematic representing the operational spectra of a standard silicon based photovoltaic cell [39]

Thermal Electricity Generation

The second technology reviewed as a method for converting the infrared radiation to electricity was to use a heat exchanger in connection with a turbine to run a generator. This method works by using the heat energy contained in the infrared portion of the spectrum to vaporize a working fluid in a closed loop system. The working fluid, when vaporized, generates a rapid expansion in volume which, and in a closed loop, causes increase in pressure. The pressure generated is then used to run a turbine (or turbo expander), which is connected to a generator to produce alternating current (AC) electricity [39, 42]. The efficiency of this system is dependent upon the temperature that can be generated from the concentrated sunlight on the heat exchanger component. The following figure, Figure 15, provides an estimation of the conversion efficiency of concentrated solar energy to electrical output using a heat engine [39]. As illustrated, the optimal efficiency of the system will be around 30 percent plus or minus a few percent, for this design 30 percent was assumed. The design of the heliostats involves a 2-axis tracking system so that the vector of the reflected light energy can be controlled. This will allow for control over the amount of light energy and thus the temperature reached at the heat exchanger.

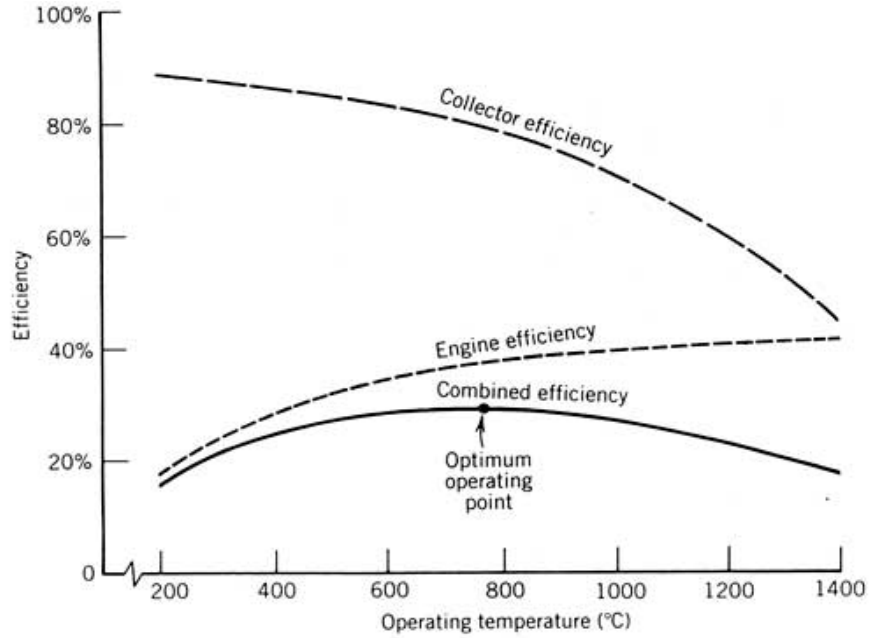


Figure 15
Combined collector and engine efficiency variation with operating temperature [39]

The most common power cycle used in solar power systems is the simple Rankine cycle with superheat, as seen in Figure 16 [39]. This cycle combines constant-pressure heat addition and rejection processes with adiabatic reversible compression and expansion processes. The system utilizes a working fluid that changes phase during the heat-transfer processes to provide essentially isothermal heat addition and rejection. Usually the working fluid is either water or an organic liquid, in this design propane was chosen as the working fluid due to a lower heat of vaporization than water.

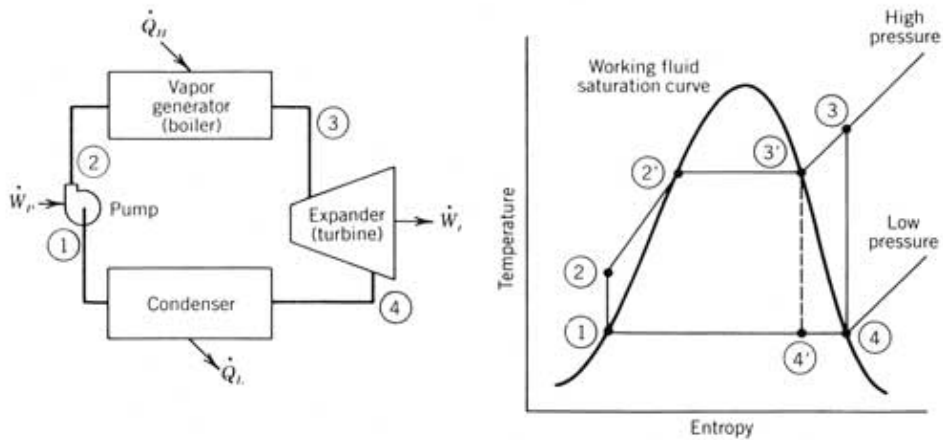


Figure 16
Simple Rankine Cycle with Superheat [39]

The cascading closed loop cycle (CCLC) operates on the same principles as the organic Rankine cycle, but involves a slightly more complex set-up. Rather than using one “boiler” (heat exchanger) it uses three heat exchangers that heat the working fluids to power two turbo expanders. This allows for a better thermal to electrical conversion efficiency. For an in depth discussion, see Part V.

3.3.4. Light Separation Equipment

Separation of the reflected light will be performed in the central towers using spectrally selective cold mirrors, or simply a cold mirror. A cold mirror is a specialized dielectric mirror that uses a dichromatic interference filter to separate wavelengths of light. To do this, a glass surface is coated with several layers of an optical coating that is chosen based upon the desired wavelengths that will be reflected or transmitted. The simplest optical coatings are thin layers of polished metals such as aluminum, silver, and gold. The reflection of the metal determines the characteristics of the mirror. Of the three, aluminum is the cheapest and most common but yields a reflectivity of around 88 – 92 percent of the visible wavelength range. Silver has a reflectivity of 95- 99 percent but reflects into the far infrared region of the spectra and is very costly to use. To this end, controlling the thickness and density of the metal coatings results in the ability to tune the reflectivity/transmissivity of the surface. This process results in what is known as a half-silvered mirror [45].

A more complex version is a dielectric optical coating that utilizes thin layers of materials such as magnesium fluoride and calcium fluoride. Again by adjusting the density and layering of these coatings it is possible to tune the optical substrate to provide the required transmission/reflection of the desired wavelengths. The reflection/transmission of light wavelengths operates on the principle of refractive index [45]. The following figure gives an illustration representing this process.

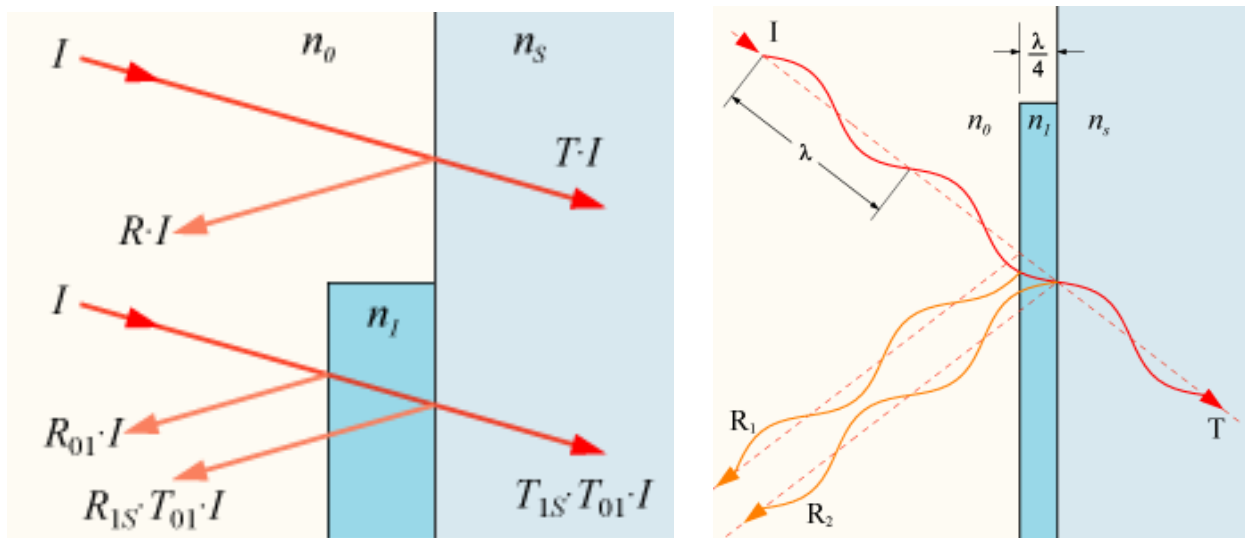


Figure 17

An illustration showing the separation of spectral wavelengths using an optical coating on a spectrally selective cold mirror. Here the blue bands (n_1) represent the optical coatings [45]

3.3.5. Discussion of Fiber Optics

Fiber optics are thin strands of either glass or plastic that are used to transmit light or signals. In this application the light in the visible wavelength range that is reflected by the cold mirror will be transmitted to the PBR using fiber optic lines. The fiber optics are grouped into a bundle and located along the inside of the tower columns with the upper end exposed to accept the concentrated light reflected from the cold mirror. The rest of the fiber optics are coated with a cladding material which keeps the light contained in the individual fiber optic line until it reaches the light plates inside the PBR. At this point the ends of fiber optics are exposed to allow the light to escape from the lines and be transmitted throughout the glass plates. Homogeneous distribution of the ends of the fiber optics within each light plate is necessary to ensure a near homogenous spread of the light across the surface of each light plate.

The fiber optics used in this design are made of borosilicate glass, which has an attenuation of 0.002% per inch (78.7% per km) in the visible light range [46]. The length of the transmission lines is estimated to be at most 150 m. Fresnel losses, or back reflection due to the difference between the refractive index of glass and air, result in an additional 4% loss per side exposed to the air (8% total). The combined losses estimated for the fiber optic transmission system are assumed to be 20%.

3.3.6. Design Summary using Photovoltaic Cells

The photovoltaic system was designed to capture the excess energy from the sunlight to supply light to the PBR so that operation could proceed 24 hours per day. The calculated input from the sunlight, in the form of visible light, was calculated to be 5.01×10^7 kWh/day. This value accounted for the losses occurred from the reflection of the sunlight to the central towers and the losses from the attenuation of the light during transmission through the fiber-optic lines. The assumed efficiency of reflection was taken as 95 percent of light collected by the heliostats would be reflected to the towers, and 80 percent of the visible portion of the light received at the towers would arrive at the PBR, assuming 20 percent loss in transmission through the fiber-optics.

The excess light required in the PBR would then be supplied using the PV system, which is composed of the PV cells mounted on the inside of the light collection towers, a DC/AC inverter, and an electricity transmission system to supply the generated electricity to the grid for "Storage". The decision was made to send the generated electricity to the grid as a storage mechanism because storage of the power in a battery would likely lead to an additional efficiency loss. There is also a potential to gain a "Green Energy" tax deduction depending on location, as the electricity supplied to the grid would be from renewable resources. This will require proper coordination with the utility company and acceptance by the governing commission. There is also the potential benefit of selling the electricity during peak hours when the cost of electricity is greater, and then buy it back at night when the cost per kilowatt-hour could be less, which could help to offset the initial capital cost for the system.

The sun's energy that is reflected to the central towers and not reflected by the spectrally selective cold mirrors will be absorbed by the PV system in the combined towers. The design also includes six towers that are present only for the generation of electricity (see Solar Collection section). The wavelengths of the light that will be absorbed by the PV cells in the combined towers are in the 700 -10,000 nm range. The "electricity generation only" towers will

be able to use the full spectrum of the sun's energy for production of electricity. As mentioned above (see Figure 14) the silicon based PV cells operate on the portion of the solar spectrum from 300 -1,200 nm and are capable of using 58 percent of the sun's energy; however, since 400 – 700 nm will be used for photosynthesis in the PBR this leaves 25 percent available for use in the PV system in the combined towers and the full 58% in the electricity generation towers. The PV cells will generate DC electricity that must be converted to AC before sending to the grid. An assumed efficiency loss of 10% is associated to this conversion from DC to AC electricity. The following figure provides an energy balance for the PV system. The equations and process used to determine the energy balance and subsequently the reflective surface area required of the heliostats is included as Appendix C.

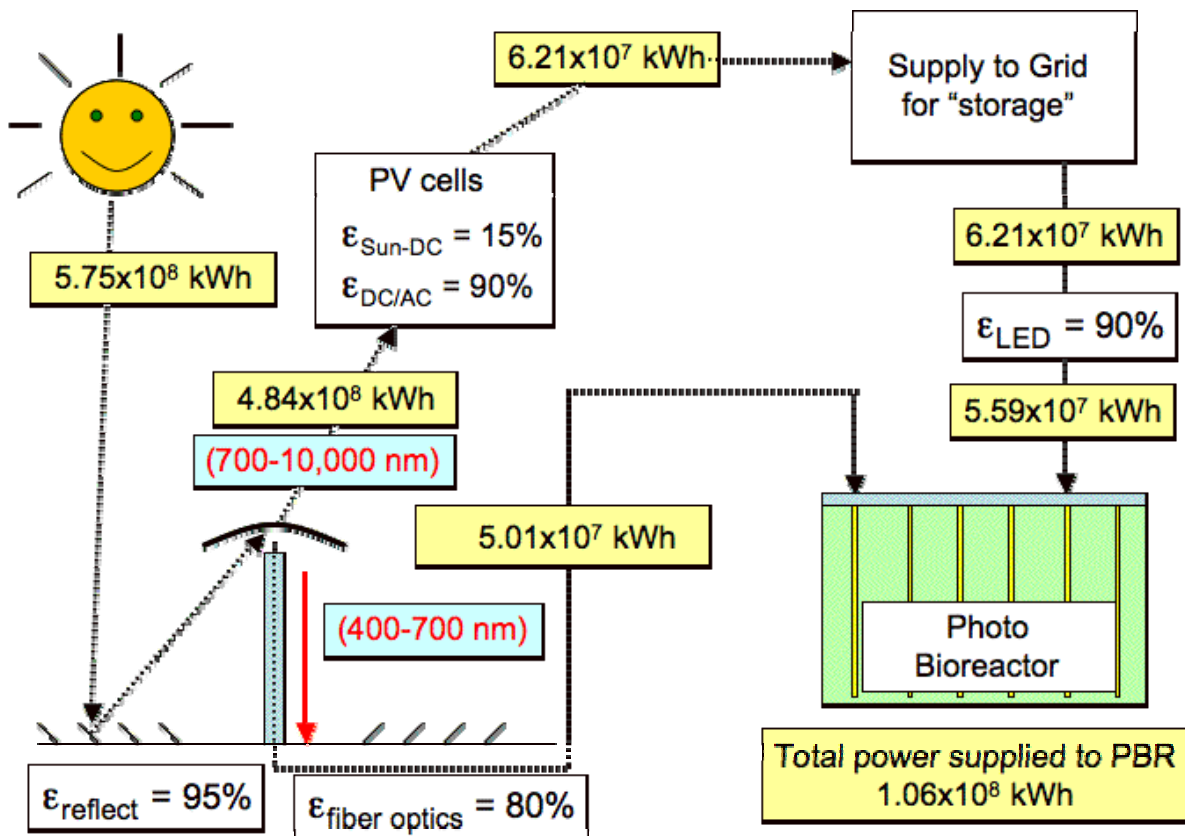


Figure 18

Average daily energy balance for the photosynthetic bioreactor using a photovoltaic system to supply the additional required energy.

3.3.7. Design Summary using Thermal Energy

The design of the thermal energy system is very similar to the PV energy system described above. The main difference is the replacement of the PV system with a cascading closed loop cycle (CCLC) for production of the required electricity. A description of the CCLC operation is described in the Thermal Electricity Generation section above. The assumed thermal energy to electrical energy efficiency of the system is estimated to be about 30%, which when compared to the 13.5% of the PV system (15% Sun to DC, 90% DC to AC = 13.5% net) allows for a sizeable reduction in the required surface area of the collector field, which results in a large decrease in capital costs. The size of the collector field for the PV system is approximately 68 km^2 while

CCLC system will require a solar collector field of 37 km², this represents a 54% decrease in the amount of area needed to produce the same amount of electricity.

The following figure, Figure 19, provides an energy balance summary for the system. The equations and process used to determine the energy balance and subsequently the reflective surface area required of the heliostats is included as Appendix C.

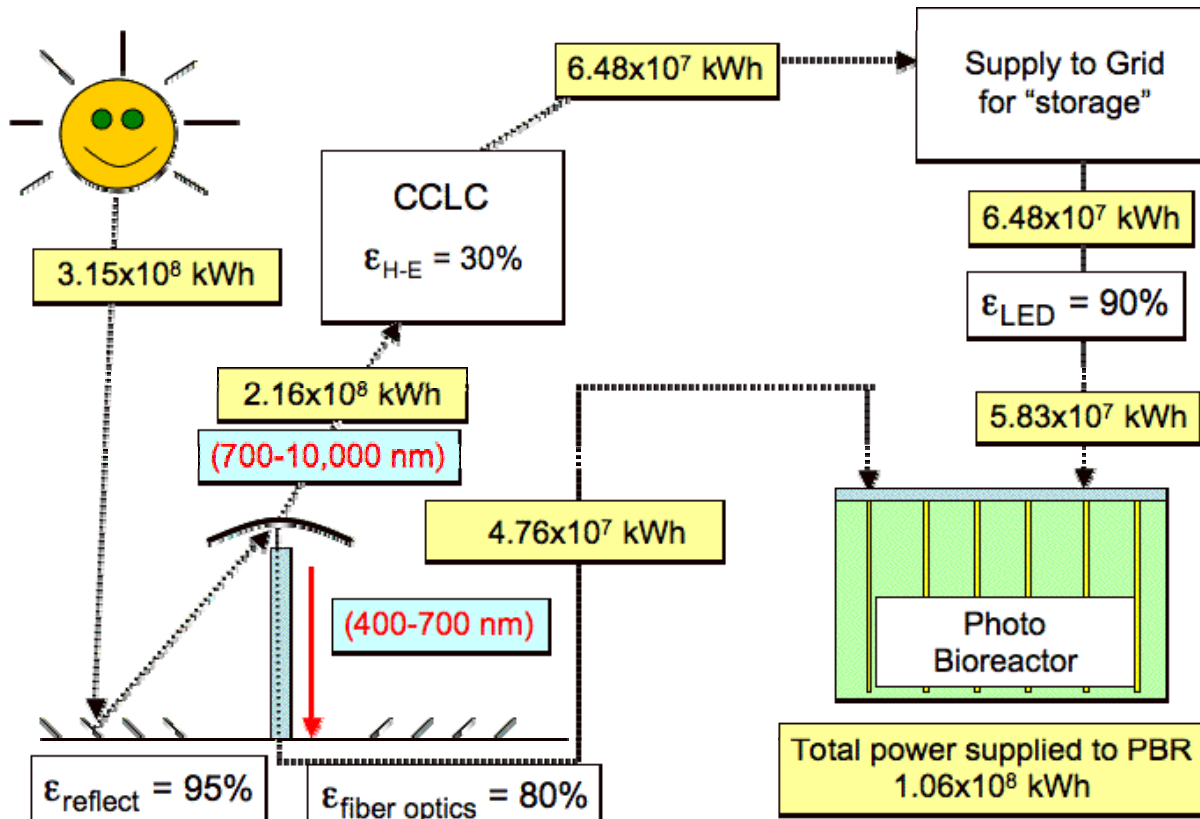


Figure 19

Average daily energy balance for the photosynthetic bioreactor using a simple Rankine cycle system to supply the additional required energy.

3.4. LIGHT COLLECTION

The function of the solar collector is to concentrate collected solar light and reflect it onto a receiver for transmission into the bioreactor and/or to generate electricity from the light. The light collection system can be described in terms of: the light wavelength that can be used by each part of the system, the types of collectors and modules for light collection, the orientation of solar collector dish, and the solar collector's efficiency. Designing considerations include optimizing the performance and cost of sunlight trackers, dish concentrators, IR cold mirrors and optical fibers.

There are several light collector types and they function in different ways and yield different collection efficiency. Several light collectors were considered for this project and are summarized hereafter. However, the heliostat/light collection tower was selected for the final design. It is important to consider that the collected light needs to be treated so that the visible light is transmitted into the PBR and the Infrared (IR) is transferred to the solar-electric

generation equipment. The light transferred to the solar-electric generation equipment, can be used to supply electric power for lighting the PBR during periods of darkness. The solar-electric generation equipment could consist of photo-voltaic (PV) cells and/or a cascading closed loop cycle (CCLC).

3.4.1. Light/Energy Requirements

Though solar energy is abundant and free, it must consist of the right level of intensity and wavelength for engineered applications such as this. This design requires collected light in the range of 400-700nm for the bioreactor and 700-11,00nm to be transmitted to the PV and/or CCLC. Because the spectrum from 400-11,00nm is utilized by the system, the collector should be optimized to receive light on those wavelengths as efficiently as possible. As stated earlier, the sunlight intensity in the southwest is approximately 8.5 kWh/m²/day. This design requires a total energy of 1.06 X 10⁸ Kwh per day in the visible spectra.

3.4.2. Types of Collectors

Growth in solar technology has lead to the production of various types of solar collectors. These solar collectors differ in shapes, orientation, operational technology, process applicability, as well as efficiencies. A solar collector/concentrator is a device for extracting or collecting the energy from the sun in a concentrated form. Solar collectors can be classified as passive, one-axis active, or two-axis active tracking collectors [47]. Examples of the one axis active tracking collectors are the parabolic trough and linear focus Fresnel reflectors. Examples of two axis active tracking collectors include parabolic dish collectors and the central tower/heliostat receivers. Active tracking systestms are capable of tracking the position of the sun at any point in time with the aid of digital computer control. Four active collectors were considered for this design and are discussed hereafter.

3.4.3. Parabolic Trough Collector

Like the name implies, these collectors have a parabolic shape that is extended in one axis and have the ability to collect light ray along a single line focus. It is a principle of geometry that a parabolic reflector pointed at the sun will reflect parallel rays of light to the focal point of the parabola. The geometry of the parabolic trough creates a focal line. A fiber optic transmission or light absorption/heat transmission system is placed along the focal line. Figure 20 is a schematic of a parabolic trough collector/concentrator. A trough system is able to track the sun by rotating the parabolic shape about an axis parallel to the focal line. It is also important that the trough be as reflective as possible. The reflectors on the parabolic trough are generally coated with aluminum or silver. Silver has the higher reflectance, but is much more expensive. It is also important to keep the reflectors clean since dirt will degrade the reflectance of light from the parabola. Due to the geometry of the design, gaps must be left between the collectors which results in low ground coverage (40-60%) [42, 47].

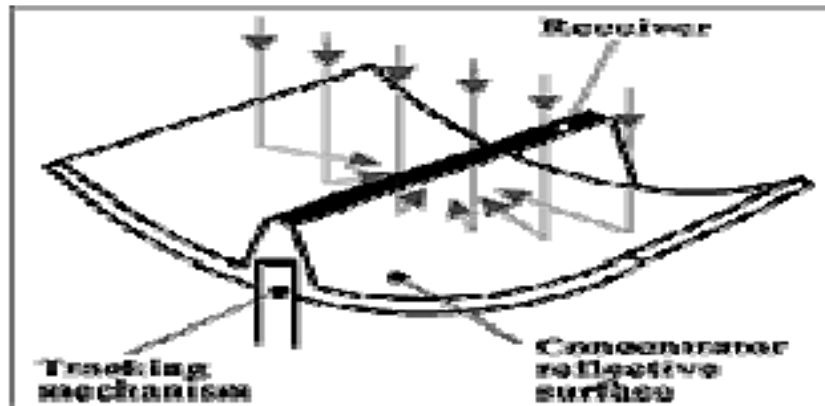


Figure 20
Parabolic Trough Collector [39]

The construction cost of a parabolic trough and its low ground coverage has been a major problem with this type of collector. For large systems the collector assembly represents the major cost. If a solar heating system is desired, these systems are capable of achieving 250-300°C [48].

3.5. LINEAR FRESNEL COLLECTOR

The linear Fresnel collector is a single axis tracking technology. This system consists of long, flat plates that are arranged so that each reflects onto a single line positioned in space above the field. At the common reflection point, there is a light transmitter or heat absorber. This is pictured in Figure 21. Tracking is achieved by rotating of each linear reflector on an axis that is parallel to the common reflection line as the sun moves throughout the day. This was a concept that was developed by Giovanni Francia in the 1960s [49].

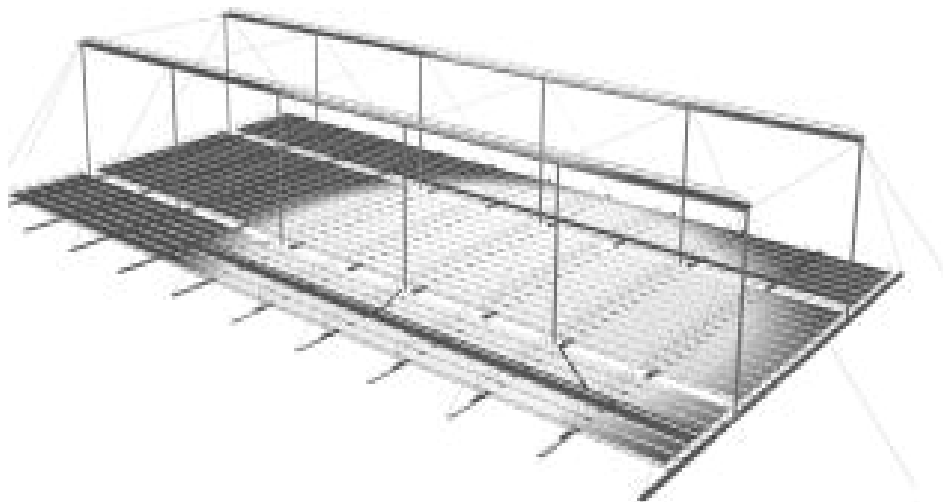


Figure 21
Linear Fresnel Reflector [50]

High densities can be attained by allowing the reflectors to change their focal point from one receiver to another during the day in order to minimize shading and achieve a dense reflector field. This arrangement is called the compact linear Fresnel reflector systems, or CLFR systems.

The reflectors are slightly curve and have a long focal length. Their mirror surfaces is made out of glass with a high reflecting performance of about 0.95. If thermal-solar generation is important, this system can achieve 250 C, which is low in comparison to 2 axis collectors that will be discussed later [47].

The operation and management cost of a linear Fresnel reflector is low because cleaning can be done manually at ground level without complication. The reflector is less costly than parabolic trough collectors. Ground coverage with this method is better than with parabolic trough.

3.6. PARABOLIC MINI DISH

This light collector can be described as a parabolic dish that is designed to collect and transmit light along a single fiber optic line. The design is based around the fiber optic cable. The size of the dish is chosen according to the amount of light is optimal for a fiber optic line and the focal point of the dish is the fiber optic endpoint as seen in Figure 22. Several mini dishes can be arranged to fit on a flat plate which can be fitted with a two-axis tracking system. The light can be transmitted along the individual fiber optic lines to any place of interest.

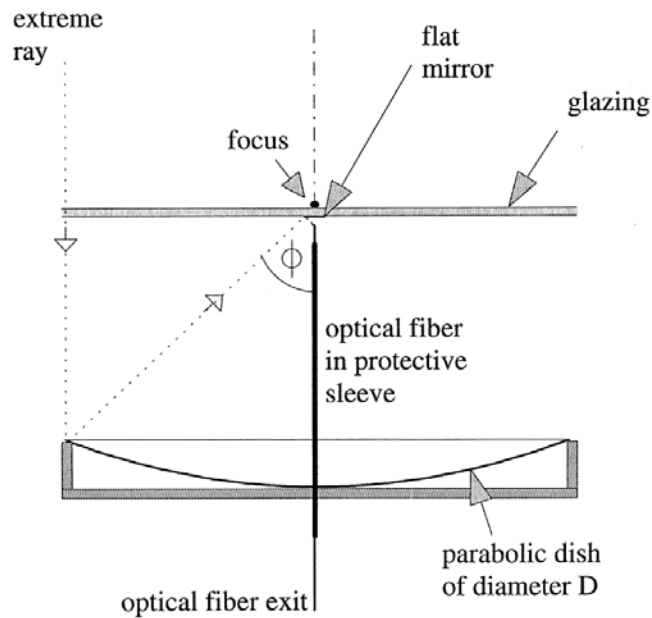


Figure 22
Schematic of a Parabolic Mini Dish [51]

For design and optimization strategies see Feurmann *et al.* [49, 51].

3.7. HELIOSTATS

3.7.1. CONCEPT OF THE MTSA

Heliostats are flat plate sun tracking mirrors designed to reflect the sun to a central tower. A new design called the mutlti towered solar array (MTSA) has emerged that has very high concentrating power, collection efficiency, and ground coverage. It will be shown that a heliostat field of an MTSA can utilize the direct solar radiation falling on the ground area of the field with a higher efficiency than the maximum efficiency of a single tower system [52].

The MTSA field differs from a conventional solar tower system which has only one tower with as the central receiver but rather a group of solar towers with closely packed neighboring heliostats. The advantage is that the MTSA can use solar radiation which would normally fall on the ground between widely spaced heliostats further away from the tower of a conventional type solar tower system. Therefore, greater ground coverage can be achieved [52]. The position of the MTSA forms a repetitive two dimensional regular pattern called bravais lattice. This lattice can then be repeated in space to cover the ground. Figure 23 bellow illustrates a field of a MTSA and the bravais lattice.

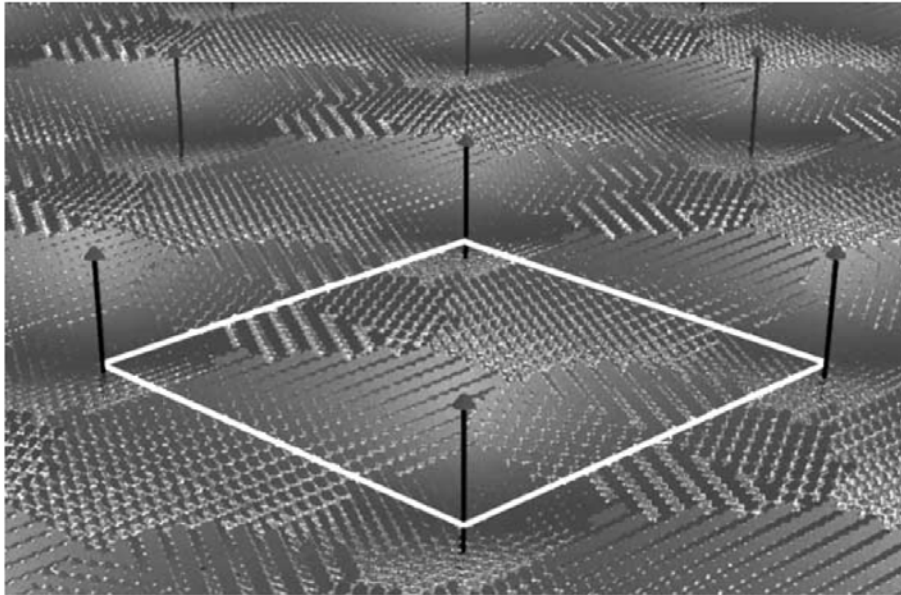


Figure 23
MTSA and Bravais Lattice [52]

3.7.2. Heliostat Design

In heliostat design it is important to ensure that the reflectors will not interfere with each other as they move through space on their axis. The concept of unimpeded space volume is important when considering the chosen shape for the heliostat. The unimpeded space volume represents the real space that could be occupied by the heliostat as it moves through space. As long as nothing enters this volume, the motion of the heliostat will not be impeded and no collision is possible. Figure 24 shows a conventional rectangular heliostat with two axis rotation. The unimpeded space is determined by rotating the heliostat about one axis and then the other and taking the confluence of the path volume as shown in Figure 25. The rectangular heliostat is first rotated about the vertical axis in Figure 25 (a) to form a cylindrical volume. The cylindrical volume is then rotated about the second axis to form a barrel shape in (b). The volume seen in Figure 25 (b) is the unimpeded space volume for the conventional rectangular heliostat. This volume defines the packing structure for the heliostat field shown in

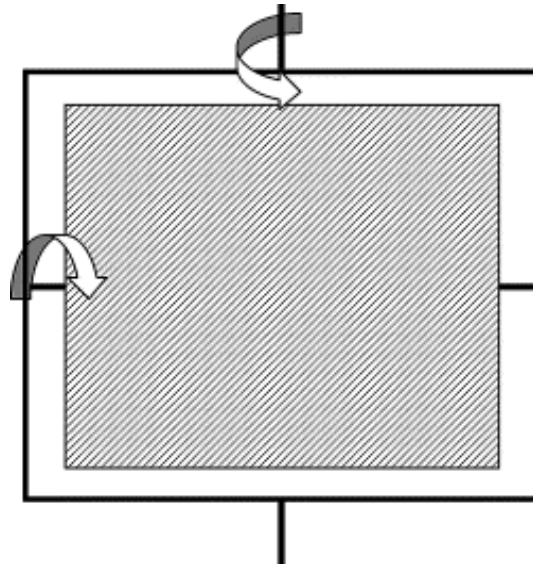


Figure 24
Conventional Heliostats [52]

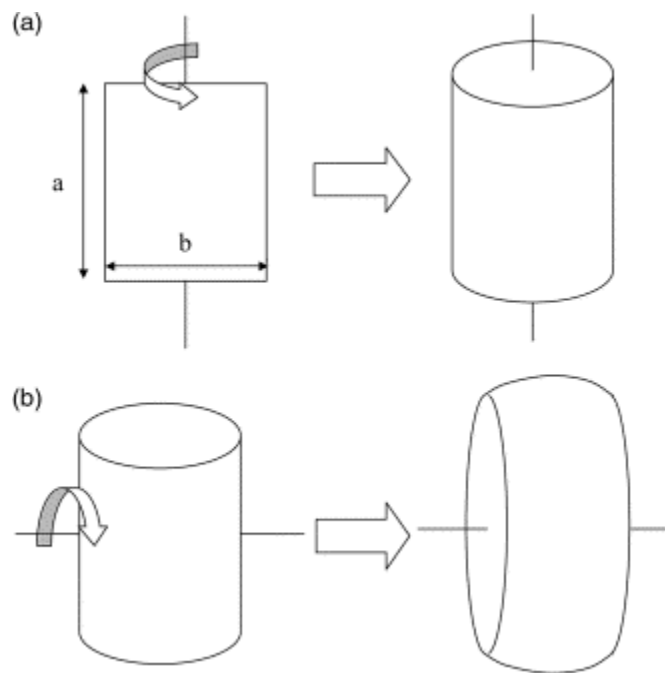


Figure 25
Unimpeded Space Volume for Conventional Heliostats [52]

The orientation of the barrel in Figure 25 (b) depends on how the heliostats are attached to the base. If the first rotational axis to the base is vertical (perpendicular to the ground), the axis of the barrel will be vertical and vice versa [52]. It is most advantageous to have the first axis be horizontal because the packing of heliostats will be tighter. The packing for a field with horizontal axis is defined by packing the unimpeded space volume next to each other is shown in Figure 26. The arrangement in Figure 26 is the tightest arrangement that can be achieved with conventional rectangular heliostats and only covers 76% of the ground.

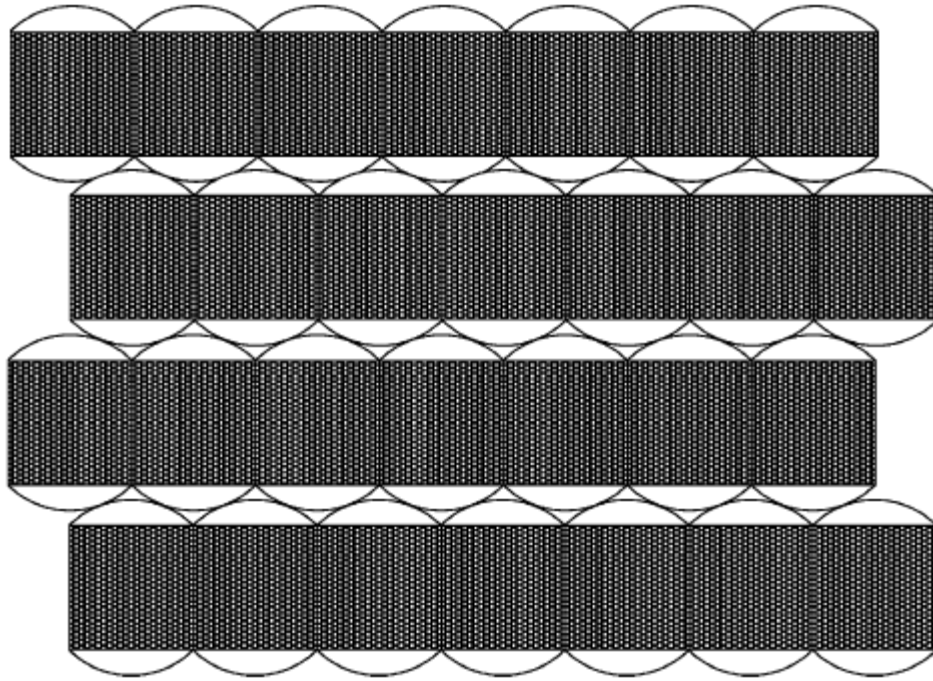


Figure 26
Ground Coverage with Horizontal Primary Axis (76%) [52]

The reason that so much space is wasted in this arrangement is because of the rounded shape of the barrel defined by the rectangular shape of the conventional heliostat. However, other shapes exist, such as a hexagon, and can yield much better packing. Figure 27 shows the unimpeded space of the rectangular and triangular portions of the heliostat. The sum of the two volumes looks like Figure 27 (a)

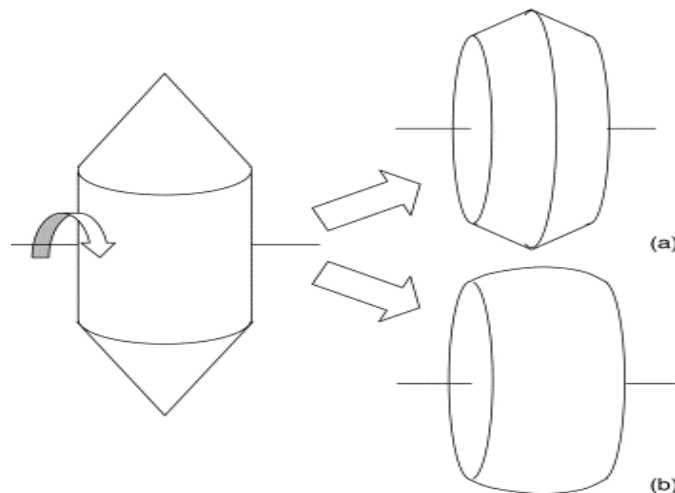


Figure 27
Unimpeded Space Volume of Hexagonal Heliostats [52]

Because of the linear sides of the pointed barrel, the heliostats can fit together with up to 100% ground coverage as seen in Figure 28.

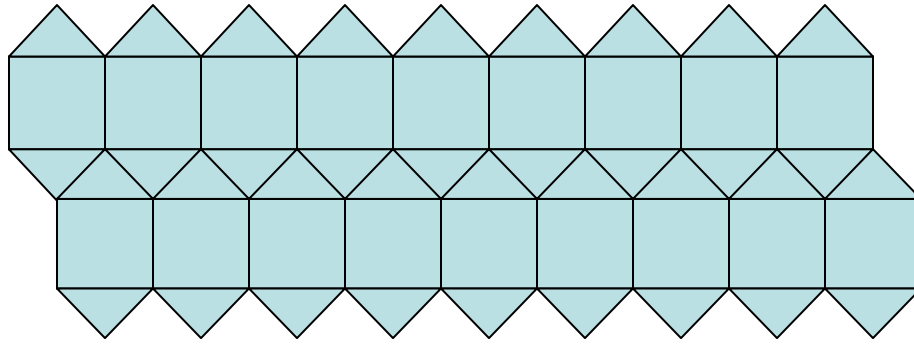


Figure 28
An orientation of a 100% ground coverage heliostats

A simple geometric relationship exists to describe the geometry that will result in a heliostat shape that will yield 100% ground coverage. Take any rectangular shape and circumscribe a circle around it. Take the tangents to the circle at the vertices of the rectangle and let them form the triangular top and bottom of the hexagon. This results in the smallest heliostat that will give 100% coverage. Figure 29 shows this relationship.

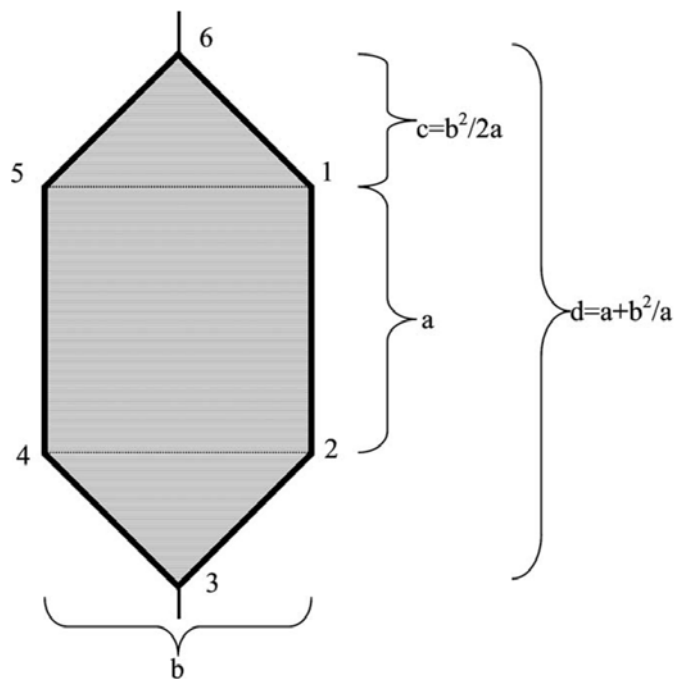


Figure 29
Proportions of a Heliostat that will Achieve 100% Ground Coverage [52]

An infinite combination of heliostat proportions is possible and shown in Figure 30. Any combination of ratios above the line will result in a hexagon that will give 100% ground coverage [52].

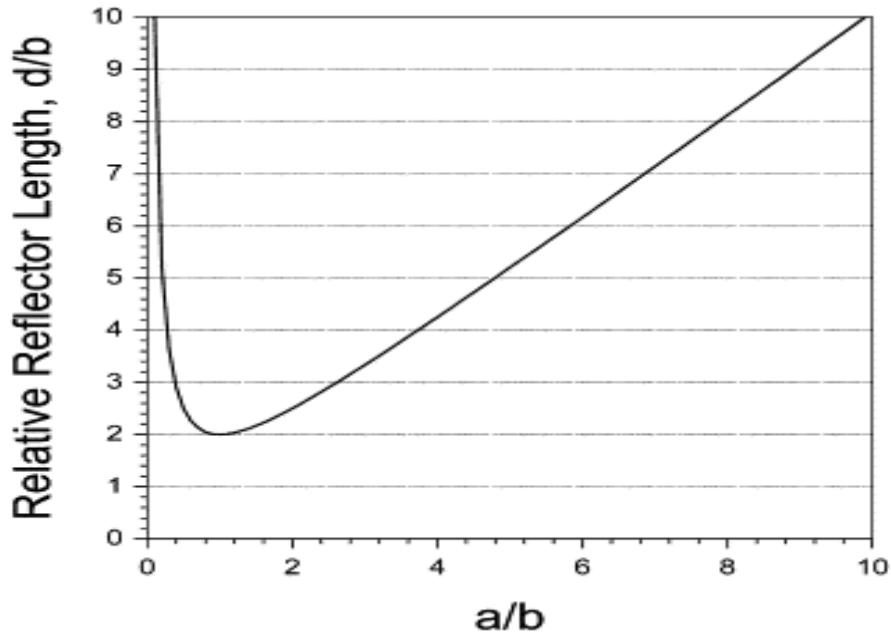


Figure 30

The length d relative to the width b of hexagonal heliostats [52]

3.8. LAND REQUIREMENTS

The land area required for a solar collector is dependent on location and the type of supplementary electrical generation. The size of the collector field is inversely proportional to the light intensity and the efficiency of the solar-electric generation equipment. This can be seen in Table 1 where the land requirement is the highest for the lowest solar intensity (Alberta) and the less efficient electrical generation system (PV) and vice versa. Table 1 summarizes the design requirements for four cases for the PBR system. The table summarizes the total heliostat area, number of heliostats and costs given the upper and lower bound projected costs.

Table 1
Area requirement for heliostats field and cost estimate for different region

Location	Alberta		South West	
Electric Generation	PV	CCLC	PV	CCLC
Heliostat Area	164 km ²	90 km ²	68 km ²	37 km ²
# of Heliostats	1.1 x 10 ⁶	6.1 x 10 ⁵	4.6 x 10 ⁵	2.5 x 10 ⁵
@ \$70/m ²	\$11.5 billion	\$6.30 billion	\$4.76 billion	\$2.59 billion
@ \$106/m ²	\$17.4 billion	\$9.54 billion	\$7.21 billion	\$3.92 billion

3.8.1. Design Summary

The design is a collector field of a MTSA of extremely closely spaced heliostats with mirror, made of ultra thin glass of about 3-4mm thickness. The glass is a di-electric silver coated mirror. It has a drive-azimuth, drive elevation, structural steel pedestal, and a digital computer control to rotate the reflectors so that the sun reflects to the tower. Also, the field is designed with multi

towers such that 9 of the towers (shown in black spots) collect light and send into the bioreactor while the other six towers (orange spots) are for the collection of sunlight to be used during peak hours/when the bioreactors are saturated with light.

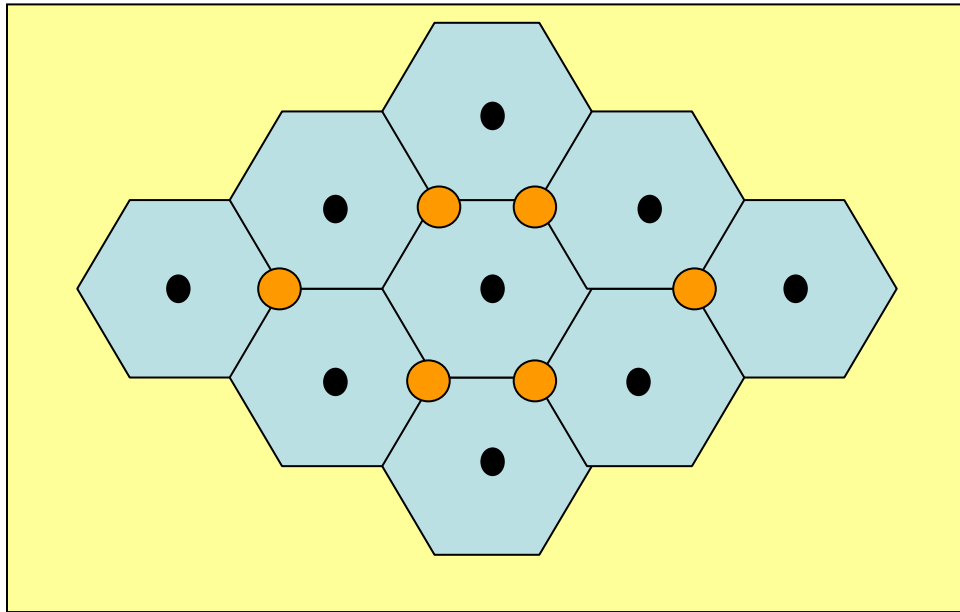


Figure 31
Plan view of the collector field showing the field cells

3.9. COST AND FEASIBILITY STUDY – PBR SYSTEM

3.9.1. Current and Future Market Conditions

The focus of the investigation was to develop a conceptual design for the sequestration of CO₂ through biological fixation. Much of the feasibility of this type of design will depend on the current and future price and market for microalgae biomass. The process investigated will produce roughly 1.3 million tons dry weight of biomass annually. The market for biomass was approximately 5 kt/year in 2004 [53]. However, the microalgae biomass market has been growing by 20-30% annually and shows no signs of slowing down as can be seen in Figure 32. At this rate, the biomass market could be large enough to support a few such plants in 25 years.

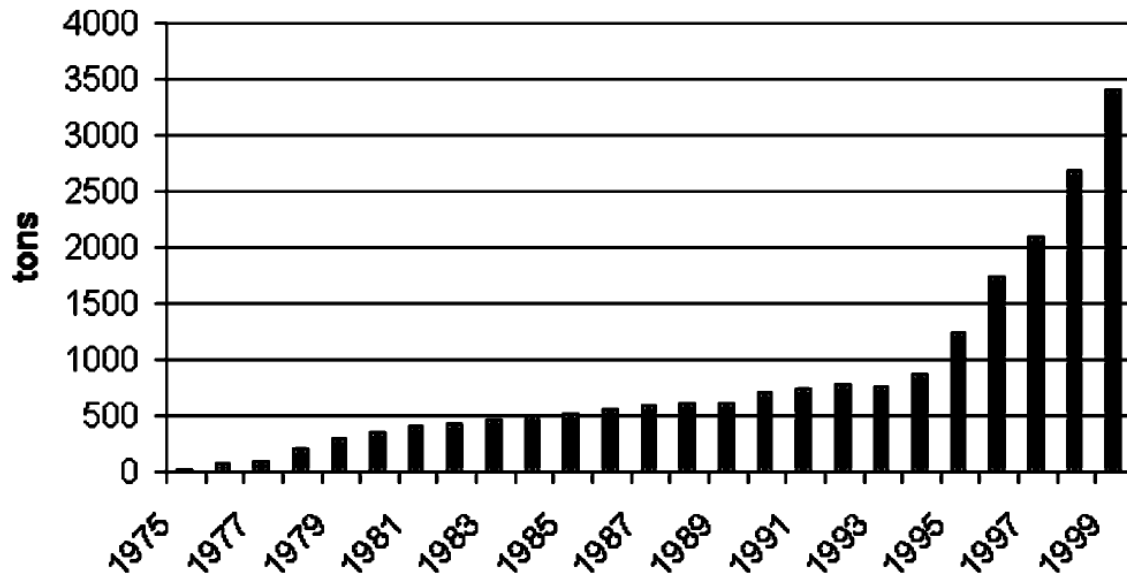


Figure 32
World Production of Spirulina biomass between 1975 and 1999 [53]

The microalgal biomass market is growing at unprecedented rates because it has been discovered that many substances within microalgae such as *Spirulina* and *Chlorella* have very positive health impacts for both humans and animals [53]. It has been estimated that microalgae in the form of processed and unprocessed foods as well as health supplements could consist of as much as 20% of the human food market within the next few years [53]. Of the significant health benefits, the autoimmune strengthening has been the largest consideration [53]. There are also very significant markets developing in animal and fish feed within farming applications because the microalgae represent a safe protein supplement [53]. It is likely that this market will see significant growth as many countries outlaw the use of animal meals in feed stocks. The proteins in microalgae have been shown to be acceptable substitutes for animal meals and have shown to have the same autoimmune benefits for livestock [53]. The fears of diseases such as avian flu, bovine and ovine encephalitis, and mad cow disease will likely further the market as the diseases can be transmitted from one animal to another in the use of processed animal meals.

The biomass market will have to drive the need for such a plant because photosynthesis is not efficient enough to be competitive with other light to electrical technologies such as photovoltaic cells and solar-thermo technology. Currently, photosynthesis can only make use of 10% of total solar irradiance. If the biomass is then burned in a power plant to produce electricity at 30% to 40% efficiency, the net solar utilization would be between 3% and 4%. This is much lower than competing and existing solar to electrical technologies. The high capital cost for generating biomass is not justified if the intention is to use the biomass for fuel to generate electricity

That said the biomass production costs for this type of system are significantly lower than existing technologies. Current technologies can produce biomass between \$50/kg and \$150/kg (\$45,000 and \$136,000/ton) [53]. As seen in the discussion to follow, the biomass production costs could be as low as \$4,371/ton. This represents a huge financial opportunity.

Because most of the costs involved scale directly with surface area (the size of the collector and the illumination plate area), the design could be fully modular and adjusted by parallel processing methods to any scale. Furthermore, the production costs from the current study would not be expected to rise significantly until the scale was reduced to at least 1/36 of the proposed size. This is due to the maximum practical volume of the bioreactors which is around 30,000m³. The current design calls for 36 such reactors operating in parallel. A 1/36th scale represents a CO₂ sequestration rate of 62 kt/year, and a biomass production rate of 36 kt/year. Certainly, the production cost will be higher for lower scales because the size and cost of supporting equipment scales inversely with production volume. However, there is a great deal of room for production costs to rise at current market prices. It would be reasonable to expect that 1/10th of the current market (0.5 kt biomass/year) could be supplied by the proposed method for a cost that is far less than \$45,000/ton algal biomass. Thus this design is feasible under current market conditions and could be a significant technology for CO₂ sequestration as the market expands.

3.9.2. Sequestration Using PBR and PV

The fixed capital investment for CO₂ Sequestration using the PBR system and PV generation have been estimated to be close to \$35.2 billion installed (See Appendix D for full capital estimation calculations). The break even biomass sale price would be \$8,375/ton. This is based on a \$35.2 billion fixed capital investment, a \$100 million land cost, a 42% taxation rate, a 6.50% interest rate, a salvage value of \$3.5 billion, a utility cost of \$100,000/year, an operating labor expense of \$900,000/year, a biomass production rate of 147.6 ton/h, a carbon dioxide credit of \$5/ton at 267 ton/hr, a nutrient rich water cost of \$0.99/ton at 60 ton/hr, a 20 year plant life, a 3 year construction period, and 10 year MARCS discounted depreciation rate.

Under the same conditions, a biomass selling price of \$12,680/ton would yield a return on investment (ROI) of 15%. This price would yield a net present value of approximately \$29.4 billion and a pay back period of 6.2 years. Figure 33 illustrates the cash flow analysis for this condition.

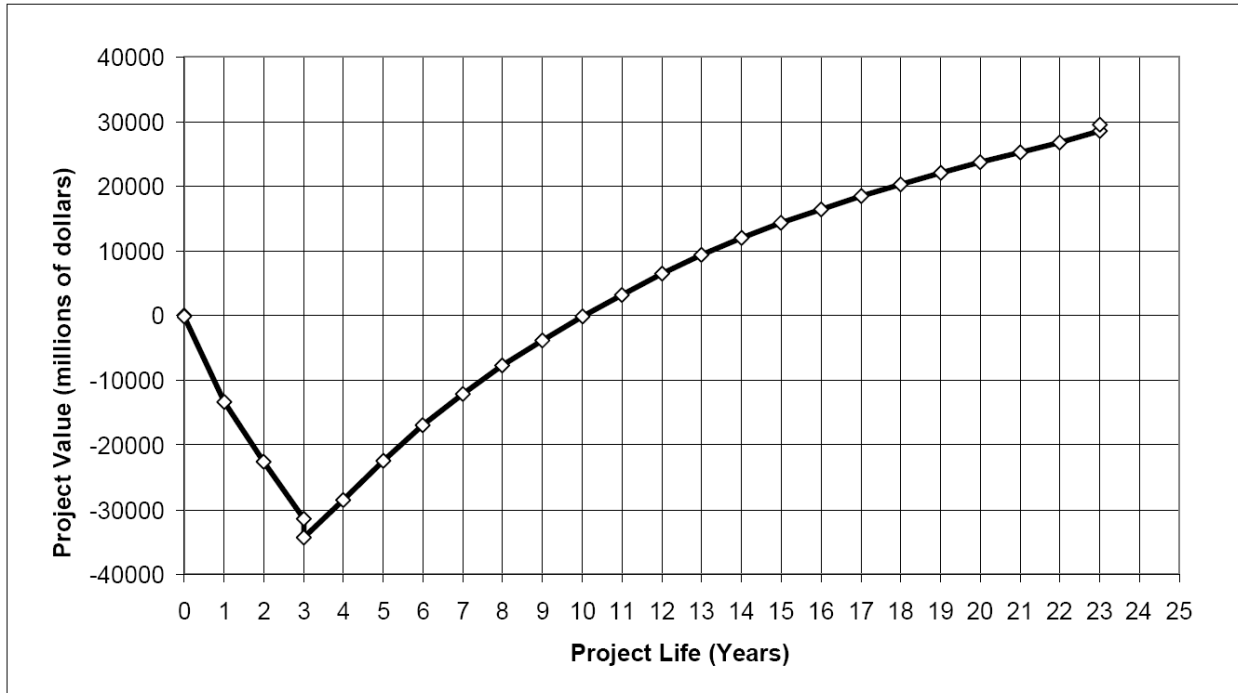


Figure 33
Cash Flow Diagram for 15% Discounted ROI for PBR with PV

3.9.3. Sequestration using PBR and CCLC

The fixed capital investment for CO₂ Sequestration using the PBR system and CCLC generation have been estimated to be close to \$18.4 billion installed (See Appendix D for full capital estimation calculations). The break even biomass sale price would be \$4,371/ton. This is based on a \$18.4 billion fixed capital investment, a \$100 million land cost, a 42% taxation rate, a 6.50% interest rate, a salvage value of \$3.5 billion, a utility cost of \$100,000/year, an operating labor expense of \$900,000/year, a biomass production rate of 147.6 ton/h, a carbon dioxide credit of \$5/ton at 267 ton/hr, a nutrient rich water cost of \$0.99/ton at 60 ton/hr, a 20 year plant life, a 3 year construction period, and 10 year MARCS discounted depreciation rate.

Under the same conditions, a biomass selling price of \$6,627/ton would yield a return on investment of 15%. This price would yield a net present value of approximately \$15.4 billion and a pay back period of 6.2 years.

4. RECOMMENDED SEQUESTRATION SYSTEM AND DESIGN

Even though the PBR system has been shown to be viable and potentially profitable under current market conditions, the market for algal biomass is not currently large enough to support a significant sequestration effort. It is because of this and the sequestration scale of the project that the final design recommendation shall consist of deep saline injection only until such point that the market conditions can support a larger scale PBR system.

5. PART IV: DEEP SALINE AQUIFER INJECTION

5.1. TEST CASE: VIKING AQUIFER

The Alberta Basin in western Canada is a typical mature continental sedimentary basin with excellent hydrocarbon potential and large oil and gas fields that is a major North American energy producer. Overall, more than 320,000 wells have been drilled in the basin to date, distributed over most of the basin area, which covers more than 900,000 km² [54]. Extensive records surrounding drilling explorations represent an unparalleled opportunity for basin scale characterization, and the Alberta Geological Survey maintains a large databank of in situ characteristics. As such, the basin represents an excellent test case to examine CO₂ storage potential. The primarily brine saturated Viking formation within the Alberta Basin will serve as an example for the brine injection design presented below.

The Viking Formation represents a wedge-shaped interval that was deposited mostly as coarse clastics (sands) in a marine environment during Early Cretaceous. The formation is deepest along its western boundary, where it is more than 3,000 m in depth, and slopes upward toward the northeast, eventually cropping out along its northeastern boundary (Figure 34). The Viking Formation consists mostly of sandstones, except for the northwestern part where shales dominate. The sandstones of the Viking Formation are saturated with saline water, forming an aquifer [54, 55]. The stratigraphy of Alberta basin is shown in Figure 35.

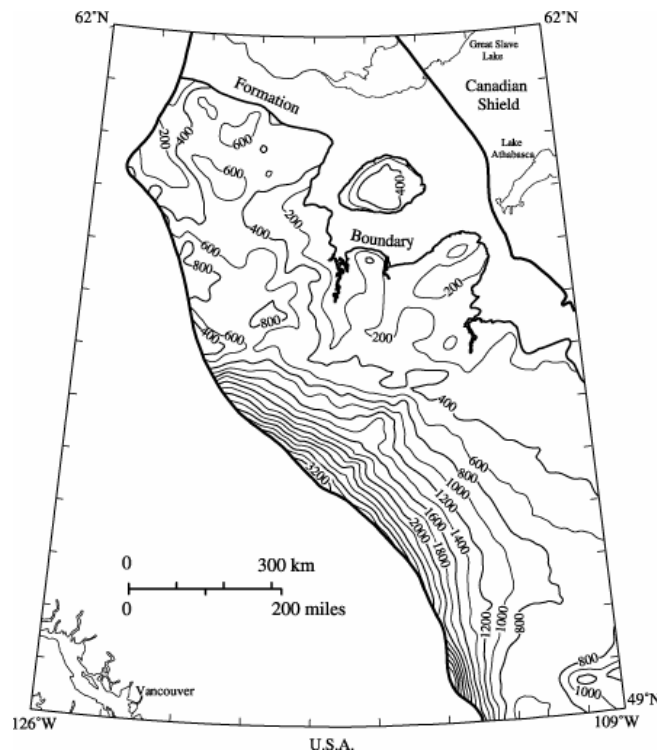


Figure 34

Depth isolines for the Viking formation. Depth (m) is to top of formation. Image modified from Bachu *et al.* [56] and Alberta Geological Survey

To date, more than 200,000 wells have been drilled through the Viking Formation. Therefore, while the Viking aquifer has good capacity for CO₂ storage, is mature and tectonically stable

[56], and is accessible from most locations in the basin, it also has potential for CO₂ leakage along the many wells that have been drilled into or through the formation. The wells are distributed over most of the 468,000 km² area, giving an overall average well density of 1 well every 2 km². Over half of all wells that penetrate the Viking aquifer are classified as abandoned wells [54]. This concern will be addressed in detail below.

5.2. TRAPPING MECHANISMS AND SEQUESTRATION CAPACITY

Upon injection into saline aquifers, CO₂ may be stored by one or more of three processes, hydrodynamic trapping, solubility trapping, or mineral trapping [7]. The most critical concern of hydrodynamic trapping is the potential for CO₂ leakage through imperfect confinement. Solubility trapping is not subject to buoyancy and is therefore less likely to leak. In mineral trapping, CO₂ is stored for very long periods by conversion into carbonate. Solubility and mineral trapping are the most important long term solutions to CO₂ sequestration in geologic media [29], while hydrodynamic trapping represents the crucial short term step in the trapping process, as CO₂ must remain hydrodynamically trapped for sufficient time to allow the other processes to take hold.

Era	Period	Group	Formation	Dominant Lithology	Maximum Thickness (meters)	Hydrostratigraphy
Cenozoic	Tertiary		Paskapoo	Sandstone	500	Aquifer
			Coalspur Brazeau	Interbedded sandstone, siltstone, and coal	1400	
Mesozoic	Cretaceous	Colorado	Wapla First White Specks	Shale	400	Aquitard
			Cardium	Sandstone	<100	Aquifer
		Colorado	Second White Specks Belle Fourche Fish Scales Westgate	Shale	400	Aquitard
			Viking	Sandstone	<100	Aquifer

Figure 35
Alberta Basin Stratigraphy [57]

5.2.1. Hydrodynamic Trapping

Crucial to all mechanisms of CO₂ capture in a reservoir system is the ability of the reservoir to maintain the injected volume of CO₂ for a sufficient residence time for other mechanisms to succeed (hydrodynamic trapping). Hydrodynamic trapping may occur via the existence of a slow transport gradient over a long distance or via structural traps which may serve to corral the CO₂ and prevent migration. In either case, caprock integrity is of primary interest to prevent leakage over an extended period of time. Accurate prediction of the hydrodynamic behavior of CO₂ is a complex venture into many critical parameters, and numerical modeling is often required. A detailed numerical modeling analysis has been conducted for this purpose, and is presented later in this report.

5.2.2. Solubility Trapping

Additional confidence in storage integrity is achieved by the eventual diffusion of CO₂ into the aqueous system, or solubility trapping. Solubility determination of CO₂ in a solvent may be accomplished via the combination of an equation of state (EOS) module, for phase distribution and fugacity determination, and a solubility model, such as the Krichevsky-Kasarnovsky (KK) equation [58]. A determination such as this applies only to CO₂ solubility in pure water, and thus must be corrected for ionic behavior intrinsic to a brine system. Such a relation, valid from 298-533K and 5-85MPa, was empirically provided by Enick and Klara [58],

$$X_b^{CO_2} = X_p^{CO_2} (1.0 - 4.893414 \times 10^{-2} S + 0.1302838 \times 10^{-2} S^2 + 0.1871199 \times 10^{-4} S^3) \quad (10)$$

for salinity, S, in mass fraction, and where the subscripts below the aqueous mole fraction of CO₂, X^{CO_2} , refer to brine and pure water. Additional correction must also be utilized for brine density under high temperature and pressure, and density alteration of brine due to CO₂ diffusion into the system. The entire sequence of determinations needed to calculate CO₂ solubility by the above mechanism is provided in Appendix E. This sequence was utilized to produce (Figure 36), where calculated CO₂ solubility in pure water, by use of the Peng-Robinson (PR) EOS (see Appendix E) and the KK equation, is compared to experimental values from Spycher *et al.* [59]. With closely matching values, the procedure is thus verified and may be extended empirically to the case of saline water via Eq. (10). The results are presented in Figure 36, and illustrate strong dependence of CO₂ solubility on state parameters and salinity, and, therefore, the need for such considerations to accurately predict CO₂ tendency under reservoir conditions.

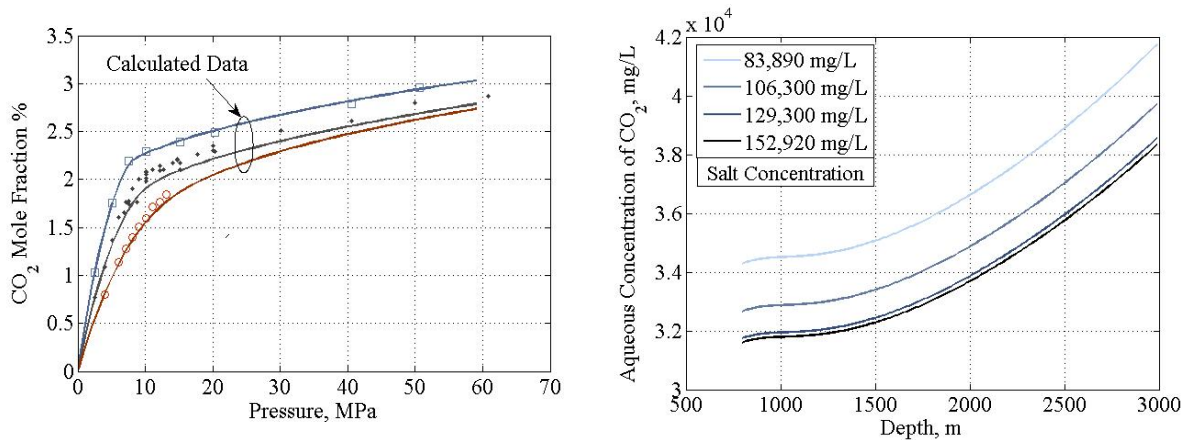


Figure 36

Impact on CO₂ solubility from, Top: pressure on isothermal bounds and Bottom: depth (pressure and temperature) on salinity bounds. Solid lines represent computer simulated results produced from Peng-Robinson equation of state and full procedure outlined in Attachment I. Data points on (a) were compiled in Spycher, *et al.* [59]

Applying this procedure to the Viking formation with average reservoir parameters (Table 2) resulted in an estimated CO₂ sequestration capacity in soluble form of 102 Gt. Through examination of similar form, Bachu and Adams [56] estimated a capacity of 106.6 Gt CO₂ for the portion of Viking suitable for sequestration. Assuming a 500MW power plant outputs 4.65 Mt CO₂ per year, this sequestration capacity (102 Gt) is sufficient to sustain injection from 100 such plants for 227 years. Such a solubility capacity is sufficient for the purposes herein,

although contribution to capacity estimates from mineralization must be considered, in addition to hydrodynamic considerations that will govern the length of time CO₂ may be safely stored as the pure phase slowly diffuses into the system for solubility and mineral trapping.

Table 2
Average characteristics of Viking formation used in
solubility estimations (e.g. [14, 56, 60])

Parameter	Assigned Value
Depth, m	2000
Temperature, deg C	55
Pressure, MPa	20
Salinity, g/l	70
Plan view area, km ²	400,000
Thickness, m	30
Porosity	0.2

5.2.3. Mineral Trapping and Capacity

Mineral trapping, as has been stated before, is a long term storage mechanism. The mechanism as described by Ortoleva *et al.* [61] is that CO₂ first dissolves in water to produce the weak carbonic acid,



This is followed by rapid dissolution of carbonic acid to form the bicarbonate ion which increases the acidity of the solution,



This leads to the dissolution of many of the primary host rock minerals, which in turn causes complexing of dissolved cations with the bicarbonate ions such as



These dissolved bicarbonate species react with divalent cations to precipitate carbonate minerals and the formation of Ca, Mg, and Fe(II) carbonates are expected to be the primary means by which the CO₂ is immobilized [62] as is shown through the following equations:



Mineral trapping is potentially attractive because it could immobilize CO₂ for very long periods of time[63]. Apart from these precipitation reactions, dissolution of alkaline aluminosilicate minerals by CO₂ will also increase the concentration of soluble carbonates and bicarbonates in solution, thereby enhancing solubility trapping.

The mineralization capacity of CO₂ in the geologic medium was determined based on the following considerations: a) redox processes that could be important in deep subsurface environments, b) the kinetics of chemical interactions between the host rock minerals and the aqueous phase, and c) CO₂ solubility dependence on pressure, temperature and salinity of the system. The mineralogy taken into consideration for this study represents general characteristics of the Viking formation. Framework grain-size ranges in diameter from 0.125 to 0.5 mm, while the clays and carbonates average about 0.008 mm in diameter. The formation water chemistry (mg/l) is Na: 28,800; K: 690; Ca: 2970; Mg: 578; HCO₃: 198; Cl: 51,600; SO₄: 366 and pH: 7.2 [64].

The equation that governs the rate of mineral dissolution [65] and precipitation is given by,

$$r_m = -\text{sgn} \left[\log \left(\frac{Q_m}{K_m} \right) \right] k_m A_m \left[\left(\frac{Q_m}{K_m} \right)^\mu - 1 \right]^\eta, \quad (17)$$

where m is the mineral index, r_m is the dissolution/precipitation rate (positive values indicate dissolution and negative values precipitation), A_m is the specific reactive surface area per kg H₂O, k_m is the rate constant (moles per unit mineral surface area and unit time) which is temperature dependent, K_m is the equilibrium constant for mineral water reaction written for one mole of mineral m, Q_m is the ion activity product, the parameters μ and η are two positive numbers normally determined by experiment and are usually but not always taken equal to unity (as in the present work). The expression “sgn(log (Q/K))” ensures that the correct sign is enforced when the exponents μ and η are not equal to one.

The mineralization was then modeled using TOUGHREACT and the changes in the volume fractions of the minerals were determined and based on the results obtained the capacity of sequestration of the medium was calculated to be roughly around 1.6 kg CO₂ per m³. Figure 37 is the mineralization behavior of Calcite (CaCO₃) and Siderite (FeCO₃), both carbonates that aid in trapping of CO₂. A more detailed explanation of the method of calculation is described in Appendix F.

With design goals to enhance and optimize the process of sequestering CO₂ from the 500 MW power plant, the ability of brackish waters to sequester a greater volume of CO₂ in soluble form than brines [66] is of importance to design considerations. Brackish waters differ from brines in

the sense that they have lower total dissolved solids (TDS < 10,000 mg/l) as compared to brines (TDS 10,000 – 100,000 mg/l) [67]. The higher salt concentrations lead to the salting out effect

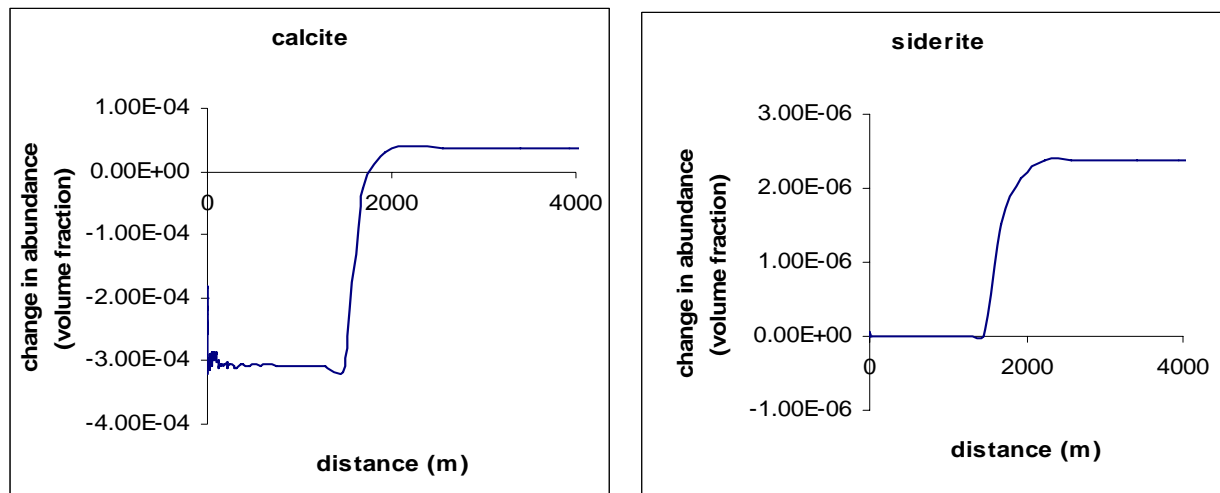


Figure 37

Change in mineral abundance for two of the minerals (negative values indicate dissolution and positive precipitation) after 50 years. Note that the scales of abundance are different for the four figures

resulting in lesser sequestration capacity of the CO₂ in the medium. Thus it is proposed to determine an area of the aquifer where the salt concentration is relatively lower and inject in that part of the formation. This possibility will be investigated as injection scenario 2 below.

5.3. AQUIFER INTEGRITY AND LEAKAGE

A crucial aspect of geologic sequestration is the leakage potential of CO₂ out of the target formation. From a global perspective, leakage of CO₂ from reservoirs would make CO₂ sequestration less effective, or even ineffective as mitigation option (depending on the leakage rate). The crucial question is what leakage rates are acceptable to assure stabilization of atmospheric greenhouse concentrations in the coming century is not endangered [68].

Leakage can occur through the seal or the cap rock on top of the storage aquifer, it may also occur through a faulted zone, especially when the fault covers all the geological layers from the surface to the basement rock. Furthermore, leakage could occur through abandoned wells. Abandoned wells may act as a bypass to the atmosphere if these were not sealed properly. Catastrophic leakage is unlikely for CO₂ injected into deep saline aquifers and probably would occur only as a result of a blowout of an injection well or existing well in the vicinity, or a seismic disturbance [7], although the tectonically stable nature of the Viking formation [56] does not favor such an occurrence.

5.3.1. Caprock Integrity

A seal or a caprock is a geological formation capable of hydraulic sealing over geological time that will maintain its sealing properties despite of geomechanical, geochemical, and hydrogeological changes [7]. It is typically a rock of low permeability that serves as a physical barrier to fluid migration. The permeability of the cap rock is typically in the range of micro-Darcy (μD) or less, as a result of small grain size and small pore diameters. The tiny pore throats

impede multi-phase fluid flow due to capillary forces trapping subjacent fluids at some finite upward (buoyant) pressure [69]. The potential for leakage depends on well and caprock (seal) integrity, overburden integrity and the trapping mechanism.

Leakage through the top seal can basically occur by three processes: 1) Diffusion through the pore system, 2) capillary transport through the pore system, and 3) multiphase migration through a micro- fracture network, or by a combination of any of these [70]. Diffusion of CO₂ dissolved in saline water is, however, a very slow process and results in very low leakage rates. Capillary transport of CO₂ through the pore system of the seal requires that CO₂ exist as a separate (non-dissolved) phase that can enter and traverses the pore space of the seal formation, under the force of buoyancy of the pure phase CO₂. In addition, a reservoir over-pressure due to reservoir fluid compression caused by the injection can constitute a driving force for capillary transport [71]. Multiphase migration through microfracture network in the seal formation, however, can be a highly efficient leakage process, provided the network has a high permeability and connectivity [71].

The Effect of Faulting

A fault is a surface at which strata are no longer continuous, but displaced. The effects of faults on fluid flow range from 1) prevention (barrier), through 2) little or none, to 3) enhancement (conduit). Because fracture porosity and resulting permeability are much higher in the damage zone than in the relatively unfractured country rock adjacent to it, fluid flow parallel to the fault is enhanced. Flow parallel to the fault is also enhanced by the presence of fractures within the fault rock, which tend to align parallel or sub-parallel to the displacement vector of the fault [72]. While the Viking formation is generally regarded as being geologically favorable for high integrity storage [56], any CO₂ injection scenario must incorporate a monitoring system to ensure capping integrity. Such a monitoring system is discussed below.

Quantification of Caprock Leakage

Multiphase flow through a caprock can be expressed by Darcy flow. The governing equation is,

$$Q_{leak} = \frac{kkrA\Delta\rho gh}{\mu\Delta z}, \quad (18)$$

where, Q is leakage rate through the caprock, k is absolute permeability of the caprock, k_r is the relative permeability of CO₂, A is the cross sectional area, μ is CO₂ viscosity, g is the gravity acceleration, D_ρ is the density difference between water and CO₂, and h is the height of CO₂ column. The estimated leakage rate per the above relation, with a caprock permeability of 10^{-18} m², relative permeability of 0.3, properties of CO₂ at reservoir conditions of injection scenario 2 in the design case presented below, and a cross sectional area determined through the numerical modeling procedure (see Injection Modeling section below) to be a circular area of radius 2000m for 50 years of injection and with a factor of safety, is 1.24×10^{-2} kg/s. Taking into consideration that the rate of injection of CO₂ into the aquifer is 155.5 kg/s, the leakage percentage is less than 0.01 % of total injected volume.

5.3.2. Well Bore Integrity

Crucial to leakage analysis is the contribution of CO₂ leakage through or along wells. CO₂ leakage through or along wells after the injection phase can be caused by casing or cementation defects due to improper design or construction, or corrosion of the casing and deterioration of cement plugs by CO₂ and/or brine [73]. Abandoned wells can be especially important migration pathways, since depleted oil/gas reservoirs are generally “punctured” by a large number of non-operative exploration and production wells, some of them in bad condition. It is uncertain how the well bore integrity (and especially the cement) is affected by CO₂ and brine considering a storage time scale of 100’s to 1000’s of years. Degradation may affect permeability of cement, which might increase leakage rates in time [73]. The potential for upward leakage is enhanced by CO₂ buoyancy where the pure phase is lighter than formation water [74].

The abandoned well leakage of CO₂ can occur via any of several possible pathways along a well: 1) In annular or degraded spaces between cement and the rock, or 2) between the cement and the casing, or 3) through the cement itself if it is damaged by chemical reactions or mechanical fracturing [54] (Figure 38). In order to assess potential leakage of a certain reservoir, detailed information must be available on the number, type and age of wells, completion technique and type of materials used [73].

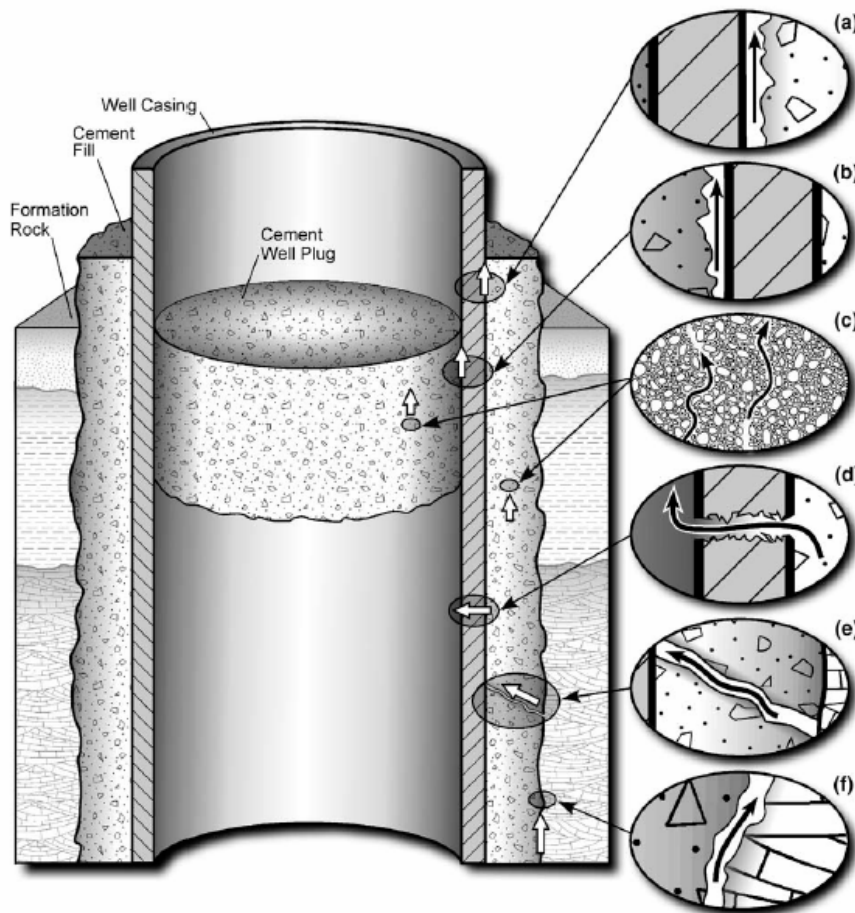


Figure 38

Quantification of Leakage from Abandoned Wells

Leakage through abandoned wells has been assumed to occur through pathways of degraded well cements or through very thin annular openings or fractures such that the multiphase version of Darcy’s law is applicable. For flow between a layer of the formation l and its neighbor layer (above), $l+1$, the expression for volumetric flow rate is [75],

$$Q_{\alpha} = -\left(\pi r_{\text{well}}^2\right) k_{\text{well}} \lambda_{\alpha} \left(\frac{p_{l+1} - p_l}{D_{l^+}} + \rho_{\alpha} g \right), \quad (19)$$

where, Q_{α} is the volumetric flow (leakage) rate of fluid α in the well, r_{well} is the effective well radius, k_{well} denotes the effective intrinsic permeability of the leaky well, p_{l+1} and p_l are the pressures in the upper and lower layers, respectively; and D_{l^+} is the vertical distance (aquitard thickness) between the two layers, and λ_{α} is the mobility of CO_2 in at aquifer conditions.

The estimated leakage through one well is 3.8×10^{-3} kg/s, assuming that 100 wells exist in the 2000m radius injection influenced area, including the 10 injection wells, the annual leakage rate will be 1.2×10^7 kg. Figure 39 shows the rate of leakage as a function of well number, and the leakage percentage assuming 1 well per 2 km^2 is 0.26%, which is within the acceptable range based on many studies that indicate the maximum acceptable leakage rate is 1% [75]

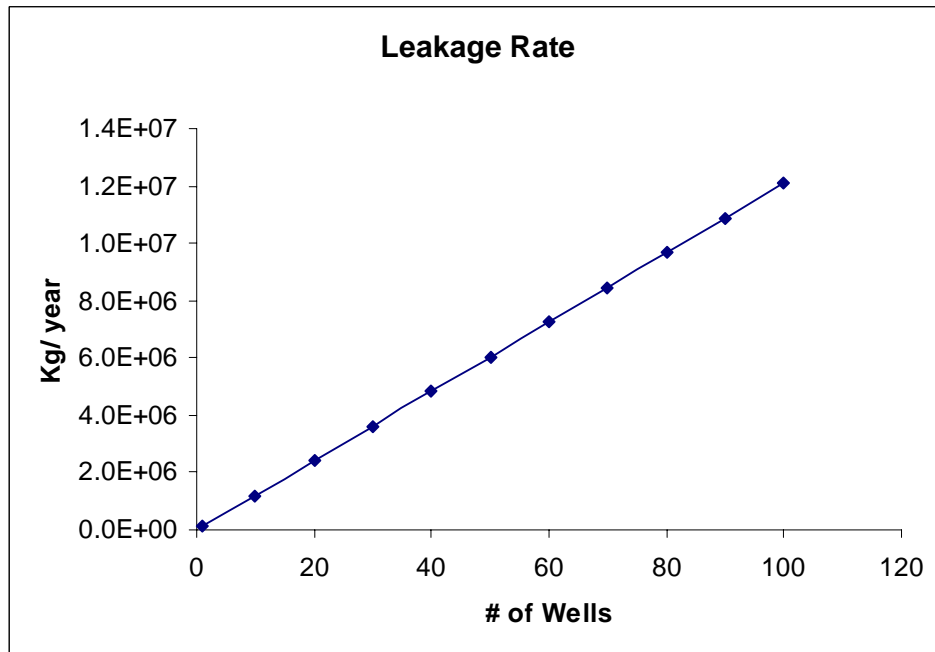


Figure 39
Leakage rate through wells

5.4. CHEMICAL CHANGES DURING INJECTION

As a result of the precipitation and dissolution of the minerals mentioned above there are various changes that take place. The precipitation of some of minerals like calcite (CaCO_3) and siderite (FeCO_3) as shown in Figure 37 lead to the trapping of the CO_2 whereas the changes in others like alkaline aluminosilicate minerals shown in Figure 40 effect the concentration of soluble carbonates and bicarbonates in solution and may thereby enhance the “solubility trapping” [67].

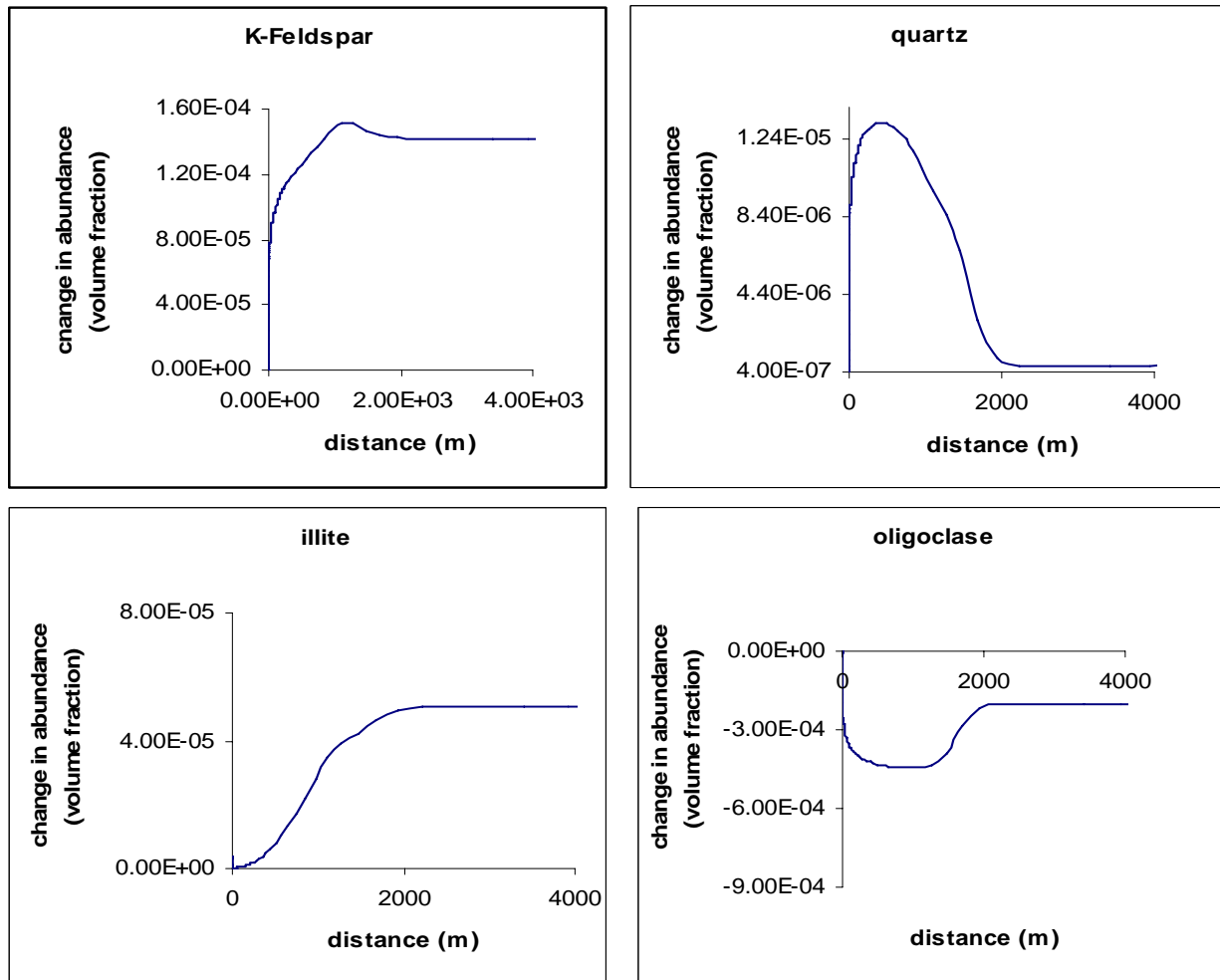


Figure 40

Change in mineral abundance (negative values indicate dissolution and positive precipitation) after 50 years.

The CO_2 plume migrates only till around 1500m during the period of 50 years for which we performed the study and it is observed that mineral abundance does not change after a distance of around 2000m. It was seen that there is no significant change in the porosity or the permeability of the medium as shown in Figure 48. The pH did not vary much as well. Hence the medium does not undergo considerable chemical degradation and thereby should not be a major concern for leakage by such means.

5.5. INJECTION MODELING

A small number of studies have utilized numerical modeling in conjunction with kinetic rate laws to examine chemically reacting reservoir CO₂ behavior [76-78]. Hydrodynamic behavior has also received numerical treatment [60, 79, 80], while the work of Rutqvist et al. [81] highlighted the combined influence of thermal, hydraulic, and mechanical interaction. Currently, the task of coupling all above behaviors in a numerical scheme which includes a detailed mechanical response component in conjunction with chemical reverberation on transport phenomena has not been accomplished. To a reasonable approximation, with the inclusion of sufficient factors of safety, predicting the two most crucial reservoir behaviors of 1) pressure build at well-bottom and 2) CO₂ radial transport may be accomplished through thermal, hydraulic, and chemical (THC) modeling.

Such a THC coupled numerical analyses may be targeted through several modeling apparatus. TOUGHREACT [82], a reactive flow addition to the pre-existing framework of TOUGH2 [83], provides a complex and thorough framework for kinetic and thermodynamic analyses of non-isothermal, reactive flow conditions. Flow simulation and thermodynamic capabilities of TOUGH2 have been thoroughly tested in the scientific community, and lend a well verified behavior to such analyses, while the reactive capability of TOUGHREACT has received considerable attention since its conception, and has behaved consistently in agreement with other reactive models [84]. In the realm of mechanical response, the inclusion of pore thermal expansivity (1/T) and pore expansivity (1/P) in TOUGHREACT may partially account for the mechanical response, to the extent that increasing pressure at well-bottom allows a calculated increase in near-well permeability.

TOUGH2 and the TOUGHREACT extension simulate by an “integral finite difference” method, thereby maintaining separation from global coordinates and relying solely on interfacial area and connection distance between nodes located at the center of each grid block. Fully implicit transient behavior is implemented in a first-order, backward finite difference scheme with upstream weighting of the flux terms. A multiphase extension of Darcy’s law describes fluid advection, while diffusive mass transport is allowed in all of three possible phases utilizing the full diffusion tensor, and thermal transport is described through conduction and convection. Of the several possible solvers provided in TOUGHREACT, the stabilized bi-conjugate gradient solver achieved the greatest reliability in convergence, and was used in all subsequent simulations.

Thermodynamic modeling for the analyses below utilized the ECO2 equation of state module, a combination of the previous state modules of EOS2, for CO₂ and water co-existence, and EWASG, incorporating water, NaCl, and a non-condensable gas and allowing precipitation and dissolution with optional permeability and porosity change. CO₂ dissolution is modeled with an extended version of Henry’s law including an EOS determined fugacity coefficient and a Poynting correction factor, and component activities are modeled using an extended Debye-Huckel relation, valid to 100,000 mg/l salinity. Vapor pressure lowering is also accommodated, but was not utilized herein. Geochemical reactions utilize the common EQ3/6 database and all considerations are valid at any pH and Eh. In the interest of brevity, the governing equations will not be described here. For a detailed analysis, the authors refer you to Pruess *et al.* [83] and Xu *et al.* [78].

5.5.1. Possible Injection Scenarios in Viking

Based upon commonly quoted gradients of 10 MPa/km and 25°C/km for pressure and temperature, respectively, CO₂ can be expected to reach supercritical state, an ideal situation for maximum storage of high density CO₂, at a depth near 800m per the thermophysical properties discussed above. However, gradients in a specific location can differ widely from these assumed values [14], as is the case for the Viking formation. To achieve sufficient hydrodynamic residence time for CO₂ to become soluble and, thus, achieve a higher state of storage confidence, the injection point must allow the CO₂ to: 1) travel at a sufficiently slow pace to not reach a portion of the aquifer where it may transition to a gaseous phase or leak directly to the surface or 2) be directed into a structural trap where migration is no longer a concern and the caprock is sufficiently impermeable to ensure minimal leakage. Each of these two scenarios is examined in detail herein.

Two specific injection scenarios are illustrated in Figure 41 and Figure 42. From these figures, injection values for each scenario are summarized in Table 3, where Scenario 1 represents the case of a continual advancement of CO₂ up-gradient and Scenario 2 presents the possibility of entrapment beneath a structural oddity as deciphered in Figure 43.

Table 3
Aquifer characteristics at conditions of Injection Scenarios 1 and 2

Comparison Variable	Injection Scenario 1	Injection Scenario 2
Depth, m	2000	800
Temperature, deg C	70	23
Pressure, MPa	12	6.5
Salinity, g/l	25	20
Porosity	0.1	0.2
Permeability, m ² (from Gasda [60])	5 × 10 ⁻¹⁴	1.9 × 10 ⁻¹³
Thickness, m	30	70

5.5.2. Number of Required Injection Wells

In its current state, modeling of CO₂ behavior in saline reservoirs has been limited to the examination of mineral precipitation/dissolution and hydrodynamic transport from the basis of full injection from a single injection well [e.g. 60, 77, 79, 82, 85, 86]. While important conclusions may be drawn from such an analysis, a realistic injection design will be limited by the amount of injective pressure an aquifer may sustain prior to hydraulic fracturing (which would be sustained and propagated throughout the injection period with constant pressure at such a value). Preliminary economic analyses [2] have assumed a standard pressure capacity of 9-18% above *in situ* pressure, leading to an estimation of the required number of injection wells for a given flow rate through a recast of Darcy's Law as [2],

$$q = \frac{\rho_r}{\rho_s} \times \frac{2\pi kh}{\ln\left(\frac{r_e}{r_w}\right)} \times \Delta p, \quad (20)$$

to determine the maximum flow rate per well, q (m³/s), with dependence on gas density (kg/m³) at reservoir conditions, ρ_r , and ambient conditions, ρ_s , reservoir thickness, h (m), permeability, k

(m^2), gas viscosity under reservoir conditions, μ (Pa.s), logarithmic ratio between well radius, r_w , and the radius of the cone of influence, r_e , and the pressure difference between well-bottom and the *in situ* reservoir pressure (Pa), which, as stated above, is taken as 9-18% of *in situ* pressure.

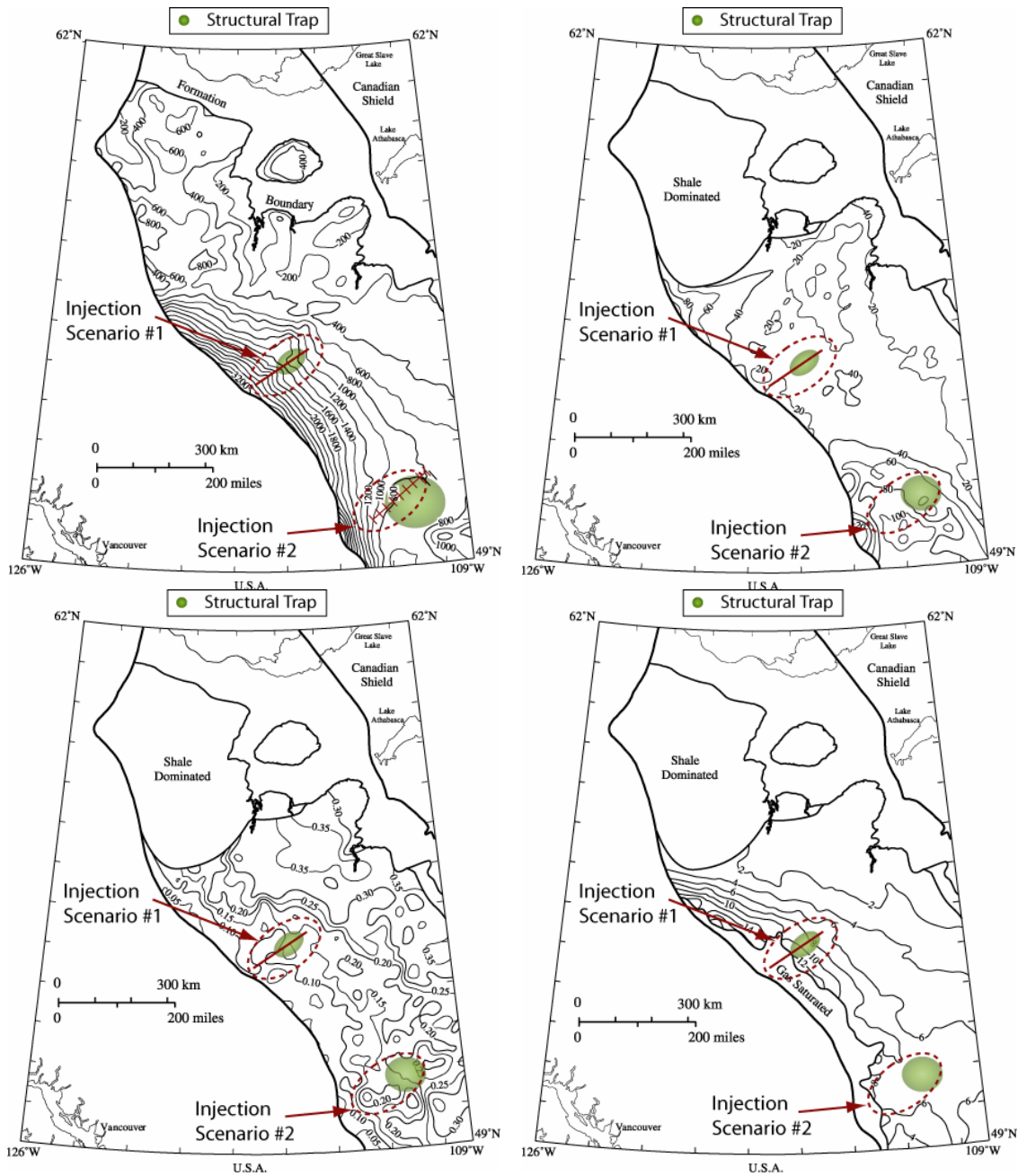


Figure 41

Isopleth maps of Viking formation for (left to right and top down) 1) Depth to top of formation (m), 2) porosity, 3) thickness (m), and 4) pressure (MPa). Two possible injection scenarios are circled generally with red-dashed ellipse, and partial structural traps are highlighted in green circles. Images are modified from Bachu *et al.* [87] and Alberta Geological Survey

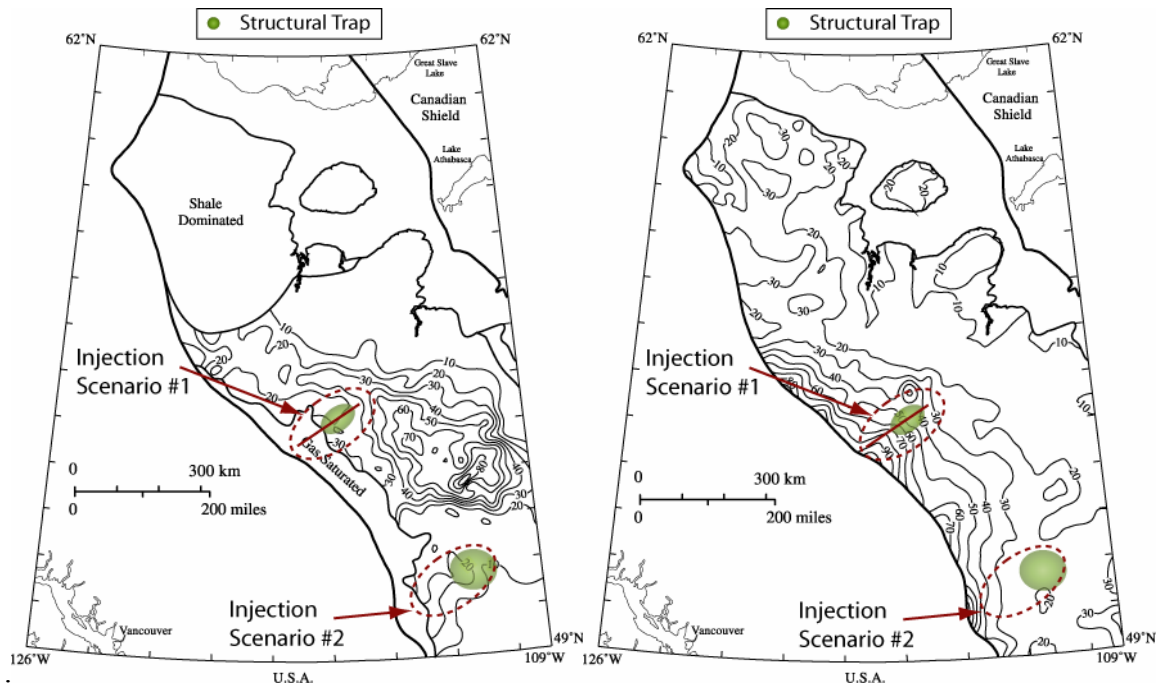


Figure 42

Isopleths of Viking formation for (left to right) 1) salinity (g/l) and 2) temperature (deg C). Symbolism is identical to Figure 41. Images modified from Bachu *et al.* [56] and Alberta Geological Survey.

The logarithmic ratio is typically assigned a value of 7.5 [2], equating to radius of influence near 2000m [88]. However, the inclusion of gas density under standard conditions is self-defeating for our purposes, where mass flow rate at well-bottom is a more desirable outcome, and has been omitted from the calculations below.

The above relation, Eq. (20), should be used with great caution, however, as the radius of influence is highly dependent on injection rate, for which the equation is forward calculating, and the assumption of 9-18% pressure capacity is highly generalized. Results from this calculation herein were used merely to provide an initial estimate of well number, thereby decreasing the number of numerical modeling attempts required to locate the optimum conditions. From Eq. (20) and the parameters of Table 3, the estimated number of wells is 17 for the 2000m injection scenario (assuming the worst case of 9% above *in situ* pressure) and 2 for the 800m injection scenario.

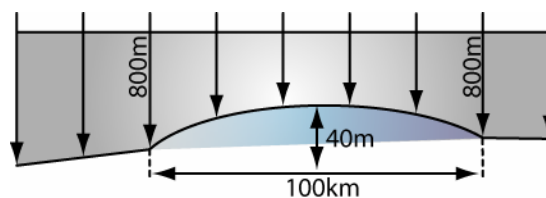


Figure 43

Injection scenario 2 depth isopleths from Figure 41 rotated to show cross section of formation. Approximate structural trap is 100km in diameter and achieves a trapping indentation of approximately 40m.

A more accurate analysis of these considerations necessitates an evaluation of the state of stress within the reservoir and numerical treatment of the pressure build surrounding the injection. These extensions are discussed below.

5.5.3. State of Aquifer Stress and Maximum Injection Pressure

Determining the stress distribution and pressure capacity of the aquifer begins by locating a representative stress/depth profile. Measured stress data has been previously compiled to provide a representative correlation between vertical and horizontal stress at depth (Figure 44). From Figure 44, a worst case stress ratio, occurring when the difference between vertical and horizontal stress reaches a maximum, may be extracted as the left-most dashed line. In further calculations, this worst case ratio was taken to be 0.48.

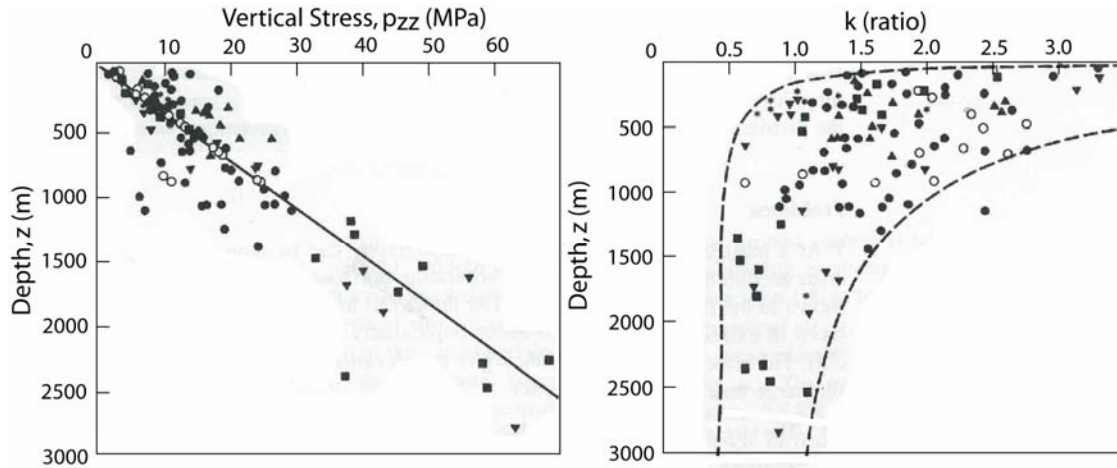


Figure 44

Variation with depth below ground surface of 1) measured *in situ* vertical stress p_{zz} and 2) ratio, k , of average measured horizontal stresses to vertical stress [88, 89].

In an ideal scenario, hydraulic fracturing will not occur until reservoir pressure climbs above the minimum principle stress (in this case the horizontal stress), at which point fracturing will propagate perpendicular to that stress. However, failure may also occur prior to reaching this pressure, as governed by a failure envelope described by Mohr's circle Figure 45. At the critical failure angle, β , the effective stress, $\sigma' = \sigma + \alpha p$, for total stress, σ , Biot modulus, α , and pressure, p , may be related as, $\sigma'_1 = \sigma'_3 N$ for the factor of safety,

$$N = \frac{1 + \sin \phi}{1 - \sin \phi}. \quad (21)$$

Rearranging these relations yields,

$$p_{\max} = \frac{\sigma_1 - N\sigma_3}{1 - N}, \quad (22)$$

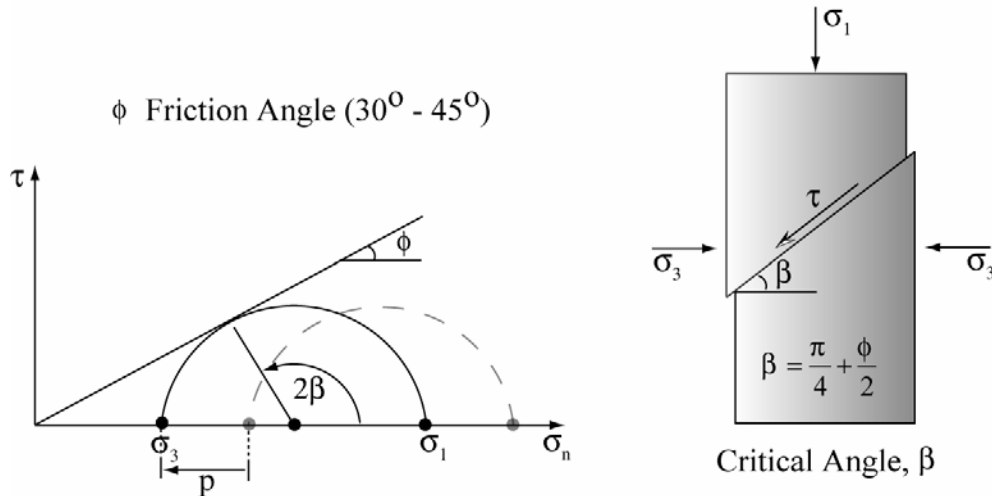


Figure 45

Mohr's circle (left) and physical representation (right) of critical angle of failure, β , as a function of friction angle, ϕ , and the principle stresses, σ_1 and σ_3 . Mohr circle is shifted by the presence of pore pressure.

for the worst case failure pressure. Applying the parameters as discussed above for the worst case minimum principle stress, a friction angle of 30° , and parameters from Table 3 yields a safe, worst case failure pressure of 15.2 MPa at 2000m depth and 8.4MPa at 800m depth. With a comfortable value for failure pressure, the number of required injection wells may then be attained through numerical modeling of injection activities.

5.5.4. Numerical Modeling of Pressure Generation

Meshing was designed for the current problem on a one-dimensional, radial geometry extending from a well radius of 0.2m (4in) to 100,000m at radial extent, which is well beyond a distance where injection influence would be felt in the system design life (see results below). One dimensional radial modeling allows verification via the existence of the similarity variable, R^2 / t [79, 90], as will be illustrated. The generalized geometry is illustrated in Figure 46, where the illustrated conditions are for the case of 800m depth injection.

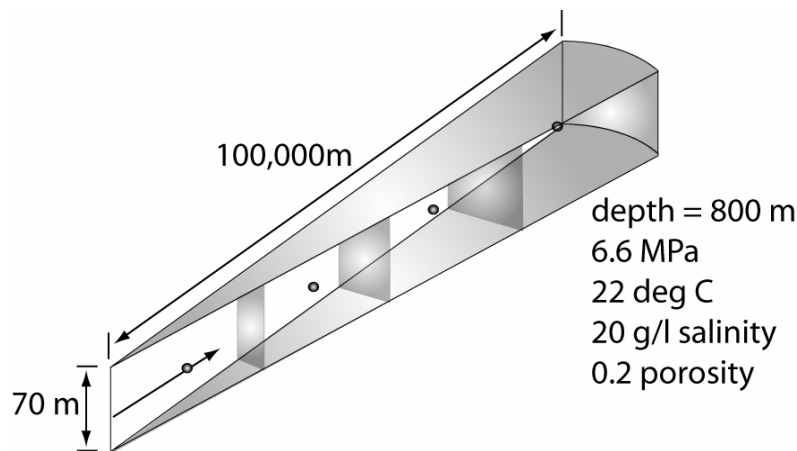


Figure 46

One dimensional radial geometry utilized in further simulations. Conditions shown are for the 800m injection depth scenario.

Scenarios of injection rate were examined by splitting the 155.5 kg/s power plant output (see above) into possible fractions in the range estimated by Eq. (20) above and for each injection depth scenario. The minimum number of wells that could be utilized without exceeding maximum aquifer pressure (see *State of Aquifer Stress and Maximum Injection Pressure*) was then adopted for future analyses. Results of the pressure analysis are shown in Figure 47.

Figure 47 illustrates the analysis for an 800m injection scenario utilizing 10 wells, where the pressure builds to approximately 8.1MPa, or slightly below the maximum (worst case) pressure of 8.4MPa. Similar analysis of the 2000m injection scenario showed a pressure build to 15MPa, or slightly below the maximum (worst case) pressure of 15.2MPa for 16 wells. To verify that permeability reduction near the well due to mineral precipitation would not alter this pressure build, an identical scenario was analyzed for chemical results.

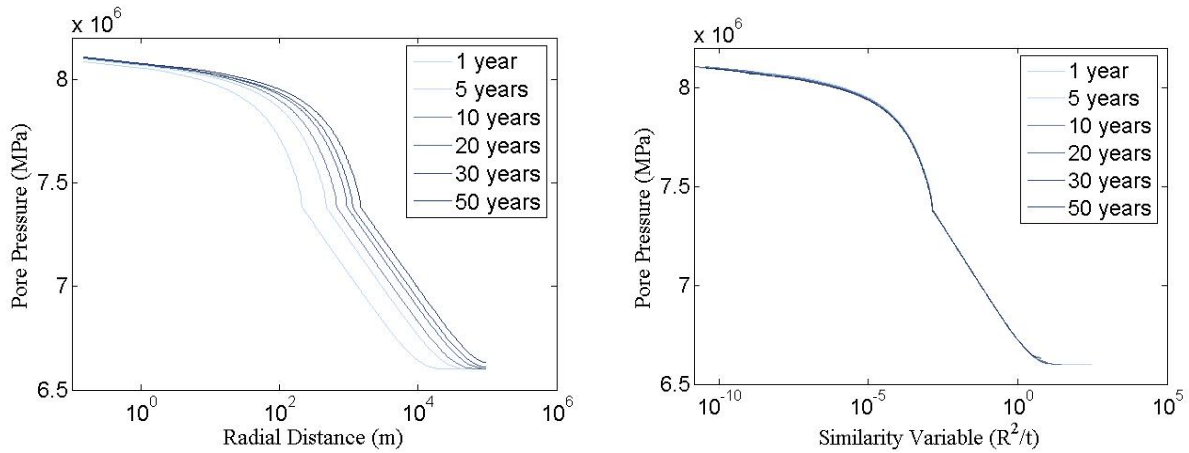


Figure 47

Pressure analysis of injection for the 800m injection depth scenario versus radial distance from the well (left) and similarity variable (right). Overlay of solution for all years is nearly indistinguishable for the similarity variable comparison, indicating valid advancement of the pressure front.

5.5.5. Permeability Reduction

Temporal changes in porosity and permeability due to mineral dissolution and precipitation can modify fluid flow. Changes in porosity can be calculated from the changes in the mineral volume fractions and a simple Kozeny-Carman grain model, which relates the porosity to the permeability as [86, 91],

$$k = \frac{R_o^2}{45} \left(\frac{\phi^3}{(1-\phi^3)} \right), \quad (23)$$

where R_o is the initial spherical close pack radius. We can hence have the ratio of the permeability k to the initial permeability k_o as,

$$\frac{k}{k_o} = \left(\frac{\phi}{\phi_o} \right)^3 \left(\frac{1-\phi_o}{1-\phi} \right)^2, \quad (24)$$

where ϕ_o is the initial porosity.

As shown in Figure 48, for a period of a year there is not much change in the porosity and the change in the permeability is quite insignificant. After this, there is hardly any change observed.

Behavior was modeled within a one-dimensional radial geometry, extending to 100km. While density gradients resulting from changes in CO₂ solubility and aqueous ions can be expected in a true scenario to increase mixing and behave slightly differently than a one-dimensional model, the extremely long time-scales over which the system must be modeled justifies its use when considering the natural spatial equilibrium that will occur over such scales. Parameters of the model are presented in Table 1, where compositions and physical characteristics are average characteristics of the Viking formation, and the injection rate is representative of one-tenth of the output from a 500MW coal-fired power plant. At the physical characteristic bounds of Viking,

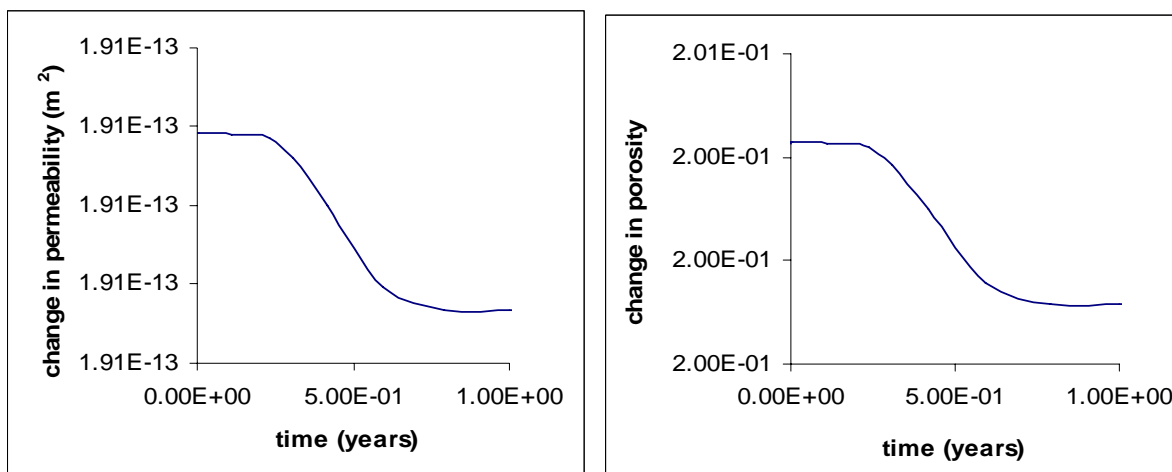


Figure 48

Change in porosity and permeability after 50 years.

ten wells will be required to inject such an output due to stress gradients in the formation and the maximum pressure (25% above *in situ*) to avoid hydraulic fracturing.

Results in Figure 4 are for 50 years of continuous injection. The impact of such mineral precipitation/dissolution on physical properties of the aquifer are still not well understood, and general cubic permeability relations coupled with generalized porosity-permeability relationships are utilized in TOUGHREACT to predict transport changes due to such chemical behavior. The generalized nature of these relations is sufficient in many cases, but may breakdown when mechanical stresses lead to pressure dissolution at contact points in aquifer soil grains (compaction and dissolution of soil) or when well-bottom pressures mechanically alter the soil matrix. Such mechanical effects may only be sufficiently modeled within a comprehensive solid mechanics model. Additionally, the development of constitutive relations specific to soil characteristics may be desired.

5.5.6. Number of Injection Wells

Because very little permeability reduction occurs due to mineral precipitation, the results attained above for pressure build remain valid. Therefore, 10 wells will be required for the 800m injection depth scenario, while 16 wells are required at 2000m. In addition to an increase in the number of wells, the well costs presented above show a dramatic difference between 800m and

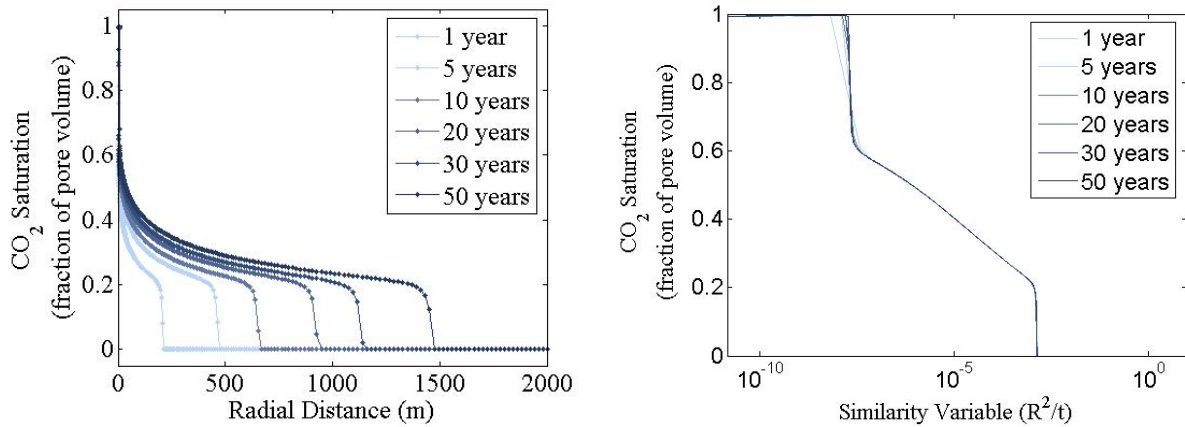


Figure 49
CO₂ saturation of matrix with radial distance (left) and similarity variable (right)

2000m, thereby indicating a dramatic cost reduction for the 800m scenario. This scenario will be further investigated below to determine well layout and the likelihood for entrapment in the structural anticline at this location (Figure 43).

5.5.7. CO₂ Transport Extent

Recalling the one-dimensional radial geometry from above, migration potential may be analyzed on an individual well basis for the ten injection wells. Utilizing the same parameters as above, Figure 49 and Figure 50 show CO₂ saturation and brine velocity, respectively. Notably, at a simulation time of 25 years, gas phase migration has achieved a mere 1000m, while 50 years yields 1500m.

Well spacing should be sufficient to prevent unacceptable interference of pure phase CO₂ from one well with the next. Pressure interference between wells, which is impossible to avoid given the large radial influence of pressure in Figure 47, is of less concern as long as the plane of symmetry between the wells (Figure 51) does not build sufficient pressure for the CO₂ to migrate outside of the structural trap.

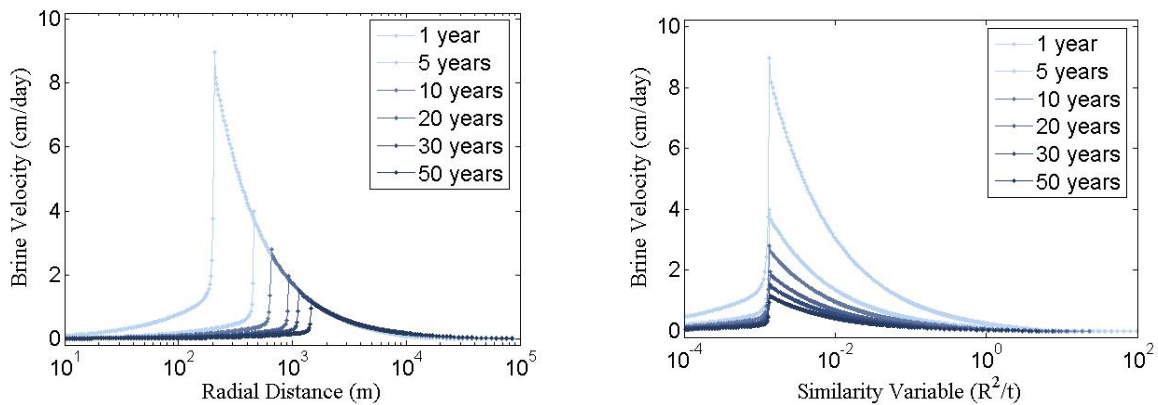


Figure 50
Brine velocity with radial distance (left) and similarity variable (right)
Well Spacing

However, given the large distance required for escape from the trap (47km) when compared to CO₂ transport distance from a single well (1500m at 50 years), this concern is negated. Therefore, the ideal situation is simply to minimize pressure interference while simultaneously minimizing well spacing, and thus pipeline cost. The optimal situation here occurs at the CO₂ migration front (Figure 47 and Figure 48), where pressure achieves its lowest value prior to an expansive slow decline to large distances. For a design life of 50 years, this distance is approximately 1500m. From this minimum value, a well spacing of 2000m has been chosen to allow some cushion to this calculation.

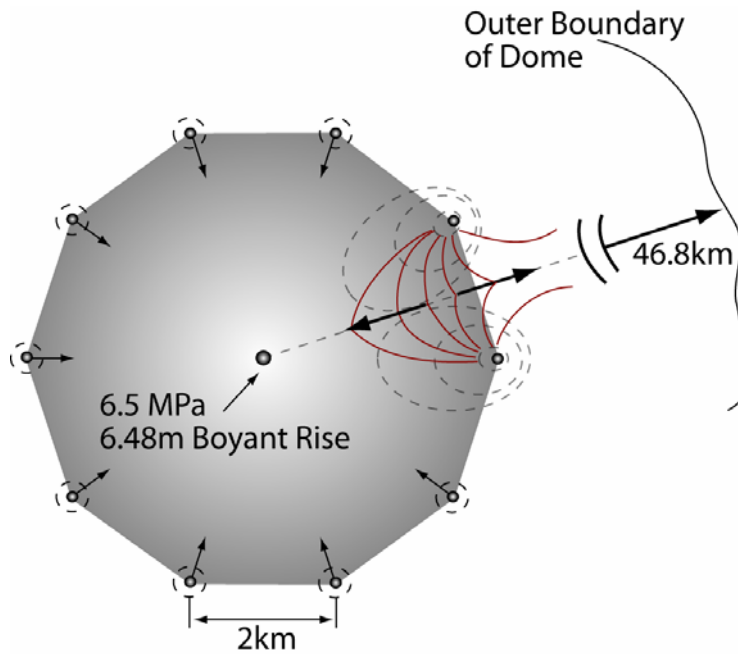


Figure 51
Layout of 10 well injection within structural dome.

5.6. COMPRESSION MODELING AND DESIGN

Once the bottom well pressure and the arrangement was determined, the compression system was designed. The design was completed using Aspen Plus. Figure 52 is a process flow diagram for the compression system. Stream 100 comes from the IGCC power plant from the palladium filter. It is delivered at 100°C and 10 atm. It is assumed that the CO in the stream has been oxidized to CO₂ before injection. The thermodynamic parameters as well as the flow rates and compositions are available in Appendix G. E100 is a counter flow heat exchanger with an area of 3,200m² in which cooling water is used to cool the flue gas to 45°C. In this process, a significant amount of water is condensed which is separated from the vapor in V100. The vapor is then compressed in MC100, which is a multistage compressor. MC100 consists of 4 compressors with 3 inter stage coolers which cool and further condense water which leaves in the liquid knock out streams, 125 to 127. The compressed flue gas is split in two and sent to the injection wells through streams 104 and 105. Only half of the wells were modeled because the injection field is symmetrical. The wells are separated by 2km as seen in Figure 51. P100 to P105 are pipe headers that are carbon steel, schedule 80, and 24 inches diameter. P100 is 1km long and P101 to P105 are 2km long. Each well, W100 to W104, is 8 inch, stainless steel, schedule 40s pipe. Each well takes 1/10th the compressed flue gas and has an elevation change

of -800m. The system was designed such that the bottom well pressure is supplied between 8.13 and 8.16 MPa. Aspen Plus can model pressure changes due to frictional losses and elevation changes for compressible fluids in pipes. The well head pressure required was found to be 6.95 MPa. The associated compression energy is 24.1 MWe.

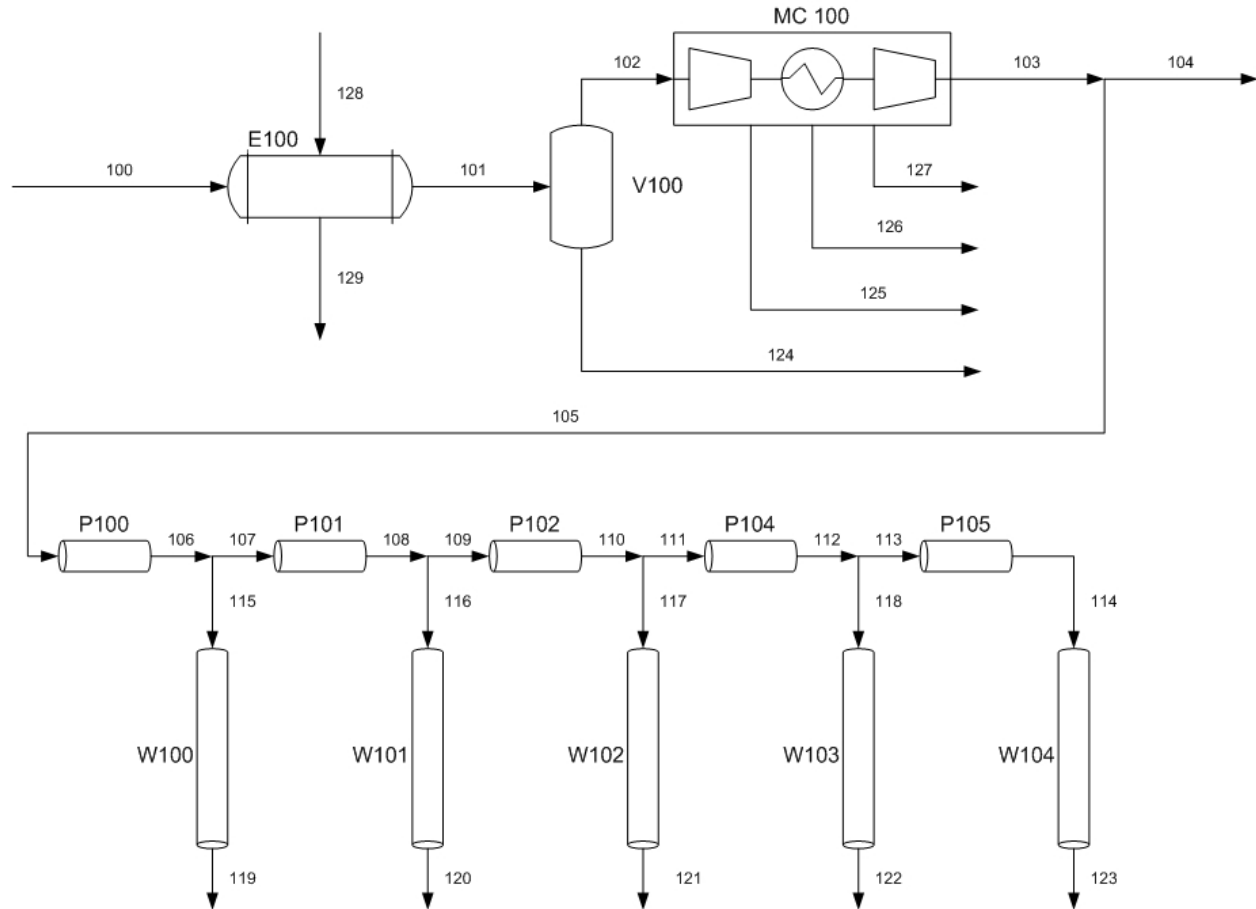


Figure 52
Process Flow Diagram for Compression and Injection System

5.7. GENERAL WELL DESIGN

The design of a CO₂ injection well is very similar to that of a gas injection well in an oil field or natural gas storage project. Most downhole components need to be upgraded for higher pressure ratings and corrosion resistance. The technology for handling CO₂ has already been developed for EOR operations and for the disposal of acid gas [92].

The injection wells function as conduits for moving supercritical CO₂ fluid from the surface down into the deep saline aquifer. The well consists of three or more concentric casings: exterior surface casing, intermediate protective casing, and injection tubing. The exterior surface casing is designed to protect underground sources of drinking water and to reduce corrosion potential by preventing water contact with the intermediate protective casing [93].

The intermediate protective casing extends from the surface into the injection zone and is cemented along its full length. The injection tubing extends from the surface into the top of the

injection zone. The injection tubing should be designed so as to be removable to facilitate well maintenance, if needed. The discharge end of the injection tubing is equipped with a backflow preventer to prevent CO₂ escape in the event of a well casing failure [93]. Typical well design is shown in Figure 53.

Injection wells commonly are equipped with two valves for well control, one for regular use and one reserved for safety shutoff. In acid gas injection wells, a downhole safety valve is incorporated in the tubing, so that if equipment fails at the surface, the well is automatically shut down to prevent back flow. A typical downhole configuration for an injection well includes a double-grip packer, an on-off tool and a downhole shutoff valve. Annular pressure monitors help detect leaks in packers and tubing, which is important for taking rapid corrective action. To prevent dangerous high-pressure buildup on surface equipment and avoid CO₂ releases into the atmosphere, CO₂ injection must be stopped as soon as leaks occur. Rupture disks and safety valves can be used to relieve built-up pressure [92]. All materials used in injection wells should be designed to anticipate peak volume, pressure and temperature. The use of corrosion-resistant material is essential.

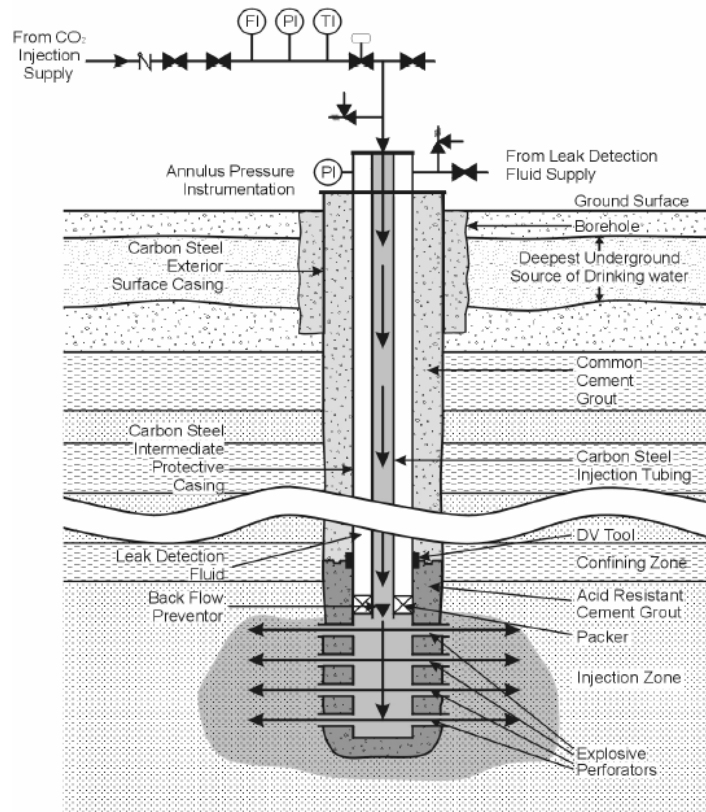
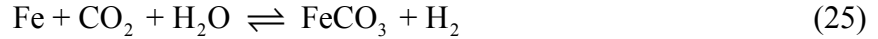


Figure 53
Typical injection well design [93]

5.8. PIPING CORROSION

A common concern is that of corrosion and we have briefly tried to address the issue. We know that the overall corrosion reaction is:



At low temperatures of 22 °C like in our case at the point of injection, the end product or the FeCO₃ formed is porous, dissolves continuously in the CO₂ solution and will not inhibit further corrosion of the pipeline [94].

The flow rate of the CO₂ too has a role in the determination of the corrosion behavior observed as shown in Figure 54. Higher flow rates generally ensure that the time of contact of the pipeline with the water present in the stream is less and hence corrosion is less pronounced as compared to lower flow rates which result in higher contact times and hence higher corrosion rates.

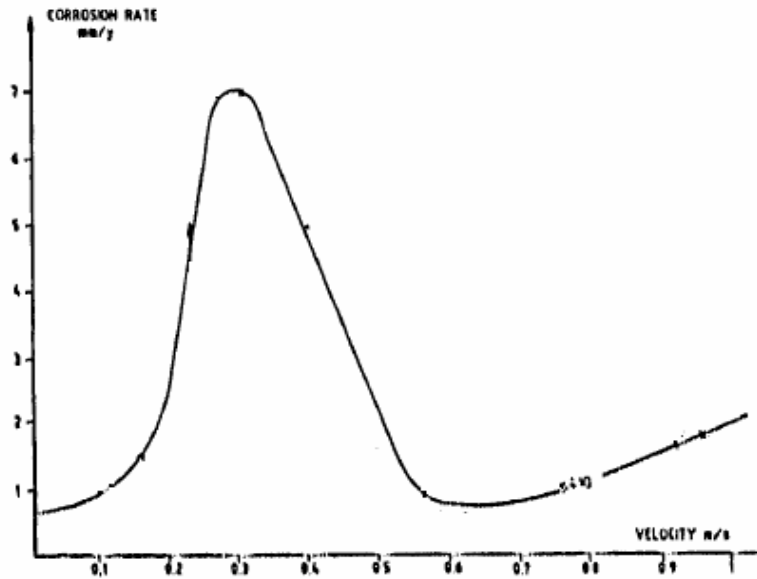


Figure 54
Variation of the corrosion rate with the flow velocity in the pipeline [95]

We have a flow rate of 11.09 m/s and hence this should considerably reduce the corrosion rate by reducing the water wetting time.

5.9. DRILLING COSTS

Drilling costs vary historically with the amount of competing activity at other projects and the availability of drilling rigs, and mainly related to the depth and diameter of the well as well as the properties of the rock formation [96]. The rock characteristics influence the initial well diameter, the number of casing strings needed and, thereby, the time required to drill the well. The chemistry of the brine determines the nature of the materials used in the well casing process; a corrosive geothermal fluid may require the use of resistant pipes and cement [96, 97].

The total average cost of per foot for drilling a well ranges between \$217/ft and \$254/ft [96, 97]. A \$300/ft has been used in this study to be more conservative.

The costs include material costs as casing, cement, and transportation to deliver materials to the drilling site. It also includes labor, materials, supplies, water, fuel, and power. Direct overhead charges are also included for operations, such as site preparation, road building, mobilization,

and demobilization and hauling costs [97]. In this study case assuming that amount that of CO₂ to inject is 4.65 MTon/year, which means 12.7 Kton/day.

5.10. MONITORING AND VERIFICATION

Monitoring and verification for geologic sequestration contains three components: modeling, plume tracking and leak detection [98]. While modeling has been examined above, monitoring aims to ensure and document effective injection well controls, also to verify the quantity of injected CO₂ that has been stored by various mechanisms. Moreover it can be used to optimize the efficiency of the storage project and to demonstrate with appropriate monitoring techniques that CO₂ remains contained in the intended storage formation(s). In addition to that, monitoring can be used to detect leakage and provide an early warning of any seepage or leakage that might require mitigating action [92].

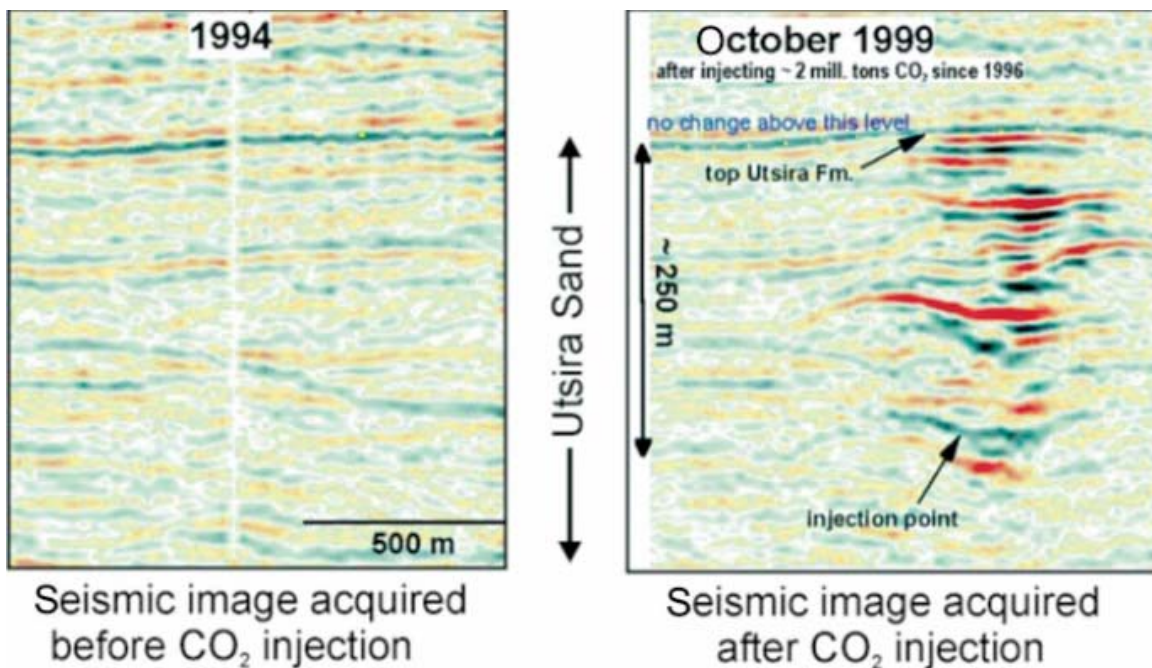


Figure 55

Seismic image of CO₂ stored in the Utsira sand at the Sleipner West field [99]

Seismic techniques are an indirect technique for measuring CO₂ distribution in the subsurface and measuring the properties of rocks by the speed of sound waves generated artificially or naturally. Seismic techniques measure the velocity and energy absorption of waves, generated artificially or naturally, through rocks. The transmission is modified by the nature of the rock and its contained fluids. In general, energy waves are generated artificially by explosions or ground vibration. Wave generators and sensors may be on the surface or modified with the sensors in wells within the subsurface and the source on the surface [92].

By taking a series of surveys over time, it is possible to trace the distribution of the CO₂ in the reservoir, assuming the free-phase CO₂ volume at the site is sufficiently high to identify from the processed data. A baseline survey with no CO₂ present provides the basis against which comparisons can be made. It would appear that relatively low volumes of free-phase CO₂ may be identified by these seismic techniques [92]. Beneath the CO₂ plume a “velocity push-down

effect” can be observed on the seismic data. This is due to seismic waves traveling more slowly through CO₂-saturated rock than through water saturated rock, and the localized pushdown thought to be caused by a ‘chimney’ of CO₂ migrating to the top of the reservoir. Figure (1) represent an example of seismic image at Sleipner West field before the injection and after the injection process, the underground situation is well imaged. Seismic and reservoir modeling is now being carried out to further quantify and constrain the CO₂ subsurface distribution and predict its future behavior [99].

Seismic resolution will decrease with depth and certain other rock-related properties; one possible way of increasing the accuracy of surveys over time is to create a permanent array of sensors or even sensors and energy sources to eliminate the problems associated with surveying locations for sensors and energy sources. For CO₂ that has migrated even shallower in the subsurface, its gas-like properties will vastly increase the detection limit; hence, even smaller threshold levels of resolution are expected [92].

To date, no quantitative studies have been performed to establish precise detection levels. However, the high compressibility of CO₂ gas, combined with its low density, indicate that much lower levels of detection should be possible. The use of passive seismic (microseismic) techniques also has potential value. Passive seismic monitoring detects microseismic events induced in the reservoir by dynamic responses to the modification of pore pressures or the reactivation or creation of small fractures. These microseismic events are extremely small, but monitoring the microseismic events may allow the tracking of pressure changes and, possibly, the movement of gas in the reservoir or saline formation [92].

CO₂ leak detection systems will serve as a backstop for modeling and plume tracking. The first challenge for leak detection is the need to cover large areas. The second challenge is to separate out CO₂ leaks from the varying fluxes of natural CO₂ respiration [98]. If CO₂ leaks out of the injection formation and escapes back to the atmosphere, the benefits gained in regard to mitigation of atmospheric CO₂ are obviously diminished.

5.11. ECONOMIC ANALYSIS

An economic analysis was performed for three cases: injection with energy supplied by CCLC, injection with purchased energy, and injection with energy from the plant. With a carbon dioxide credit of \$5/ton CO₂, the sequestration costs were \$14.9 million/year, \$10.3 million/year, and \$8.9million/year or \$2.93/ton CO₂, \$2.03/ton CO₂, and \$1.74/ton CO₂ respectively. See Appendix D for full details. Based on this analysis, it is recommended that the capacity of the power plant be reduced and the energy to compress the flue gas comes from the reduced capacity.

6. PART V: ENERGY SUPPLY STUDY

6.1. INTRODUCTION

The fuel and environment costs necessary to reduce emissions will drive the search for new ways to improve efficiency and extract more energy from fuel sources. On average, only 35 percent of the energy in a fossil fuel is converted to electrical output in a conventional power plant. The remaining 65 percent is discharged into the environment as waste heat at temperatures ranging from 300°F to 1,200°F in the form of hot water or vented steam and stack gasses from sources such as internal combustion engines, gas turbines, boilers, incinerators, furnaces, kilns, foundries

and many more. Steam turbines are commonly used to convert this waste heat to power [100]. However, steam turbine power plants with higher efficiencies (over 33 percent) require a heat input above 1,000°F (Figure 56).

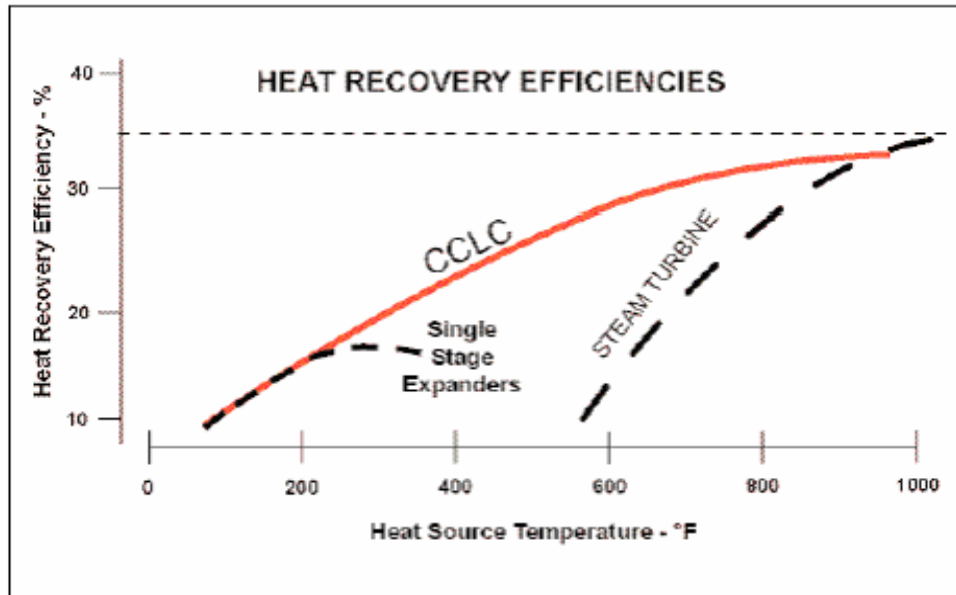


Figure 56
Heat Recovery Efficiency of CCLC as a Function of Inlet Temperature [101]

When the heat source temperature is much below 700°F, steam turbine systems are an inefficient method to generate electrical power. Below 500°F, thermal efficiencies for steam turbine systems approach zero. Wow Energies, Houston, Texas, has developed the patent-pending CCLC based on the Organic Rankin Cycle (ORC) with components that have been tested and in operation for decades. The CCLC can significantly increase waste heat recovery as seen in Figure 56. For example, it can extract 207 GW of power from existing waste heat sources in the U.S. and also help provide a low cost solution to many of the emission challenges [25].

6.2. THE CASCADING CLOSED LOOP CYCLE

The CCLC uses propane as the working fluid. It can capture heat from nearly any heat source and efficiently convert it to power. Until development of the CCLC, there has not been an efficient method to convert to electrical power the majority of waste heat generated by industrial processes. Thermodynamically, it represents one of the most efficient ways to generate power is with an ORC [102].

Three key principles were united to create the CCLC [101]:

- The heat energy (BTUs) required to convert liquid propane to a vapor is approximately 130 Btu/lb. It takes approximately 1,000 Btu/lb to vaporize water.
- At CCLC operating pressures, propane will vaporize and condense near ambient temperatures. At steam turbine operating pressures, heat source temperatures well above 600°F are necessary to produce efficient steam turbine power.

- Cascading multiple turbo-expanders and multiple heat exchangers in a series-parallel arrangement extract maximum energy from the heat source by keeping the propane in a vapor state between heat transfer stages.

The CCLC consists of two hermetically sealed propane loops as presented in Figure 57. Propane is neither consumed nor discharged to the environment. Its working pressures in the CCLC are the same as the natural gas fuel supply pressures required for a gas turbine power plant. The propane pump (P) in Figure 57 pressurizes a single propane stream to working pressure where it is divided into two propane streams. The first propane stream is vaporized with the waste heat source using a heat exchanger (HX1). This first stream of vaporized propane is then expanded across the first turbo-expander (EX1). The heat from the discharge of the first and second turbo-expanders is used to vaporize a second propane stream using multiple shell and tube heat exchangers (HX2 & HX3). This second stream of vaporized propane is expanded in a second turbo-expander to produce additional power (EX2). The two streams of propane are then recombined and condensed to a liquid using an air-to-air or air-to-water heat exchanger. The condensed propane liquid is returned to the pump (P) where it is pressurized to operating pressure to repeat the hermetically sealed, closed loop cycle.

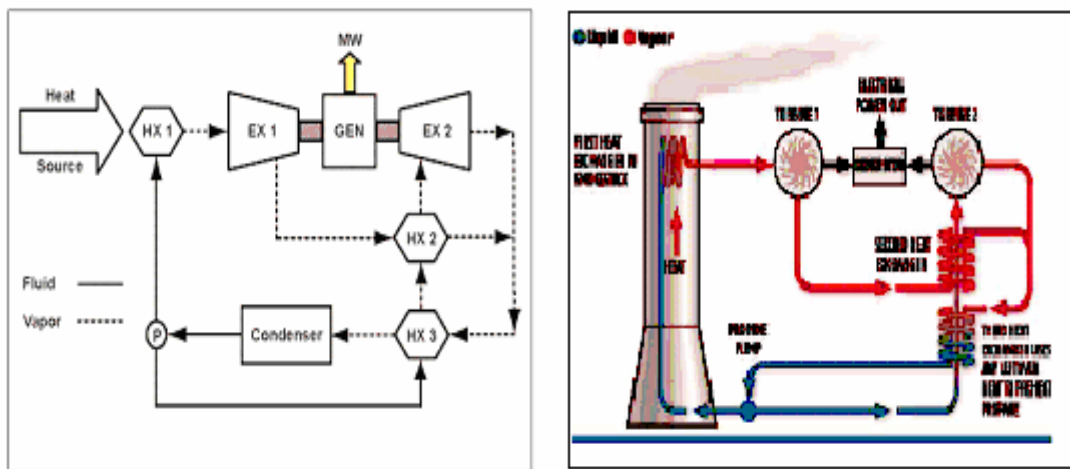


Figure 57
Schematic of CCLC Power Generating Plant [101]

Controlling the discharge pressure of EX1 and EX2 is important in achieving high efficiencies using the CCLC technology. The actual pressure level is dictated by the temperature of the cooling source, air or water, which is used to condense the propane and is set to maintain a vapor at the discharge of each turbo-expander. A high temperature vapor state is required to allow pre-heating the second stream of propane – a key to capturing nearly all the heat from the heat source. As ambient temperatures decrease during the day, month and year, the turbo-expander discharge pressure is reduced to allow additional expansion, and get more power. On average, the output of the CCLC is 15 to 20 percent higher than its design point rating [103]. Figure 58 represents the heat transfer and expansion process for a CCLC, superimposed on a pressure-enthalpy diagram.

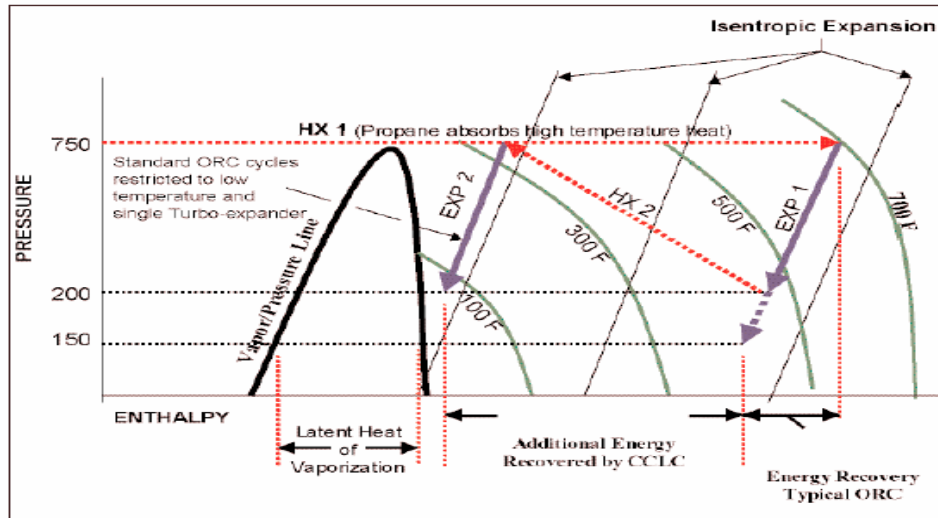


Figure 58
CCLC Pressure-Enthalpy Curve [101]

This graphic shows that nearly all the heat from the heat source is converted to power, resulting in final flue gas exhaust temperatures that are near-ambient

6.3. AVAILABILITY

The CCLC system uses commercially available turbo-expanders, heat exchangers and pumps, which can be sourced from numerous manufacturers. The CCLC system components have millions of hours of reliable and nearly maintenance free service, primarily in refineries and petrochemical plants. Turbo-expanders have been used for decades in thousands of applications and are used to drive generators, pumps and compressors in the most demanding of applications. Turbo-expander companies offer reliable turbo-expanders in both radial inflow (centrifugal) and axial configurations in sizes ranging from a fraction of a HP up to 50,000 HP [104]. Turbo-expanders are essential components in air separation plants; cryogenic processes; LNG plants; natural gas and propane pressure letdown applications; and for waste heat recovery systems. It is common to have two or more turbo-expanders driving a single generator, pump or compressor as shown on the right. The CCLC dual turbo-expanders can be connected to the generator through a common gearbox or connected to opposite ends of a double-ended generator or provided as two separate generators. WOW Energies estimates there are over 2000 MW of installed ORC turbo-expander driven electrical generation systems currently operating in refineries, petrochemical plants, air separation plants, LNG plants and geothermal plants. CCLC component manufacturers guarantee performance and provide warranties for their specific equipment, which can be sourced globally [104]. GE, for example, will guarantee the electrical output of the generator set consisting of skid mounted dual turbo-expanders with gearbox, electrical generator, lube oil system, controls, instrumentation and switchgear. GE, however, would expect a specific flow, pressure and temperature of propane vapor to be delivered to the dual expanders, just as they would expect a specific flow, pressure and temperature of steam to be delivered to a steam turbine. Heat exchanger and pump suppliers guarantee and warrant performance as well, based on a specific flow, pressure and temperature being supplied to their respective components. WOW Energies provides the process flow for the CCLC system, specifications for all the components and a guarantee for the total system.

Propane is a naturally occurring hydrocarbon and by-product of natural gas production and a common fluid used in petrochemical plants and refineries in refrigeration and waste heat recovery cycles. The use and distribution of propane is a major industry and the propane used in the CCLC closed loop system is the same as used by families for cooking and heating as well as a clean vehicular fuel for trucks, automobiles and forklifts. Propane storage tanks are prolific in remote locations where propane is used as a daily source of clean energy for industries and communities that do not have access to natural gas [105]. A CCLC system is similar to a gas turbine fuel gas compressor skid in terms of handling hydrocarbon vapors. Natural gas fuel for gas turbines requires compression to pressures equivalent to those used in the CCLC. However, unlike an open loop gas turbine fuel gas compressor system, the CCLC system is a hermetically sealed closed loop system and propane is neither consumed nor discharged to the environment.

6.4. DESIGN CONSIDERATIONS

At reduced temperatures, vaporized pollutants such as heavy metal oxides of mercury, vanadium, cadmium and lead are forced to condense and therefore can't be discharged to the atmosphere. CCLC component costs assume that the heat exchanger and exhaust ducting will be constructed of stainless steel since condensate will be acidic. The condensate continuously collected, neutralized and used in other processes or disposed of as per existing regulatory requirements. Flue gases containing high levels of both SO_x and NO_x currently require multiple emission reduction systems to remove pollutants. The primary systems in use today are Flue Gas Desulfurization (FGD) units for removal of sulfur compounds and Selective Catalytic Reduction (SCR) systems to remove nitrogen compounds. The need to install multiple systems to clean up flue gas pollutants is eliminated with the CCLC power generation system when combined with a Final Flue Gas Cleanup (FFGC). This inherent pollution reduction capability of the CCLC system combined with a FFGC system is a powerful and cost effective method to reduce emissions (See Figure 59) [106].

The FFGC consists of a multistage Wet Electrostatic Precipitator (WESP) with an integrated chemical additive system. Low flue gas temperatures are conducive to rapid and complete chemical reactions when using additives to oxidize nitrogen and sulfur compounds to convert these pollutants to fertilizers or stable salts. Environmental permitting is much easier for CCLC systems and can be done quickly. CCLC can use a variety of heat sources. However, many plants have multiple sources of waste heat that can be adjacent or located hundreds of feet apart. Unless these heat sources have a significant level of waste heat, it may not be practical to install a separate CCLC on each waste heat source. Other considerations include: the applicability of air-to-propane heat exchangers in line with the flue gas; some heat sources only have low-grade heat available; heat sources may consist of different mediums such as hot water, vented steam or a flue gas; and space constraints. For these applications, an alternate method of capturing heat is available using multiple fluid loops to bring the heat to the CCLC system.

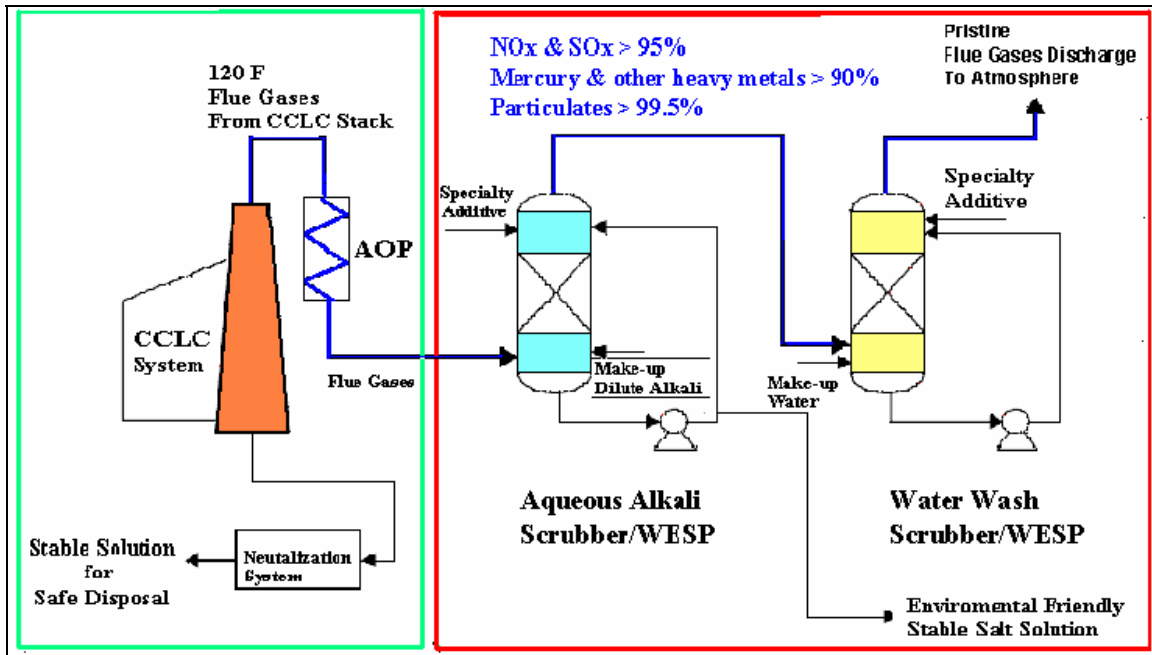


Figure 59
Final Flue Gas Cleanup FFGC integrated to CCLC

6.5. PROPOSED APPLICATION

The CCLC has three potential applications within the proposed sequestration schemes discussed in Parts III and IV. Because the CCLC only needs heat, potentially any source will suffice. Thus, it is not only possible to recover heat from a flue (gas stream as discussed above), but also from solar applications, and the output of other thermal cycles. The system is very flexible in its application. It could be used to cool flue gasses that are input to a biological reactor (depending on the type of power plant), to generate electricity in a thermo-solar application, and/or as an addition to a steam cycle to improve system efficiency and generate electricity for system components such as the compressors for well injection. The following is a discussion of the use for generating the electrical energy needed for compression in saline injection from and IGCC power plant.

6.6. ADDITION TO THE STEAM TURBINE CYCLE IN THE IGCC

Considering the evident ductility of this thermodynamic cycle, the CCLC could be employed to generate the energy necessary for the compression equipment in the saline injection. The CCLC can be added to the steam cycle inside the IGCC configuration.

Considering that the optimum steam turbine cycle works at a temperature range between 1300°C and 250°C and that the outlet temperature of the HRSG must be 60°C to maintain high system efficiency [24], it may be reasonable to apply a CCLC to recover the heat in the temperature range of 250°C and 60°C, represented in Figure 60. It is likely that the CCLC will be able to convert the heat energy at higher efficiencies than the steam cycle in this temperature range as can be seen in Figure 56. Optionally, the system could be applied to the condenser of the steam cycle to make use of Q2 in Figure 56. The optimum scheme would have to be found by modeling the system and integrating it into the IGCC design. This is beyond the scope of the

investigation. However, the case shown in Figure 60 was investigated for the purposes of demonstration.

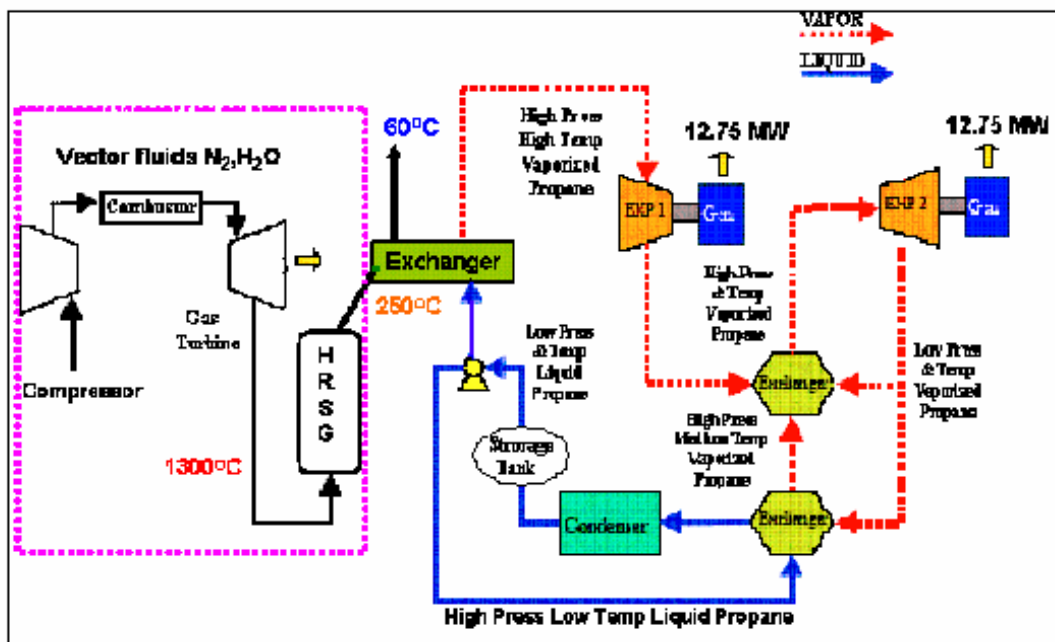


Figure 60
CCLC Proposed Addition to Steam Turbine Cycle

The stream coming from the HSRG will have a molar composition of 14.6% H₂O, 12.2% O₂, and 73.2% N₂ and a total flow rate of 94,248 kmol/hr [24]. The total heat energy available between 250°C and 60°C is 150 MWt. The heat recovery was modeled in Aspen Plus. The large amount of heat is due to the condensation of water in this temperature range. The flue gas is cooled to 60.8°C and the propane is heated to 169°C (336°F). The propane flow rate will be 245 kg/sec. From Figure 56 the efficiency value of the cycle at 336°F is approximately 20%. Furthermore it has been assumed that the turbines operate at an efficiency of 85%. Based on those assumptions the amount of produced electricity is 25.5 MWe. The remaining 75% of the heat energy (120 MWt) is dissipated at the condenser. This energy is sufficient to operate the compression equipment for saline injection.

7. SUMMARY AND CONCLUSIONS

Two scenarios were developed for sequestration of CO₂ from a 500 MW coal-fired power plant operating on an integrated gasification combined cycle process. Utilizing a photosynthetic bioreactor to sequester half of the CO₂ emissions has been shown not economically viable at the current market demand for algal biomass. However, because most of the costs involved scale directly with surface area (the size of the collector and the illumination plate area), the design could be fully modular and adjusted by parallel processing methods to any scale. Furthermore, the production costs from the current study would not be expected to rise significantly until the scale was reduced to at least 1/36 of the proposed size. This is due to the maximum practical volume of the bioreactors which is around 30,000m³. The current design calls for 36 such reactors operating in parallel. A 1/36th scale represents a CO₂ sequestration rate of 62 kt/year,

and a biomass production rate of 36 kt/year. Certainly, the production cost will be higher for lower scales because the size and cost of supporting equipment scales inversely with production volume. However, there is a great deal of room for production costs to rise at current market prices. It would be reasonable to expect that 1/10th of the current market (0.5 kt biomass/year) could be supplied by the proposed method for a cost that is far less than \$45,000/ton algal biomass. Thus this design is feasible under current market conditions and could be a significant technology for CO₂ sequestration as the market expands.

Alternatively, saline injection has been shown viable at full scale plant operation via a 10 well injection scenario. The injection scheme is conceptually shown to trap CO₂ hydrodynamically beyond the design period with little risk to aquifer integrity by pressure or chemical means. Hydrodynamic, solubility, and mineral trapping are quantified for the design period, and leakage of CO₂ through the shale caprock and local abandoned wells is shown to approach 0.05 percent of the total injected volume in a 20 year design scheme. Energy supply to the compression equipment was investigated via several possible origins. An economic analysis was performed for three cases: injection with energy supplied by CCLC, injection with purchased energy, and injection with energy from the plant. With a carbon dioxide credit of \$5/ton CO₂, the sequestration costs were \$14.9 million/year, \$10.3 million/year, and \$8.9million/year or \$2.93/ton CO₂, \$2.03/ton CO₂, and \$1.74/ton CO₂ respectively.

8. REFERENCES

1. Special Report on Carbon Dioxide Capture and Storage, in *Summary of Policymakers and Technical Summary*, B Metz, O Davidson, Hd Coninck, M Loos, and L Meyer, Editors. 2004, Intergovernmental Panel on Climate Change.
2. Shafeen, A, E Croiset, PL Douglas, and I Chatzis. CO₂ sequestration in Ontario, Canada. Part II: cost estimation. *Energy Conversion and Management*, 2004;**45**(20): 3207-17.
3. Freund, P and J Davidson. General overview of cost. IEA Greenhouse Gas R&D Programme. in *IPCC Workshop on Carbon Capture and Storage*. 2002. Regina, Canada.
4. Keith, DW, JA Giardina, MG Morgan, and EJ Wilson. Regulating the underground injection of CO₂. *Environmental Science & Technology*, 2005;**39**(24): 499A-505A.
5. West, J, J Pearce, M Bentham, and P Maul. Issue Profile: Environmental Issues and the Geological Storage of CO₂. *European Environment*, 2005;**15**: 250–9.
6. Wilson, EJ, TL Johnson, and DW Keith. Regulating the ultimate sink: Managing the risks of geologic CO₂ storage. *Environmental Science & Technology*, 2003;**37**(16): 3476-83.
7. Bruant, RG, AJ Guswa, MA Celia, and CA Peters. Safe storage of CO₂ in deep saline aquifers. *Environmental Science & Technology*, 2002;**36**(11): 240A-5A.
8. Klara, SM, RD Srivastava, and HG McIlvried. Integrated collaborative technology, development program for CO₂ sequestration in geologic formations - United States Department of Energy R&D. *Energy Conversion and Management*, 2003;**44**(17): 2699-712.
9. Farrar, C, J Neil, and J Howle, U.S. Geological Survey Water-Resources Investigations Report. 1999, U.S. Geological Survey.
10. Holloway, S. Storage of fossil fuel-derived carbon dioxide beneath the surface of the earth. *Annual Review of Energy and the Environment*, 2001;**26**: 145-66.
11. Hawkins, DG. No exit: thinking about leakage from geologic carbon storage sites. *Energy*, 2004;**29**(9): 1571-8.
12. Mintzer I, LJ, Schwartz P,. US Energy scenarios for the 21st century: Appendix B: Technology Assessments. 2003.
13. Friedmann, SJ, JJ Dooley, H Held, and O Edenhofer. The low cost of geological assessment for underground CO₂ storage: Policy and economic implications. *Energy Conversion and Management*, In Press, Corrected Proof.
14. Bachu, S. The potential for carbon dioxide sequestration in geological media in Alberta. in *Combustion and Global Climate Change: Canada's Challenges and Solutions*. 1999. Calgary, AB.
15. Reeves, S, Assessment of CO₂ sequestration and ECBM potential of U.S. coalbeds, in *Topical report for U.S. Department of Energy*. 2003.
16. Stevens, SH, VA Kuuskraa, D Spector, and P Riemer. CO₂ sequestration in deep coal seams: Pilot results and worldwide potential. in *4th International Conference on Greenhouse Gas Control Technologies*. 1998. Interlake, Switzerland.
17. Proceeding of workshop NETL Mineral CO₂ sequestration. 2001: National Energy Technology Laboratory.
18. O'Connor, WK, DC Dahlin, DN Nilsen, SJ Gerdemann, GE Rush, RP Walters, and PC Turner. Research status on the sequestration of carbon dioxide by direct aqueous mineral carbonation. in *18th annual international Pittsburgh coal conference*. 2001. Newcastle, Australia.

19. Guthrie, GD, JW Carey, D Bergfeld, D Byler, S Chipera, HJ Ziock, and KS Lackner. Geochemical aspects of the carbonation of magnesium silicates in an aqueous medium. in *NETL Conference on Carbon Sequestration*. 2001.
20. O'Connor, WK, DC Dahlin, DN Nilsen, GE Rush, RP Walters, and PC Turner. CO₂ storage in solid form: a study of direct mineral carbonation. in *5th international conference on greenhouse gas technologies*. 2000. Cairns, Australia.
21. O'Connor, WK, DC Dahlin, DN Nilsen, RP Walters, and PC Turner. Carbon dioxide sequestration by direct mineral carbonation with carbonic acid. in *25th international technical conference on coal utilization and fuel systems*. 2000. Clearwater, Florida.
22. O'Connor, WK, DC Dahlin, PC Turner, and R Walters. Carbon dioxide sequestration by exsitu mineral carbonation. in *Second Dixy Lee Memorial Symposium: Utilization of fossil fuel generated carbon dioxide in agriculture and industry*. 1999. Washington DC.
23. Lackner, KS. Carbonate chemistry for sequestering fossil carbon. *Annual Review of Energy and the Environment*, 2002;**27**: 193-232.
24. Soundarrajan, N, MA Hill, J Guo, R Sundararaman, HJ Kim, VG Dhar, O Mustafaoglu, and R Sundararaman. Towards an Optimal Design for Integrating CO₂ Capture and Fuel Conversion Technologies in a 500 MWe Coal-Based Power Plant. *EGEE* 580, 2006.
25. Stinger, D. Getting more power from waste heat. *Turbomachinery International* 2004.
26. Bayless, D, M Vis, G Kremer, and M Prudich, Carbon Dioxide Mitigation through Controlled Photosynthesis. 2000. p. 32.
27. Bayless, DJ, GG Kremer, ME Prudich, BJ Stuart, ML Vis-Chiasson, K Cooksey, and J Muhs. Enhanced Practical Photosynthetic CO₂ Mitigation. 2001.
28. Torzillo, G, B Pushparaj, J Masojidek, and A Vonshak. Biological constraints in algal biotechnology. *Biotechnology and Bioprocess Engineering*, 2003;**8**(6): 338-48.
29. Allen, DE, BR Strazisar, Y Soong, and SW Hedges. Modeling carbon dioxide sequestration in saline aquifers: Significance of elevated pressures and salinities. *Fuel Processing Technology*, 2005;**86**(14): 1569-80.
30. Ogbonna, J and H Tanaka. Industrial-size photobioreactors. *Chemtech*, 1997;**27**(7): 43-9.
31. Radmer, R, P Behrens, and K Arnett. Analysis of the productivity of a continuous algal culture system. *Biotechnology and Bioengineering*, 1987;**29**(4): 488-92.
32. Suh, IS and SB Lee. A light distribution model for an internally radiating photobioreactor. *Biotechnology and Bioengineering*, 2003;**82**(2): 180-9.
33. Anderson, S and R Newell. Prospects for carbon capture and storage technologies. *Annual Review of Environment and Resources*, 2004;**29**: 109-42.
34. Direct Ocean Sequestration Expert's Workshop, in *Final Report - US Dept. of Energy, National Energy Technology Laboratory*. 2001, US DOE and Monterey Bay Aquarium Research Institute. p. 1-59.
35. Chae, SR, EJ Hwang, and HS Shin. Single cell protein production of *Euglena gracilis* and carbon dioxide fixation in an innovative photo-bioreactor. *Bioresource Technology*, 2006;**97**(2): 322-9.
36. Doucha, J, F Straka, and K Livansky. Utilization of flue gas for cultivation of microalgae (*Chlorella* sp.) in an outdoor open thin-layer photobioreactor. *Journal of Applied Phycology*, 2005;**17**(5): 403-12.
37. Lee, HY, LE Erickson, and SS Yang. Kinetics and bioenergetics of light-limited photoautotrophic growth of *Spirulina platensis*. *Biotechnology and Bioengineering*, 1987;**29**(7): 832-43.

38. Bennewitz, P. Designing an apparatus for measuring bidirectional reflection/transmission. in *Optical Materials Technology XIII*. 1994: Fraunhofer Institute for Solar Energy Systems.
39. Stine, WB and M Geyer, Power From The Sun. www.powerfromthesun.net. 2004.
40. U.S. Solar Radiation Resource Maps. National Renewable Energy Laboratory. http://rredc.nrel.gov/solar/old_data/nsrdb/redbook/atlas/. 2004.
41. Annual Average Solar Irradiance NREL. www.nrel.gov/gis/images/us_csp_annual_may2004.jpg. 2004.
42. Mills, D. Advances in solar thermal electricity technology. *Solar Energy*, 2004;**76**(1-3): 19-31.
43. Solar-Cells. Wikipedia on-line encyclopedia. <http://en.wikipedia.org/wiki/solar-cells>.
44. Sun Power Corporation. <http://www.sunpowercorp.com/pdf/A-300.pdf>.
45. Hecht, E, Optics. 2nd Edition ed. 1990, Reading, Mass.: Addison Wesley. 676.
46. Fiberoptics transmission losses. Fiberoptics Technology Incorporated. <http://www.fiberoptix.com/technical/transmission-loss.html>.
47. Dewinter, F, Solar Collectors, Energy Storage, and Materials. Solar heat technologies. Vol. 5. 1990: The MIT Press Cambridge, Massachusetts. 1073.
48. Coventry, J. Performance of a concentrating photovoltaic/thermal solar collector. *Solar energy*, 2004;**78**: 211-22.
49. Feuermann, D, JM Gordon, and M Huleihil. Solar fiber-optic mini-dish-concentrators: First experimental results and field experience. *Solar Energy*, 2002;**72**(6): 459-72.
50. Mills, D. Advances in solar thermal electric technology. *Solar energy*, 2004;**76**: 19-31.
51. Feuermann, D and JM Gordon. Solar fiber-optic mini-dishes: A new approach to the efficient collection of sunlight. *Solar Energy*, 1999;**65**(3): 159-70.
52. Philipp, S and D Mills. Multi-Tower solar array. *Solar energy*, 2003;**75**: 249-60.
53. Pulz, O and W Gross. Valuable products from biotechnology of microalgae. *Applied Microbiology and Biotechnology*, 2004;**65**(6): 635-48.
54. Gasda, SE, S Bachu, and MA Celia. Spatial characterization of the location of potentially leaky wells penetrating a deep saline aquifer in a mature sedimentary basin. *Environmental Geology*, 2004;**46**(6-7): 707-20.
55. Michael, K and K Haug, Hydrodynamic Trapping of Injected Acid Gas in the Alberta Basin, Western Canada. 2005, Alberta Energy and Utilities Board - Alberta Geological Survey: Edmonton, Alberta.
56. Bachu, S and JJ Adams. Sequestration of CO₂ in geological media in response to climate change: capacity of deep saline aquifers to sequester CO₂ in solution. *Energy Conversion and Management*, 2003;**44**(20): 3151-75.
57. Bekele, E, M Person, B Rostron, and R Barens. Modeling secondary oil migration with core-scale data: Viking formation, Alberta Basin. *AAPG Bulletin*, 2002;**86**(1): 55-74.
58. Enick, R and SM Klara. CO₂ solubility in water and brine under reservoir conditions. *Chemical Engineering Communications*, 1990;**90**: 23-33.
59. Spycher, N, K Pruess, and J Ennis-King. CO₂-H₂O mixtures in the geological sequestration of CO₂. I. Assessment and calculation of mutual solubilities from 12 to 100 degrees C and up to 600 bar. *Geochimica Et Cosmochimica Acta*, 2003;**67**(16): 3015-31.
60. Gasda, S, CO₂ sequestration into a mature sedimentary basin: determining the capacity and leakage potential of a saline aquifer formation, in *Department of Civil and Environmental Engineering*. 2004, Princeton University. p. 121.

61. Ortoleva, PJ, P Dove, and F Richter. Geochemical Perspectives on CO₂ Sequestration. in *US Department of Energy Workshop on Terrestrial Sequestration of CO₂-An Assessment of Research Needs*. 1998. Gaithersburg, MD.
62. Gunter, WD, B Wiwchar, and EH Perkins. Aquifer disposal of CO₂-rich greenhouse gases: extension of the time scale of the experiment for CO₂ sequestering reactions by geochemical modelling. *Mineral. Petrol.*, 1997;**59**: 121-40.
63. Bachu, S, WD Gunter, and EH Perkins. Aquifer disposal of CO₂ - hydrodynamic and mineral trapping. *Energy Conversion Management*, 1994;**35**(4): 269-79.
64. Gunter, WD, EH Perkins, and I Hutcheon. Aquifer disposal of acid gases: modelling of water-rock reactions for trapping of acid wastes. *Applied Geochemistry*, 2000;**15**: 1085-95.
65. Lasaga, KR. Chemical kinetics of water rock interactions. *J. Geophys. Res.*, 1984;**89**: 4009-25.
66. Gunter, WD, EH Perkins, and TJ McCann. Aquifer Disposal of CO₂-Rich Gases: Reaction Design for Added Capacity. *Energy Conversion Management*, 1993;**34**(9-11): 941-8.
67. Xu, T, JA Apps, and K Pruess. Numerical simulation of CO₂ disposal by mineral trapping in deep aquifers. *Applied Geochemistry*, 2004;**19**(6): 917-36.
68. Damen, K, A Faaij, and W Turkenburg, Health, safety and environmental risks of underground CO₂ sequestration. 2003, Department of Science, Technology and Society Utrecht University: Utrecht, Netherlands.
69. Friedmann, SJ. Storing carbon in Earth. *Geotimes*, 2003;**48**(3): 16-20.
70. Lindeberg, E and D WesselBerg. Vertical convection in an aquifer column under a gas cap of CO₂. *Energy Conversion and Management*, 1997;**38**: S229-S34.
71. Zweigel, P, E Lindeberg, A Moen, and D Wessel-Berg, Towards A Methodology for Top Seal Efficiency Assesment for Underground CO₂ Stoarage. 2004.
72. Lindeberg, E. Escape of CO₂ from aquifers. *Energy Conversion and Management*, 1997;**38**: S235-S40.
73. Nordbotten, JM, MA Celia, and S Bachu. Analytical solutions for leakage rates through abandoned wells. *Water Resources Research*, 2004;**40**.
74. Nordbotten, JM, MA Celia, and S Bachu. Injection and storage of CO₂ in deep saline aquifers: analytical solution for CO₂ plume evolution during injection. *Transport in Porous Media*, 2005;**58**: 339-60.
75. Nordbotten, JM, MA Celia, S Bachu, and HK Dahle. Semianalytical solution for CO₂ leakage through abandoned well. *Environmental Science Technology*, 2005;**39**: 602-11.
76. Xu, T, JA Apps, and K Pruess. Mineral sequestration of carbon dioxide in a sandstone-shale system. *Chemical Geology*, 2005;**217**: 295-318.
77. Xu, T and K Pruess. Modeling multiphase non-isothermal fluid flow and reactive geochemical transport in variably saturated fractured rocks: 1. Methodology. *Americal Journal of Science*, 2001;**301**: 16-33.
78. Xu, TF, E Sonnenthal, N Spycher, and K Pruess. TOUGHREACT - A simulation program for non-isothermal multiphase reactive geochemical transport in variably saturated geologic media: Applications to geothermal injectivity and CO₂ geological sequestration. *Computers & Geosciences*, 2006;**32**(2): 145-65.
79. Pruess, K and J Garcia, Solutions of test problems for disposal of CO₂ in saline aquifers. 2003, Lawrence Berkeley National Laboratory. p. 44.

80. Pruess, K, T Xu, J Apps, and J Garcia. Numerical modeling of aquifer disposal of CO₂. in *SPE/EPA/DOE Exploration and Production Environmental Conference, Paper SPE 66537*. 2001. San Antonio, Texas.
81. Rutqvist, J, YS Wu, CF Tsang, and G Bodvarsson. A modeling approach for analysis of coupled multiphase fluid flow, heat transfer, and deformation in fractured porous rock. *International Journal of Rock Mech Min Sci*, 2002;**39**: 429-42.
82. Xu, T, E Sonnenthal, N Spycher, and K Pruess. TOUGHREACT - A simulation program for non-isothermal multiphase reactive geochemical transport in variably saturated geologic media: Applications to geothermal injectivity and CO₂ geological sequestration. *Computers and Geosciences*, 2006;**32**(32): 145-65.
83. Pruess, K, C Oldenburg, and G Moridis, TOUGH2 users guide, version 2.0. 1999, Lawrence Berkeley Laboratory Report p. 192 pp.
84. Pruess, K, J Garcia, T Kavscek, C Oldenburg, J Rutqvist, C Steefel, and T Xu. Code intercomparison builds confidence in numerical simulation models for geologic disposal of CO₂. *Energy*, 2004;**29**: 1431-44.
85. Pruess, K, T Xu, J Apps, and J Garcia. Numerical modeling of aquifer disposal of CO₂. in *Exploration and Production Environmental Conference*. 2001. San Antonio, Texas: SPE, EPA, DOE
86. Xu, T, JA Apps, and K Pruess. Reactive geochemical transport simulation to study mineral trapping for CO₂ disposal in deep arenaceous formations. *Journal of Geophysical Research*, 2003;**108**(B2): 2071.
87. Bachu, S. Screening and ranking of sedimentary basins for sequestration of CO₂ in geological media in response to climate change. *Environmental Geology*, 2003;**44**(3): 277-89.
88. Brady, BHG and ET Brown, *Rock mechanics for underground mining*, Second Edition. 1985, London: Chapman & Hall. 571.
89. Brown, ET and E Hoek. Trends in relationships between measured in-situ stresses and depth. *International Journal of Rock Mechanics and Mining Science*, 1978;**15**: 211-5.
90. O'Sullivan, MJ. A similarity method for geothermal well test analysis. *Water Resources Research*, 1981;**17**(2): 390-8.
91. Bolton, EW, AC Lasaga, and DM Rye. Long-term flow/chemistry feedback in a porous medium with heterogenous permeability: Kinetic control of dissolution and precipitation. *American Journal of Science*, 1999;**299**: 1-68.
92. Benson, S and P Cook, *IPCC Special Report on Carbon dioxide Capture and Storage*. 2005.
93. Smith, L, N Gupta, B Sass, T Bubenik, C Byrer, and PD Bergman, *Engineering and Economic Assessment of Carbon Dioxide Sequestration in Saline Formations*. 2001.
94. Das, GS and AS Khanna. *Corrosion Behavior Of Pipeline Steel In CO₂ Environment*. *Trans. of Indian Inst. of Met.*, 2004;**57**(3): 277-81.
95. Gunaltun, Y. *Carbon Dioxide Corrosion in Oil Wells*. Society of Petroleum Engineers, 1991.
96. *Joint Association Survey on Drilling Costs*. 2003, American Petroleum Institute.
97. Bloomfield, K and P Laney, *Estimating Well Costs for Enhanced Geothermal System Applications*. 2005, Battelle Energy Alliance.
98. *Carbon Sequestration, Technology Roadmap and Program Plan*. 2005, United States Department of Energy.

99. Holloway, S. Underground sequestration of carbon dioxide - a viable greenhouse gas mitigation option. *Energy*, 2005;**30**(11-12): 2318-33.
100. Stinger, D, System converts smokestack heat to electricity. www.NewScientist.com. 2004.
101. Stinger, D, Cascading Closed Loop Cycle (CCLC). 2004, Texas Energy Center.
102. Larjola, J. Electricity from industrial waste heat using high-speed organic Rankine cycle (ORC). *Int. J. Production Economics*, 1994;**41**: 227-35.
103. Stinger, D. Propane Heat Exchange Technology Would Harness Significant Waste Heat. . *Power Engineering* 2004.
104. Walker, G, Combined Heat & Power. www.enatec.com.
105. Stinger, D. New Electricity Technology Gathers S. *Houston Business Journal* 2004.
106. Stinger, D. Cascading Closed Loop CycleSM (CCLC) A Renewable Energy. *Meeting the World's Energy & Environmental Challenges*, 2005.

Appendix A

Literature Review

CO₂ Sequestration Team Critical Literature Review

EGEE 580

2/14/06

Joshua Taron
Apurba Sakti
Abdallah Abdel-Hafez
Mike Fitzgerald
Ojogbane Achimugu
Igor Faoro
Dirk Van Essendelft

Table of Contents

Team Objectives	A4
Planetary Sequestration: Common Issues	A5
Capture of CO ₂	A5
Compression Energy	A5
Transportation	A8
Injection	A9
Safety, Health and Environmental Risks	A10
Legal Issues	A11
Public Perception/Policy	A11
Geologic Sequestration: Coal Bed Sequestration	A13
Potential Storage Capacity and Methane Recovery Potential	A13
Confidence in Storage Integrity	A14
Environmental Impact and Public Perception	A15
Economic Viability	A15
Conclusion	A16
Geologic Sequestration: Oil/Gas Well Injection	A17
Geologic Sequestration: Deep Saline Aquifers	A20
General Process	A20
Suitable Aquifer Criteria	A21
Storage Capacity	A22
Conclusion	A22
Oceanic Sequestration: Active and Passive	A23
Active Sequestration Methods	A23
Residence Time for CO ₂ in the Deep Ocean	A24
Ecological Impact Considerations	A25
Offshore Disposal Distances	A26
Passive Sequestration Methods	A27
Public Opinion	A29
Biological Sequestration: Terrestrial Ecosystem	A30
Land Use Management	A30
Limitations and Uncertainties	A33
Conclusion	A33
CO ₂ sequestration by mineral carbonation	A35
Selection of minerals	A35
Alkaline solid wastes	A36
Pre-treatment	A37
Size reduction	A37
Magnetic separation	A37
Thermal treatment	A37
Direct carbonation	A37
Direct gas-solid carbonation with CO ₂	A37
Aqueous scheme	A37
Indirect carbonation	A38
HCl extraction route	A38
Molten salt process	A38

Wollastonite carbonation using acetic acid.....	A39
Dual alkali approach	A39
Thermodynamics.....	A39
Kinetics	A39
Dry carbonation	A39
Aqueous carbonation	A40
Economic and energetic consideration	A40
Economic consideration.....	A40
Energetic balance	A40
Biological Sequestration: Industrial-Bioreactor	A42
Microbial Selection.....	A42
Photobioreactor Systems.....	A43
Light Collection	A47
Thermal Pretreatment.....	A48
Cost Estimates.....	A48
Conclusion	A49
Team Conclusion	A49
References.....	A50

Team Objectives

As awareness of the increasing level of atmospheric CO₂ from anthropogenic sources progresses further into public consciousness, fear of possible consequences has fueled advancement toward the forefront of global environmental concerns. From this basis, the viability of newly constructed power plants is now, and will be increasingly so in the future, largely dependent upon an available method of sequestering a significant portion of the CO₂ it will generate. The need for technologies capable of accomplishing this task is apparent. Due to such necessity, the purpose of this study is to examine possible methods to sequester the CO₂ emitted from a 500MW power plant and to do so in the most efficient manner possible.

Method viability will be governed by several controlling criteria including the location of the power plant, sustainability of the sequestration method, environmental health and safety issues, potential storage capacity, public acceptance of the method, and economic viability. The sequestration methods include: biological fixation, planetary storage, and mineralization. Biological fixation methods include terrestrial-forestation, oceanic fertilization, and microbial fixation in industrial-bioreactors. Planetary methods include deep ocean injection, coal-bed injection, brine reservoir injection, and oil/natural gas injection. Mineralization methods include dry and aqueous mineralization.

Presented hereafter is a literature review, analysis, and discussion of sequestration methods by topic.

Planetary Sequestration: Common Issues

Geologic sequestration of anthropogenic CO₂ emissions is perhaps one of the most widely known methods of sequestration. Typically, geologic methods of sequestration involve the capture of CO₂ emissions from the waste streams of fossil-fuel burning power plants, as well as other high volume CO₂ producing plants. The captured gas is then purified to a more concentrated stream before it is subsequently compressed, where it can then be transported to a suitable disposal site. In the geologic medium, suitable disposal sites include: oil/natural gas wells which are either under producing or no longer in production; un-mineable coal seams; deep saline aquifers; and deep ocean methods where the liquefied gas is injected to the ocean floor where pressures are high enough to keep the liquefied CO₂ in its liquid phase. Each of these methods presents some unique benefits and challenges. Below is a more detailed discussion of the reviewed geologic methods.

Capture of CO₂

The estimated costs of CO₂ capture at large power plants are based on the engineering design studies of technologies in commercial use today. The three most efficient designs currently under evaluation are pulverized coal (PC), natural gas combined cycle (NGCC), and integrated gasification combined cycle (IGCC). Of these three designs, only the PC and IGCC are applicable for bituminous coals, the same fuel-source for the proposed 500 MW power plant.

The energy requirement for capturing the CO₂ from a PC design plant ranges from 24-40% (0.02-0.03, “2002 US\$”/kWh) of the energy value of the fuel stream. While an IGCC design plant has an energy requirement that ranges from 14-25% (0.01-0.02, “2002 US\$”/kWh) of the energy value for capture [1]. These capture costs include the cost of compressing the CO₂ (typically to about 11-14 MPa). System improvements in the future could reduce energy penalties to between 9-15%. These energy penalties result in an increase in the amount of fuel consumed for the same net output of energy. This results in an overall increase in the production of CO₂ that has to be sequestered. Based on current markets, an overall monetary cost estimate of CO₂ sequestration through deep ocean injection has been estimated to be around \$5-30/tCO₂ (2002 US\$) injected [1].

Compression Energy

The physical properties of CO₂ are relevant to its storage underground because they define the density at which it can be stored [2]. They are also relevant because large volume changes are associated with CO₂ phase changes, so it might be desirable to store CO₂ under physical conditions that are not close to the phase boundary conditions. Figure 1 shows the phase diagram of CO₂.

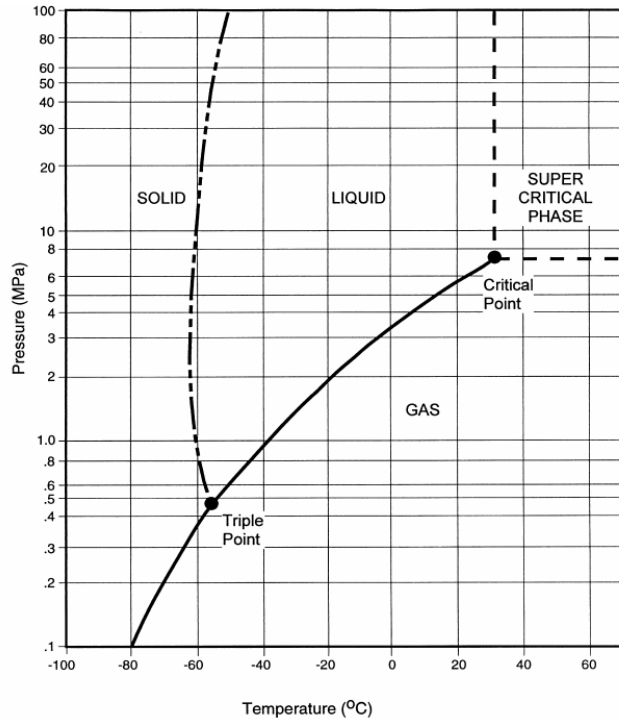


Figure 1
CO₂ Phase Diagram [3]

As is evident from the phase diagram, CO₂ occurs as a solid, a liquid, a gas, or a supercritical fluid. Above its critical temperature of 31.1°C and critical pressure of 7.38 MPa (72.8 bars), CO₂ exists in the so-called dense phase condition, i.e., as a supercritical fluid. A supercritical fluid is a gas-like compressible fluid in that it fills and takes the shape of its container, but it has liquid-like densities (0.2–0.9 g/ml). It is desirable to store CO₂ as a supercritical fluid because it would be much denser than the gas phase and therefore would occupy much less space in the subsurface. One tonne of CO₂ at a pressure of 10 MPa at a density of 700 kg/m³ occupies 1.43 m³, while at standard temperature and pressure, at the ground surface, one tonne of CO₂ occupies 509 m³ [4]. The extreme change in volume makes compression necessary for storage in a geologic medium.

Preliminary calculations were made to determine the energy required to compress CO₂ generated by the proposed 500MW power plant. There are two basic modes of compression: adiabatic and isothermal. Adiabatic compression is compression that takes place with no heat transfer ($dQ=0$). Isothermal compression is compression that takes place at constant temperature, therefore $dH=dU=0$. These two modes determine the compression energy. In practice, a single stage compression occurs very quickly. Because of this, there is little time for heat to be released from the fluid as it is compressed. For that reason, it is considered to be near adiabatic. If high pressures are needed, interstage cooling is used and several stages of compression are employed. In that way the compression becomes a mixture of isothermal and adiabatic. Isothermal compression is always less work than adiabatic, and real, multistage compression is bounded by those compression energies. Figure 2 shows the isothermal and adiabatic compression energy per mol for CO₂.

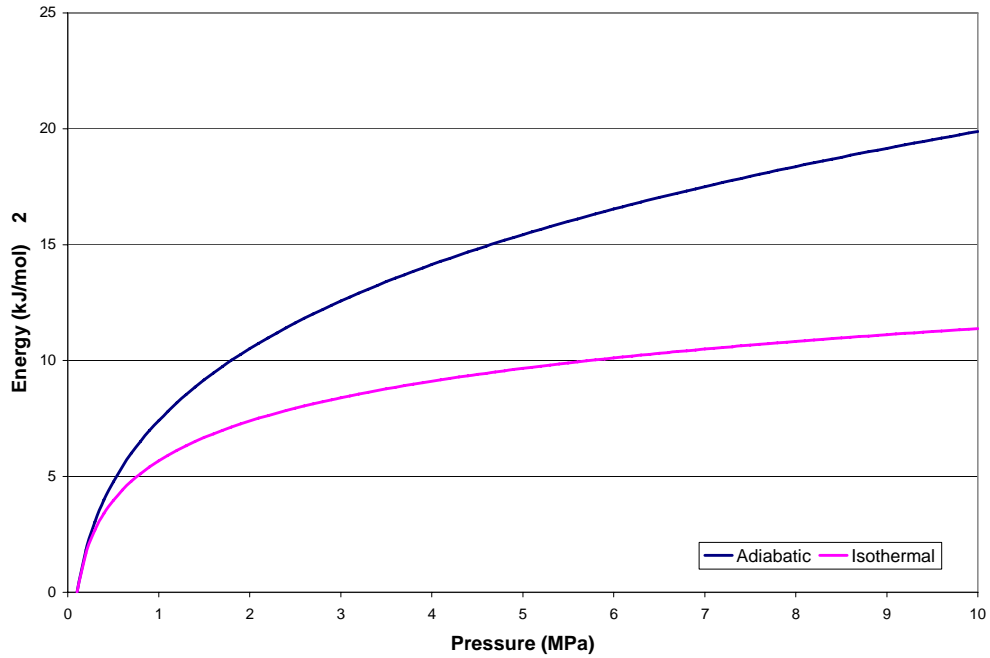


Figure 2
Compression Energy Boundaries

The compression pressure needed is offset by the depth of injection. If critical pressure is needed at the injection depth, the gravitational pull on fluid above the injection point will help to compress the gas. Figure 3 shows that as the injection depth increases, the compression needed at the surface decreases. The calculations were based on a compressible fluid.

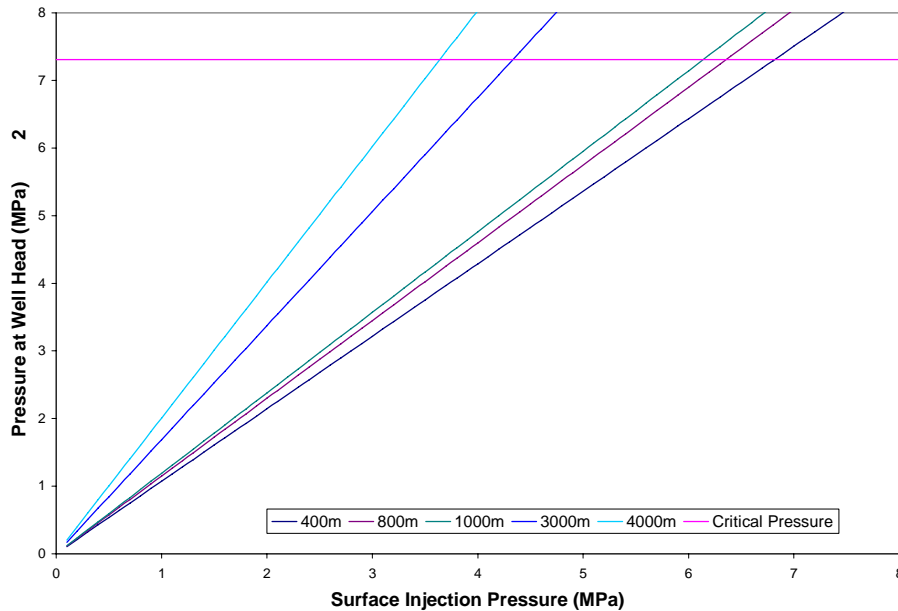


Figure 3
Pressure at Depth vs Pressure at Surface as a Function of Injection Depth

Transportation

It is preferred to transport the CO₂ at a pressure beyond its supercritical pressure threshold so as to avoid any two phase mixtures. This enhances liquid phase transportation and enhances the economic benefits. The operating pressure and temperature lies in between 8619 kPa at 4°C and 15,300 kPa at 38°C. The upper and lower limits are set, respectively, by the ASME-ANSI 900# flange rating and ambient condition coupled with the phase behavior of CO₂ [5]. Literature suggests that the CO₂ emissions from a 500 MW coal power plant will be approximately 10,000 to 14,000 ton per day which is equivalent to 53 to 83 m³/s [6]. For this a 14 to 16 inch diameter pipeline will be required. A larger diameter pipeline gives a higher margin of safety for occasional higher CO₂ flows.

For successful injection, the well pressure should be sufficiently higher than the reservoir in situ pressure. This often calls for the installation of booster compressor to enhance the pressure of the CO₂. The pressure should be high enough to penetrate the reservoir but not damage it. It should be typically 9–18% above the reservoir in situ pressure [5]. The pressure at the bottom can be determined as a function of the density of CO₂ at the different temperature and pressure, using compressibility factors. The graph shown in Figure 4 was generated by Hendriks [7] using the aforesaid method. It shows the change of the well head pressure along the injection tubing with the increase in the depth [5].

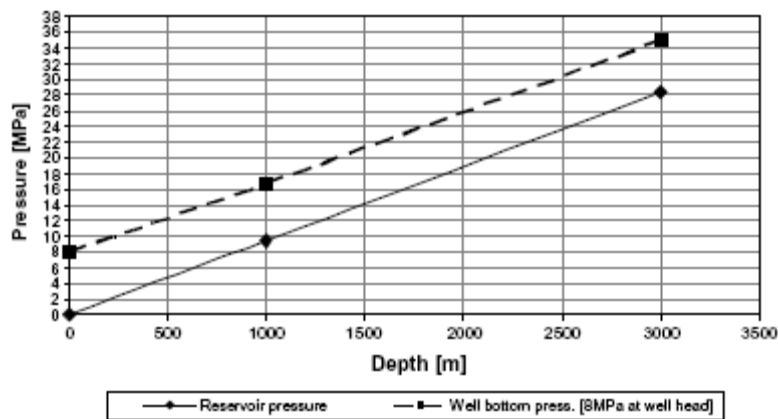


Figure 4

Well bottom and reservoir pressure at well head pressure of 8 MPa [5, 7]

Figure 5 shows the variation of CO₂ density along a pipeline with different inlet temperatures with initial inlet pressure of 15MPa and for isothermal and adiabatic conditions. This is representative of the condition without boosters.

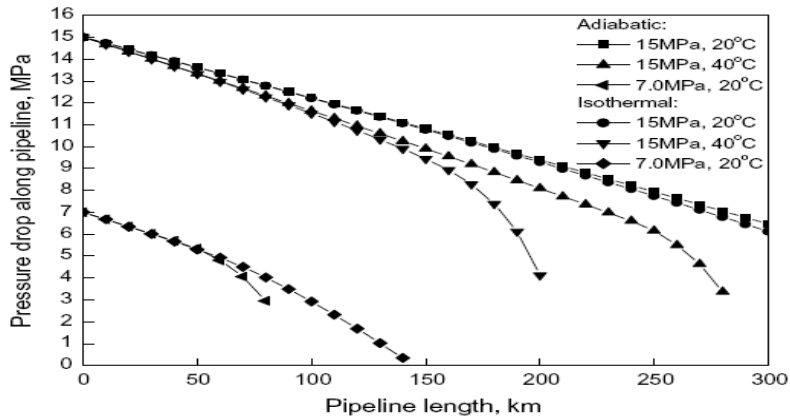


Figure 5

Pressure drop along pipeline at different pipe inlet conditions (without boosters) [8]

As is evident from the Figure 5, the lower temperature and higher pressure scenario allows the transport of the CO₂ to greater distances. At these conditions the CO₂ exists as a subcooled liquid. Simulation studies of the transport of CO₂ as a subcooled liquid have reported to increase energy efficiency by 9% (relating to the input work saved in keeping the state unchanged) [8]. However this is a very site specific option and will depend largely on the pressure needed at the point of injection, the distance from the point of CO₂ capture, and on the type of climate prevailing for the maintenance of low temperatures.

Another issue is the presence of townships and other local authorities. In such cases obtaining right-of-way for the pipelines may become more difficult. The CO₂ must also be dehydrated before it is transported because hydrated CO₂ is very corrosive and can shorten the life of the pipelines drastically [9].

Injection

The following equation can be used to determine the flow rate for injection: [5, 7]

$$q_s = \frac{\rho_r}{\rho_s} \times \frac{2\pi kh}{\ln\left(\frac{r_e}{r_w}\right)\mu} \times \Delta P$$

where q_s = flow rate (m³/s), ρ_r = density of the gas under reservoir conditions (700 kg/m³), ρ_s = density of the gas under standard conditions (1.95 kg/m³N), k = permeability of the reservoir, h = thickness of the reservoir, r_w = radius of the well (m), r_e = radius of the influence sphere of the injection well (m), μ = viscosity of CO₂ at the well bottom and ΔP = pressure difference between reservoir and well bottom pressure. As a rule of thumb, the value of the logarithmic term can be assumed as 7.5 [5, 10].

The ΔP term is a major source of uncertainty since it changes the flow rate and hence the number of injection wells and hence the cost. Figure 6a shows the sensitivity of flow rate and the number of injection wells on the pressure difference and Figure 6b shows the sensitivity of cost and number of injection wells on different flow rates.

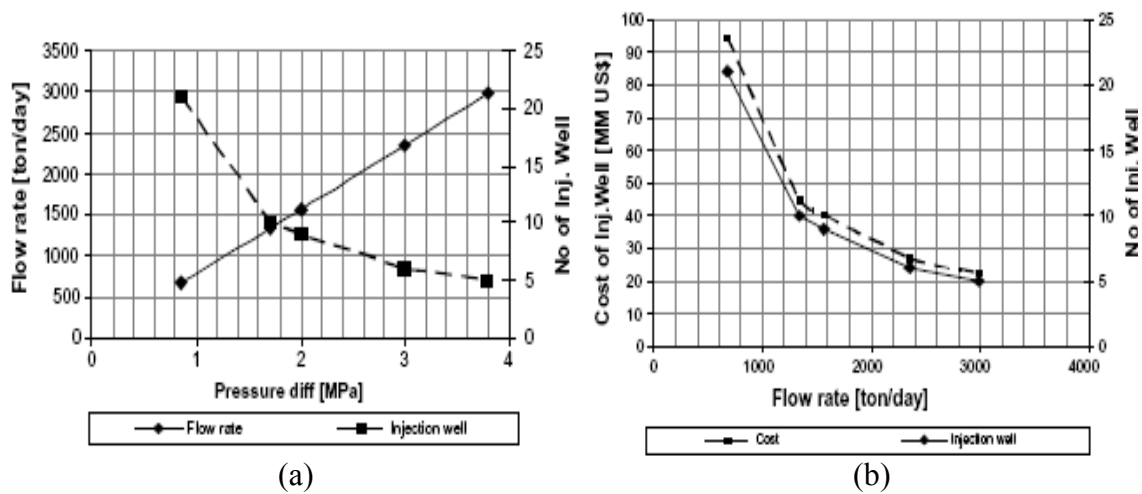


Figure 6

Sensitivity of flow rate and no. of injection wells on the pressure difference (a) and the sensitivity of cost of injection well and the no. of injection wells on the flow rate (b) [5]

Crucial to this analysis is the cost. Fortunately, the United States currently transports over 40 MtCO₂ across a total of 2500km of pipeline for use in Enhanced Oil Recovery (EOR) [11], and so the economics of this endeavor are well documented. The transportation costs for a chosen distance of 250km range from 1 to 8 US\$/tCO₂ with changes in mass flow rate [11]. At our rate of CO₂ emission, near 4.6 Mt/yr, the cost is narrowed to approximately 3 US\$/tCO₂/250km, or 13.8 million US\$/yr, and the cost increases significantly to near 32 US\$/tCO₂ at a distance of 3000km [11], or 147 million US\$/yr. Undoubtedly, transportation costs are a dominant concern, and in the case that a CO₂ source is not located near a possible injection site, will likely negate it as an option when compared to an alternate, ideal proximity technology.

Safety, Health and Environmental Risks

The geologic storage sites should be selected to minimize the potential for leakage. Although CO₂ at low concentrations is not directly hazardous to human health, it may detrimentally alter environmental processes [12]. Leakages could occur over small areas from discrete point sources, such as abandoned wells. Uncontrolled leakages would have widespread implications for the environment. Leakages might damage crops, groundwater quality and/or human and animal health. Other concerns include acidification, changes in biological diversity and species composition and asphyxiation at high CO₂ concentrations. In addition, biogeochemical processes may be affected as increased CO₂ concentrations could change pH, microbial populations and nutrient supply [12, 13].

The risks of geologic sequestration fall in two categories: Global and local risks. Global risks arise from leaks that return stored CO₂ to the atmosphere. Additionally, global risks involve the release of CO₂ that may contribute significantly to climate change. Moreover, the global risk may alternatively be viewed as uncertainty in the effectiveness of CO₂ containment [14].

Local risks are classified as hazards for things like humans, ecosystems and groundwater [11]. Local risks arise from the elevated CO₂ concentrations associated with the flux of CO₂ through the shallow subsurface to the atmosphere. Additionally, local risks occur as a result of the chemical effects of dissolved CO₂ in the subsurface. Moreover, local effects could arise from the displacement of fluids by the injected CO₂ [14]. If leakage to the atmosphere were to occur in low-lying areas with little wind, or in sumps and basements overlying these diffuse leaks, humans and animals could be harmed [11].

Catastrophic releases could occur as a result of a blowout of an injection well or existing well in the vicinity, or as a result of seismic disturbance [15]. Groundwater can be affected by CO₂ leaking directly into an aquifer or by brines displacement into overlying aquifers, with concomitant potential to contaminate potable water supplies. There may also be acidification of soils and displacement of oxygen in soils [16].

Risks can be minimized by the avoidance of vulnerable areas, monitoring of the injection process and CO₂ plume delineation. Remote sensing techniques and water quality analyses also may be explored for near-surface monitoring of injection sites and for detection of leaks. Seismic monitoring must be conducted to avoid potential seismic catastrophes [17].

Legal Issues

Legal issues are important because they give the framework by which the techniques must be implemented. At present however not many countries have developed such guidelines for onshore CO₂ storage. Long term liability issues need to be addressed like the transfer of information between institutions for long term monitoring of the wells. Essentially the legal framework for the successful working of long term sequestration needs to be drafted so that changing times and institutions do not in any way have an obliterating effect on the project. Also issues like the property rights need to be addressed since the pore space is owned by the surface property owners [11]. Also when it comes to issues involving more than one jurisdiction or sovereign powers, international treaties need to be in place so that the process is not stalled. Current treaties which address these are the UN Convention on the Law of the Sea, and the London and OSPAR Conventions [11]. However they are mainly for the protection of offshore environments.

Public Perception/Policy

Public perception is an interesting issue and is of significant importance. As yet, little has been published on the question of whether people will find CO₂ sequestration underground to be acceptable. Some [4] state that CO₂ removal, as a dedicated single technology, is an option that does not enjoy enthusiastic public support and conclude that these barriers can only be overcome by research and design and effective demonstration of the technology. It will not be possible to overcome them by communication alone. The IPCC report of 2005 states that two conditions will have to be met before the CO₂ sequestration is considered as a credible technology namely anthropogenic global climate change has to be regarded as a relatively serious problem and there must be acceptance of the need for large reductions in CO₂ emissions to reduce the threat of global climate change. Also people in business, government, or NGO's must seek out and hear objections raised by skeptics and come out with answers to them for this technique to be accepted [9, 18]. To further maximize by the advocacy community and the public, policymakers

will need to convince those sectors that the storage option is needed, that it will not crowd out more desirable strategies, and that it will perform effectively and safely [9].

With regards to policy related issues, geologic CO₂ storage capacity need to be seen and understood to be an investment in a nation or regions future economic and environmental well being in the way that estimates of hydrocarbon resources/reserves are viewed today. The potential to store CO₂ should be treated as a natural resource [19].

Geologic Sequestration: Coal Bed Sequestration

As previously presented, selection criteria for coal bed sequestration with enhanced methane recovery (ECBM) include potential storage capacity and methane recovery potential, confidence of storage integrity for the sequestration time-span, environmental impact, public health concerns and perceptions, and comparable economics. Each issue will be addressed independently in the following.

Potential Storage Capacity and Methane Recovery Potential

Assessing CO₂ storage capacity in a single, unmineable coal seam necessitates consideration of many site-specific parameters; including sorption pressure and volume, temperature, coal surface pH, water saturation, permeability, and the complex framework of the fractured, dual-porosity system. Transient conditional changes, such as permeability reductions and pH, temperature, and pressure variations, will also play a role. Among such transients, CO₂-induced coal swelling has been well documented [20-22] and, more recently, quantified under characteristics of coals in the San Juan Basin of Colorado and New Mexico, where pilot studies showed an extreme, approximately 99%, reduction in coal permeability with the onset of CO₂ injection [21, 23].

Expanding these considerations to the scale of national or worldwide storage potential must include such concerns in addition to proximity of each sink to the CO₂ source, accessibility of the location, and depth of injection. To the author's knowledge, no such analysis has been conducted on a worldwide scale. The study of Stevens [24] concluded in the finale 225 GT of worldwide storage capacity based on a broad sweeping assumption of 2:1 CO₂/CH₄ recovery potential. Nationally, however, the U.S. Department of Energy *Coal-Seq* project undertook a more rigorous analysis of national sequestration capacity. This analysis [25] included consideration of methane recoverability, CO₂ adsorption capacity distributed by coal rank, proximity of coal beds to CO₂ sources, and the care not to build CO₂ pressures above the in-situ CH₄ pressure. Location of U.S. coal seams sorted by rank and their proximity to CO₂ producing locations and 1000MW coal-fired power plants are shown in Figure 7.

Utilizing the CO₂ and CH₄ isotherm data from studies on the San Juan Basin [26], Black Warrior coal bed, Alabama [27], and the Powder River basin [28], sorption ratio as a function of coal rank, in percent vitrinite, was plotted as shown in Figure 8. The curve fit in Figure 8 is for the higher pressure case of 1000 psi, as to be reflective of unmineable coal bed conditions.

Conclusions of DOE's study [25] suggest approximately 90 Gt of national CO₂ sequestration capacity, including 38 Gt in Alaska. Referencing Figure 7, this quantity may be divided into 14 Gt for the Powder River basin, 10 Gt for San Juan, and 8 Gt for the Greater Green River basin. Alternately, ECBM recovery potential was estimated at approximately 150 Tcf including 47 Tcf in Alaska and divided into 20 Tcf for Powder River, 16 for San Juan, and 19 for Greater Green River. With approximately 2 Gt/year of CO₂ currently being emitted from U.S. power plants, the literature would thus suggest sufficient capacity exists for sequestration via ECBM. However, design of a sequestration system under conditions of a specific power plant will require full analysis of the specific site.

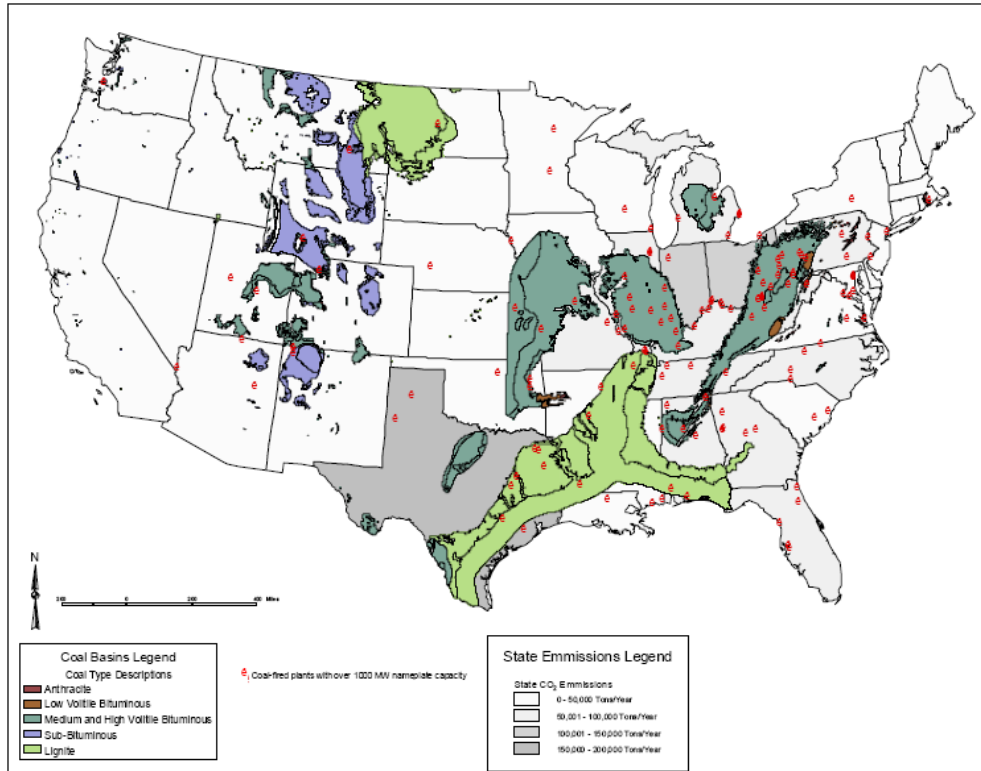


Figure 7

U.S. coal seams distributed by rank. High CO₂ emission states are shaded in light gray and >1000MW coal-fired power plants are indicated by red [25]

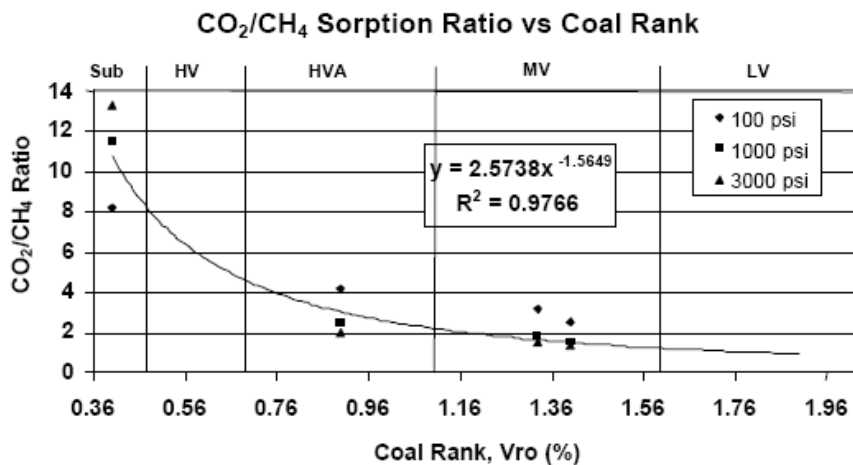


Figure 8

Sorption ratio as a function of coal rank, in percent vitrinite [25]

Confidence in Storage Integrity

To the author's knowledge, no study has yet been conducted on the volume of CO₂ lost from an injection reservoir. Of the possible mechanisms of leakage, pathways along existing wells and failure in cap-rock integrity present the most probable, for which Celia and Bachu [15] suggest probability in the former and Saripalli [29] favor the latter over a possibility of well-head failure. Alternately, Ha-Duong and Keith [30] present an economic analysis including the offset likely to

be incurred from an assumingly certain percentage loss of injected CO₂, but no independent and quantitative representation is presented. Of field studies currently underway in the San Juan basin [23, 31], the Ishikari coal field, Japan [32], and the Upper Silesian basin, Poland [33], none have made effort to confront the difficult task of monitoring any loss of CO₂ from the reservoir. Alternately, in the Fenn-Big Valley, Alberta, Gunter [34], suggest that the ultra-low permeability shale serving as caprock will prevent any slow leakage by such means.

Method integrity in this sense is harshly dependent upon the specific coal seam and the hydrodynamics of its caprock. As some leakage is likely by any number of means, determining an acceptable amount is necessary. In studies of possible surface leakage, Pacala and Hepple and Benson simultaneously conclude that a seepage rate of less than 0.1%/year is acceptable for stabilization of atmospheric CO₂ [35, 36]. Celia presented analytical solutions to leakage from abandoned or other wells, and suggest a high probability of leakage due the frequent existence of pre-existing wells in explored reservoirs [36]. This possibility will receive further, detailed attention in later submissions, but is beyond the scope of this literature review.

One additional consideration, pH in the subsurface environment as CO₂ concentrations increase can be expected to acidify under many conditions. The effects of such acidification on storage integrity will depend on subsurface composition and should not be excluded from consideration. As many coalbed waters are alkaline in their natural state, however, the influence of injected CO₂ may be minimal, but will depend on the geochemistry of each coalbed.

Environmental Impact and Public Perception

Beginning in April 2001, EPA oversaw a phase I analysis of drinking water surrounding various coalbed methane activities [37]. This study was in response to citizen concerns in Wyoming, Montana, Alabama, Virginia, Colorado, and New Mexico, with the highest concentration of citizen concerns from the San Juan, Black Warrior, Central Appalachian, and Powder River basins. EPA monitored water activity through document publication [37] in June 2004 and concluded that "...the injection of hydraulic fracturing fluids into coalbed methane wells poses little or no threat to USDWs and does not justify additional study at this time." Long term impact of ECBM activity on surrounding drinking water can, at present, only be postulated, but remains unlikely provided sufficiently low permeability in the caprock. However, that sufficient public concern warranted EPA study suggests a high probability of public resistance to ECBM activity now or in the future.

Economic Viability

Crucial to this analysis is the cost of transportation. Fortunately, the United States currently transports over 40 MtCO₂ across a total of 2500km of pipeline for use in EOR [11], and so the economics of this endeavor are well documented. These pipelines operate under elevated pressure and ambient temperature in the "dense phase mode" [11], where no distinct phase change occurs in the continuous progression from gaseous to liquid phase. Under such conditions, transportation costs for a chosen distance of 250km range from 1 to 8 US\$/tCO₂ with changes in mass flow rate [11]. At our rate of CO₂ emission, near 4.6 Mt/yr, the cost is narrowed to approximately 3 US\$/tCO₂/250km, or 13.8 million US\$/yr, and the cost increases significantly to near 32 US\$/tCO₂ at a distance of 3000km [11], or 147 million US\$/yr. Undoubtedly, transportation costs are a dominant concern, and in the case that a CO₂ source is not located near a possible injection site, will likely negate it as an option when compared to an alternate, ideal

proximity technology. Capture costs will also be of primary concern, but will not be addressed here as they are presented elsewhere in this literature review (see Ocean Sequestration).

Cost of CO₂ injection to depths of approximately 1000m will pose the dominant portion of sequestration costs. A detailed discussion of CO₂ critical state and compression topics was presented previously (see sections on EOR and brine injection), and so a brief but well developed (in its components) economic analysis is called for.

Via the same methods used to estimate potential storage capacity above, Reeves [25] provided a thorough economic analysis of national CO₂ sequestration capacity. This analysis suggests that 25-30 Gt of CO₂ can be sequestered at a profit, while the next 80-85 Gt can be sequestered for below US\$5/ton, excluding transportation and capture. On a larger scale, Stevens [24] estimated 5-15 Gt of CO₂ may be injected at a profit, 60 Gt at less than US\$50 per ton, and 150 Gt at between US\$100 and US\$120 per ton on a worldwide basis. Again, this analysis utilized a CO₂/CH₄ ratio of 2:1.

Conclusion

At its current state, literature review of ECBM-CO₂ suggests viability from a retracted viewpoint. In the event that a precise location for the CO₂ source is known, this information would likely be a show-stopper or proponent of ECBM, depending on proximity to other sequestration options. Attention to more specified details of the ECBM process, such as analytical and numerical analyses of the dual porosity and thermodynamic system, will be required for further advancement of this research assessment. The decision to conduct such analyses is pending information from alternate sequestration options.

Geologic Sequestration: Oil/Gas Well Injection

CO₂ can either be sequestered in a depleted oil/gas well or it can be co-optimized with the process of enhanced oil recovery (EOR) or enhanced gas recovery (EGR). It is estimated that the storage capacity of depleted and active fossil fuel reservoirs could be as high as 900 billion metric tones of CO₂ equivalent worldwide. Depleted oil fields and EOR fields offer a storage capacity of approximately 130 Gt of CO₂ [38].

More than a century of intensive petroleum exploitation has left thousands of oil and gas fields near the end of their lives [39]. Some of these exhausted fields could act as storage sites for CO₂. It follows the concept that because there were hydrogeological conditions that led to the trapping of hydrocarbons, the same conditions will allow the sequestration of CO₂ in the space vacated by the recovered hydrocarbons [39, 40]. Depleted hydrocarbon reservoirs which have been invaded by water offer limited storage capacity, since the CO₂ will have to displace the water, as such underpressured oil reservoirs that have not yet been invaded by water offer greater and better sequestration potentials. In the case of depleted gas reservoirs, they can be regarded as excellent geological traps for CO₂ storage [39, 40]. There is large capacity for storage since the primary recovery in the case of gas wells is to the tune of 95% whereas it is around 5-40% in the case of oil fields [39, 41]. The good thing about this concept is that it repressurizes the wells back to their original pressures. Also the geologic data for these sites are well established and the surface and down-hole infrastructure used for the hydrocarbon recovery can be used for the sequestration. However currently the option of sequestration into depleted oil/gas reservoirs doesn't have many buyers because of the fact that it is not economically beneficial and also because of the fact that the reservoirs may still have oil/gas reserves that haven't yet been recovered using the contemporary technology [16, 41].

This leads to the concept of carbon sequestration through enhanced oil recovery (CSEOR) and through enhanced gas recovery (CSEGR) which offers more economic feasibility.

The petroleum industry has been injecting CO₂ into underground formations for several decades to improve oil recovery from light and medium oil reservoirs [40]. Supercritical CO₂ acts as a powerful solvent reducing the viscosity of the oil and making it more mobile. The traditional approach is to reduce the amount of CO₂ injected per barrel of oil produced. For a sequestration process, however, the aim is to maximize both the amount of oil produced and the amount of CO₂ stored. This calls for the co-optimization of both the processes. To reduce atmospheric CO₂ the source of CO₂ for EOR should be anthropogenic and not natural reservoirs.

With regards to EGR, reservoir simulation and laboratory studies have suggested that injecting CO₂ into mature natural gas reservoirs for carbon sequestration with enhanced gas recovery (CSEGR) is technically feasible. Reservoir simulations show that the high density of CO₂ can be exploited to favor displacement of methane with limited gas mixing by injecting CO₂ in low regions of a reservoir while producing from higher regions in the reservoir [42].

In the case of EOR, an analysis on the Permian Basin of West Texas has shown that the greenhouse gas emissions generated by the combustion of gasoline from the additional oil produced would almost be offset by CO₂ storage in the reservoir. Table 1 shows the summary of their findings.

Table 1
EOR Injection Statistics [38]

	CO ₂	CH ₄
injected	5.5	0.29
emitted	0.4	1.5×10^{-3}
emissions avoided (Figure 2 A)	2.6	0.29
storage capacity	3	0.1
net storage	2.6	0.1

As shown in Table 1 the net CO₂ storage is 2.6kg/kg of oil produced which amounts to 4.5kg of CO₂ per kg of gasoline taking into consideration the production ratio of gasoline from crude oil. When the average emission from a car is considered to be 380g CO₂/km traveled the net emission amounts to 4.8 kg of CO₂/kg of gasoline consumed as is stated by the authors of this work [38].

However considering the fact that Europe aims at reducing the emissions to 120g/km [21] and co-optimization strategies for sequestering more amount of CO₂ per kg of incremental oil produced, it will mean that a lot more CO₂ will be sequestered than generated.

This brings us back to the critical issue of co-optimization of storage and recovery. A variety of injection scenarios are being considered to increase the amount of CO₂ sequestered to the amount of incremental oil being produced. Among them are gas injection after water flooding (GAW), water-alternating-gas drive (WAG), gas injection with active production and injection well constraints (well control or WC), switch from solvent gas injection to pure CO₂ injection. GAW and WAG resemble conventional oil recovery methods. “Gas injection after water flooding represents a project where water is used to maintain pressure and drive oil from the reservoir. After some volume of water injection, the project is converted to gas injection as a means of sequestering CO₂. The WAG scheme injects water and CO₂ in alternating slugs. The water helps to reduce the mobility of CO₂ within the reservoir, making CO₂ a more effective displacement agent. The more dense water sweeps the lower portions of the reservoir while the more buoyant gas sweeps the upper portions. The third scheme aims to maximize the mass of CO₂ injected while not reducing oil recovery. The well control parameters are the producing gas–oil ratio (GOR) and the injection pressure, where the producing GOR is the volumetric flow rate of gas produced upon the oil production rate. The final scheme employs initially a solvent gas that is rich in light hydrocarbon components. Miscibility of the injection gas with the oil leads to excellent recovery. Later, during injection, the solvent gas is switched to pure CO₂. This helps to reduce the volume of relatively expensive solvent required and promotes recovery of the hydrocarbon gas components as well as leading to maximum concentration of CO₂ in the gas filled pore space. Wells are operated as in the well control scenario. [43]. This increases sequestration by 7-12% as compared to the other schemes.

Literature review of a report published for cost analysis has indicated that for the case of coal powered plants cogeneration concepts together with process optimization strategies can bring down the cost of CO₂ to around \$0.50 to \$ 2.00/mscf and assuming this to be \$1.25 the cost of a barrel of incremental oil produced will be \$18 which indicates definite room for profit (all values

in Canadian dollars, 1992) [44]. There is however considerable variation in the costs stated in literature which is understandable since the process depends on a lot of factors which vary the cost for different cases. The main cost is incurred in the capture and compression of CO₂ and as per a 2005 report range in between US\$25-40/t CO₂ for an integrated gasification combined cycle (IGCC) plant [19]. The cost of transportation and injection vary from US\$0 to \$15.3/t CO₂ [5, 19]. Gentzis in his analysis report of CO₂ sequestration in Alberta in 2000, Canada states that the cost can be as high as US\$56/t C [40]. In a 2005 report, CSEGR for a particular field in California is reported to be economically feasible with CO₂ supply costs of up to US\$ 4–12/t (US\$ 0.20–0.63/Mcf) [19]. The IPCC report of 2005 states that the cost for storage to be typically between 0.5–8 US\$/tCO₂ injected and the monitoring costs of US\$ 0.1–0.3 /tCO₂ are additional. When storage is combined with EOR or EGR, the economic value of CO₂ can reduce the total cost of carbon capture and storage (CCS) and based on data and oil prices prior to 2003 (\$15-20/ barrel), enhanced oil production for onshore EOR with CO₂ storage could yield net benefits of 10–16 US\$/tCO₂ (37–59 US\$/t C) [11] which definitely adds to its feasibility.

Geologic Sequestration: Deep Saline Aquifers

Deep saline aquifers represent an attractive option for CO₂ sequestration. These aquifers are wide spread and underlie many parts of the world, which in turn reduce the costs of infrastructure associated with pipeline construction. The storage capacity accompanied with this option is high [45]. Residence time in saline aquifers is long ranging from hundreds to several thousands years [5]. Such aquifers are typically not suitable for irrigation and other uses, so injection of CO₂ has limited environmental impacts and less likely to present a problem for potential future use [16]. Furthermore, these aquifers are often close to stationary point-source CO₂ emission sites [15]. Availability of subsurface rights makes this option more viable [46]. Moreover, deep saline aquifers sequestration has general public acceptance and mature technology [3].

General Process

CO₂ is injected through well or wells into a permeable and porous saline aquifer that covered with impermeable cap layer located at suitable depth that enables storing the CO₂ beyond the critical condition, temperatures greater than 31.18C and pressures greater than 7.38 MPa. As seen in Figure 1, at this condition CO₂ behaves still like a gas by filling all the available volume, but has a liquid density that increases, depending on pressure and temperature, from 200 to 900 kg/m³ [47]. Some of the injected CO₂ (up to 29%) will dissolve in the water and the rest will form a plume that will over-ride at the top of the aquifer [3]. A minimum depth of 800 m is necessary for CO₂ to remain in its critical state, this depth may vary according to the location of the aquifer and the subsurface temperature and pressure gradient [5].

The solubility of CO₂ at ground-surface conditions, in pure water is about 1.7 kg CO₂/m³, and this solubility increases at the critical conditions to reach 35 kg/m³ with 15% total dissolved solids by mass [15], Figure 9 shows the variation of liquid CO₂ density as a function of temperature and pressure.

Upon injection into saline aquifers, CO₂ may be stored by one or more of three processes, hydrodynamic trapping, solubility trapping, or mineral trapping [15]. The most critical concern of hydrodynamic trapping is the potential for CO₂ leakage through imperfect confinement. Solubility trapping is not subject to buoyancy and is therefore less likely to leak. In mineral trapping, CO₂ is stored for very long periods by conversion into carbonate. Solubility and mineral trapping are the most important long term solutions to CO₂ sequestration in geologic media [48] these trapping processes shown in Figure 10.

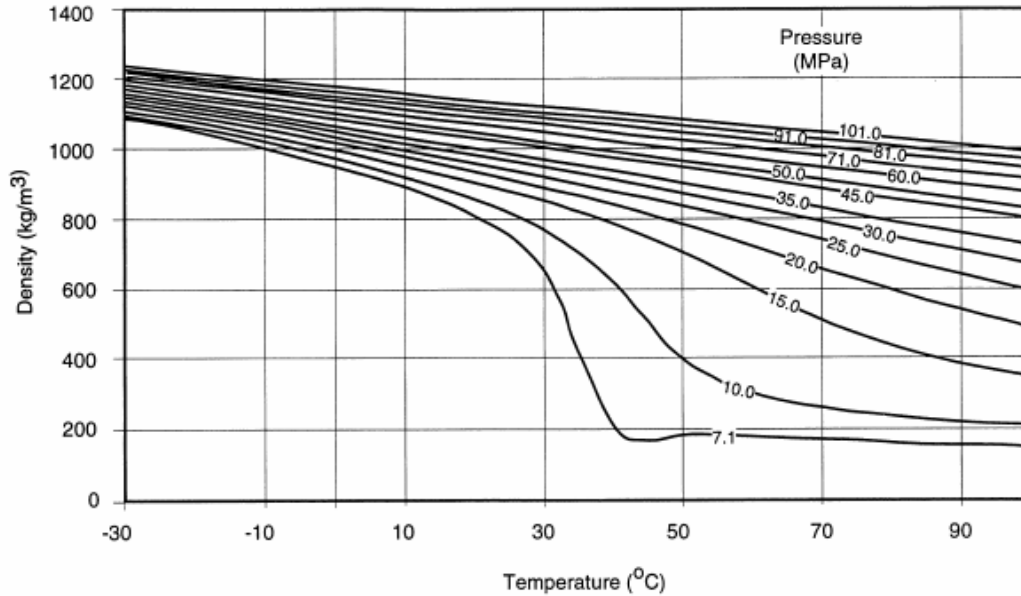


Figure 9
Variation of liquid CO₂ density as a function of temperature and pressure [3]

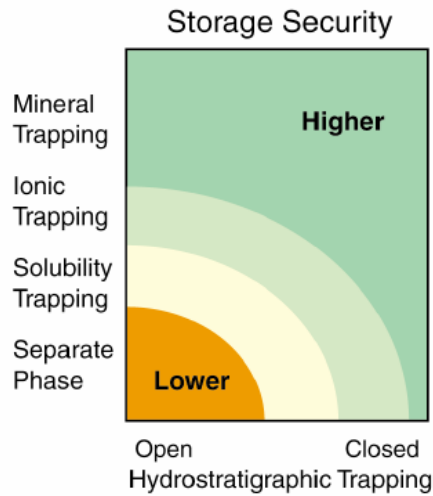


Figure 10
Physical and geochemical processes that enhance storage security [35]

Suitable Aquifer Criteria

Most studies suggest that adverse effects can be mitigated by choosing suitable locations [36]. The target aquifer should have a minimum 800 m depth, which represents the threshold depth for CO₂ injection, based on the average pressure and geothermal gradient, which 10 MPa /km and 25- 30 C°/km respectively, Figure 11 shows the subsurface temperature and pressure gradients for the Michigan basin [5].

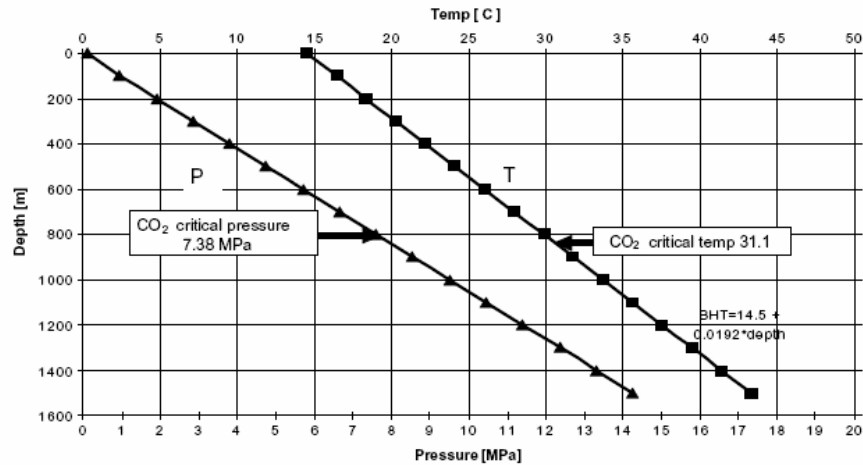


Figure 11

Subsurface temperature and pressure gradients for the Michigan basin [5]

A suitable aquifer has high pore space volume and high permeability, is stable in terms of seismicity and tectonic setting and has no major faulting or fracturing. The aquifer should be capped by an extensive aquitard (shales) or aquiclude (salt and anhydrite beds) to ensure CO₂ sequestration and prevent its escape into overlying layers which could contain fresh water, and ultimately to the surface [15].

Storage Capacity

Storage capacity represents the maximum amount of CO₂ that can be sequestered in an aquifer without undesirable effects, such as an unacceptable rise in the aquifer pressure, contamination of potable water by CO₂ or by displacement of the saline/fresh groundwater interface, and escape of CO₂ into the atmosphere via an unidentified migration pathway through the cap rock [47].

Storage capacity depends mainly on the area of the aquifer and its thickness, permeability, porosity and CO₂ solubility. The solubility of CO₂ in water varies according to the degree of salinity as well as according to temperature and pressure [5]. Globally, deep saline aquifers offer the greatest storage capacity, estimated between 300 and 10,000 GtCO₂ [15].

Conclusion

Most of the adverse effects can be mitigated by choosing suitable location. This can be achieved by conducting proper geophysical and hydrogeological studies and investigations. Once the suitable target aquifer has been located, the risks accompanied with this method will be minimized. Deep saline aquifers have, by far, the largest potential for CO₂ sequestration in geological media in terms of volume, duration, economics and minimum or null environmental impact [3].

Oceanic Sequestration: Active and Passive

The oceans are very vast covering 71% of the earth's surface and with an average depth of around 3,800 meters they present a large potential reservoir for storing CO₂ emissions generated by the burning of fossil fuels for energy. To date, a lot of research has gone into understanding the oceans and whether they will make a good sequestration option for CO₂. Presented below is a summary of some of the good's, bad's, and unknown's related to oceanic sequestration of anthropogenic CO₂.

On planet earth, the oceans represent the largest global reservoir of carbon; containing approximately 40,000 Gt of carbon, primarily in the inorganic form of bicarbonate [49]. Carbon enters the ocean in many forms, one of which is CO₂, through naturally occurring runoff, direct diffusion, and biological uptake processes. The component of runoff adding to the carbon in the ocean will not be considered here. The direct diffusion process is an equilibrium process between the atmosphere and the ocean waters. As the concentration of atmospheric CO₂ increases, a gradient emerges for the atmospheric CO₂ to be "forced" into the ocean. In fact, at present there is a current flux of about 7 GtCO₂ per year of CO₂ going in to the oceans; with the oceans having already taken up about 500 GtCO₂ of the 1,300 GtCO₂ anthropogenic emissions released to the atmosphere over the past 200 years [1]. One of the main problems with this is that the process is occurring is too slow for today's needs. Remember at present human activity is accounting for the production of about 23.5 GtCO₂/year (from year 2000) [1]. To increase the rate of sequestration in several mechanisms have been suggested as potentially viable methods of sequestering the CO₂ from the atmosphere. Reviewed in this literature survey are the findings of proposed methods that appear to have some merit, and include both active and passive means. The active means reviewed include capturing the CO₂ emissions from point sources, such as fossil fuel burning power plants and cement factories, and injecting it into various depths of the ocean in either liquid or gaseous phases. Passive means reviewed are through direct diffusion and biological uptake by marine organisms. All the proposed methods provide benefits as well as negatives and involve the understanding of key issues involved with each option.

Active Sequestration Methods

Active sequestration methods involve the capture of CO₂ being emitted at point sources and then its subsequent injection into the ocean. Proposed methods include injecting the compressed emissions in a gaseous phase to the shallow ocean (depths less than 1000 meters) where it is expected to diffuse into the water column and react to form bicarbonates. This method was briefly reviewed and subsequently deemed not reliable as a sequestration method by the authors, due to its lack of supporting evidence that it will work and the assumed potential for early re-release to the atmosphere. A more reliable method of active ocean sequestration is through injection of the CO₂ in a liquid phase via a pipeline to the deep ocean (depths greater than 3000 meters) [1, 49]. At depths greater than 3,000 meters the liquefied CO₂ will remain in a liquid-phase form and has the potential to stay sequestered for a long period of time. CO₂, as mentioned in a preceding section, will be at its critical point at pressures greater than 7.38 MPa. The following figure, Figure 12, represents the density of seawater and the density of liquid CO₂ at various depths in the ocean.

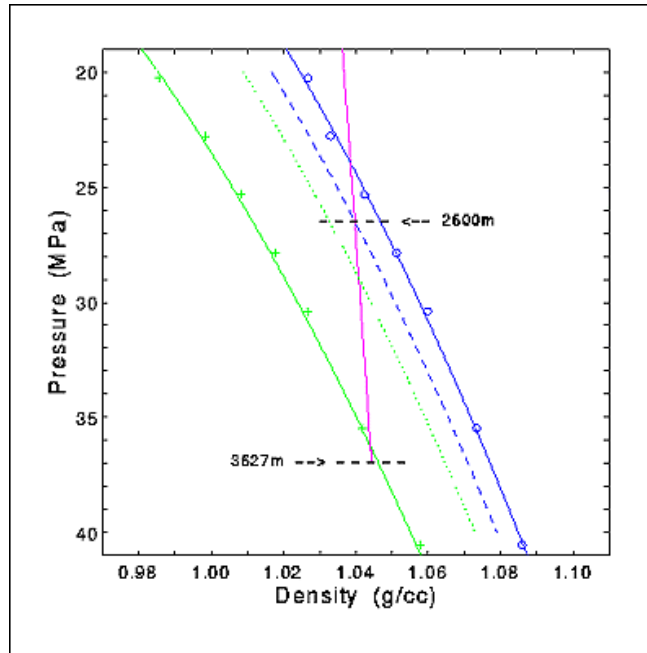


Figure 12

The magenta line represents the density of sea-water, and the other lines represent liquid CO₂ at 10°C, 4°C, 2°C, and 0°C from left to right, respectively [50]

As illustrated in Figure 12, the density of liquid CO₂ is less than sea-water up to about 2,600 meters in depth, assuming the sea-water is 2°C, a reasonable assumption. Below this depth, the density of liquid CO₂ surpasses that of the seawater; meaning that the compressed CO₂ injected at or below 2,600 meters depth will be denser than the surrounding waters and will sink to the ocean floor. The target depth generally proposed is at least 3,000 meters to ensure sufficient depth below the neutrally buoyant depth of 2,600 meters [50, 51]. For reference the density of CO₂ at 3,000 meters is 1.06 g/cc and the density of the surrounding seawater is 1.04 g/cc, at a pressure of 30.6 MPa.

The key issues involved with this methods of sequestration are: the additional energy required to capture and compress CO₂ to liquid phase; the effect that injecting the CO₂ will have on the oceans pH levels as well as marine organism; the residence time that one can assume the CO₂ will be effectively sequestered from the atmosphere; and the costs/energy associated with getting the CO₂ to a suitable location in the ocean.

Residence Time for CO₂ in the Deep Ocean

The length of time with which CO₂ will stay sequestered in the deep ocean has been largely debated by, with estimates ranging from only a few hundred years to a few thousand years, depending on the method in which CO₂ was deposited into the ocean. If the CO₂ is released below 3,000 meters it will sink and form a “lake” in depressions in the oceans floor. In this scenario, a retention time of more than a thousand years has been assumed, barring any catastrophic releases. Which in turn do not appear likely due to the fact that the density of the CO₂ is greater than seawater at that depth. Upwelling of the liquid CO₂ from the “lakes” will likely result in the subsequent settlement further down current, and should reduce the likelihood that the CO₂ will be released early from the ocean floor. In addition, hydrate layers will form on

the surface of CO₂ droplets above 44.5 bars (4.45 MPa) and below 10°C (conditions present at depths of 500m or greater) [52]. The hydrate layer will act as a barrier against the dissolution of the liquid-phase CO₂ into the surrounding seawater. Table 2 provides an estimate of the fraction of CO₂ retained for ocean storage at given depths of injection; based on a summary of seven ocean models as presented in the Technical Summary of the IPCC Special Report on CO₂ Capture and Storage [1]:

Table 2
Retention time of CO₂ injected in the ocean at different depths

Year	Injection depth		
	800 m	1500 m	3000 m
2100	0.78 ± 0.06	0.91 ± 0.05	0.99 ± 0.01
2200	0.50 ± 0.06	0.74 ± 0.07	0.94 ± 0.06
2300	0.36 ± 0.06	0.60 ± 0.08	0.87 ± 0.10
2400	0.28 ± 0.07	0.49 ± 0.09	0.79 ± 0.12
2500	0.23 ± 0.07	0.42 ± 0.09	0.71 ± 0.14

As shown in Table 2, the CO₂ will be sequestered for a much longer percentage of time if injection is below 3,000 meters. However, this also shows that after about 500 years about 21% of initial CO₂ injected into the deep ocean will have escaped back to the atmosphere.

Ecological Impact Considerations

High concentrations of CO₂ in the atmosphere or direct sequestration of CO₂ in the oceans can influence the pH level in ocean water. Current research already indicates that the pH of the shallow ocean has decreased by 0.1 units, over the past 200 years, due to the natural diffusion of atmospheric CO₂ into the ocean [1], and has the potential to decrease even more over the next several centuries, based on current projections of CO₂ emissions [53]. This potential decrease in ocean water pH could potentially be larger than any inferred from the geologic record of the past 300 million years [53]. The impact of this could be detrimental to the oceans ecology, though at present there is a limited understanding of the effects of pH reduction on marine biota. This comes mainly from a lack of data, though some data does suggest that coral reefs, calcareous plankton, and other organisms whose skeletons or shells contain calcium carbonate may be particularly affected [53]. In addition, some other marine biota may not be affected except at high pH changes. Experiments on bacteria and nematodes have shown that the survival and growth rates of these organisms are affected only at pH levels of 6.5 units or lower. In the deep ocean, CO₂ sequestration can reduce the pH level from its normal value of about 8.0 units to around 4.0 units near the injection points [54], where biota may be more sensitive to pH changes [53]. Nakashiki and Ohsumi [55] modeled the dispersion of CO₂ in the North Pacific Ocean from continuous injection of CO₂ at a depth of 1,000 meters. Consistent with other reported findings [54], the study suggests that the potential impact might be limited to small regions around the injection point. Adams [56] have also shown that zooplankton mortality is minimized when liquid CO₂ is introduced to a 4000-meter seafloor depression forming a deep lake. In this sense, at increasing depths in the ocean the density of the benthic organisms decreases exponentially [57]. Another potential method to reduce the local effects of the high CO₂ concentrations would be to distribute the liquid via multiple release ports along a fixed pipe laid on the ocean floor. This would help to spread out the high concentrations to a larger area potentially yielding a lower impact to the benthic communities near the pipeline.

Although there is little data to suggest whether injection of liquid CO₂ to the ocean floor will create disastrous outcomes, there is data to suggest that the pH will be affected. The injection of a few GtCO₂ would produce a measurable change in ocean chemistry in the region of injection, whereas injection of hundreds of GtCO₂ would produce larger changes in the region of injection and eventually produce measurable changes over the entire ocean [1]. pH changes of more than 0.4 units, over a approximately 1% of the ocean volume have been predicted based on model simulations. Without the case of ocean storage (direct injection), a pH change of more than 0.25 units is expected to occur in the shallow ocean waters due to equilibrium with the elevated CO₂ concentrations in the atmosphere [1]. In either case, a change in pH between 0.2-0.4 units is greater than has been recorded previously in the oceans [1, 53]. In a high estimate, one ocean model has indicated that the continued release of CO₂ to the atmosphere at the current IPCC predicted rate could lead to a pH decrease of up to 0.7 units [53]. At present, impact to the pH of the oceans deep waters has not yet been identified [1].

Offshore Disposal Distances

As indicated earlier, for injection of liquid CO₂ to the ocean floor, in the form a CO₂ lake, pressures of greater than 3,000 meters deep are necessary. Also, the average depth of the ocean is around 3,800 meters, so it can be assumed that for most coastal areas suitable injection locations exist within a reasonable distance from the point source [1]. Figure 13 below, shows locations, near the United States, which are close enough to be considered suitable sites for deep ocean injection; and summarized on the following table are calculated travel distances and pipe lengths from onshore collection centers to offshore disposal sites [58]. Table 3 provides a summary of the transportation distances between onshore collection sites and offshore disposal sites. As indicated in Table 3 offshore distances of around 300 to 600 km are required to reach a suitable depth in the ocean for disposal of liquefied CO₂ and are found on both the Pacific and Atlantic Ocean sides of the United States.

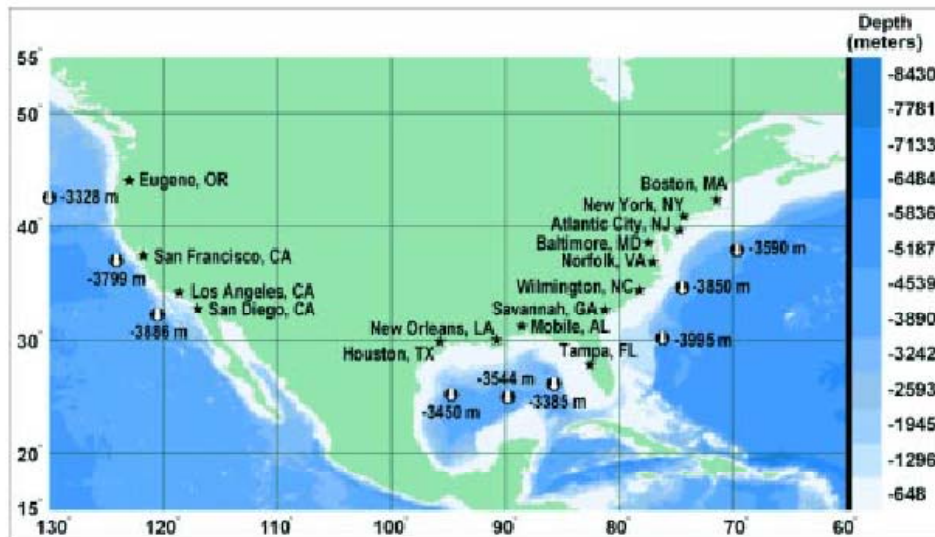


Figure 13
Potential CO₂ collection and ocean storage sites in North America [58]

Table 3
Offshore travel distances from onshore collection sites [58]

Onshore Collection Center			Offshore Disposal Site				Travel Distance/ Pipe Length (km)
City	o Longitude	o Latitude	Body of Water	o Longitude	o Latitude	Depth (m)	
Atlantic City (NJ)	74.42	39.36	Atlantic	68.00	39.00	3590	556
Boston (MA)	71.06	42.36	Atlantic	68.00	39.00	3590	457
New York (NY)	74.01	40.71	Atlantic	68.00	39.00	3590	553
Baltimore (MD)	76.61	39.29	Atlantic	73.50	35.00	3850	555
Norfolk (VA)	76.29	36.85	Atlantic	73.50	35.00	3850	326
Wilmington (NC)	77.95	34.23	Atlantic	73.50	35.00	3850	414
Savannah (GA)	81.10	32.08	Atlantic	76.00	30.50	3995	519
Tampa (FL)	82.46	27.95	Gulf of Mexico	85.50	26.50	3385	343
Mobile (AL)	88.04	30.69	Gulf of Mexico	85.50	26.50	3385	530
New Orleans (LA)	90.08	29.95	Gulf of Mexico	89.00	25.00	3544	561
Houston (TX)	95.36	29.76	Gulf of Mexico	94.50	25.50	3450	482
San Diego (CA)	117.16	32.72	Pacific	120.50	32.00	3886	325
Los Angeles (CA)	118.24	34.05	Pacific	120.50	32.00	3886	312
San Francisco (CA)	122.42	37.78	Pacific	124.00	37.00	3799	165
Eugene (OR)	123.09	44.05	Pacific	130.00	43.00	3328	574

Figure 14 provides an estimate of transport costs related to the shipping/piping of liquefied CO₂ to suitable distances offshore. As illustrated in the figure offshore pipeline transport costs, for a distance of up to about 1,000 km offshore, will be around \$5-15 USD/tCO₂ (year 2000). After this distance offshore, it appears to be more economically feasible to ship the CO₂ via a tanker.

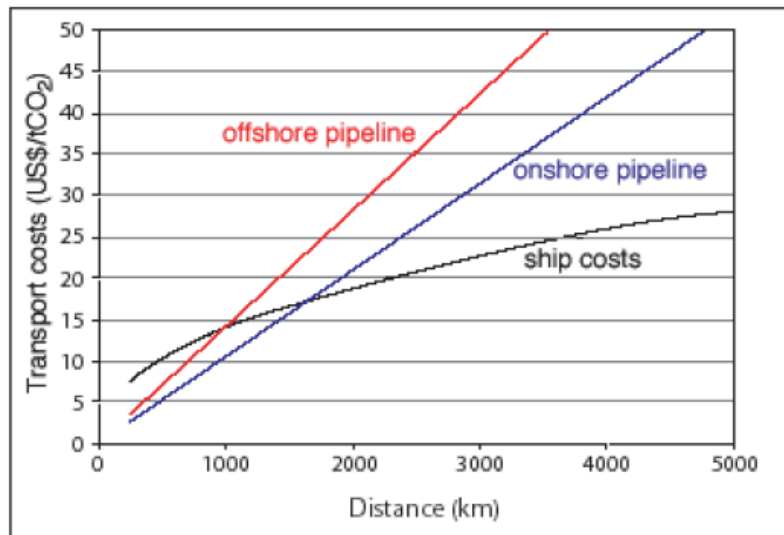


Figure 14

CO₂ transport costs per km (year 2000). Costs, plotted as US \$/tCO₂ transported against distance, for onshore pipelines, offshore pipelines, and ship transport. Pipeline costs are given for a mass flow of 6 MtCO₂/yr. Ship costs include intermediate storage facilities, harbour fees, fuel costs, and loading and unloading activities. Costs include also additional costs for liquefaction compared to compression [1]

Passive Sequestration Methods

The oceans are currently sequestering around 7.0 Gt CO₂/year (2.0GtC/year) through the natural carbon cycle [1]. This occurs both by direct diffusion in the ocean and by biological uptake

through marine organisms. It has been suggested that the oceans are capable of sequestering much more CO₂ through the biological uptake of marine organisms, than is currently happening. This is due to limiting concentrations of a few nutrients, mainly iron, phosphorous, and fixed nitrogen with iron being by far the most important [59]. One method, called ocean fertilization, proposes to stimulate ocean productivity by fertilizing the ocean surface with the necessary nutrients. The premise of this method is to stimulate photosynthetic biological activity, which will draw dissolved CO₂ out of the water and into biomass, thus under-saturating the surface waters, which will cause more atmospheric CO₂ to diffuse into the ocean through the above mentioned equilibrium process. The generated biomass is then expected to increase in density and sink to the ocean floor or be consumed by larger marine organisms and then travel to the ocean floor in their feces [60].

The volume of nutrients needed to support this method is moderately not that significant. In general, 100,000 moles of carbon biomass requires 16,000 moles of fixed nitrogen, 1,000 moles of soluble phosphorous and one mole of available iron [59]. At present the main premise is to fertilize the oceans with only iron, which will not require extremely large volumes. Though this has not yet been shown in experimental data. Previous experiments to date include (but not limited to) the following [59]:

IronEx I (1993) – performed in the equatorial pacific, spread 880 lbs of Fe as FeSO₄ on a 25 square mile patch of ocean resulting in an increase in phytoplankton but no measurable decrease in the CO₂ content of the water.

IronEx II (not sure) – performed in the equatorial pacific, spread 990 lbs of Fe as FeSO₄ on a 28 square mile patch of ocean resulting in a bloom of diatoms. The chlorophyll increased by a factor of 27 times, and the pCO₂ decreased by 90 atm in the patch.

Ocean Farming, Inc. Voyage I (Jan. 1998) – performed in the Gulf of Mexico, fertilized three 9 square mile patches. This resulted in a bloom of large diatoms to 4.3 times their initial concentration in a little over a day. While the results gave a positive indication of a large bloom, they were not definitive and did not provide a verifiable measure of phytoplankton increase over the period of the expected bloom of about two weeks.

Ocean Farming, Inc. Voyage II (May 1998) – performed in the Gulf of Mexico, one 9-square mile patch was fertilized using iron pellets designed to release the chelated iron over four days. This resulted in a large bloom of diatoms that averaged five to seven times background concentrations. It was suspected that a further increase phytoplankton was restricted by the absence of the next limiting nutrient, likely phosphorous, nitrate, or both. Extrapolating over the increased size of the patch gave an estimated 600 tons of diatoms per ton of fertilizer pellets or 1,800 tons of diatoms per ton of chelated iron added to the waters.

SOIREE (not listed) – performed in the Southern Ocean south of New Zealand, one 20-square mile patch was fertilized with iron sulfate over four days. This resulted in a chlorophyll concentration increase of six times and a biomass increase of three times mostly in the form of diatoms.

In summary, to date there has been little success in determining reliable values for attributing ocean fertilization nutrient volumes to a volume of CO₂ being sequestered from the atmosphere. Assuming that a reasonable amount of atmospheric CO₂ could be sequestered by this method a residence time has been estimated to be about 1,600 years, as measured by the C¹⁴ to C¹² ratio of upwelling of deep ocean water off of Peru [61].

One of the main proposed benefits of this method was that it imitates a naturally occurring process and should not pose a significant environmental risk. However, information has been found that suggests that the benefits of this method may be outweighed by some potentially hazardous outcomes. These hazardous outcomes include possible increase in the amount of dimethylsulfide produced by several species of phytoplankton, deoxygenation of the oceans surface waters, and potential for and increase in methanogenesis that could greatly increase the atmospheres methane concentration. It should be noted that methane is a potent greenhouse gas with a global warming potential 21 times higher than CO₂ when integrated over a 100-year period. N₂O concentrations may also be increased do to nitrogen cycling in the ocean. N₂O is a potent greenhouse gas about 206 times as effective, per molecule, as CO₂ in radiative heating of the atmosphere [60]. In summary, there is not enough data available to properly evaluate this methods application to the at-hand problem of sequestering a portion of the atmospheric anthropogenic CO₂ emissions.

Public Opinion

In all, there is a lot of opposition against the above-proposed methods of oceanic sequestration of CO₂. Deep ocean injection faces opposition based on the fact that there is no conclusive evidence that injection of CO₂ to the deep ocean, in the form of lakes, will not cause catastrophic changes to the ecosystem [51]. Furthermore, the associated costs involved with capturing, compressing, and transporting the CO₂ to the deep ocean is potentially costly in both energy utilized, thus an increase in the volume of CO₂ produced, and capital/operational costs [49]. The CO₂ sequestered is not entirely removed from the atmosphere, it will be stored for a around 1,000 to 2,000 years before being naturally released to the atmosphere [1]. Ocean fertilization is opposed based on some similar reasons as deep ocean injection. One major issue is the fact that there is again no conclusive evidence that dispersal of CO₂ into HNLC waters will not cause a disruption to the oceans ecosystem. This method is also not sustainable because it will always require available supplies of nitrogen, phosphorous, and iron to remain in operation. There is also the energy penalty associated with the processing and distribution of the nutrients to the ocean, which has been estimated to be around 25% [49] of the total fuel costs. The processing of these nutrients will result in an increase of the amount of CO₂ produced in the overall process.

Biological Sequestration: Terrestrial Ecosystem

Knowing that the terrestrial ecosystem is a natural carbon sink, changes in agricultural management can potentially increase the accumulation rate of soil organic carbon (SOC) and vegetative CO₂ uptake, thereby offsetting atmospheric CO₂ production from fossil fuel combustion and land use changes [62]. For this reason, a critical literature review explaining the various methods for improving CO₂ sequestration in the terrestrial ecosystem as well as its limitations and uncertainties is presented below.

Terrestrial sequestration incorporates net removal of CO₂ from the atmosphere or the prevention of CO₂ emission from the ecosystem. Since the terrestrial ecosystem includes both soil and vegetation, research in the field focuses on means of improving land use management and soil texture to enhance CO₂ sequestration while considering environmental effects, economics of the methods, and public acceptance. As a result of land misuse, the table below, shows loss of carbon when a tropical forest is converted into different land use. With the aid of this table, we can calculate the loss from the forest fire of 1997-1998 in Indonesia national forest (world center of bio-diversity) which resulted to a loss of US\$9.3 billion. Considering an estimated rate of US\$20 for every tonne of carbon released, conversion of an open forest to agriculture or pasture land result in a global warming damage worth about US\$600 to US\$1,000/ha, also, conversion of a closed to secondary forest causes a damage between US\$2,000 to US\$3,000/ha while converting from primary forest to agriculture causes a damage between US\$4,000 to US\$4,400 [63]. To offset and avoid this amount of money requires proper land management assuming that the land misuse leads to loss in this amount of carbon.

Table 4
Changes in Carbon with land use changes (tC/ha) [63]

	Original C	Shifting agriculture	Permanent agriculture	Pasture
Original C		79	63	63
Closed primary forest	283	-204	-220	-220
Closed secondary forest	194	-106	-152	-122
Open forest	115	-36	-52	-52

Methods of terrestrial sequestration include: (1) Afforestation, reforestation and restoration of graded land (2) Agroforestry on agricultural lands (3) Improving growth rate with the aid of required nutrients.

Land Use Management

In the 1980s and 1990s, increases in CO₂ emissions from land mismanagement, either by deforestation, biomass burning, or conversion of natural to agricultural systems, was estimated to be 1.7 billion ton C/yr and 1.6 billion ton C/yr, respectively, while emissions from fossil fuel combustion and cement production were estimated to be between 5.0 billion tons and 6.3 billion tons C/yr, respectively [62]. Sequestering a reasonable amount of this CO₂ requires improving land management practices, reducing the decomposition of organic matter; increasing the photosynthetic carbon fixation of trees and other vegetation; and creating energy offsets through biomass and other products. The Food and Agricultural Organization (FAO) of the United Nations reported that since afforestation depends mostly on political decisions, agroforestry will be an option for a good technical and ecological management plan [64]. Agroforestry is a

farming method that integrates crops with trees and shrubs. Crops are grown with no mulching, tillage and plant covers. This type of farming system has a very high sequestration rate in croplands and can sequester about 2 to 9 ton C/yr through the duration of 15 to 40 years depending on the type of soil; it is attractive to small farmers but requires a lot of space [64]. Comparing data evaluation for periods of 20 to 50 years for the FAO project and data from IPCC [65], Lal [62] showed that practicing agroforestry with 1 billion ha will sequester 0.2-3.1 tons C/ha/yr and 0.5 t C/ha/yr respectively. Also, Robert [64] evaluated carbon storage in different ecoregions and showed that 21 to 50 tons C/ha could be offset for a period of 5 to 8 years from plant uptake alone, whereas the roots (soil uptake) alone could increase this value by 10%. However, using cacao/erythrina as the dominant plant species could have an increase of 10 and 22 ton C/ha for a period of 10 years. This numbers agreed with those from Nor [65] as stated earlier. Adopting agroforestry can triple the carbon stock from 23 to 70 ton/ha through a period of 25 years, it can mitigate the CO₂ emission from deforestation, provide a sustainable system, however, social and cultural issues may be difficult to manage. As stated by FAO Global Resources Assessment, “the current global rate of deforestation is around 17 million ha per year” [64]. As a result of deforestation on this huge amount of land, the terrestrial ecosystem has lost much carbon into the atmosphere and to offset this amount of carbon, there is need to improve aforestation. Aforestation practice can sequester significant amounts of carbon through conserving old forests and planting new species of timbers (saplings) to replace the very old ones before they begin to burn or decompose. The old timbers are turned into useful products and have carbon stored in them for as long as 50 years, according to Friends of the Earth International.

In the U.S., different types of forests cover approximately 750 million ha [64], and since photosynthesis by plants determines how much carbon is stored in soil, trees, and vegetation, improving forest growth is of benefit to carbon sequestration in the terrestrial ecosystem. It is reported that typical sequestration potential available in the tropics through aforestation and reforestation may be estimated between 3.2 to 10.0 t C/ha/yr, assuming land availability of 700 million ha which is projected to sequester 42 to 59 t C for 50 years [36]. The forest as a carbon sink can increase its CO₂ fixation if afforestation is enhanced through planting species of trees that suit various climatic regions at the appropriate time of the year. However, the rate of carbon sequestration depends on the growth characteristics of the species, the density of the tree's wood and the condition for growth where the tree is planted. To maintain the forest, small stems are removed at various development stages to permit higher growth rates. The rate of carbon fixation is higher in younger stages of trees, between 20 to 50 years, and growth rate has been improved through a tree improvement campaign [66] to about 30 cubic meters/ha/yr. FAO estimates that there are between 1.5 and 2.0 million ha of trees planted every year to increase the forestry CO₂ sequestration rate, and the available land for planting is between 300 to 400 million ha in developing countries. This could be a good spot for afforestation in addition to the natural forests in Brazil and Papua New Guinea, which could potentially have more than 70% of land as natural forests [36] if the Canadian International Development Agency (CIDA) project for improving forestry management is adhered to. Therefore, planting species of plants such as aspen, which can serve as a carbon storage and also as biofuel, will sequester up to 4.5Mg C/ha yr [65]. Furthermore, forestry products can serve as carbon store when substituted for building materials such as bricks, concrete, steel, and aluminum, but they need to be replaced with fast growing saplings. Also, substituting fossil fuels with biofuels crops (sugarcane, corn, potatoes,

wheat, bamboo) and wood is being projected to replace 3.5 Gt of fossil fuel by 2050 [65]. This is based on the classification of biofuels, unlike fossil fuels, as “carbon-free” [66].

Species of trees like *Eucalyptus* grow in excess of 50 cu. m/ha/yr and this rate can be increased by proper selection and breeding with help from modern biotechnology. Similar species are the *Pinus spp*, *Tectona granids* and *Acaci spp*. As a result of their growth rate and ability to withstand harsh environment, they can serve in the reclamation of degraded mine lands for afforestation. With this option, abandoned mine lands may be reclaimed through the use of flue gas desulphurization (FGD) slurry byproducts from a coal fired power plant. The calcinataed slurry can be used to neutralize acid mine drainage and make lands available for planting of trees like *sweet-gum* and *cycoma* which have the potential to sequester 70 to 90 metric tons of carbon per 1.5 to 2.0 ha of land per year [67]. This is a sequestration method that is likely to be efficient in the U.S, which has countless acres of mined lands. In the U.S., out of a total of 118 million tons per year of flue gas desulphurization solid, fly ash, and other products, only 31% is put into use while the rest end up in landfills. To increase this 31%, the high alkalinity level of fly ash produced during the combustion process buffers the high acid mine drainage (AMD) and provide nutrients for new generation. Though not all fly ash can be used because of their different chemical composition based on the type of coal burned. Some fly ash contains insoluble silicon, iron oxide and aluminum and can also contain soluble metal and metal oxide which when exposed to water; the metal in fly ash could leach into the environment polluting surface or ground water.

While developing this strategy, there is need to protect the terrestrial soil. Knowing that the soil is a large body estimated to contain 70% of all terrestrial carbon, research shows that adapting Recommended Management Practice (RMP) can improve the soil fixation on agricultural soil while having positive impact on food security, water quality and the environment [62]. Soil organic carbon (SOC) depletion has emitted 78 billion ton of carbon into the atmosphere as a result of low soil nutrients, improper mulching, and erosion, and practicing RMP will offset this enormous amount of CO₂. RMP involves maximizing energy, nutrients application, irrigation, no-tillage, and low or zero fallowing. With no tillage farming, records show that carbon sequestration ranging from 200 Kg/ha/yr in the dry region to 600 Kg/ha/yr in cold region and this rate can be increased to 300 to 1000 kg/ha/yr by applying appropriate cover crops [64]. Conservation tillage (growing crops with minimal cultivation) was estimated to sequester 0.1-0.2 tC on 3 billion ha of dry land and 0.2-0.5 on 2 billion ha of tropical forest [64]. Fallowing, for instance, should be eliminated in the summer because it keeps the soil moist and enhances mineralization [62]. In essence, the objective is to maintain a dense vegetal cover on the soil surface such that biomass carbon can be returned to the soil.

Other RMP that can enhance terrestrial CO₂ sequestration is erosion prevention, where 150 to 1500 million tC/yr were estimated as the global loss of carbon due to erosion [64]. Also, increases in soil temperature will alter the rate of soil decomposition most strongly in the boreal and Polar Regions, where projected climate change impact on soil quality shows that an increase in the soil temperature by 3°C results in depletion of the soil organic pool by 28% [62]. So, preventing soil erosion can be done through the use of cover crops, wind break, and boundary planting with the aid of trees and other shade crops (*erythrina spp*, *Inga spp*, *cacao-E* and *poepigiana*) which are capable of increasing SOM by 42 and 16 Mg C/ha [68]. On the other hand, boundary planting shield an area from wind damage and have positive effect on soil

characteristics/crop production. Studies show that the potential of *Calliandra Calthyrus* as a live fence in species in Costa-Rica can sequester 20Mg C/ha while in Mexico, C sequestration using fencing trees were reported to store 24 to 36 Mg C/ha during a cycle of 25-30yrs [68]. Previous research also shows that improved fallow in western Kenya enhances CO₂ sequestration rate [68].

For the success of the above mentioned methods in land management, the soil requires application of nutrients such as fertilizers and manure/compost, which can manipulate the terrestrial ecosystem for the uptake and sequestration of CO₂. A study on U.S. forests shows that forest growth increases by 25% with the application of fertilizers, improving CO₂ storage by 0.45 Mg C/ha/yr [64]. Soil nutrients such as compost or manure are traditionally used to add organic matter to the soil with a relatively high carbon sequestration rate of 0.2 to 0.5 tons C per 20 tons of compost/ha. However, the problem with composting is the inability to maintain the microbial temperature and its decreasing source due to animal husbandry. Also, increases input of soil carbon can lead to progressive immobilization of soil nutrients, and hence decreases in nutrients uptake which, in-turn, lowers the amount of nitrogen in the leaves and reduces photosynthesis.

Limitations and Uncertainties

While considering various RMP, previous research shows that the terrestrial ecosystem requires a tropical forest approximately the size of Texas for 30 yrs to reduce CO₂ by 7%. Friends of the earth international went further to analyze the long term security of forests as a carbon sink and stated that this depends on the relative temperature sensitivity of soil species and the rate of decomposition of organic matter; such that certain conditions could result in sink becoming source. An example was in the high latitude boreal forest of Canada where the Russia-Canadian forest transitioned into a CO₂ source following two decades of growth. Other benefits include the possibility that developing countries could be the beneficiary of carbon trading, since they could sell areas of rain forest in a carbon credit.

Offsetting emissions from a 500MW (0.8Mt C/yr) coal fired power station requires a tropical forest between 200,000ha and 400,000ha with an upper bound sequestration rate of 2 to 4 tons C/ha/yr and lower bound of 0.5t C/ha/yr and a cost of \$24-\$120/ha [69]. Furthermore, a plantation of *Acacia mernsii* can sequester 7.8t C/ha/yr to offset the 0.8Mt C using about one quarter to one third of land space needed by the rain forest. However, a report by Roper [66] explained that the forests are normally the responsibility of government that at the present time does not have the budget and staff to manage the forest by today's standard. Recent studies also show that Nitrogen inputs from agroforestry practice can exceed the required level of some crops resulting in the volatilization of excess nitrogen in the form of N₂O. In the same way, CH₄ can be produced during the production and cultivation of rice paddy in agroforestry system [68]. In this paper, financial consideration was limited, though previous work explained that "costs, benefits and profits varies like biophysical parameters and ought to to be contextualized" while management practices should be very economical to make them attractive to farmers [70]. In addition, Robert [64] asks an important question, "How can good data for validating and running carbon models be obtained?"

Conclusion

This paper outlined a review of potential for terrestrial CO₂ sequestration based on various management practices inline with the RMP. Comparing previous work done, Albrecht and

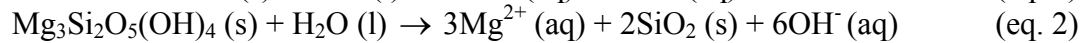
Kandji stated that the carbon sequestration potential of agroforestry system is estimated between 12-228Mg /ha. And with 585-1215 x 10⁶ ha suitable for practice, about 1.1 to 2.2 billion C would be stored in the terrestrial ecosystem over a period of 50yrs if agricultural systems are implemented on a global scale. This implies that improved land management and farming practices can sequester a reasonable amount of CO₂ along with a suit of co-benefits such as reducing run off and erosion, protecting water quality etc. Analyses so far shows that there is potential for terrestrial CO₂ sequestration, although this potential is limited by land availability and other drawbacks as discussed above. However, proper land and soil management will sequester a reasonable amount of CO₂ in to the terrestrial biosphere while improving the environment and finding general support from the public sector.

CO₂ sequestration by mineral carbonation

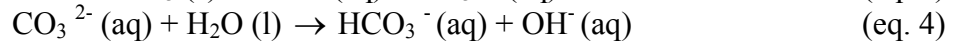
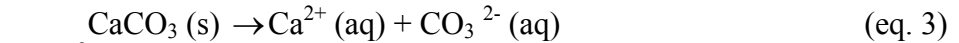
The identified critical issues relating to CO₂ sequestration by mineral carbonation are: selection of minerals; process routes: pre-treatment, direct & indirect carbonation; thermodynamics and kinetics; and economic and energetic consideration. The results of the literature research in regards of these themes will be present in the following report.

Selection of minerals

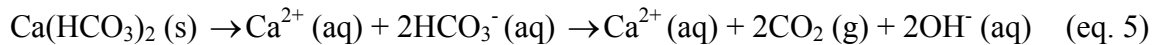
To be able to react with acid CO₂, the mineral has to provide alkalinity. Not all alkali or alkaline earth metals containing minerals provide alkalinity. Alkalinity is derived from oxides or hydroxide. This can be explained by showing the processes occurring during dissolution, e.g.:



Another (weaker) source of alkalinity is carbonates. This can be illustrated by the dissolution of calcite and the subsequent second dissociation step of carbonic acid.



Although it is easier to convert carbonates into bicarbonates than to carbonate a silicate mineral (Lackner, 2002), oxides and hydroxides are preferred. Controlled storage is only possible for carbonates, because carbonates are almost insoluble in water while bicarbonates are fairly soluble. Part of the sequestered CO₂ would be released, if bicarbonates were dissolved in rainwater.



Calcium and magnesium rarely occur as binary oxides in nature. They are typically found in silicate minerals. These minerals are capable of being carbonated because carbonic acid is a stronger acid than silicic acid (H₄SiO₄). Thus silica present in the mineral is exchanged with carbonate and the mineral is carbonated. Igneous rocks are particularly suitable for CO₂ fixation because they are essentially free of carbonates. The main candidate magnesium-rich ultramafic rocks are dunites, peridotites and serpentinites. The first two can be mined for olivine, a solid solution of forsterite (Mg₂SiO₄) and fayalite (Fe₂SiO₄). Ore grade olivine may contain alteration products, such as serpentine (Mg₃Si₂O₅(OH)₄) and talc (Mg₃Si₄O₁₀(OH)₂). Serpentine can take the form of antigorite, lizardite and chrysotile. The main calcium-containing candidate is wollastonite (CaSiO₃). The composition of various minerals and their specific CO₂ sequestration capacity are given in Table 5 and the distribution of magnesium silicate mineral deposits worldwide is reported in Figure 15.

Table 5
Composition of various minerals and CO₂ sequestration characteristics [71, 72]

Rock	MgO [wt%]	CaO [wt%]	R _c [kg/kg]	R _{CO₂} [kg/kg]
Dunite (olivine)	49.5	0.3	6.8	1.8
Serpentine	~40	~0	~8.4	~2.3
Wollastonite	-	35	13.0	3.6
Talc	44	-	7.6	2.1
Basalt	6.2	9.4	26	7.1

R_c = mass ratio of rock needed for CO₂ fixation to carbon burned. R_{CO₂} = corresponding mass ratio of rock to CO₂.

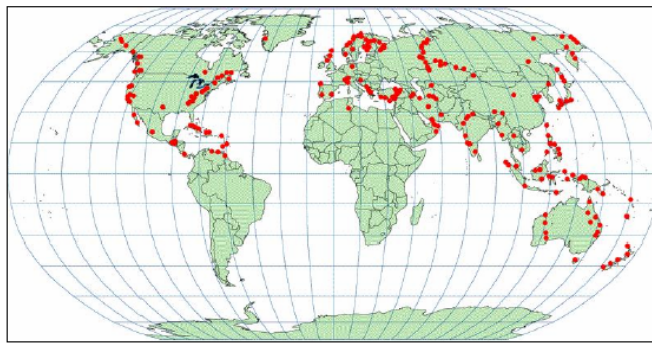


Figure 15
Distribution of magnesium silicate mineral deposits worldwide [73]

The worldwide resources that can actually be mined are, however, unknown. Studies have been performed at individual peridotite/serpentinite bodies. Two selected reservoirs in the United States are Twin Sisters, Washington, and Wilbur Springs, California, which are capable of sequestering the globally emitted CO₂ for 2 and 5 years respectively [74]. Lackner indicated a deposit in Oman of 30,000km³ magnesium silicates which alone would be able to store most of the CO₂ generated by combustion of the world's coal reserves [75, 76]. Basalt, which is rich in calcium, is ubiquitous, but it is difficult to extract the reactive components from the mineral matrix [77]. In the DOE research program olivine and serpentine are selected because of their large abundance in nature and the high molar ratio of the alkaline earth oxides within the minerals [74]. Other researchers, including Wu, concluded that talc and wollastonite would be the most appropriate minerals [71].

Alkaline solid wastes

Most available literature deals with mineral CO₂ sequestration using mineral rock as feedstock. An alternative source of alkalinity could be the use of solid alkaline waste materials, which are available in large amounts and are generally rich in calcium. Possible candidates are, among others, asbestos waste, iron and steel slag and coal fly ash [78]. The carbonation of alkaline waste materials has two potential advantages: these materials constitute an inexpensive source of mineral matter for the sequestration of CO₂ and the environmental quality of the waste materials (i.e. the leaching of contaminants) can be improved by the resulting pH-neutralization and mineral neoformation.

Pre-treatment

The pre-treatment options that will be taken in consideration are: size reduction, magnetic separation and thermal treatment.

Size reduction

To achieve a reasonable reaction rate the minerals have to be ground. The reaction rate increases with the surface area. Among others, O'Connor examined the influence of the particle size on the conversion. These authors found that a reduction from 106-150 μm to <37 μm increased the conversion in their experiments from 10% to 90% [79]. Attrition grinding, however, is energy intensive and difficult to conduct on a large scale.

Magnetic separation

The oxidation of iron (magnetite) slows down the carbonation of serpentine due to the formation of a layer of hematite on the mineral surface [80]. To execute the process in a non-oxidising atmosphere complicates the process and increases the costs significantly. Magnetic separation of the iron compounds prior to the carbonation process resolves this complication [78]. Furthermore, a potentially marketable iron ore by product is formed [81] When a combination of magnetic separation and thermal treatment is used, it is more effective first to conduct the magnetic treatment step [82].

Thermal treatment

Serpentine contains up to 13% by weight of chemically bound water. By heating the serpentine to 600-650 $^{\circ}\text{C}$ the water is removed and an open structure is created [79]. This significantly improves the reaction kinetics owing to the increase reactive surface. For example heat-treatment of antigorite increased the surface areas from 8.5 m^2/g to 18.7 m^2/g [78]. The heating process can be further extended to higher temperatures in order to separate, for example, MgO from its matrix. Temperatures above 900 $^{\circ}\text{C}$ are needed for serpentine and even higher values for olivine [83]. The mineral porosity can also be increased by treatment with steam [78] or supercritical water (T=385 $^{\circ}\text{C}$, p=272atm) [79].

Direct carbonation

Direct carbonation of a mineral can be conducted in two ways: as a direct dry gas-solid reaction or in an aqueous solution.

Direct gas-solid carbonation with CO₂

The most straightforward process route is the direct gas-solid carbonation. This was first studied by Lackner [84]. Various reactions depending on the feedstock are possible. High CO₂ pressures are necessary in order to obtain reasonable reaction rates. The reaction rate can further be improved by the use of supercritical CO₂ [83]. The produced water dissolves in supercritical CO₂.

Aqueous scheme

From natural rock weathering it is known that water greatly improves the reaction rate. A process developed on based on this principle is the carbonic acid route [79, 85], in which CO₂ reacts at high pressure in an aqueous suspension of forsterite or serpentine. First, CO₂ dissolves in the water and dissociates to bicarbonate and H⁺ resulting in a pH of about 5.0 to 5.5 at high CO₂

pressure; then the Mg^{2+} is liberated from the mineral matrix by H^+ ; finally, the Mg^{2+} reacts with bicarbonate and precipitates as magnesite. A bicarbonate/salt mixture ($NaHCO_3/NaCl$) can be used to accelerate the reaction [79]. The sodium bicarbonate increases the HCO_3^- concentration and thus accelerates the carbonation reaction. An increase of 0.5-1.0g/l CO_2 in distilled water to 20g/l CO_2 in a $NaHCO_3/NaCl$ -solution has been reported [80]. The reaction can take place at a lower pressure. Used concentrations are about 1M $NaCl$ and 0.5-0.64M $NaHCO_3$ and a 15% containing slurry solids is used. The solution is buffered at pH 7.7 to 8.0 [81]. The addition of $NaCl$ increases the release of Mg^{2+} ions from the silicate by creating soluble complexes and thus lowering the magnesium activity in solution [81]. The solution chemistry can be further improved by adding alkali metal hydroxides. Thus the pH of the solution is elevated and the absorption of CO_2 is further improved. The hydroxide is also not consumed. Another option that could improve the dissolution of serpentine and simultaneously elevate the pH is the addition of Na_2CO_3 .

Indirect carbonation

HCl extraction route

To extract the magnesium from the mineral matrix hydrochloric acid can be used [72, 84]. The process was originally developed during World War II as an alternative route producing magnesium. As an example, the process steps using serpentine as feedstock are given. First, the magnesium is extracted from the mineral with the help of HCl . The use of an excess HCl results in an acid solution in which the magnesium dissolves as $MgCl_2 \cdot 6H_2O$. The HCl is recovered by heating the solution from 100 to $\pm 250^\circ C$. During this temperature increase, the $MgCl_2 \cdot 6H_2O$ first loses its associated water, resulting in $MgCl_2 \cdot H_2O$ and, finally, HCl separates instead of further water release. The $MgCl(OH)$ reforms to magnesium hydroxide when water is reintroduced and finally, the $Mg(OH)_2$ is carbonated. The thermodynamics of the process have been studied in detail by Wendt [86]. The third step of the process in which $Mg(OH)_2$ is formed has a positive Gibbs energy change and therefore the energy consumption of the process is considerable [87].

Molten salt process

A first approach towards lowering energy consumption is the use of a molten salt ($MgCl_2 \cdot 3.5H_2O$) as an alternative extraction agent [86]. The salt is recycled within the process. There are two options. In the first process, $Mg(OH)_2$ is produced and carbonated separately. In the second process, the steps are integrated into one step. The steps for the first process are: $MgCl_2 \cdot 3.5H_2O$ is used as solvent to produce $Mg(OH)_2$; the serpentine is dissolved in the molten salt ($T = \pm 200^\circ C$); then the silica is precipitated ($T = \pm 150^\circ C$), water is added and $Mg(OH)_2$ precipitates: the $MgCl_2$ is partially dehydrated in order to recover the solvent ($T = \pm 110-250^\circ C$) and finally the magnesium hydroxide is separated and carbonated.

In the second process the carbonation takes place directly in $MgCl_2 \cdot 3.5H_2O(l)$, the CO_2 pressure is about 30 bar [88]. Important drawback of this route is the corrosive nature of the solvent. This causes construction and operational difficulties. Furthermore, in spite of recycling, make-up $MgCl_2 \cdot 3.5H_2O$ is needed. Based on a detailed assessment, Newall concluded that a commercial supply of $MgCl_2$ of this scale is probably unrealistic and if at all possible, unaffordable [88].

Wollastonite carbonation using acetic acid

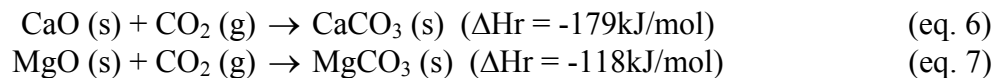
A second approach towards the reduction of energy consumption is the use of other acids than HCl. Kakizwawa selected acetic acid to extract calcium ions from wollastonite [89]. The route consists of two steps. First, wollastonite is treated with acetic acid, then the calcium is carbonated and the acetic acid recovered in a combined step. So far, this route has not received much attention in the literature. The main advantage of the route is the ability to speed up the carbonation process by extracting reactive compounds from the matrix without using hydrochloric acid.

Dual alkali approach

The dual alkali approach is based on the Solvay process in which sodium carbonate is produced from sodium chloride using ammonia as a catalyst [90], then the ammonia is recovered and, finally, if desired the bicarbonate can be converted to a carbonate. In order to improve energy efficiency, research on the modification of the process has been done. In the modified process HOCH₂CH₂(CH₃)NH is used instead of ammonia [90].

Thermodynamics

Carbonate is the lowest energy-state of carbon. The carbonation reactions of magnesium and calcium oxide are strongly exothermic[72]:



The carbonation reaction with gaseous CO₂ proceeds very slowly at room temperature and pressure. Increasing the temperature increases the reaction rate. However, because of entropy effects, the chemical equilibrium favours gaseous CO₂ over solid-bound CO₂ at high temperatures (calcination reaction). The highest temperature at which the carbonation occurs spontaneously depends on the CO₂ pressure and the type of mineral.

Kinetics

Dry carbonation

Research focuses on the dry carbonation of calcium and magnesium oxides and hydroxides. The carbonation of CaO and Ca(OH)₂ progresses very rapidly and proceeds towards completion in several minutes at elevated temperature and pressure [84]. The advantage of a fast reaction of calcium minerals, however, is counterbalanced by their low concentrations in naturally occurring ores, which makes them less suitable as feedstock. The concentrations of magnesium in ores are generally higher, but the carbonation rate of MgO is slow. The reaction of Mg(OH)₂ can be fast enough for an industrial process [84]. The kinetics of the carbonation of Mg(OH)₂ have been investigated in detail by McKelvy [91, 92].

The activation energy of the dehydroxylation of magnesium hydroxide is 146 kJ/mol and the net activation energy of the combined carbonation and dehydroxylation is 304 kJ/mol. The optimum temperature is 375°C. At this temperature the reaction proceeds quickly and the carbonated product is thermodynamically favoured [93].

Aqueous carbonation

In an aqueous process the magnesium or calcium first has to dissolve from the matrix into the water. Two possible routes of the carbonation reaction are: a direct conversion of Mg^{2+} into magnesium carbonate and an indirect route via hydromagnesite [78]. A detailed analysis of the rates of the various aqueous route process steps was made by Guthrie [94]. These authors concluded that the dissolution of the magnesium silicate is an important step that probably determines the reaction rate. The dissolution rate differs for the various minerals. Thermal pre-treatment is known to increase the dissolution rate of serpentine. Another important factor is the role of silica. On the dissolving particles a silica-enriched layer may develop that changes the rate and mechanism of dissolution. This layer is formed by incongruent dissolution [94]. This is the subject of further studies. Wu concluded that the rate-determining steps for the carbonation of wollastonite are the dissolution of calcium from the matrix and the carbonation in aqueous solution [71]. These authors also suggested that the slow reaction rate might result from the development of a thin product layer on the surface.

For the aqueous route this effect is counteracted by a decreasing solubility of CO_2 in the water phase, thereby resulting in an optimum temperature. Gerdemann *et al.* found an optimum temperature for olivine at $185^\circ C$ and $155^\circ C$ for serpentine [95]. Fernandez found that the kinetics of the carbonation of MgO at atmospheric pressure can be described by a shrinking reaction core model [96]. The activation energy these authors found is 29.1 kJ/mol. The rate-determining step seems to be the reaction between the precipitated magnesium carbonate on the surface and the CO_2 to form bicarbonate. This looks contradictory to remarks made by Lackner [77]. However, the formed magnesium carbonate precipitates on the surface and thus hinders further carbonation. If bicarbonate is formed the magnesium dissolves and new magnesium oxide can react.

Economic and energetic consideration

Economic consideration

For mineral CO_2 sequestration the costs can be further divided into costs for the pre-treatment of minerals and for the sequestration process itself. Second, costs can be split up in fixed (investment costs) and variable costs (energy consumption, raw materials needed, etc.). Very few detailed cost analyses of mineral CO_2 sequestration are available. As an indication, scale-up of current laboratory practices leads to costs of about 70€/ton. A major part of the costs comes from the heat treatment step. If this problem can be overcome, costs of about 20-30€/ton seem a realistic target [77]. The mining costs for mineral CO_2 sequestration are small and are estimated at 3-5€/ton [78]. As an indication, the costs for extraction, concentration and transport of CO_2 are estimated at 31€/ton CO_2 [78].

Energetic balance

A single 500 MW power plant generates about 10,000 ton CO_2 /day. To sequester this amount of CO_2 via the mineral route would require approximately 23,000 ton/day of magnesium silicate ore. Feedstock minerals are produced as by-products at several existing mines, but a massive increase in mining activities would be necessary to facilitate large-scale mineral CO_2 sequestration [74]. In addition to these considerations, mineral CO_2 sequestration technologies involve other environmental impacts such as the consumption of extra energy. Assuming that the

required energy is provided by fossil fuels, mineral sequestration would enhance the use of fossil fuels. When mineral sequestration is applied at a power plant, the extra energy consumption would consequently decrease its efficiency. Kakizawa calculated a decrease from 40% to 32% for a thermal power plant [89].

A large part of the energy consumption comes from the pre-treatment of the feedstock. Heat treatment of 1 ton of serpentine to remove chemically bound water requires 200-250kWh of energy [81]. In addition, Kojima and co-workers estimated that an extra 18.7kg CO₂ has to be sequestered to crush 1 ton of wollastonite from 0.2m to 75μm; 1ton CaSiO₃ can sequester 278kg CO₂ [97].

To determine the overall energy consumption, the capture of CO₂ also has to be taken into account. As an indication the amount of energy needed for separation and compression of CO₂ from power plants has been calculated at the Massachusetts Institute of Technology [98]. The energy costs for CO₂ capture are 0.147 MW for the IGCC, 0.256 MW for the PC and 0.138 MW for the NGCC power plant per net megawatt power output of the power plant. Kakizawa and co-workers have estimated an energy consumption of 0.07MW per MW produced by a thermal power plant [89]. The overall energy consumption of mineral carbon sequestration would be 125-250 MW for a 500MW power plant.

Biological Sequestration: Industrial-Bioreactor

Sequestering CO₂ by biological means through photosynthesis represents an attractive option because it is clean and renewable. However, several challenges exist. Primarily, the rate is slow for most photosynthetic processes, which creates large land requirements. In an effort to make the process faster and to reduce land requirements, many have begun work on designing and industrializing process that utilize photosynthetic microbes because of their relatively quick growth rates, biological growth density potential, and ease of utilization. Previously, several key issues had been identified with regards to the design of an industrial bioreactor system. The following is a literature review, analysis, and discussion relating to the key issues.

Microbial Selection

Microalgae can be considered as any microscopic, unicellular microbe that is, at least some of the time, photoautotrophic [99]. There are tens if not hundreds of thousands of species believed to exist. However, as a class of organisms in biology, there is relatively little known about these organisms. Of the vast numbers of species that exist, only a few (maybe hundreds) have been investigated for their potential usefulness in society and in industry [99]. In recent times, many investigators have been attempting to apply these microbes to the issue of CO₂ sequestration because of their relatively fast fixation rates (more than 10 times that of a typical tree [100]). Vast numbers of microbes have been screened for potential and many have been found to work [100-103]. The microbes must have the highest fixation rates possible, efficiently convert light into high value biomass, survive at the highest possible temperature, and have tolerance to the flue gas [101]. The species that have demonstrated the most promise include *Synechocystis aquatilis* SI-2 [100, 103], *Botryococcus braunii* SI-30 [100, 103], several strains of *Chlorella* [99-101, 104], and *Nostoc* 86-3 [99, 102].

Synechocystis aquatilis SI-2 showed the highest CO₂ fixation rate of 1.5 g/l/day [100, 103]. *Botryococcus braunii* SI-30 showed a similar fixation rate of close to 1.25 g/l/day, but also had the advantage of high hydrocarbon production within the cell of approximately 15wt% by dry weight basis [100, 103]. However, these species were not found to have optimal growth rates at temperatures around 25-35°C [100, 103]. This makes them less desirable for direct flue gas injection and their tolerance to flue gas contaminants is not reported. *Chlorella* showed decent fixation rate of approximately 0.78 g/l/day [101] on a volumetric base and high biomass growth on an area base of almost 23g/m²/day [104]. In addition, it demonstrated good thermal resistance and tolerance to flue gas composition [101, 104]. *Nostoc* 86-3 was used in a DOE project to grow on films and showed a decent fixation rate of approximately 10g/m² film area/day under conditions of almost 50°C and being fed flue gas [102].

There is hope that genetic engineering will lead to improved fixation and production. For example, carbonic anhydrase is responsible for the catalytic formation of CO₂ from bicarbonate within the cell. Enhancing the concentration of carbonic anhydrase has been shown to have positive impact on the fixation rate [105]. *Synechococcus* sp. PCC7942 was genetically enhanced to improve the carbonic anhydrase concentration and was shown to have a higher fixation rate [103]. There is also work being done to increase the yield of valuable byproducts such as Astaxanthin, Phycocyanin, Phycoerythrin, β-Carotene, Tocopherol, ARA, and DHA [104-106]. Most of these markets are fast growing or burgeoning today [105].

Photobioreactor Systems

Perhaps the greatest challenge is to maximize the production of photosynthetic microbes through the design of the photobioreactors (PBR). There are several bioreactor types which can be classified as closed, open, indoor, and outdoor as seen in

Table 6. Issues to consider in the selection and design of a PBR include the control of light intensity and efficiency, temperature, and nutrient mix as well as cell culture protection, CO₂ injection and loss to the atmosphere, biomass harvesting, land footprint, and capital and operating costs.

Table 6
Common Reactor Types

	Open	Closed
Indoor		Mixed Tank [100] Vertical Film [102]
Outdoor	Pond [100, 107] Raceway [101] Thin film [104]	Tubular [99, 101, 108] Flat Plate [71, 101]

Outdoor open systems are the simplest type of PBR's. The entire solution is exposed to direct sunlight in an open atmosphere. Outdoor open systems share the benefit of inexpensive operating costs. However, the land requirements are quite large in comparison because they do not make efficient use of light. Moreover, there is little to no control of culture environment (temperature, protection, etc). In addition, there can be quite a large loss of CO₂ to the atmosphere. In experimentation with thin film, outdoor reactors it was found that as much as 21% of the CO₂ dissolved into aqueous media escaped to the atmosphere [104]. The amount escaping to the atmosphere from the other types of outdoor reactors would be expected to be much less because the atmosphere exposed area to reaction volume ratio is much lower. Even so, this kind of loss poses serious efficiency losses and could pose work and environmental hazards. Further, regulations may prohibit such quantities of emissions at ground level. Typical aerial productivities for pond and raceway reactors are between 8 and 14 gBDW/m²/day [101]. BDW stands for BioMass on a Dry Weight basis and is equal to half the weight of CO₂ that went into it [102].

Outdoor closed systems have the advantage of cell culture protection and relatively small aerial footprints [71, 108]. Within this class of reactors, the organisms and growth media are pumped through a network of photo transmitting tubes or plates which are in direct exposure to sunlight. This prevents loss of CO₂ to the atmosphere and can generally increase the production per square meter of land because one has more control over the light exposure conditions [71, 101, 108]. Furthermore, because the organisms are contained within a closed circulating loop, harvesting and control of nutrient mix is much easier [101]. Aerial productivities have been reported to be as high as 130 gBDW/m²/day by this method [101, 108].

Indoor closed systems have the advantage of complete control over microbial environment. Productivities should be the highest for this method because the environment is as close to optimum in growth conditions as possible all of the time. However, these systems are complex and expensive because they now need to have a light collection and delivery system. Even so, the cost may be offset through high productivity and the ability to hybridize the collected light. That is to say that only the photosynthetically active radiant (PAR – 400 to 700nm [71, 104, 109]) is sent to the PBR, while the rest is filtered off and used elsewhere for something like photovoltaic generation or heat [100, 102, 110].

The greatest challenge in designing a PBR is controlling the light intensity that the microbes are exposed to. This is an important issue because it greatly affects the required size of the light collection system. There is a light saturation point for which the photoactive molecules can no longer convert all active light into chemical energy at maximum efficiency. Below this saturation point the photosynthetic efficiency is in the range of 20-24% of PAR (roughly 10-12% total solar irradiation) [107, 109]. Above the saturation point, the efficiency drops rapidly and then levels out around 30 times the light saturation intensity at a thermodynamic efficiency of about 3% of PAR [109]. This is shown in Figure 16.

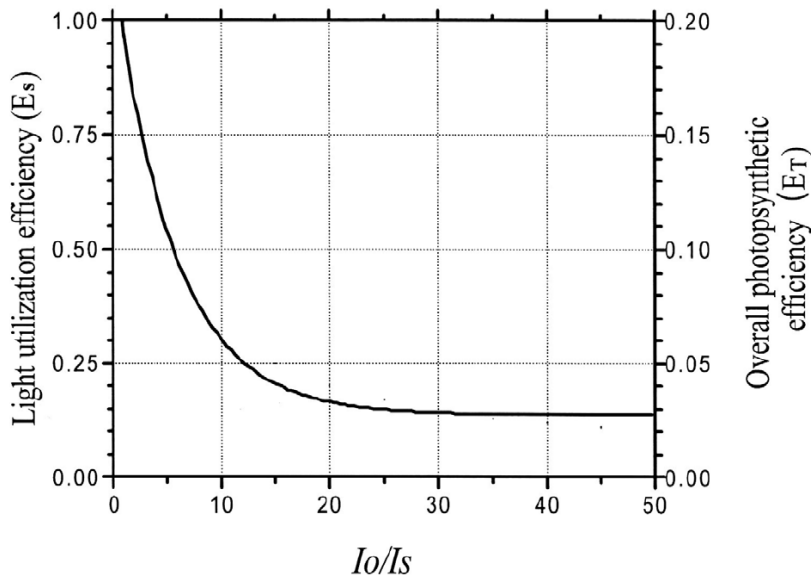


Figure 16
Photosynthetic Efficiency vs Light Intensity [109]

Here, I_o is the incident light intensity, I_s is the saturation light intensity, $E_s = I_s/I_o(\ln(I_o/I_s+1))$ is the light utilization efficiency as proposed by V. Bush, and E_T is the over all efficiency defined as the higher heating value of the biomass over the light energy in the PAR [109]. E_s is a measure of the absorption of photons by photosynthetic pigments [109]. E_T scales with E_s but is not equal to it because the conversion efficiency of excited pigment states to chemical energy is approximately 20% [109]. For most microbes, the saturation intensity (measured in moles of photons per area per time) is in the region of $200 \mu\text{mol}/\text{m}^2/\text{s}$ and the typical light intensity of a summer day is around $2000 \mu\text{mol}/\text{m}^2/\text{s}$ [109].

This principle can be seen in the study done on the outdoor thin film reactor by Doucha. In this experiment, reaction slurry that contains nutrients, dissolved CO₂, and the microbes was pumped over a slightly inclined plane that was exposed to direct sunlight. In doing so, a thin, consistent falling film was developed over the surface of the inclined plane. Figure 17 shows the flux of oxygen out of the thin film culture as a function of PAR light intensity. The flux of oxygen should be directly proportional to the rate of photosynthesis. The data is consistent with the theory set forth by V. Bush as seen in Figure 18 [104, 109].

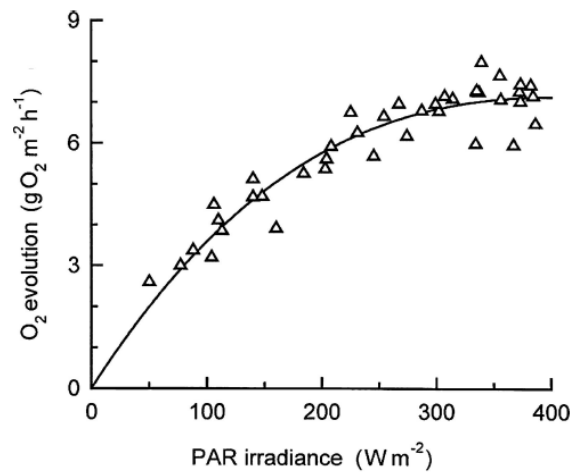


Figure 17

Oxygen Evolution vs PAR irradiance for Thin Film Outdoor Reactor [104]

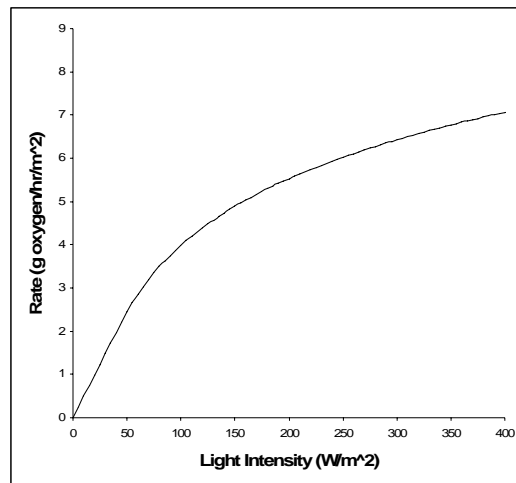


Figure 18

Theoretical Calculation of Oxygen Evolution as a Function of PAR Irradiance

Notice that the authors fit to the data is somewhat different than the expected theory, but also notice that the theory also closely predicts the trends in the data. It is reasonable to expect that the rate of photosynthesis is proportional to $E_T = 0.2 * E_s$ from Bush's theory, and the PAR light intensity. It is also known that photosynthesis produces glucose, for every mole of glucose, 6 moles of oxygen are evolved, and that the heat of reaction is 2805 kJ/mol glucose. The theory then predicts the rate of oxygen evolution as: $Rate = k * E_T * I_o$, where $k = \text{Molar Ratio}(O_2:\text{Glucose}) * \text{Mwt}(O_2) / \text{Heat of Rxn}(\text{Glucose}) * 3600$ which has units of gO₂/hr, E_s and I_o

are defined above, and I_s was 45W/m^2 . The Molar ratio is 6, the Mwt is 32, and the Heat of reaction is

Figure 19 is data from the same study that shows light intensity and cell culture temperature vs the time of day. From Figure 19, it can be seen that for the majority of the day, the light intensity is above 300 W/m^2 . It is quite evident that for the majority of the day the microbes are being forced to work in an intensity region that is quite inefficient. It is a small wonder then, that the overall efficiency was found to be between 5.5 to 6.9% of PAR rather than closer to 20% [104]. It is also not surprising that the utilization of PAR energy percentage grew as the data collection date moved away from the summer solstice because the exposure angle grew lowering the light intensity. For the same reason, placing plate or tube banks at an angle to the incident radiation can improve the overall productivity per square meter of land area by an order of magnitude [101, 108]. Placing the tube banks at an angle allows the light to be spread out over the reactor area, thereby reducing the light flux per square meter of reactor.

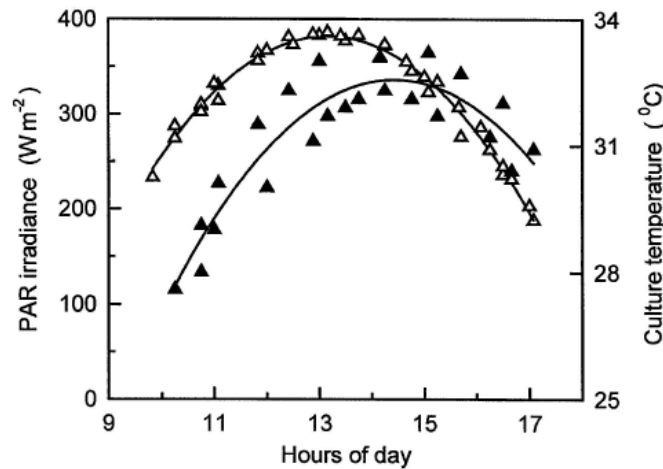


Figure 19

Light Intensity (white triangles) and Culture Temperature (black triangles) vs Time of Day [104]

If operating at high light intensities, a large change in angle to incident light (change in light flux) results in a small change in photosynthetic rate per square meter of reactor area as seen in Figure 17; however, a large change in angle to incident light can result in a large change in total reactor area exposed to light. It was found that an angle of approximately 80° between the sun at its highest point in the day and the plane of the reactor results in highest productivities per square meter of land [108]. Furthermore, placing the reactor at an angle has the effect of evening out the solar flux throughout the day as seen in Figure 20. The incident angle is given above the line.

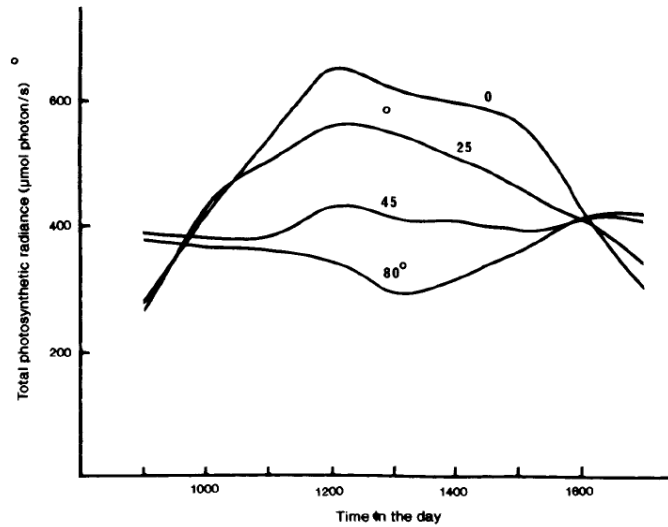


Figure 20

Total Reactor Photon exposure per second vs Time of day [108]

From what was observed from inclined tube and plate designs, it is beneficial to lower light intensity while shortening the light path distance. This would be applicable to volume normalized production (as opposed to area normalized production schemes such as film and plate PBR) as well. It will be good to increase the luminous sources within an indoor PBR while lowering the intensity of each source. This will lower the average light path within the reactor and provide consistent, lower light at levels that maximize efficiency. These conditions will allow for the maximum cell density within the reactor and maximize the productivity.

Light Collection

Active light collection and transmission is only necessary if used with an indoor reactor. There are four standard light collectors used in the solar industry: parabolic dish array, parabolic trough, linear Fresnel reflector, and light tower [110]. In the parabolic dish array, a reflector/collector is used that is much the same as a satellite dish. It actively tracks the sun in two axis. The light is reflected off of the parabolic surface to a focal point at which it is collected and utilized or transmitted through fiber optics [110-112]. The parabolic trough is quite similar except it is one axis tracking and instead of a focal point, a focal line is created. Thus the collector is linear and placed along the focal line [110]. The light can be utilized there or transmitted by fiber optics [100, 113]. The linear Fresnel reflector is similar to the trough except an array of flat, narrow mirrors is distributed collinearly to the focal line. The array of mirrors can be adjusted in a single axis to focus the light on a linear collector [110]. The light tower works somewhat differently. An array of flat plate reflectors is spread out around a central tower. Each mirror actively tracks the sun such that the reflected light of each mirror hits the tower at a common point [110]. At this point, the light would be collected, utilized, or transmitted by fiber optics to the reactor. This kind of array has been widely developed and commercialized. It also has the potential to be most cost effective in a biological application. Beam splitting technology has been developed for this kind of system and light collection efficiencies of >90% incident ground radiation has been demonstrated [110]. The beam splitting

technology was developed to allow for collected light to be split and active wavelengths sent to photovoltaic cells and the rest to thermal generation. This technology could be adapted to allow for photosynthetically active wavelengths to be sent to a bioreactor, photovoltaically active wavelengths sent to PV cells, and for the remainder to generate heat for a heat cycle. This could help generate capital to pay for the expense of the solar collector.

Another potentially interesting technology is that of micro dish arrays. Micro dish arrays were developed for the transmission of sunlight through fiber optic lines. Each dish is sized to the optimal transmission intensity of a single fiber optic line. The dishes are then arrayed on a larger panel and the lines collected in a bundle and taken elsewhere for use [111, 112]. If this can be done cost effectively and efficiently, it may be a good solution for indoor PBR's.

The size and subsequent cost of the solar collector may be prohibitive. Given a target sequestration rate of 4.65Mt CO₂/year, a reaction energy of 467.5kJ/mol CO₂, a thermodynamic, photosynthetic efficiency of 10%, and a daily average solar energy density of roughly 0.375 W/m² [114], it was calculated that a minimum of 37.9km² is needed to support the photosynthesis at that rate. It can also be expected that the cost of the solar collector will be in the range of \$100/m², resulting in a capital investment of \$3.7 billion [110, 115].

It is because of this cost that the light utilization efficiency is critical. The lower the efficiency, the more light energy it takes to complete the photosynthesis and the larger the collector size must be. This must be balanced by the complexity and the cost of the reactor system. As seen in Figure 17, the rate does decrease when light intensity decreases. When the rate decreases, the size of the reactor increases. Increasing the light utilization will reduce the size and cost of the collector, but will increase the size and cost of the reactor. The largest variable in this is the saturation light intensity for given types of organisms. The response of the rate to changes in temperature, pH, nutrient content, etc will be critical to the design.

Thermal Pretreatment

For direct flue gas injection methods, the temperature of the flue gas is a problem for the growth of microalgae. The majority of microalgae cannot survive above 35 to 40°C, though some have been reported to survive as high as 50°C [101, 102]. Little has been proposed as a solution. However, one solution was identified as part of a DOE funded project. A type of heat exchanger termed a translating slug flow exchanger was proposed. This type of exchanger consists of a tube lined with a helical coil through which cooling water is circulated. The diameter is set such that the water condensate forms slugs that travel down the length of the exchanger with the flue gas. During this process the condensate and flue gas are cooled together and the water becomes saturated with carbonic acid. The water and flue gas are then sent to the PBR to be fed to the microbes [116]. This represents an interesting blend of technology. It may also be advantageous to include a low temperature heat cycle within the process to recover some energy and do useful work.

Cost Estimates

Cost estimates range from \$0 to \$250 per ton CO₂ [100, 101, 107, 117]. Some argue that the venture could be profitable based on the sale of high value products [99]. The most reasonable and in depth study gave a cost of \$30 per ton CO₂ in 1997 [117]. This, however, will have to be amended because of the near doubling of the price of a barrel of oil since that time. It is also

important to note that the markets for microalgae and microalgae products are new and growing fast. In 1999, the world production of microalgae biomass was around 7,300 tons/year and the market for the major microalgae product, *Spirulina*, grew by almost 21% [105]. If that is an indication of the market trend today, the market for microalgae would be around 18kt. Even with the small market it is important to realize that most markets for microalgae derived products are in their infancy. It is impossible to predict what the value or market potential for certain microalgae will be, but it looks promising and large [105]. It may very well be that microalgae sequestration will have the market support and value to be profitable in the future.

Conclusion

Industrial PBRs represent an interesting blend of technology which, if done in a carefully considered manner and if applied to the correct situation, could provide a solution to excess CO₂ generation in a renewable, sustainable, and economical fashion. Given that the solar field collector costs are comparable for indoor, closed systems, the most cost effective solution may be to implement a volume normalized system with a central tower array which can split and individually utilize the different wavelengths of light.

Team Conclusion

Under the right circumstances, any of the methods investigated above may prove to be viable. However, based on our team interests, public perception issues, and logistical issues, a combination of an industrial bioreactor system and the geological storage methods will be further investigated and recommended as a design.

References

1. IPCC, Special Report on Carbon Dioxide Capture and Storage, in *Summary of Policymakers and Technical Summary*, B. Metz, O. Davidson, H.d. Coninck, M. Loos, and L. Meyer, Editors. 2004, Intergovernmental Panel on Climate Change: United Nations.
2. Celia, MA and S Bachu. Geological sequestration of CO₂: Is leakage unavoidable and acceptable? in *6th International Conference on Greenhouse Gas Control Technologies (GHGT-6), September 30 - October 4, 2002*. 2002. Kyoto, Japan.
3. Bachu, S. Sequestration of CO₂ in geological media: criteria and approach for site selection in response to climate change. *Energy Conversion and Management*, 2000;**41**(9): 953-70.
4. Holloway, S. Storage of fossil fuel-derived carbon dioxide beneath the surface of the earth. *Annual Review of Energy and the Environment*, 2001;**26**: 145-66.
5. Shafeen, A, E Croiset, PL Douglas, and I Chatzis. CO₂ sequestration in Ontario, Canada. Part II: cost estimation. *Energy Conversion and Management*, 2004;**45**(20): 3207-17.
6. Freund P, DJ. General overview of cost. IEA Greenhouse Gas R&D Programme., IPCC Workshop on Carbon Capture and Storage, Regina, Canada, 2002.
7. Hendriks, C. Carbon Dioxide removal from coal fired power plants. Dordrecht: Kluwer Academic Publishers, 1994.
8. Zhang, ZX, GX Wang, P Massarotto, and V Rudolph. Optimization of pipeline transport for CO₂ sequestration. *Energy Conversion and Management*, 2006;**47**(6): 702-15.
9. Hawkins, DG. No exit: thinking about leakage from geologic carbon storage sites. *Energy*, 2004;**29**(9): 1571-8.
10. Hendriks, CA and K Block. Underground storage of carbon dioxide. *Energy Conversion Management*, 1993;**34**(9): 949-57.
11. Metz, B, O Davidson, H de Coninck, M Loos, L Meyer, and Eds., Carbon dioxide capture and storage, summary for policymakers, in *IPCC Special Report*. 2005.
12. Keith, DW, JA Giardina, MG Morgan, and EJ Wilson. Regulating the underground injection of CO₂. *Environmental Science & Technology*, 2005;**39**(24): 499A-505A.
13. West, J, J Pearce, M Bentham, and P Maul. Issue Profile: Environmental Issues and the Geological Storage of CO₂. *European Environment*, 2005;**15**: 250-9.
14. Wilson, EJ, TL Johnson, and DW Keith. Regulating the ultimate sink: Managing the risks of geologic CO₂ storage. *Environmental Science & Technology*, 2003;**37**(16): 3476-83.
15. Bruant, RG, AJ Guswa, MA Celia, and CA Peters. Safe storage of CO₂ in deep saline aquifers. *Environmental Science & Technology*, 2002;**36**(11): 240A-5A.
16. Klara, SM, RD Srivastava, and HG McIlvried. Integrated collaborative technology, development program for CO₂ sequestration in geologic formations - United States Department of Energy R&D. *Energy Conversion and Management*, 2003;**44**(17): 2699-712.
17. Farrar, C, J Neil, and J Howle, U.S. Geological Survey Water-Resources Investigations Report, WRI98-4217, in *U.S. Geological Survey*. 1999.
18. Mintzer I, LJ, Schwartz P,. US Energy scenarios for the 21st century: Appendix B: Technology Assessments. 2003.
19. Friedmann, SJ, JJ Dooley, H Held, and O Edenhofer. The low cost of geological assessment for underground CO₂ storage: Policy and economic implications. *Energy Conversion and Management*, In Press, Corrected Proof.

20. Schroeder, K, E Ozdemir, and BI Morsi. Sequestration of carbon dioxide in coal seams. in *First National Conference on Carbon Sequestration, U.S. DOE and NETL, May 14-17, 2001*. 2001. Washington.
21. Callison, D, J Jones, and B Shelley. Field studies of enhanced methane recovery and CO₂ sequestration in coal seams. *World Oil*, 2002;**223**(12): 56-60.
22. Mahajan, OP. CO₂ surface area of coals: The 25-year paradox. *Carbon*, 1991;**29**: 735-42.
23. Reeves, S and A Oudinot. The Allison Unit CO₂-ECBM Pilot - A reservoir and economic analysis. in *Proceedings of the 2005 International Coalbed Methane Symposium*. 2005. Tuscaloosa, AL.
24. Stevens, SH, VA Kuuskraa, D Spector, and P Riemer. CO₂ sequestration in deep coal seams: Pilot results and worldwide potential. in *4th International Conference on Greenhouse Gas Control Technologies*. 1998. Interlake, Switzerland.
25. Reeves, S. Assessment of CO₂ sequestration and ECBM potential of U.S. coalbeds. Topical report for U.S. Department of Energy, (DE-FC26-00NT40924), February, 2003, 2003.
26. Gasem, KAM, RL Robinson, and SR Reeves. Adsorption of pure methane, nitrogen, and carbon dioxide and their mixtures on San Juan Basin coal. DOE Topical Report (DE-FC26-00NT40924), May, 2002, 2002.
27. Pashin, JC, RE Carroll, RH Groshong, DE Raymond, MR McIntyre, and WJ Payton. Geologic screening criteria for sequestration of CO₂ in coal: Quantifying potential of the Black Warrior Coalbed Methane Fairway, Alabama. Annual Technical Progress Report, U.S. Department of Energy, National Technology Laboratory (DE-FC-00NT40927), 2003: 190 pp.
28. Nelson, CR, DG Hill, and TJ Pratt, Properties of Paleocene Fort Union Formation Canyon Seam coal at the Triton Federal Coalbed methane well, Campbell County, Wyoming, in (*SPE 59786*) Presented in *CERI/SPE Gas Technology Symposium, April 3-5, 2000*. 2000: Calgary.
29. Saripalli, KP, NM Mahasenan, and EM Cook. Risk and hazard assessment for projects involving the geological sequestration of CO₂. in *6th International Conference on Greenhouse Gas Control Technologies (GHGT-6), September 30 - October 4, 2002*. 2002. Kyoto, Japan.
30. Ha-Duong, M and D Keith. Carbon storage: the economic efficiency of storing CO₂ in leaky reservoirs. *Clean Technologies and Environmental Policy*, 2003;**5**(3): 181-9.
31. Reeves, S and A Oudinot. The Tiffany Unit CO₂-ECBM Pilot - A reservoir and economic analysis. in *2005 International Coalbed Methane Symposium*. 2005. Tuscaloosa, AL.
32. Yamaguchi, S, K Ohga, M Fujioka, and S Muto. Prospect of CO₂ sequestration in the Ishikari coal field, Japan. in *7th International Conference on Greenhouse Gas Control Technologies*. 2004. Vancouver, Canada.
33. Pagnier, H, F van Bergen, P Krzystolik, J Skiba, B Jura, J Hadro, P Wentink, G De-Smedt, H-J Kretzschmar, J Frobel, G Muller-Syring, B Krooss, A Busch, K-H Wolf, S Mazumder, D Bossie-Codreanu, X Choi, D Grabowski, D Hurtevent, J Gale, P Winthaegen, B van der Meer, Z Kobiela, H Bruining, S Reeves, and S Stevens. Field experiment of ECBM-CO₂ in the Upper Silesian Basin of Poland (RECOPOL). in *7th International Conference on Greenhouse Gas Control Technologies, September 5-9, 2004*. 2004. Vancouver, Canada.

34. Gunter, WD, MJ Mavor, and JR Robinson. CO₂ storage and enhanced methane production: Field testing at Fenn-Big Valley, Alberta, Canada, with application. in *7th International Conference on Greenhouse Gas Control Technologies, September 5-9, 2004*. 2004. Vancouver, Canada.
35. Hepple, RP and SM Benson. Implications of surface seepage on the effectiveness of geologic storage of carbon dioxide as a climate change mitigation strategy. in *6th International Conference on Greenhouse Gas Control Technologies (GHGT-6)*. 2002. Kyoto, Japan.
36. Celia, MA, S Bachu, JM Nordbotten, S Gasda, and HK Dahle. Quantitative estimation of CO₂ leakage from geological storage: Analytical models, numerical models, and data needs. in *7th International Conference on Greenhouse Gas Control Technologies*. 2004. Cheltenham, UK.: IEA Greenhouse Gas Programme.
37. EPA. Evaluation of impacts to underground sources of drinking water by hydraulic fracturing of coalbed methane reservoirs. EPA Publication 816-R-04-003, 2004.
38. Aycaguer, A-C, M Lev-On, and AM Winer. Reducing Carbon Dioxide Emissions with Enhanced Oil Recovery Projects: A Life Cycle Assessment Approach. *Energy & Fuels*, 2001;**15**: 303-8.
39. Voormeij, DA and GJ Simandl. Geological, ocean, and mineral CO₂ sequestration options: A technical review. *Geoscience Canada*, 2004;**31**(1): 11-22.
40. Gentzis, T. Subsurface sequestration of carbon dioxide - an overview from an Alberta (Canada) perspective. *International Journal of Coal Geology*, 2000;**43**(1-4): 287-305.
41. Bachu, S. Sequestration of CO₂ in geological media in response to climate change: road map for site selection using the transform of the geological space into the CO₂ phase space. *Energy Conversion and Management*, 2002;**43**(1): 87-102.
42. Oldenburg, CM, SH Stevens, and SM Benson. Economic feasibility of carbon sequestration with enhanced gas recovery (CSEGR). *Energy*, 2004;**29**(9): 1413-22.
43. Kovscek, AR and MD Cakici. Geologic storage of carbon dioxide and enhanced oil recovery. II. Cooptimization of storage and recovery. *Energy Conversion and Management*, 2005;**46**(11-12): 1941-56.
44. Tontiwachwuthikul, P, CW Chan, W Kritpiphat, D Demontigny, D Skoropad, A Gelowitz, and A Aroonwilas. Large Scale Carbon Dioxide Production from Coal-fired Stations for Enhanced Oil Recovery: A New Economic Feasibility Study. *Journal of Canadian Petroleum Technology*, 1998;**37**(11): 48-55.
45. Bergman, PD and EM Winter. Disposal of Carbon-Dioxide in Aquifers in the Us. *Energy Conversion and Management*, 1995;**36**(6-9): 523-6.
46. Bachu, S and JJ Adams. Sequestration of CO₂ in geological media in response to climate change: capacity of deep saline aquifers to sequester CO₂ in solution. *Energy Conversion and Management*, 2003;**44**(20): 3151-75.
47. Holloway, S. Underground sequestration of carbon dioxide--a viable greenhouse gas mitigation option. *Energy*, 2005;**30**(11-12): 2318-33.
48. Allen, DE, BR Strazisar, Y Soong, and SW Hedges. Modeling carbon dioxide sequestration in saline aquifers: Significance of elevated pressures and salinities. *Fuel Processing Technology*, 2005;**86**(14): 1569-80.
49. Johnston, P, D Santillo, and R Stringer, Ocean Disposal/Sequestration of Carbon Dioxide from Fossil Fuel Production and Use: An Overview of Rationale, Techniques, and

- Implications, in *Technical Note 01/99*. 1999, Greenpeace Research Laboratories: Amsterdam, Netherlands. p. 1-51.
50. MBARI, Density of CO₂ at Pressure, in *Ocean Chemistry of Greenhouse Gases*. 2004, Monterey Bay Aquarium Research Institute: Monterey Bay, California.
 51. DOE, U. Direct Ocean Sequestration Expert's Workshop. in *Final Report - US Dept. of Energy, National Energy Technology Laboratory*. 2001. Monterey Bay Aquarium Research Institute: US DOE.
 52. Shindo, Y, Y Fujioka, and H Komiyama. Dissolution and Dispersion of CO₂ from a Liquid CO₂ Pool in the Deep Ocean. *International Journal of Chemical Kinetics*, 1995;**27**: 1089-95.
 53. Caldeira, K and M Wickett. Anthropogenic carbon and ocean pH. *Nature*, 2003;**425**(September): 365.
 54. Caulfield, JA, DI Auerbach, EE Adams, and HJ Herzog. Near Field Impact of Reduced pH from Ocean CO₂ Disposal. *Energy Conversion and Management*, 1997;**38**(Suppl.): S337-S41.
 55. Nakashiki, N and T Ohsumi. Dispersion of CO₂ Injected in the Ocean at Intermediate Depth. *Energy Conversion Management*, 1997;**38**(Suppl.): S343-S8.
 56. Adams, EE, JA Caulfield, HJ Herzog, and DI Auerbach. Impacts of Reduced pH from Ocean CO₂ Disposal: Sensitivity of Zooplankton Mortality to Model Parameters. *Waste Management*, 1997;**17**(5/6): 381-4.
 57. Shirayama, Y. Biodiversity and Biological Impact of Ocean Disposal of Carbon Dioxide. *Waste Management*, 1997;**17**(5/6): 381-4.
 58. Sarv, H, Large-Scale CO₂ Transportation and Deep Ocean Sequestration, in *Phase I Final Report*, U.D.o. Energy, Editor. 1999, US DOE.
 59. Markels, MJ and RT Barber. Sequestration of CO₂ by Ocean Fertilization. in *NETL Conference on Carbon Sequestration*. 2001.
 60. Fuhrman, JA and DG Capone. Possible biogeochemical consequences of ocean fertilization. *Limnology and Oceanography*, 1991;**36**(8): 1951-9.
 61. Williams, PM and ERM Druffel. Radiocarbon in Dissolved Organic Carbon in the Central North Pacific Ocean. *Nature*, 1987;**330**: 246-8.
 62. Lal, R. Soil carbon sequestration to mitigate climate change. *Geoderma*, 2004;**123**: 1-22.
 63. Nor, SM, C Pinso, and AHA Ali. Tropical forestry and carbon sequestration. in *Workshop on Emission Trading & Clean Development Mechanism (CDM) in Asia*. 2001. Singapore.
 64. Robert, M, Soil carbon sequestration for improved land management. 2001, Rome: Food and Agriculture Organization of the United Nations, World Soil Resources Report. 57.
 65. IPCC, Land use change, and forestry: A special report of the IPCC, ed. R. Watson, I.R. Noble, B. Bolin, N.H. Ravindranath, D.J. Verardo, and D.J. Dokken. 2000, New York: Cambridge University Press. 377.
 66. Roper, J, Tropical forests and climate change, C.C.F.A. Network, Editor. 2001.
 67. Litynski, JT and SM Klara, Terrestrial Sequestration Program: Capture and storage of carbon in terrestrial ecosystems, in *Program Facts*, N.E.T.L. U.S. Department of Energy, Editor. 2003.
 68. Albrecht, A and ST Kandji. Carbon sequestration in tropical agroforestry systems. *Agriculture Ecosystems and Environment*, 2003;**99**: 15-27.
 69. Barbier, E. Tropical deforestation. *Nature*, 1989;**339**(29): 655-6.

70. Tschakert, P. The costs of soil carbon sequestration: An economic analysis for small-scale farming systems in Senegal. *Agricultural Systems*, 2004;**81**: 227-53.
71. Richmond, A and Z Cheng-Wu. Optimization of a flat plate glass reactor for mass production of *Nannochloropsis* sp outdoors. *Journal of Biotechnology*, 2001;**85**(3): 259-69.
72. Lackner, KS, CH Wendt, DP Butt, EL Joyce, and DH Sharp. Carbon dioxide disposal in carbonate minerals. *Energy*, 1995;**20**: 1153-70.
73. Kohlmann, RZaJ. Second Nordic Minisymposium on Carbon Dioxide Capture and Storage. available at <http://www.entek.chalmers.se/~anly/symp/symp2001.html>, 2001.
74. Goff, FL, K. S. Carbon dioxide sequestering using ultramafic rocks. *Environmental Geosciences*, 1998;**5**(89-101).
75. Lackner, KS, DP Butt, CH Wendt, and DH Sharp. Carbon dioxide disposal in solid form. in *21st international conference on coal utilization and fuel systems*. 1996. Clearwater, Florida.
76. Lackner, KS and HJ Ziock. From low to no emissions. *Modern Power Systems*, 2000;**20**(3): 31-2.
77. Lackner, KS. Carbonate chemistry for sequestering fossil carbon,. *Annual Review of Energy and the Environment*, 2002(27): 193-232.
78. NETL. Proceeding of workshop NETL Mineral CO₂ sequestration. 2001.
79. O'Connor, WK, DC Dahlin, DN Nilsen, RP Walters, and PC Turner. Carbon dioxide sequestration by direct mineral carbonation with carbonic acid. in *25th international technical conference on coal utilization and fuel systems, Clearwater, Florida*. 2000.
80. Fauth, DJ, PM Goldberg, JP Knoer, Y Soong, WK O'Connor, DC Dahlin, DN Nilsen, RP Walters, KS Lackner, H-J Ziock, MJ McKelvy, and Z-Y Chen. Carbon dioxide storage as mineral carbonates. *American Chemical Society, Division Fuel Chemistry*, 2000: 708-12.
81. O'Connor, WK, DC Dahlin, DN Nilsen, SJ Gerdemann, GE Rush, RP Walters, and PC Turner. Research status on the sequestration of carbon dioxide by direct aqueous mineral carbonation. in *18th annual international Pittsburgh coal conference, Newcastle, Australia*. 2001.
82. O'Connor, WK, DC Dahlin, DN Nilsen, GE Rush, RP Walters, and PC Turner. CO₂ storage in solid form: a study of direct mineral carbonation. *5th international conference on greenhouse gas technologies, Cairns, Australia.*, 2000.
83. Zevenhoven, RK, J. CO₂ sequestration by magnesium silicate mineral carbonation in Finland. in *R'02 Recovery, Recycling, Re-integration*. 2002. Geneva, Switzerland.
84. Lackner, KS, DP Butt, and CH Wendt. Progress on binding CO₂ in mineral substrates. *Energy Conversion and Management*, 1997;**38**(S259-S264).
85. O'Connor, WK, DC Dahlin, PC Turner, and R Walters. Carbon dioxide sequestration by exsitu mineral carbonation. *Second Dixy Lee Memorial Symposium: Utilization of fossil fuelgenerated carbon dioxide in agriculture and industry, Washington DC.*, 1999.
86. Wendt, CH, DP Butt, KS Lackner, and H-J Ziock. Thermodynamic calculations for acid decomposition of serpentine and olivine in MgCl₂ melts. *Los Alamos National Laboratory, Los Alamos, New Mexico, LA-UR-98-4528.*, 1998.
87. Butt, DP, KS Lackner, and CH Wendt. The kinetics of binding carbon dioxide in magnesium carbonate. in *23th international conference on coal utilization and fuel systems*. 1998. Clearwater, Florida, USA.

88. Newall, PS, SJ Clarke, HM Haywood, H Scholes, NR Clarke, and PA King. CO₂ storage as carbonate minerals. in *IEA*. 1999. Cheltenham, UK.
89. Kakizawa, MY, A. & Yanagisawa, Y. A new CO₂ disposal process using artificial rock weathering of calcium silicate accelerated by acetic acid. *Energy*, 2001(26): 341-54.
90. Huang, HP, Y Shi, W Li, and SG Chang. Dual alkali approaches for the capture and separation of CO₂. *Energy and Fuels*, 2001;15: 263-8.
91. McKelvy, MJ, AVG Chizmeshya, H Bearat, R Sharma, and RW Carpenter. Developing a mechanistic understanding of lamellar hydroxide mineral carbonation reaction processes to reduce CO₂ mineral sequestration process cost. NETL Conference on Carbon Sequestration., 2001.
92. McKelvy, MJ, R Sharma, AVG Chizmeshya, RW Carpenter, and K Streib. Magnesium hydroxide dehydroxylation: in situ nanoscale observations lamellar nucleation and growth. *Chemistry of Materials*, 2001;13(3): 921-6.
93. Butt, DP, KS Lackner, CH Wendt, SD Conzone, H Kung, YC Lu, and JK Bremser. Kinetics of thermal dehydroxylation and carbonation of magnesium hydroxide. *Journal of American Ceramic Society*, 1996;79(7): 1892-8.
94. Guthrie, GD, JW Carey, D Bergfeld, D Byler, S Chipera, HJ Ziock, and KS Lackner. Geochemical aspects of the carbonation of magnesium silicates in an aqueous medium. NETL Conference on Carbon Sequestration., 2001.
95. Gerdemann, SJ, DC Dahlin, and WK O'Connor. Carbon dioxide sequestration by aqueous mineral carbonation of magnesium silicate minerals. in *6th international conference on greenhouse gas control technologies*. 2002. Kyoto, Japan.
96. Fernandez, AI, JM Chimenos, M Segarra, MA Fernandez, and F Espiell. Kinetic study of carbonation of MgO slurries. *Hydrometallurgy*, 1999;53(2): 155-67.
97. Kojima, T, A Nagamine, N Ueno, and S Uemiya. Absorption and fixation of carbon dioxide by rock weathering. *Energy Conversion and Management*, 1997;38: S461-S6.
98. David, J. Economic evaluation of leading technology options for sequestration of carbon dioxide. Massachusetts Institute of Technology., 2000.
99. Olaizola, M. Commercial development of microalgal biotechnology: from the test tube to the marketplace. *Biomolecular Engineering*, 2003;20(4): 459-66.
100. Stewart, C and MA Hessami. A study of methods of carbon dioxide capture and sequestration - the sustainability of a photosynthetic bioreactor approach. *Energy Conversion and Management*, 2005;46(3): 403-20.
101. Lee, JS and JP Lee. Review of advances in biological CO₂ mitigation technology. *Biotechnology and Bioprocess Engineering*, 2003;8(6): 354-9.
102. Bayless, D, M Vis, G Kremer, and M Prudich, Carbon Dioxide Mitigation through Controlled Photosynthesis, in *PBD: 1 Oct 2000*. 2000. p. 32 pages ; PDFN.
103. Murakami, M and M Ikenouchi. The biological CO₂ fixation and utilization project by RITE .2. Screening and breeding of microalgae with high capability in fixing CO₂. *Energy Conversion and Management*, 1997;38: S493-S7.
104. Doucha, J, F Straka, and K Livansky. Utilization of flue gas for cultivation of microalgae (*Chlorella* sp.) in an outdoor open thin-layer photobioreactor. *Journal of Applied Phycology*, 2005;17(5): 403-12.
105. Pulz, O and W Gross. Valuable products from biotechnology of microalgae. *Applied Microbiology and Biotechnology*, 2004;65(6): 635-48.

106. Singh, S, BN Kate, and UC Banerjee. Bioactive compounds from cyanobacteria and microalgae: An overview. *Critical Reviews in Biotechnology*, 2005;**25**(3): 73-95.
107. Benemann, JR. CO₂ mitigation with microalgae systems. *Energy Conversion and Management*, 1997;**38**: S475-S9.
108. Yuan-Kun Lee, C-SL. Effect of photobioreactor inclination on the biomass productivity of an outdoor algal culture. *Biotechnology and Bioengineering*, 1991;**38**(9): 995-1000.
109. Torzillo, G, B Pushparaj, J Masojidek, and A Vonshak. Biological constraints in algal biotechnology. *Biotechnology and Bioprocess Engineering*, 2003;**8**(6): 338-48.
110. Mills, D. Advances in solar thermal electricity technology. *Solar Energy*, 2004;**76**(1-3): 19-31.
111. Feuermann, D and JM Gordon. Solar fiber-optic mini-dishes: A new approach to the efficient collection of sunlight. *Solar Energy*, 1999;**65**(3): 159-70.
112. Feuermann, D, JM Gordon, and M Huleihil. Solar fiber-optic mini-disit-concentrators: First experimental results and field experience. *Solar Energy*, 2002;**72**(6): 459-72.
113. Coventry, JS. Performance of a concentrating photovoltaic/thermal solar collector. *Solar Energy*, 2005;**78**(2): 211-22.
114. NREL, U.S. Solar Radiation Resource Maps, http://rredc.nrel.gov/solar/old_data/nsrdb/redbook/atlas/.
115. Price, H and D Kearney. Reducing the Cost of Energy from Parabolic Trough Solar Power Plants. in *ISES 2003*. 2003. Hawaii Island, Hawaii.
116. Bayless, DJ, GG Kremer, ME Prudich, BJ Stuart, ML Vis-Chiasson, K Cooksey, and J Muhs. Enhanced Practical Photosynthetic CO₂ Mitigation. 2001.
117. Kadam, KL. Plant flue gas as a source of CO₂ for microalgae cultivation. Economic impact of different process options. *Energy Conversion and Management*, 1997;**38**: S505-S10.

Appendix B

Matlab Code for Light Distribution Modeling

```

syms axd adx x d lo c
em=50;
kc=2.7;
kx=4.7;
saturated_light=45;
dist=.7;

cellconc=2;
pct=.95;

ccmin=0;
ccmax=3;
n=10000;
stepsize=(ccmax-ccmin)/n;
cellconc=zeros(1,n);
photorate=zeros(1,n);
laparent=zeros(1,n);
INoLoss=zeros(1,n);

into=saturated_light;
lapp=1;
for p = 0:1000
    for i = 1:n
        latd=0;
        llost=0;
        cellconc(i)=ccmin+(i-1)*stepsize;
        for z=0:100
            latd=lapp*exp(-em*cellconc(i)/((kc+cellconc(i))*(kx+dist))*dist^2);
            lappold=lapp;
            lapp=into+pct^2*latd;
            Inorefloss=into+latd;
            if abs(lapp-lappold) < .00001
                break
            end
        end
        laparent(i)=lapp;
        Em=0.2;
        K=0.156;
        G=2.04;
        A=1;

R=1.85379905333786/(2.58240989468827+cellconc(i))^5.81859065287705+0.0027152
6957864673;
        lutil=(into-(Inorefloss-lapp))^2;
        Y=Em*lutil*A*K-G*R*cellconc(i)*A*dist*10;
        photorate(i)=Y^44/(12*G*10*A*dist)*1000;
    end
end

```

```

INoLoss(i)=Inorefloss;
end

maxrate=max(photorate);
for i = 1:n
if photorate(i) == maxrate
break
end
end

apparent_light=laparent(i);
axd=em*cellconc(i)/((kc+cellconc(i))*(kx+x));
adx=em*cellconc(i)/((kc+cellconc(i))*(kx+dist-x));
l=apparent_light*(exp(-axd*x)+exp(-adx*(dist-x)));
latzero=subs(l,x,0);

if abs(latzero-saturated_light)/saturated_light < 0.0001
break
else
into=into+(saturated_light-latzero)*.05;
end
end

apparent_light
maxrate=maxrate/1000*24
ASR=maxrate*dist*10
cellconcentration=cellconc(i)
latd=lapp*exp(-em*cellconc(i)/((kc+cellconc(i))*(kx+dist))*dist);
light_lost=INoLoss(i)-laparent(i);
into

figure(1)
plot(cellconc,photorate)
axis([0 ccmx 0 max(photorate)*1.05])
xlabel('Cellular Concentration [g dry weight/L]')
ylabel('CO2 Fixation Rate [g CO_2/m^3/h]')

latzero;
lave=eval(1/dist*int(l,0,dist))

figure(2)
ezplot(l,[0 dist])
axis([0 dist 0 1.05*saturated_light])
title('')
xlabel('Position Between Plates [cm]')

```

ylabel('PAR Light Intensity [W/m^2]')

co2perday=4.65/2*1000000*2000*453.59237/365;

TotalVolume=co2perday/maxrate/1000

TotalArea=co2perday/ASR

PARLightRequired=TotalArea*into*2/1000

TotalLightCollectionReq=PARLightRequired*2

LightUtilizationEff=1-light_lost/into

Appendix C

Solar Sizing Calculations

The following procedure was used in the calculation of the solar collector surface area required to supply the necessary amount of light to the photosynthetic bioreactor. One main presumption here is that the system is optimized so that all the energy produced is used in the PBR. Also, initially all visible light is sent for use in photo-bioreactor but once enough power from visible light is collected and sent to the photo-bioreactor that some of the heliostats would be adjusted so that the excess visible light power would be sent to central towers to aid in electricity production.

Variables:

Variable Name	Symbol	Value	Description
Reflective surface area of solar collector	$A_{\text{collector}}$	Solved for	The area of the reflective area of the solar collector is the value that was solved for
Solar collector reflection	$\epsilon_{\text{collector}}$	95 %	Assumes 5% of light energy reaching heliostat surface does not make it to central towers for various reasons. (dust on mirrors, dust in air, ect.)
Fiber-optic transmission	$\epsilon_{\text{fiber-optics}}$	80 %	Accounts for all losses incurred over the length of the fiber-optics
Photovoltaic electricity generation	$\epsilon_{\text{sun - DC}}$	15 %	Solar cells used in design have sun light energy to electrical (DC) output of up to 21.5%, but a working efficiency of 17.7%. We used 15% to include a safety factor.
DC to AC conversion	$\epsilon_{\text{DC - AC}}$	90 %	10% loss is estimated to occur during DC to AC conversion
Heat engine efficiency	$\epsilon_{\text{Heat - AC}}$	30%	Assumes 30% of thermal energy can be converted to electrical power (AC)
LED grow-lights	$\epsilon_{\text{collector}}$	90 %	The operational efficiency of LED based grow lights is 90%
Fraction of visible light	$f_{\text{visible_light}}$	45%	Fraction of total light energy present in 400 – 700 nm range
Max. intensity of sun energy	I_o	1.112 kW/m ²	Intensity of sun's energy in southwest US at solar noon

Equations used:

Equation Number	Description	Units	Equation
1	Solar intensity at time (t)	(kWh/m ² /day)	$I_{total} = I_o \sin\left(\frac{\pi t}{720}\right)$
2	Energy from the sun	(kW)	$P_{solar} = A_{collector} * I_{total}$
3	Power from sun collected for PBR	(kW)	$P_{to_reactor} = P_{solar} * f_{visible_light}$
4	Power from sun inside PBR	(kW)	$P_{in_reactor} = P_{to_reactor} * \epsilon_{fiberoptics} * \epsilon_{collector}$
5	Excess power sent to electricity generation system (Includes IR and part of visible light spectra)	(kW)	$P_{excess} = (P_{solar} - P_{to_reactor}) * \epsilon_{collection}$
6	Power from sun converted to AC (PV system)	(kW)	$P_{AC} = P_{excess} * \epsilon_{PV} * \epsilon_{DC-AC}$
7	Power from sun converted to AC (Heat engine system)	(kW)	$P_{AC} = P_{excess} * \epsilon_{CCLC}$
8	Electrical power converted to visible light using LED's in photo-bioreactor	(kW)	$P_{LED} = P_{AC} * \epsilon_{LED}$
9	Total Power sent to reactor	(kW)	$P_{total} = P_{to_reactor} + P_{AC}$

Procedure:

1. Solve for the intensity of the sun at time (t) from 0 – 720 minutes (equals a 12 hr period) using equation 1
2. Calculate power from sun for each time (t) using equation 2
3. Calculate sunlight power, visible portion, collected for photo-bioreactor at each time (t) using equation 3
4. Calculate amount of power from sun that is actually received in photo-bioreactor at each time (t) using equation 4 – use if then statement to adjust amount of visible light power going to photo-bioreactor so that excess light is not sent.
 - a. Total power required in 4.41×10^6 kW
 - b. Cell = if($P_{\text{inside reactor}} > 4.41 \times 10^6$, then 4.41×10^6 , else $P_{\text{inside reactor}}$)
5. Calculate rest of power that will be available for electricity generation using equation 5
6. Calculate amount of power converted to electricity (AC) using equation 6 if PV system or equation 7 if heat exchanger system
7. Calculate amount of power (light generated from electric system) sent to photo-bioreactor using equation 8
8. Sum all columns to get power in kWmin for each column then divide by 60 to get kWhr for each column
9. The total power needed in the PBR on a continuous basis is 4.41×10^6 kW
10. Calculate total amount of power (light from sun plus light from electric) sent to photo-bioreactor using equation 9
11. To solve for the minimum surface area required for the solar collectors use the difference of squares method on Total power required – Total power available, use the surface area of the solar collector as the changeable variable and solve for the minimum value of the difference of squares.
12. Repeat all steps to solve for the minimum required surface area given the other electricity generation system.

Appendix D

Capital Estimations

- D.1 – PBR System, Break Even with PV
- D.2 – PBR System, 15% ROI with PV
- D.3 – PBR System, Break Even with CCLC
- D.4 – PBR System, 15% ROI with CCLC
- D.5 – Saline Injection with CCLC for power
- D.6 – Saline Injection by Purchasing Power
- D.7 – Saline Injection by Reducing Plant Capacity

Add Equipment

Unit Number 100

Edit Equipment

CEPCI 462.4

User Added Equipment

Storage Tanks	Tank Type	Volume (cubic meters)	Volume (gallons)	Purchased Equipment Cost	Bare Module Cost
Tk-101	Fixed Roof	30000		\$ 1,080,000	\$ 1,190,000
Tk-102	Fixed Roof	30000		\$ 1,080,000	\$ 1,190,000
Tk-103	Fixed Roof	30000		\$ 1,080,000	\$ 1,190,000
Tk-104	Fixed Roof	30000		\$ 1,080,000	\$ 1,190,000
Tk-105	Fixed Roof	30000		\$ 1,080,000	\$ 1,190,000
Tk-106	Fixed Roof	30000		\$ 1,080,000	\$ 1,190,000
Tk-107	Fixed Roof	30000		\$ 1,080,000	\$ 1,190,000
Tk-108	Fixed Roof	30000		\$ 1,080,000	\$ 1,190,000
Tk-109	Fixed Roof	30000		\$ 1,080,000	\$ 1,190,000
Tk-110	Fixed Roof	30000		\$ 1,080,000	\$ 1,190,000
Tk-111	Fixed Roof	30000		\$ 1,080,000	\$ 1,190,000
Tk-112	Fixed Roof	30000		\$ 1,080,000	\$ 1,190,000
Tk-113	Fixed Roof	30000		\$ 1,080,000	\$ 1,190,000
Tk-114	Fixed Roof	30000		\$ 1,080,000	\$ 1,190,000
Tk-115	Fixed Roof	30000		\$ 1,080,000	\$ 1,190,000
Tk-116	Fixed Roof	30000		\$ 1,080,000	\$ 1,190,000
Tk-117	Fixed Roof	30000		\$ 1,080,000	\$ 1,190,000
Tk-118	Fixed Roof	30000		\$ 1,080,000	\$ 1,190,000
Tk-119	Fixed Roof	30000		\$ 1,080,000	\$ 1,190,000
Tk-120	Fixed Roof	30000		\$ 1,080,000	\$ 1,190,000
Tk-121	Fixed Roof	30000		\$ 1,080,000	\$ 1,190,000
Tk-122	Fixed Roof	30000		\$ 1,080,000	\$ 1,190,000
Tk-123	Fixed Roof	30000		\$ 1,080,000	\$ 1,190,000
Tk-124	Fixed Roof	30000		\$ 1,080,000	\$ 1,190,000
Tk-125	Fixed Roof	30000		\$ 1,080,000	\$ 1,190,000
Tk-126	Fixed Roof	30000		\$ 1,080,000	\$ 1,190,000
Tk-127	Fixed Roof	30000		\$ 1,080,000	\$ 1,190,000
Tk-128	Fixed Roof	30000		\$ 1,080,000	\$ 1,190,000
Tk-129	Fixed Roof	30000		\$ 1,080,000	\$ 1,190,000
Tk-130	Fixed Roof	30000		\$ 1,080,000	\$ 1,190,000
Tk-131	Fixed Roof	30000		\$ 1,080,000	\$ 1,190,000
Tk-132	Fixed Roof	30000		\$ 1,080,000	\$ 1,190,000
Tk-133	Fixed Roof	30000		\$ 1,080,000	\$ 1,190,000
Tk-134	Fixed Roof	30000		\$ 1,080,000	\$ 1,190,000
Tk-135	Fixed Roof	30000		\$ 1,080,000	\$ 1,190,000
Tk-136	Fixed Roof	30000		\$ 1,080,000	\$ 1,190,000

User Added Equipment	Description	BMF ₀	Actual BMF	Purchased Equipment Cost	Bare Module Cost
Z-101	Solar Collector	1	1	\$ 6,768,053,469	\$ 6,768,053,469
Z-102	glass for reactor	1	1	\$ 62,000,000	\$ 62,000,000
Z-103	supporting equipment	1	1	\$ 2,000,000,000	\$ 2,000,000,000
Z-104	PV cells	1	1	\$12,900,000,000	\$12,900,000,000

Name	Total Module Cost	Grass Roots Cost	Utility Used	Efficiency	Actual Usage	Annual Utility Cost
Tk-101	\$ 1,640,000	\$ 2,330,000	NA			
Tk-102	\$ 1,640,000	\$ 2,330,000	NA			
Tk-103	\$ 1,640,000	\$ 2,330,000	NA			
Tk-104	\$ 1,640,000	\$ 2,330,000	NA			
Tk-105	\$ 1,640,000	\$ 2,330,000	NA			
Tk-106	\$ 1,640,000	\$ 2,330,000	NA			
Tk-107	\$ 1,640,000	\$ 2,330,000	NA			
Tk-108	\$ 1,640,000	\$ 2,330,000	NA			
Tk-109	\$ 1,640,000	\$ 2,330,000	NA			
Tk-110	\$ 1,640,000	\$ 2,330,000	NA			
Tk-111	\$ 1,640,000	\$ 2,330,000	NA			
Tk-112	\$ 1,640,000	\$ 2,330,000	NA			
Tk-113	\$ 1,640,000	\$ 2,330,000	NA			
Tk-114	\$ 1,640,000	\$ 2,330,000	NA			
Tk-115	\$ 1,640,000	\$ 2,330,000	NA			
Tk-116	\$ 1,640,000	\$ 2,330,000	NA			
Tk-117	\$ 1,640,000	\$ 2,330,000	NA			
Tk-118	\$ 1,640,000	\$ 2,330,000	NA			
Tk-119	\$ 1,640,000	\$ 2,330,000	NA			
Tk-120	\$ 1,640,000	\$ 2,330,000	NA			
Tk-121	\$ 1,640,000	\$ 2,330,000	NA			
Tk-122	\$ 1,640,000	\$ 2,330,000	NA			
Tk-123	\$ 1,640,000	\$ 2,330,000	NA			
Tk-124	\$ 1,640,000	\$ 2,330,000	NA			
Tk-125	\$ 1,640,000	\$ 2,330,000	NA			
Tk-126	\$ 1,640,000	\$ 2,330,000	NA			
Tk-127	\$ 1,640,000	\$ 2,330,000	NA			
Tk-128	\$ 1,640,000	\$ 2,330,000	NA			
Tk-129	\$ 1,640,000	\$ 2,330,000	NA			
Tk-130	\$ 1,640,000	\$ 2,330,000	NA			
Tk-131	\$ 1,640,000	\$ 2,330,000	NA			
Tk-132	\$ 1,640,000	\$ 2,330,000	NA			
Tk-133	\$ 1,640,000	\$ 2,330,000	NA			
Tk-134	\$ 1,640,000	\$ 2,330,000	NA			
Tk-135	\$ 1,640,000	\$ 2,330,000	NA			
Tk-136	\$ 1,640,000	\$ 2,330,000	NA			
Z-101	\$ 9,301,900,000	\$ 18,201,550,000				
Z-102	\$ 85,200,000	\$ 121,300,000	Unspecified			
Z-103	\$ 2,748,800,000	\$ 3,913,500,000	Unspecified			
Z-104	\$ 12,900,000,000	\$ 12,900,000,000				
Totals	\$ 25,094,900,000	\$ 35,220,200,000				\$ -

Add Materials

<u>Material</u>	<u>Classification</u>	<u>Price (\$/ton)</u>	<u>Consumption (ton/h)</u>	<u>Material Costs (\$/y)</u>
Biomass	Product	\$ 8,374.500	147.62	\$ 10,829,494,724
Carbon Dioxide Credits	Product	\$ 5.000	266.55	\$ 11,674,890
water	Raw Material	\$ 0.985	60	\$ 517,716

- 1 Chemical Marketing Reporter for black iron oxide, synthetic, baged, truck loaded, free on board, warehouse value
- 2 based on values for fillers for rubber, plastic etc.
- 3 Based on 1998 value from Chem marketing reporter - freight equilized

Economic Options

Cost of Land \$	100,000,000
Taxation Rate	42%
Annual Interest Rate	6.50%
Salvage Value \$	3,522,020,000
Working Capital \$	3,522,161,772
FCIL \$	35,220,200,000
Total Module Factor	1.18
Grass Roots Factor	0.50

Economic Information Calculated From Given Information

Revenue From Sales \$	10,841,169,614
C _{RM} (Raw Materials Costs) \$	517,716
C _{UT} (Cost of Utilities) \$	100,000
C _{WT} (Waste Treatment Costs) \$	-
C _{OL} (Cost of Operating Labor) \$	900,000

Factors Used in Calculation of Cost of Manufacturing (COM)

$$Comd = 0.18*FCIL + 2.76*COL + 1.21*(CUT + CWT + CRM)$$

Multiplying factor for FCIL	0.18
Multiplying factor for C _{OL}	2.76
Facotrs for C _{UT} , C _{WT} , and C _{RM}	1.21
COM _d \$	6,342,867,436

Factors Used in Calculation of Working Capital

$$Working\ Capital = A*C_{RM} + B*FCIL + C*C_{OL}$$

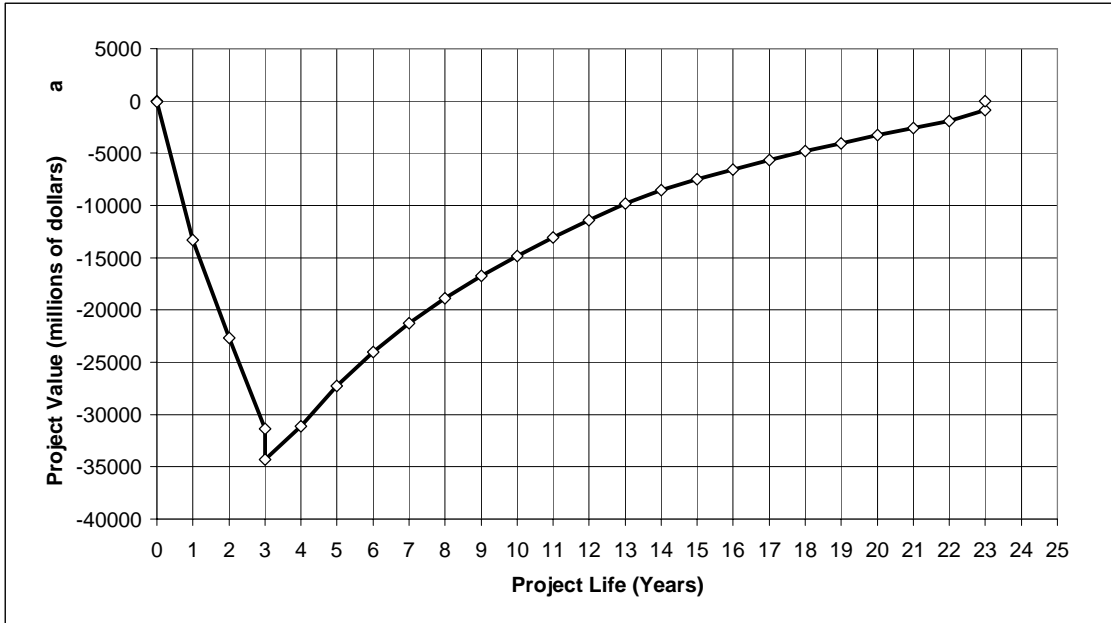
A	0.10
B	0.10
C	0.10

Project Life (Years after Startup)	20
------------------------------------	----

Construction period	3
---------------------	---

Distribution of Fixed Capital Investment (must sum to one)

End of year One	40%
End of year Two	30%
End of year Three	30%
End of year Four	
End of year Five	



Generate CFD

Discounted Profitability Criterion

Net Present Value (millions)	0.06
Discounted Cash Flow Rate of Return	6.50%
Discounted Payback Period (years)	17.4

Non-Discounted Profitability Criteria

Cumulative Cash Position (millions)	33795.36
Rate of Return on Investment	4.80%
Payback Period (years)	8.6

Year	Investment	d_k	$FCI_t - Sd_k$	R	COM_d	$(R - COM_d - d_k) * (1 - t) + d_k$	Cash Flow (Non-discounted)	Cash Flow (discounted)	Cumulative Cash Flow (discounted)
0	0.00		35220.20				0.00	0.00	0.00
0	100.00		35220.20				(100.00)	(100.00)	(100.00)
1	14088.08		35220.20				(14088.08)	(13228.24)	(13328.24)
2	10566.06		35220.20				(10566.06)	(9315.66)	(22643.91)
3	10566.06		35220.20				(10566.06)	(8747.10)	(31391.01)
3	3522.16		35220.20				(3522.16)	(2915.82)	(34306.83)
4		3522.02	31698.18	10841.17	6342.87	4088.26	4088.26	3177.90	(31128.93)
5		6339.64	25358.54	10841.17	6342.87	5271.66	5271.66	3847.69	(27281.24)
6		5071.71	20286.84	10841.17	6342.87	4739.13	4739.13	3247.89	(24033.35)
7		4050.32	16236.51	10841.17	6342.87	4310.15	4310.15	2773.61	(21259.75)
8		3240.26	12996.25	10841.17	6342.87	3969.92	3969.92	2398.75	(18860.99)
9		2606.29	10389.96	10841.17	6342.87	3703.66	3703.66	2101.28	(16759.71)
10		2324.53	8065.43	10841.17	6342.87	3585.32	3585.32	1909.99	(14849.72)
11		2324.53	5740.89	10841.17	6342.87	3585.32	3585.32	1793.42	(13056.30)
12		2289.31	3451.58	10841.17	6342.87	3570.53	3570.53	1677.02	(11379.28)
13		2289.31	1162.27	10841.17	6342.87	3570.53	3570.53	1574.66	(9804.62)
14		1162.27	-	10841.17	6342.87	3097.17	3097.17	1282.54	(8522.08)
15		-	-	10841.17	6342.87	2609.02	2609.02	1014.45	(7507.63)
16		-	-	10841.17	6342.87	2609.02	2609.02	952.54	(6555.09)
17		-	-	10841.17	6342.87	2609.02	2609.02	894.40	(5660.68)
18		-	-	10841.17	6342.87	2609.02	2609.02	839.82	(4820.87)
19		-	-	10841.17	6342.87	2609.02	2609.02	788.56	(4032.31)
20		-	-	10841.17	6342.87	2609.02	2609.02	740.43	(3291.88)
21		-	-	10841.17	6342.87	2609.02	2609.02	695.24	(2596.64)
22		-	-	10841.17	6342.87	2609.02	2609.02	652.81	(1943.83)
23		-	-	10841.17	6342.87	4651.79	4651.79	1092.90	(850.94)
23		-	-	-	-	-	3622.16	850.99	0.06

Probable Variation of Key Parameters over Plant Life

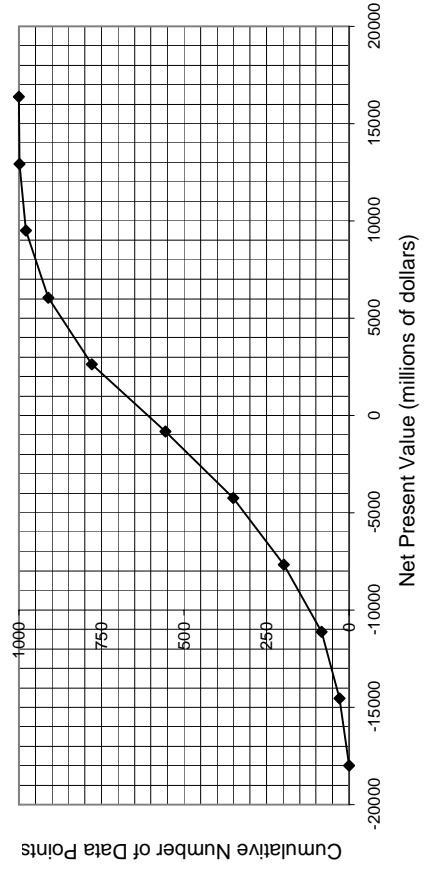
	<u>Lower Limit</u>	<u>Upper Limit</u>	<u>Base Value</u>
FCIL	-20%	30%	#####
Price of Product	-10%	10%	#####
Working Capital	-50%	10%	#####
Income Tax Rate*	-20%	20%	\$ 3,522,161,772
Interest Rate*	-10%	20%	42%
Raw Material Price	-10%	15%	6%
Salvage Value	-80%	20%	\$ 517,716
			\$ 3,522,020,000

* Please note that variations for percentages are a percent of a percent. For example, a 10% variance on a 12% interest rate would imply a 1.2% uncertainty

Run Economic Analysis

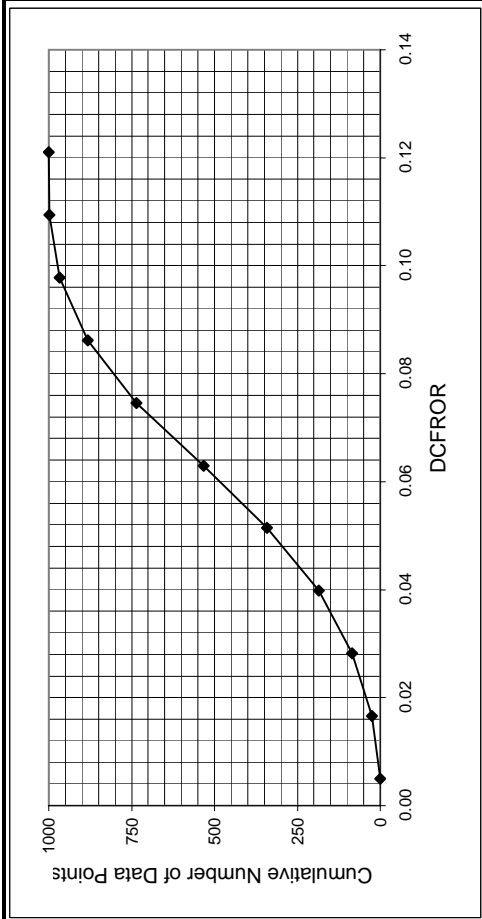
Net Present Value Data

Low NPV	-17986.3		
High NPV	16369.1		
<u>Bins</u>	<u>Upper Value</u>	<u># points/bin</u>	<u>Cumulative</u>
0	-17986.3	0	0
1	-14550.8	29	29
2	-11115.2	54	83
3	-7679.7	114	197
4	-4244.1	154	351
5	-808.6	205	556
6	2626.9	223	779
7	6062.5	131	910
8	9498.0	68	978
9	12933.6	20	998
10	16369.1	2	1000



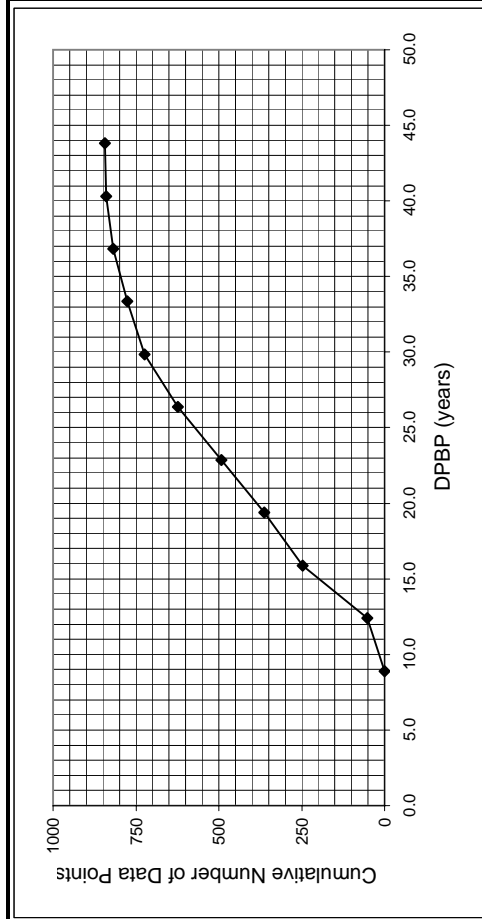
Discounted Cash Flow Rate of Return Data

Low DCFROR	0.00	Upper	#/bin	Cumulative
High DCFROR	0.12	0.00	0	0
Bins		0.02	26	26
		0.03	58	84
		0.04	102	186
		0.05	156	342
		0.06	190	532
		0.07	204	736
		0.09	146	882
		0.10	86	968
		0.11	30	998
		0.12	2	1000



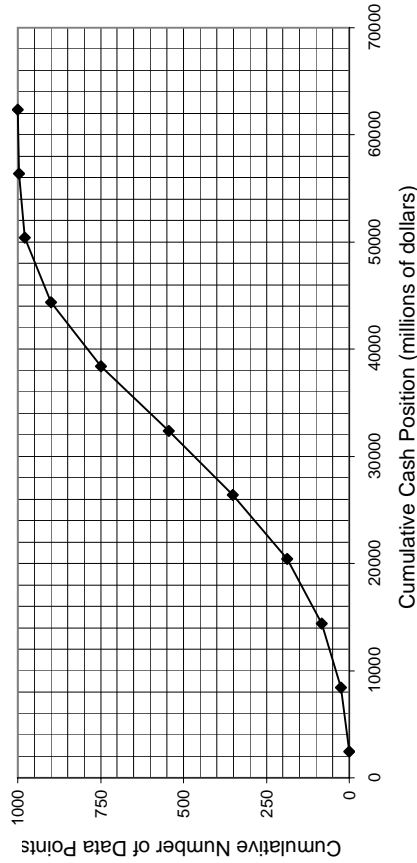
Discounted Payback Period Data

Low DPBP	8.9	Upper	#/bin	Cumulative
High DPBP	43.8	8.9	0	0
Bins		12.4	52	52
		15.9	196	248
		19.4	115	363
		22.9	130	493
		26.4	131	624
		29.8	100	724
		33.3	52	776
		36.8	42	818
		40.3	22	840
		43.8	3	843



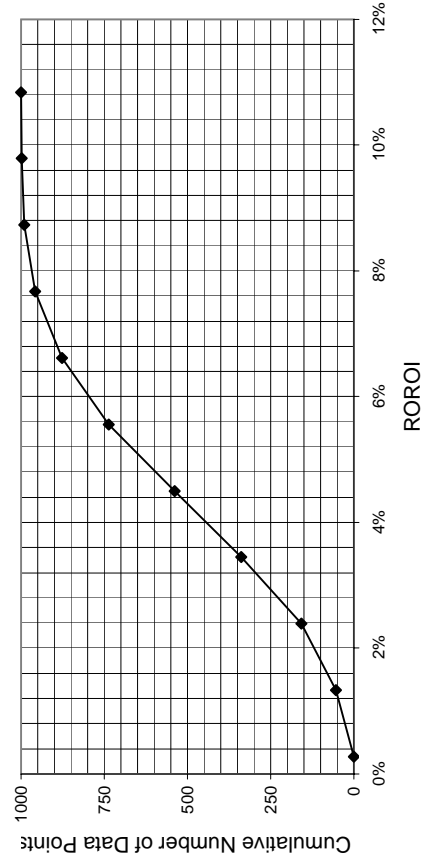
Cumulative Cash Position Data

Low CCP	2435.86		
High CCP	62366.41		
Bins	Upper Value	# points/bin	Cumulative
0	2435.86	0	0
1	8428.91	25	25
2	14421.97	58	83
3	20415.02	104	187
4	26408.08	164	351
5	32401.13	193	544
6	38394.19	205	749
7	44387.25	151	900
8	50380.30	79	979
9	56373.36	17	996
10	62366.41	4	1000



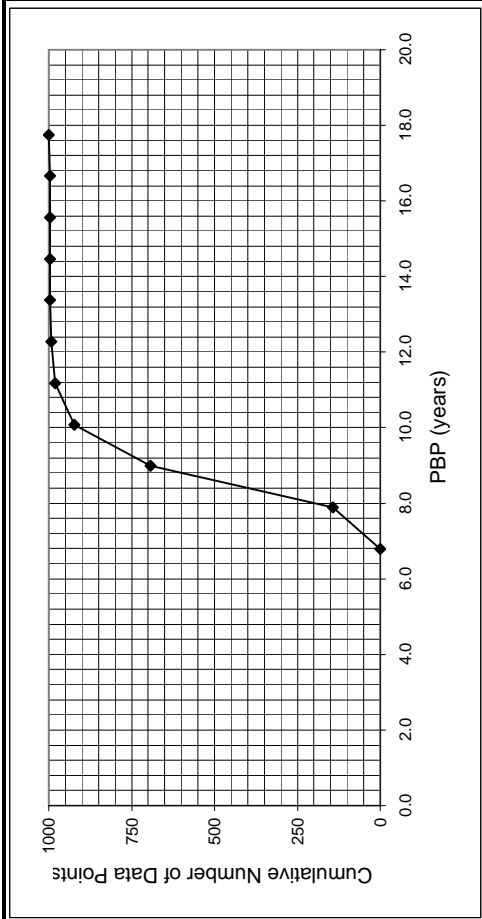
Rate of Return on Investment Data

Low RORO	0%		
High RORO	11%		
Bins	Upper Value	# points/bin	Cumulative
0	0%	0	0
1	1%	54	54
2	2%	103	157
3	3%	182	339
4	5%	199	538
5	6%	198	736
6	7%	141	877
7	8%	80	957
8	9%	33	990
9	10%	9	999
10	11%	1	1000



Payback Period Data

Low DPBP	6.8	Upper	#/bin	Cumulative
High DPBP	17.8	6.8	0	0
Bins		7.9	142	142
		9.0	552	694
		10.1	229	923
		11.2	58	981
		12.3	11	992
		13.4	4	996
		14.5	1	997
		15.6	0	997
		16.7	0	997
		17.8	3	1000



Update Preferences

Hours per Operating Year 8760

	<u>Cost (\$/GJ)</u>
Common Utilities	
Electricity (110V - 440V)	16.8
Cooling Water (30°C to 45°C)	0.354
Refrigerated Water (15°C to 25°C)	4.43
Steam from Boilers	
Low Pressure (5 barg, 160°C)	6.08
Medium Pressure (10 barg, 184°C)	6.87
High Pressure (41 barg, 254°C)	9.83
Fuels	
Fuel Oil (no. 2)	6.0
Natural Gas	6
Coal (FOB mine mouth)	1.07
Thermal Systems	
Moderately High (up to 330°C)	6.67
High (up to 400°C)	7
Very High (up to 600°C)	7.5
Refrigeration	
Moderately Low (5°C)	4.43
Low (-20°C)	7.89
Very low (-50°C)	13.11
Cost (\$/tonne)	
Waste Disposal (solid and liquid)	
Non-Hazardous	36
Hazardous	200

Power Preference

kilowatts

Pressure Preference

barg

Heat Duty Preference

MJ/h

Length Preference

meters

Area Preference

square meters

Volume Preference

cubic meters

Gas Flow Preference

cubic meters/s

Cost Preference

\$/kg

Flowrate Preference

kg/h

Energy Price Preference

\$/Gigajoule

Cost of Steam used in Steam Drives

	<u>Cost (\$/GJ)</u>
Steam used for steam-powered drives \$	9.83

Equipment Efficiencies

Pump Efficiency	85%
Drive Efficiency	90%
Fan Efficiency	80%
Furnace Efficiency	90%
Turbine Efficiency	85%

Process Equipment

Operators per shift per equipment

Cost of Labor (per operator/year) \$ 50,000

Compressor Data (without electric motors)

Compressor Type	K ₁	K ₂	K ₃	F _{BMCS}	F _{BMS}	F _{BMNi}	W _{min} (kW)	W _{max} (kW)
Centrifugal	2.2891	1.3604	-0.1027	2.7	5.8	11.5	450	3000
Axial	2.2891	1.3604	-0.1027	3.8	8.0	15.9	450	3000
Rotary	5.0355	-1.8002	0.8253	2.4	5.0	9.9	18	950
Reciprocating	2.2891	1.3604	-0.1027	3.4	7.0	13.9	450	3000

Drive Data

Electric Drives	K ₁	K ₂	K ₃	F _{EM}	W _{min} (kW)	W _{max} (kW)
Explosion Proof	2.4604	1.4191	-0.1798	1.5	75	2600
Totally Enclosed	1.956	1.7142	-0.2282	1.5	75	2600
Open/Drip Proof	2.9508	1.0688	-0.1315	1.5	75	2600

Non-Electric Drives	K ₁	K ₂	K ₃	F _{EM}	W _{min} (kW)	W _{max} (kW)
Gas Turbine	-21.7702	13.2175	-1.5279	3.5	7500	23000
Steam Turbine	2.6259	1.4398	-0.1776	3.5	70	7500
Internal Combustion	2.7635	0.8574	-0.0098	2.0	10	10000

Fan Data (include electric motors)

Fan Type	K ₁	K ₂	K ₃	F _{BMCS}	F _{BMberglass}	F _{BMS}	F _{BMNi}	Threshold	C ₁	C ₂	C ₃	V _{min} (m/s)	V _{max} (m/s)	P _{max} (barg)
Centrifugal Radial Fan	3.5391	-0.3533	0.4477	2.7	5.0	5.8	11.5	0.01	0.00	0.209	-0.033	1	100	0.16
Centrifugal Backward curv	3.3471	-0.0734	0.3090	2.7	5.0	5.8	11.5	0.01	0.00	0.209	-0.033	1	100	0.16
Axial Tube Fan	3.0414	-0.3375	0.4722	2.7	5.0	5.8	11.5	0.04	0.00	0.209	-0.033	1	100	0.16
Axial Vane Fan	3.1761	-0.1373	0.3414	2.7	5.0	5.8	11.5	0.04	0.00	0.209	-0.033	1	100	0.16

Fired Heater Data

Reactive Heaters	K ₁	K ₂	K ₃	Q _{min} (kW)	Q _{max} (kW)	P _{max} (barg)	C ₁	C ₂	C ₃	Bare Module Factor		
										CS	Alloy Steel	SS
Reformer Furnace	3.068	0.8597	0.0194	3000	100000	200	0.1405	-0.2698	0.1293	2.13	2.51	2.81
Pyrolysis Furnace	2.3859	0.9721	-0.0206	3000	100000	200	0.1017	-0.1957	0.09403	2.13	2.51	2.81

Non-reactive Heaters	K ₁	K ₂	K ₃	Q _{min} (kW)	Q _{max} (kW)	P _{max} (barg)	C ₁	C ₂	C ₃	Bare Module Factor		
										CS	Alloy Steel	SS
Process Heater	7.3488	-1.1666	0.2028	1000	100000	200	0.1347	-0.2368	0.1021	2.13	2.51	2.81

Thermal Fluid Heaters	K ₁	K ₂	K ₃	Q _{min} (kW)	Q _{max} (kW)	P _{max} (barg)	C ₁	C ₂	C ₃	F _{bm}	Steam Superheat Factor		
											F _{T1}	F _{T2}	F _{T3}
Hot Water	2.0829	0.9074	-0.0243	650	10750	200	-0.0163	0.0569	-0.0088	2.17			
Molten Salt, Mineral Oil,	1.1979	1.4782	-0.0958	650	10750	200	-0.0163	0.0569	-0.0088	2.17			
Diphenyl Based Oils	2.2628	0.8581	0.0003	650	10750	200	-0.0163	0.0569	-0.0088	2.17			
Packaged Steam Boilers	6.9617	-1.48	0.3161	1200	9400	40	2.5941	-4.2348	1.7224	2.2	1.000	0.00184	3.35E-06

Heat Exchanger Data

Exchanger Type	K ₁	K ₂	K ₃	C ₁	C ₂	C ₃	B ₁	B ₂	A _{min} (m ²)	A _{max} (m ²)	P _{max} (barg)	
Double Pipe	3.3444	0.2745	-0.0472	13.1467	-12.6574	3.0705	1.74	1.55	1	10	300	
40 barg < P < 100 barg				0.6072	-0.912	0.3327						
P < 40 barg				0	0	0						
Multiple Pipe	2.7652	0.7282	0.0783	13.1467	-12.6574	3.0705	1.74	1.55	10	100	300	
40 barg < P < 100 barg				0.6072	-0.912	0.3327						
P < 40 barg				0	0	0						
Fixed tube, sheet, or U tut tubes only > 5 barg	4.3247	-0.303	0.1634	0.03881	-0.11272	0.08183	1.63	1.66	10.0	1000	140	
Floating Head tubes only > 5barg	4.8306	-0.8509	0.3187	0.03881	-0.11272	0.08183	1.63	1.66	10.0	1000	140	
Bayonet tubes only > 5 barg	4.2768	-0.0495	0.1431	0.03881	-0.11272	0.08183	1.63	1.66	10.0	1000	140	
Kettle Reboiler tubes only > 5 barg	4.4646	-0.5277	0.3955	0.03881	-0.11272	0.08183	1.63	1.66	10.0	100	140	
Scraped Wall	3.7803	0.8569	0.0349	13.1467	-12.6574	3.0705	1.74	1.55	2.0	20	300	
40 barg < P < 100 barg				0.6072	-0.912	0.3327						
P < 40 barg				0	0	0						
Teflon Tube	3.8062	0.8924	-0.1671	0	0	0	1.63	1.66	1.0	10	15	
Air Cooler	4.0336	0.2341	0.0497	-0.125	0.15361	-0.02861	0.96	1.21	10	10000	100	
Spiral Tube - shell and tut tube only	3.9912	0.0668	0.243	-0.4045	0.1859	0	1.74	1.55	1	100	400	
Spiral Plate	4.6561	-0.2947	0.2207	0	0	0	0.96	1.21	1	100	19	
Flat Plate	4.6656	-0.1557	0.1547	0	0	0	0.96	1.21	10	1000	19	

Material Factors, F_M

Exchanger Type	Shell - CS		Cu		SS		Ni		Ti	
	Tube - CS	Cu	Cu	SS	SS	Ni	Ni	Ti	Ti	
Double Pipe	1.00	1.35	1.69	1.81	2.73	2.68	3.73	4.63	11.38	
Multiple Pipe	1.00	1.35	1.69	1.81	2.73	2.68	3.73	4.63	11.38	
Fixed tube, sheet, or U tut	1.00	1.35	1.69	1.81	2.73	2.68	3.73	4.63	11.38	
Floating Head	1.00	1.35	1.69	1.81	2.73	2.68	3.73	4.63	11.38	
Bayonet	1.00	1.35	1.69	1.81	2.73	2.68	3.73	4.63	11.38	
Kettle Reboiler	1.00	1.35	1.69	1.81	2.73	2.68	3.73	4.63	11.38	
Scraped Wall	1.00	1.35	1.69	1.81	2.73	2.68	3.73	4.63	11.38	
Spiral Tube	1.00	1.35	1.69	1.81	2.73	2.68	3.73	4.63	11.38	

Shell Material					
Type of Exchanger	CS	Cu	SS	Ni	Ti
Teflon Tube Exchanger	1.00	1.20	1.30	1.40	3.30

Material In Contact with Process Fluid					
Type of Exchanger	CS	Cu	SS	Ni	Ti
Spiral Plate	1.00	1.35	2.45	2.68	4.63
Flat Plate	1.00	1.35	2.45	2.68	4.63

Tube Material			
Type of Exchanger	CS	Al	SS
Air Cooler	1.00	1.42	2.93

Pump Data (including electric drives)

Pump Type	K ₁	K ₂	K ₃	C ₁	C ₂	C ₃	B ₁	B ₂	F _{mCl}	F _{mCS}	F _{mCu}	F _{mSS}	F _{mNi}	F _{mTi}	P _{max} (barg)	W _{min} (kW)	W _{max} (kW)
-----------	----------------	----------------	----------------	----------------	----------------	----------------	----------------	----------------	------------------	------------------	------------------	------------------	------------------	------------------	-------------------------	-----------------------	-----------------------

Centrifugal pump	3.3892	0.0536	0.1538	-0.3935	0.3957	-0.00226	1.89	1.35	1.0	1.6	NA	2.3	4.4	NA	100	1	300
Positive Displacement	3.4771	0.1350	0.14380	-0.24538	0.259016	-0.01363	1.89	1.35	1.0	1.4	2.7	4.7	10.7	100	1	100	
Reciprocating pump	3.8696	0.3161	0.12200	-0.2454	0.2590	-0.0136	1.89	1.35	1.0	1.5	1.3	2.4	4.0	6.4	100	0.1	200

Tank Data

Tank Type	K ₁	K ₂	K ₃	B ₁	B ₂	V _{min} (m ³ /s)	V _{max} (m ³ /s)
Fixed Roof	4.8509	-0.3973	0.1445	1.10	0	90	30000
Floating Roof	5.9567	-0.7585	0.1749	1.10	0.00	1000	40000

Turbine Data

Turbine Type	K ₁	K ₂	K ₃	F _{BMC1}	F _{BMC5}	F _{BMCu}	F _{BMS5}	F _{BMNI}	F _{BMTI}	W _{min} (kW)	W _{max} (kW)
Axial	2.7051	1.4398	-0.1776	NA	3.5	NA	6.1	11.7	NA	100	4000
Radial	2.2476	1.4965	-0.1618	NA	3.5	NA	6.1	11.7	NA	100	1500

Vaporizer and Evaporator Data

Evaporator Types	K ₁	K ₂	K ₃	A _{min} (m ²)	A _{max} (m ²)	P _{max} (barg)	C ₁	C ₂	C ₃
Forced Circulation	5.0238	0.3475	0.0703	5	1000	150	0.1578	-0.2992	0.1413
Falling Film	3.9119	0.8627	-0.0088	50	500	150	0.1578	-0.2992	0.1413
Agitated (Scraped Wall)	5	0.149	-0.0134	0.5	5	150	0.1578	-0.2992	0.1413
Short Tube	5.2366	-0.6572	0.35	10	100	150	0.1578	-0.2992	0.1413
Long Tube	4.642	0.3698	0.0025	100	10000	150	0.1578	-0.2992	0.1413

Vaporizer Types	K ₁	K ₂	K ₃	V _{min} (m ³)	V _{max} (m ³)	P _{max} (barg)	C ₁	C ₂	C ₃
Jacketed Vessel	3.8751	0.3328	0.1901	1	100	320	0.1578	-0.2992	0.1413
Internal Coil	4.038	0.09142	0.2766	1	100	320	0.1578	-0.2992	0.1413
Jacketed Vessel w/ Coil	4.038	0.09142	0.2766	1	100	320	0.1578	-0.2992	0.1413

Evaporator Types	Bare Module Factors, F _{BM}				
	CS	Cu Alloy	SS	Ni Alloy	Ti
Forced Circulation	2.9	3.63	5.08	9.66	14.5
Falling Film	2.25	2.81	3.94	7.49	11.25
Agitated (Scraped Wall)	2.25	2.81	3.94	7.49	11.25
Short Tube	2.9	3.63	5.08	9.66	14.5
Long Tube	2.9	3.63	5.08	9.66	14.5

Vaporizer Types	Bare Module Factors, F _{BM}									
	CS	Cu	s Lined SS	s Lined Ni	SS	SS Clad	Ni Alloy	Ni Alloy Cla	Ti	Ti Clad
Jacketed Vessel	2.7	3.4	4.7	4.9	4.8	3.8	9.1	5.9	13.7	9.5
Internal Coil	3.0	3.8	5.2	5.5	5.2	4.1	10.1	6.6	15.2	10.6
Jacketed Vessel w/ Coil	3.0	3.8	5.2	5.5	5.2	4.1	10.1	6.6	15.2	10.6

Vessel Data (including data for distillation towers and packed columns)

	Vertical Vessels					Horizontal Vessels					
	K ₁	K ₂	K ₃	V _{min}	V _{max}	K ₁	K ₂	K ₃	V _{min}	V _{max}	P _{max} (barg)
	3.4974	0.4485	0.1074	0.3	520	3.5565	0.3776	0.0905	0.1	628	400

Vessel B-Values

	B1	B2
Horizontal	1.49	1.52
Vertical	2.25	1.82

F_{BM}

MOC	Sieve	Valve	Demister
CS	1.0	1	
SS	1.8	1.83	1.0
Fluorocarbon			1.8
Ni-alloy	5.6	5.58	5.6

F₃

Tray Type	K ₁	K ₂	K ₃	A _{min} (m ²)	A _{max} (m ²)
Sieve	2.9949	0.4465	0.3961	0.07	12.3
Valve	3.3322	0.4838	0.3434	0.7	10.5
Demister	3.2353	0.4838	0.3434	0.7	10.5

Materials of Construction

F _M CS	1.0
F _M SS clad	1.7
F _M SS	3.1
F _M Ni clad	3.6
F _M Ni	7.1
F _M Ti clad	4.7
F _M Ti	9.4

Tower Packing

Materials of Construction	K ₁	K ₂	K ₃	V _{min} (m ³)	V _{max} (m ³)
Ceramic	3.0664	0.9744	0.0055	0.03	628
304 SS	3.2999	0.9744	0.0055	0.03	628
Plastic Saddle	2.4493	0.9744	0.0055	0.03	628

Add Equipment

Unit Number 100

Edit Equipment

CEPCI 462.4

User Added Equipment

Storage Tanks	Tank Type	Volume (cubic meters)	Volume (gallons)	Purchased Equipment Cost	Bare Module Cost
Tk-101	Fixed Roof	30000		\$ 1,080,000	\$ 1,190,000
Tk-102	Fixed Roof	30000		\$ 1,080,000	\$ 1,190,000
Tk-103	Fixed Roof	30000		\$ 1,080,000	\$ 1,190,000
Tk-104	Fixed Roof	30000		\$ 1,080,000	\$ 1,190,000
Tk-105	Fixed Roof	30000		\$ 1,080,000	\$ 1,190,000
Tk-106	Fixed Roof	30000		\$ 1,080,000	\$ 1,190,000
Tk-107	Fixed Roof	30000		\$ 1,080,000	\$ 1,190,000
Tk-108	Fixed Roof	30000		\$ 1,080,000	\$ 1,190,000
Tk-109	Fixed Roof	30000		\$ 1,080,000	\$ 1,190,000
Tk-110	Fixed Roof	30000		\$ 1,080,000	\$ 1,190,000
Tk-111	Fixed Roof	30000		\$ 1,080,000	\$ 1,190,000
Tk-112	Fixed Roof	30000		\$ 1,080,000	\$ 1,190,000
Tk-113	Fixed Roof	30000		\$ 1,080,000	\$ 1,190,000
Tk-114	Fixed Roof	30000		\$ 1,080,000	\$ 1,190,000
Tk-115	Fixed Roof	30000		\$ 1,080,000	\$ 1,190,000
Tk-116	Fixed Roof	30000		\$ 1,080,000	\$ 1,190,000
Tk-117	Fixed Roof	30000		\$ 1,080,000	\$ 1,190,000
Tk-118	Fixed Roof	30000		\$ 1,080,000	\$ 1,190,000
Tk-119	Fixed Roof	30000		\$ 1,080,000	\$ 1,190,000
Tk-120	Fixed Roof	30000		\$ 1,080,000	\$ 1,190,000
Tk-121	Fixed Roof	30000		\$ 1,080,000	\$ 1,190,000
Tk-122	Fixed Roof	30000		\$ 1,080,000	\$ 1,190,000
Tk-123	Fixed Roof	30000		\$ 1,080,000	\$ 1,190,000
Tk-124	Fixed Roof	30000		\$ 1,080,000	\$ 1,190,000
Tk-125	Fixed Roof	30000		\$ 1,080,000	\$ 1,190,000
Tk-126	Fixed Roof	30000		\$ 1,080,000	\$ 1,190,000
Tk-127	Fixed Roof	30000		\$ 1,080,000	\$ 1,190,000
Tk-128	Fixed Roof	30000		\$ 1,080,000	\$ 1,190,000
Tk-129	Fixed Roof	30000		\$ 1,080,000	\$ 1,190,000
Tk-130	Fixed Roof	30000		\$ 1,080,000	\$ 1,190,000
Tk-131	Fixed Roof	30000		\$ 1,080,000	\$ 1,190,000
Tk-132	Fixed Roof	30000		\$ 1,080,000	\$ 1,190,000
Tk-133	Fixed Roof	30000		\$ 1,080,000	\$ 1,190,000
Tk-134	Fixed Roof	30000		\$ 1,080,000	\$ 1,190,000
Tk-135	Fixed Roof	30000		\$ 1,080,000	\$ 1,190,000
Tk-136	Fixed Roof	30000		\$ 1,080,000	\$ 1,190,000

User Added Equipment	Description	BMF ₀	Actual BMF	Purchased Equipment Cost	Bare Module Cost
Z-101	Solar Collector	1	1	\$ 6,768,053,469	\$ 6,768,053,469
Z-102	glass for reactor	1	1	\$ 62,000,000	\$ 62,000,000
Z-103	supporting equipment	1	1	\$ 2,000,000,000	\$ 2,000,000,000
Z-104	PV cells	1	1	\$12,900,000,000	\$12,900,000,000

Name	Total Module Cost	Grass Roots Cost	Utility Used	Efficiency	Actual Usage	Annual Utility Cost
Tk-101	\$ 1,640,000	\$ 2,330,000	NA			
Tk-102	\$ 1,640,000	\$ 2,330,000	NA			
Tk-103	\$ 1,640,000	\$ 2,330,000	NA			
Tk-104	\$ 1,640,000	\$ 2,330,000	NA			
Tk-105	\$ 1,640,000	\$ 2,330,000	NA			
Tk-106	\$ 1,640,000	\$ 2,330,000	NA			
Tk-107	\$ 1,640,000	\$ 2,330,000	NA			
Tk-108	\$ 1,640,000	\$ 2,330,000	NA			
Tk-109	\$ 1,640,000	\$ 2,330,000	NA			
Tk-110	\$ 1,640,000	\$ 2,330,000	NA			
Tk-111	\$ 1,640,000	\$ 2,330,000	NA			
Tk-112	\$ 1,640,000	\$ 2,330,000	NA			
Tk-113	\$ 1,640,000	\$ 2,330,000	NA			
Tk-114	\$ 1,640,000	\$ 2,330,000	NA			
Tk-115	\$ 1,640,000	\$ 2,330,000	NA			
Tk-116	\$ 1,640,000	\$ 2,330,000	NA			
Tk-117	\$ 1,640,000	\$ 2,330,000	NA			
Tk-118	\$ 1,640,000	\$ 2,330,000	NA			
Tk-119	\$ 1,640,000	\$ 2,330,000	NA			
Tk-120	\$ 1,640,000	\$ 2,330,000	NA			
Tk-121	\$ 1,640,000	\$ 2,330,000	NA			
Tk-122	\$ 1,640,000	\$ 2,330,000	NA			
Tk-123	\$ 1,640,000	\$ 2,330,000	NA			
Tk-124	\$ 1,640,000	\$ 2,330,000	NA			
Tk-125	\$ 1,640,000	\$ 2,330,000	NA			
Tk-126	\$ 1,640,000	\$ 2,330,000	NA			
Tk-127	\$ 1,640,000	\$ 2,330,000	NA			
Tk-128	\$ 1,640,000	\$ 2,330,000	NA			
Tk-129	\$ 1,640,000	\$ 2,330,000	NA			
Tk-130	\$ 1,640,000	\$ 2,330,000	NA			
Tk-131	\$ 1,640,000	\$ 2,330,000	NA			
Tk-132	\$ 1,640,000	\$ 2,330,000	NA			
Tk-133	\$ 1,640,000	\$ 2,330,000	NA			
Tk-134	\$ 1,640,000	\$ 2,330,000	NA			
Tk-135	\$ 1,640,000	\$ 2,330,000	NA			
Tk-136	\$ 1,640,000	\$ 2,330,000	NA			
Z-101	\$ 9,301,900,000	\$ 18,201,550,000				
Z-102	\$ 85,200,000	\$ 121,300,000	Unspecified			
Z-103	\$ 2,748,800,000	\$ 3,913,500,000	Unspecified			
Z-104	\$ 12,900,000,000	\$ 12,900,000,000				
Totals	\$ 25,094,900,000	\$ 35,220,200,000				\$ -

Add Materials

<u>Material</u>	<u>Classification</u>	<u>Price (\$/ton)</u>	<u>Consumption (ton/h)</u>	<u>Material Costs (\$/y)</u>
Biomass	Product	\$ 12,680.000	147.62	\$ 16,397,157,216
Carbon Dioxide Credits	Product	\$ 5.000	266.55	\$ 11,674,890
water	Raw Material	\$ 0.985	60	\$ 517,716

- 1 Chemical Marketing Reporter for black iron oxide, synthetic, baged, truck loaded, free on board, warehouse value
- 2 based on values for fillers for rubber, plastic etc.
- 3 Based on 1998 value from Chem marketing reporter - freight equalized

Economic Options

Cost of Land \$	100,000,000
Taxation Rate	42%
Annual Interest Rate	6.50%
Salvage Value \$	3,522,020,000
Working Capital \$	3,522,161,772
FCIL \$	35,220,200,000
Total Module Factor	1.18
Grass Roots Factor	0.50

Economic Information Calculated From Given Information

Revenue From Sales \$	16,408,832,106
C _{RM} (Raw Materials Costs) \$	517,716
C _{UT} (Cost of Utilities) \$	100,000
C _{WT} (Waste Treatment Costs) \$	-
C _{OL} (Cost of Operating Labor) \$	900,000

Factors Used in Calculation of Cost of Manufacturing (COM)

$$Comd = 0.18*FCIL + 2.76*COL + 1.21*(CUT + CWT + CRM)$$

Multiplying factor for FCIL	0.18
Multiplying factor for C _{OL}	2.76
Facotrs for C _{UT} , C _{WT} , and C _{RM}	1.21
COM _d \$	6,342,867,436

Factors Used in Calculation of Working Capital

$$Working\ Capital = A*C_{RM} + B*FCIL + C*C_{OL}$$

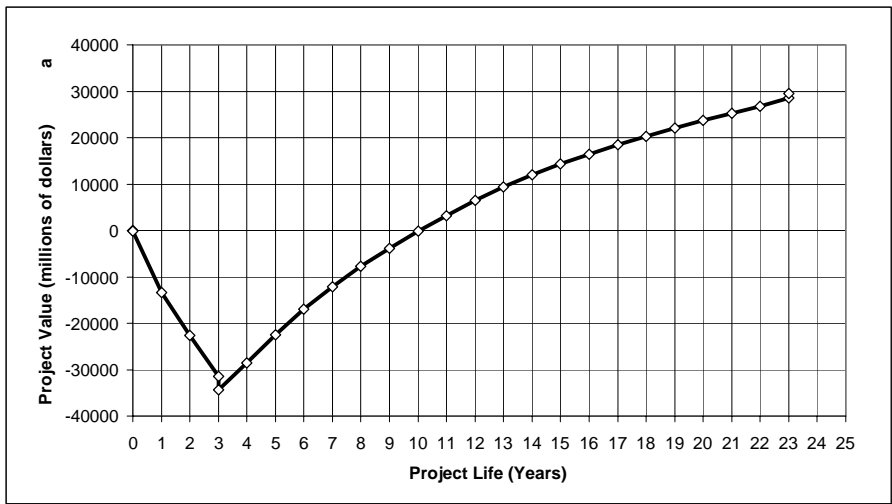
A	0.10
B	0.10
C	0.10

Project Life (Years after Startup)	20
------------------------------------	----

Construction period	3
---------------------	---

Distribution of Fixed Capital Investment (must sum to one)

End of year One	40%
End of year Two	30%
End of year Three	30%
End of year Four	
End of year Five	



Generate CFD

Discounted Profitability Criterion

Net Present Value (millions)	29456.13
Discounted Cash Flow Rate of Return	15.00%
Discounted Payback Period (years)	6.2

Non-Discounted Profitability Criteria

Cumulative Cash Position (millions)	98380.25
Rate of Return on Investment	13.97%
Payback Period (years)	4.5

Year	Investment	d_k	$FCI_t - Sd_k$	R	COM_k	$(R - COM_k - d_k) * (1-t) + d_k$	Cash Flow (Non-discounted)	Cash Flow (discounted)	Cumulative Cash Flow (discounted)	Cumulative Cash Flow (Non-discounted)
0	0.00		35220.20				0.00	0.00	0.00	0.00
0	100.00		35220.20				(100.00)	(100.00)	(100.00)	(100.00)
1	14088.08		35220.20				(14088.08)	(13228.24)	(13328.24)	(14188.08)
2	10566.06		35220.20				(10566.06)	(9315.66)	(22643.91)	(24754.14)
3	10566.06		35220.20				(10566.06)	(8747.10)	(31391.01)	(35320.20)
3	3522.16		35220.20				(3522.16)	(2915.82)	(34306.83)	(38842.36)
4		3522.02	31698.18	16408.83	6342.87	7317.51	7317.51	5688.07	(28618.76)	(31524.85)
5		6339.64	25358.54	16408.83	6342.87	8500.91	8500.91	6204.65	(22414.11)	(23023.95)
6		5071.71	20286.84	16408.83	6342.87	7968.38	7968.38	5461.00	(16953.11)	(15055.57)
7		4050.32	16236.51	16408.83	6342.87	7539.40	7539.40	4851.65	(12101.47)	(7516.17)
8		3240.26	12996.25	16408.83	6342.87	7199.17	7199.17	4349.96	(7751.50)	(317.01)
9		2606.29	10389.96	16408.83	6342.87	6932.90	6932.90	3933.41	(3818.10)	6615.90
10		2324.53	8065.43	16408.83	6342.87	6814.56	6814.56	3630.30	(187.80)	13430.46
11		2324.53	5740.89	16408.83	6342.87	6814.56	6814.56	3408.73	3220.93	20245.02
12		2289.31	3451.58	16408.83	6342.87	6799.77	6799.77	3193.74	6414.66	27044.79
13		2289.31	1162.27	16408.83	6342.87	6799.77	6799.77	2998.81	9413.47	33844.57
14		1162.27	-	16408.83	6342.87	6326.41	6326.41	2619.77	12033.24	40170.98
15		-	-	16408.83	6342.87	5838.26	5838.26	2270.07	14303.31	46009.24
16		-	-	16408.83	6342.87	5838.26	5838.26	2131.52	16434.83	51847.50
17		-	-	16408.83	6342.87	5838.26	5838.26	2001.43	18436.26	57685.76
18		-	-	16408.83	6342.87	5838.26	5838.26	1879.28	20315.54	63524.01
19		-	-	16408.83	6342.87	5838.26	5838.26	1764.58	22080.12	69362.27
20		-	-	16408.83	6342.87	5838.26	5838.26	1656.88	23737.00	75200.53
21		-	-	16408.83	6342.87	5838.26	5838.26	1555.76	25292.75	81038.79
22		-	-	16408.83	6342.87	5838.26	5838.26	1460.80	26753.56	86877.05
23		-	-	16408.83	6342.87	7881.03	7881.03	1851.58	28605.14	94758.08
23		-	-				3622.16	850.99	29456.13	98380.25

Probable Variation of Key Parameters over Plant Life

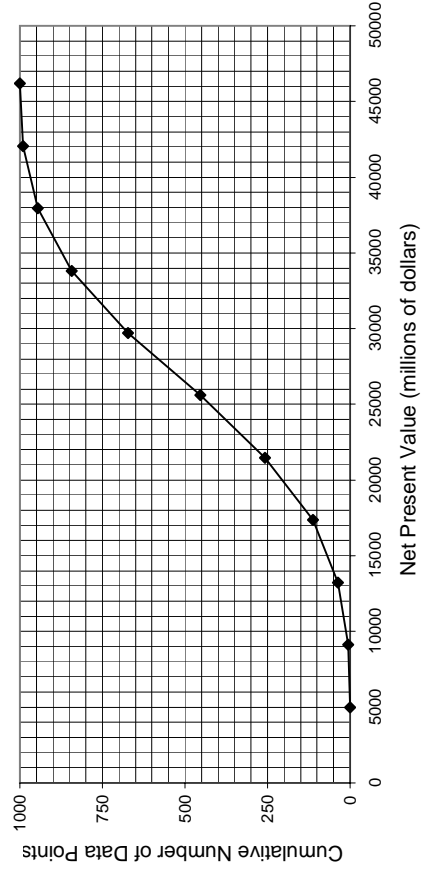
	<u>Lower Limit</u>	<u>Upper Limit</u>	<u>Base Value</u>
FCIL	-20%	30%	#####
Price of Product	-10%	10%	#####
Working Capital	-50%	10%	#####
Income Tax Rate*	-20%	20%	\$ 3,522,161,772
Interest Rate*	-10%	20%	42%
Raw Material Price	-10%	15%	6%
Salvage Value	-80%	20%	\$ 517,716
			\$ 3,522,020,000

* Please note that variations for percentages are a percent of a percent. For example, a 10% variance on a 12% interest rate would imply a 1.2% uncertainty

Run Economic Analysis

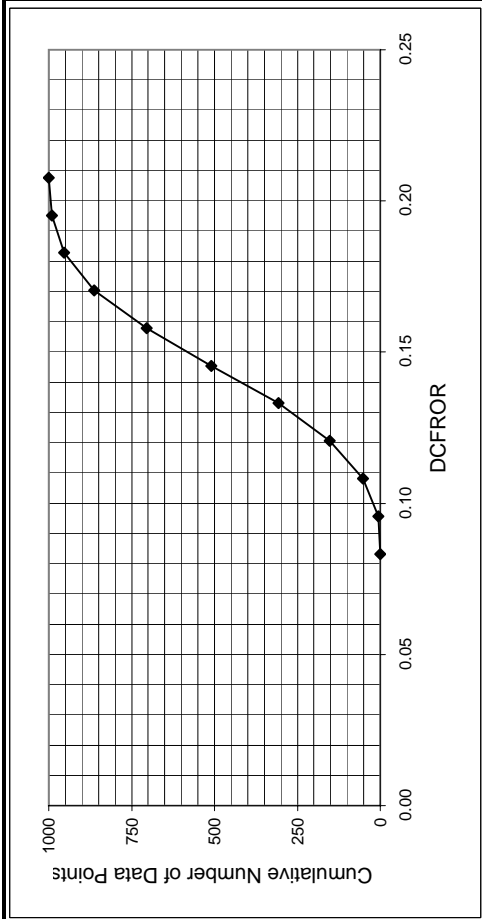
Net Present Value Data

Low NPV	5006.3		
High NPV	46186.0		
<u>Bins</u>	<u>Upper Value</u>	<u># points/bin</u>	<u>Cumulative</u>
0	5006.3	0	0
1	9124.2	5	5
2	13242.2	31	36
3	17360.2	77	113
4	21478.1	145	258
5	25596.1	195	453
6	29714.1	220	673
7	33832.1	170	843
8	37950.0	102	945
9	42068.0	45	990
10	46186.0	10	1000



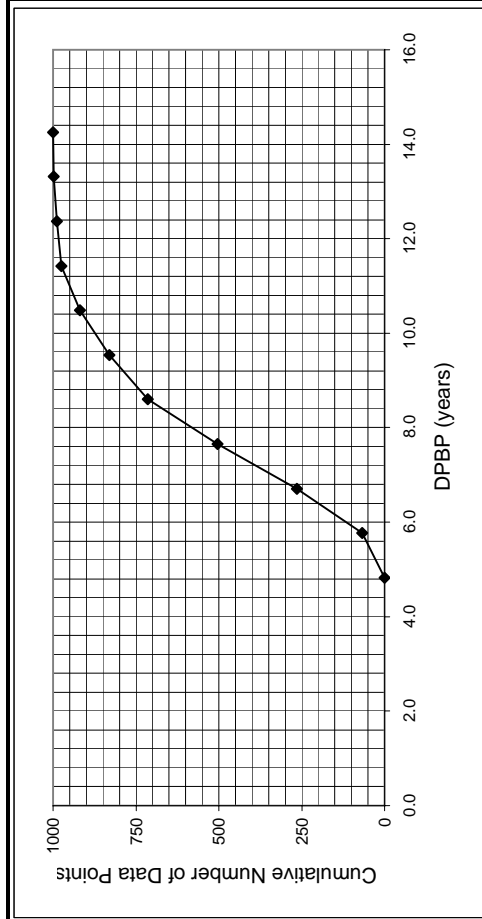
Discounted Cash Flow Rate of Return Data

Low DCFROR	0.08		
High DCFROR	0.21		
Bins	Upper	#/bin	Cumulative
0	0.08	0	0
1	0.10	6	6
2	0.11	47	53
3	0.12	99	152
4	0.13	155	307
5	0.15	202	509
6	0.16	196	705
7	0.17	158	863
8	0.18	91	954
9	0.20	36	990
10	0.21	10	1000



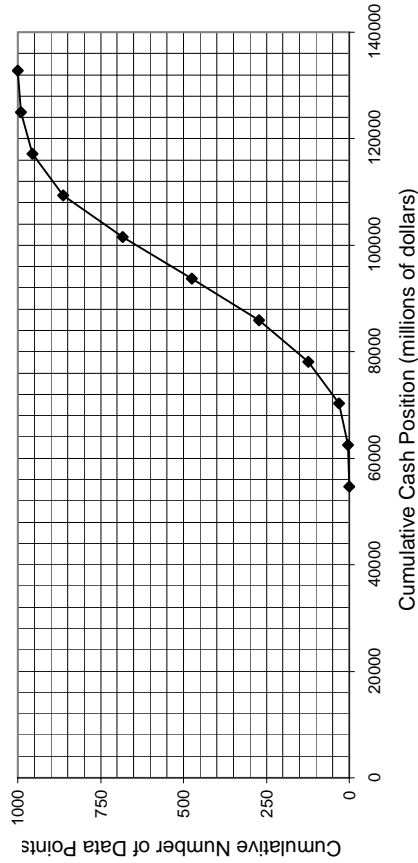
Discounted Payback Period Data

Low DPBP	4.8		
High DPBP	14.3		
Bins	Upper	#/bin	Cumulative
0	4.8	0	0
1	5.8	67	67
2	6.7	197	264
3	7.7	240	504
4	8.6	210	714
5	9.5	117	831
6	10.5	88	919
7	11.4	55	974
8	12.4	14	988
9	13.3	10	998
10	14.3	2	1000



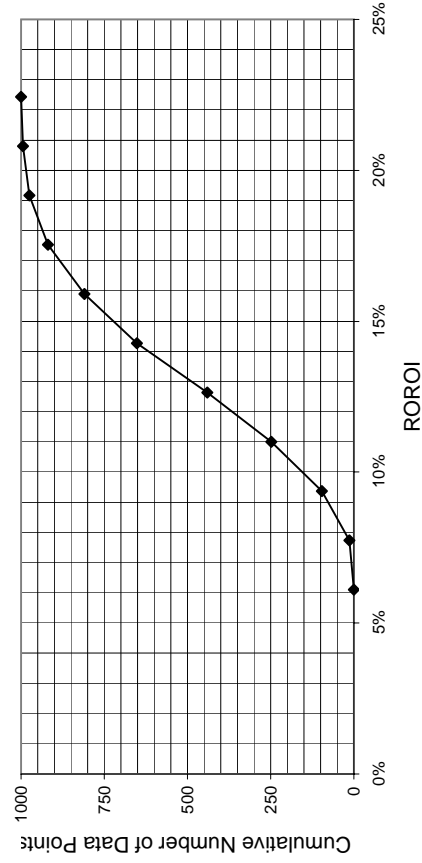
Cumulative Cash Position Data

Low CCP	54685.65		
High CCP	132810.66		
<u>Bins</u>	<u>Upper Value</u>	<u># points/bin</u>	<u>Cumulative</u>
0	54685.65	0	0
1	62498.15	3	3
2	70310.66	28	31
3	78123.16	93	124
4	85935.66	148	272
5	93748.16	203	475
6	101560.66	209	684
7	109373.16	179	863
8	117185.66	92	955
9	124998.16	35	990
10	132810.66	10	1000



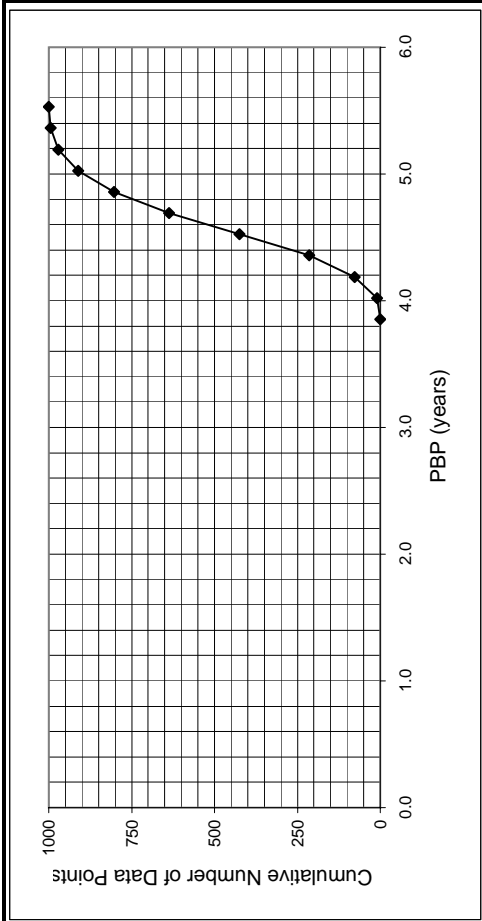
Rate of Return on Investment Data

Low RORO	6%		
High RORO	22%		
<u>Bins</u>	<u>Upper Value</u>	<u># points/bin</u>	<u>Cumulative</u>
0	6%	0	0
1	8%	13	13
2	9%	83	96
3	11%	152	248
4	13%	192	440
5	14%	211	651
6	16%	159	810
7	18%	109	919
8	19%	56	975
9	21%	20	995
10	22%	5	1000



Payback Period Data

Low DPBP	3.9	Upper	#/bin	Cumulative
High DPBP	5.5	3.9	0	0
		4.0	10	10
		4.2	67	77
		4.4	137	214
		4.5	210	424
		4.7	213	637
		4.9	166	803
		5.0	109	912
		5.2	59	971
		5.4	23	994
		5.5	6	1000



Hours per Operating Year	8760
---------------------------------	------

	<u>Cost (\$/GJ)</u>
Common Utilities	
Electricity (110V - 440V)	16.8
Cooling Water (30°C to 45°C)	0.354
Refrigerated Water (15°C to 25°C)	4.43
Steam from Boilers	
Low Pressure (5 barg, 160°C)	6.08
Medium Pressure (10 barg, 184°C)	6.87
High Pressure (41 barg, 254°C)	9.83
Fuels	
Fuel Oil (no. 2)	6.0
Natural Gas	6
Coal (FOB mine mouth)	1.07
Thermal Systems	
Moderately High (up to 330°C)	6.67
High (up to 400°C)	7
Very High (up to 600°C)	7.5
Refrigeration	
Moderately Low (5°C)	4.43
Low (-20°C)	7.89
Very low (-50°C)	13.11
Waste Disposal (solid and liquid)	
<u>Cost (\$/tonne)</u>	
Non-Hazardous	36
Hazardous	200

Cost of Steam used in Steam Drives	
	<u>Cost (\$/GJ)</u>
Steam used for steam-powered drives \$	9.83

Equipment Efficiencies	
Pump Efficiency	85%
Drive Efficiency	90%
Fan Efficiency	80%
Furnace Efficiency	90%
Turbine Efficiency	85%

Process Equipment	
Operators per shift per equipment	
Cost of Labor (per operator/year) \$	50,000

Update Preferences

Power Preference
kilowatts

Pressure Preference
barg

Heat Duty Preference
MJ/h

Length Preference
meters

Area Preference
square meters

Volume Preference
cubic meters

Gas Flow Preference
cubic meters/s

Cost Preference
\$/kg

Flowrate Preference
kg/h

Energy Price Preference
\$/Gigajoule

Compressor Data (without electric motors)

Compressor Type	K ₁	K ₂	K ₃	F _{BMCS}	F _{BMSS}	F _{BMNS}	W _{min} (kW)	W _{max} (kW)
Centrifugal	2.2891	1.3604	-0.1027	2.7	5.8	11.5	450	3000
Axial	2.2891	1.3604	-0.1027	3.8	8.0	15.9	450	3000
Rotary	5.0355	-1.8002	0.8253	2.4	5.0	9.9	18	950
Reciprocating	2.2891	1.3604	-0.1027	3.4	7.0	13.9	450	3000

Drive Data

Electric Drives							
	K ₁	K ₂	K ₃	F _{BM}	W _{min} (kW)	W _{max} (kW)	
Explosion Proof	2.4604	1.4191	-0.1798	1.5	75	2600	
Totally Enclosed	1.956	1.7142	-0.2282	1.5	75	2600	
Open/Drip Proof	2.9508	1.0688	-0.1315	1.5	75	2600	
Non-Electric Drives							
	K ₁	K ₂	K ₃	F _{BM}	W _{min} (kW)	W _{max} (kW)	
Gas Turbine	-21.7702	13.2175	-1.5279	3.5	7500	23000	
Steam Turbine	2.6259	1.4398	-0.1776	3.5	70	7500	
Internal Combustion	2.7635	0.8574	-0.0098	2.0	10	10000	

Fan Data (include electric motors)

Fan Type	K ₁	K ₂	K ₃	F _{BMCS}	F _{BM fiberglass}	F _{BMSS}	F _{BMNS}	Threshold	C ₁	C ₂	C ₃	V _{min} (m3/s)	V _{max} (m3/s)	P _{max} (barg)
Centrifugal Radial Fan	3.5391	-0.3533	0.4477	2.7	5.0	5.8	11.5	0.01	0.00	0.209	-0.033	1	100	0.16
Centrifugal Backward curv	3.3471	-0.0734	0.3090	2.7	5.0	5.8	11.5	0.01	0.00	0.209	-0.033	1	100	0.16
Axial Tube Fan	3.0414	-0.3375	0.4722	2.7	5.0	5.8	11.5	0.04	0.00	0.209	-0.033	1	100	0.16
Axial Vane Fan	3.1761	-0.1373	0.3414	2.7	5.0	5.8	11.5	0.04	0.00	0.209	-0.033	1	100	0.16

Fired Heater Data

Reactive Heaters	K ₁	K ₂	K ₃	Q _{min} (kW)	Q _{max} (kW)	P _{max} (barg)	C ₁	C ₂	C ₃	Bare Module Factor		
										CS	Alloy Steel	SS
Reformer Furnace	3.068	0.6597	0.0194	3000	100000	200	0.1405	-0.2698	0.1293	2.13	2.51	2.81
Pyrolysis Furnace	2.3859	0.9721	-0.0206	3000	100000	200	0.1017	-0.1957	0.09403	2.13	2.51	2.81

Non-reactive Heaters	K ₁	K ₂	K ₃	Q _{min} (kW)	Q _{max} (kW)	P _{max} (barg)	C ₁	C ₂	C ₃	Bare Module Factor		
										CS	Alloy Steel	SS
Process Heater	7.3488	-1.1666	0.2028	1000	100000	200	0.1347	-0.2368	0.1021	2.13	2.51	2.81

Thermal Fluid Heaters	K ₁	K ₂	K ₃	Q _{min} (kW)	Q _{max} (kW)	P _{max} (barg)	C ₁	C ₂	C ₃	F _{bm}	Steam Superheat Factor		
											F _{T1}	F _{T2}	F _{T3}
Hot Water	2.0829	0.9074	-0.0243	650	10750	200	-0.0163	0.0569	-0.0088	2.17			
Molten Salt, Mineral Oil,	1.1979	1.4782	-0.0958	650	10750	200	-0.0163	0.0569	-0.0088	2.17			
Diphenyl Based Oils	2.2628	0.8581	0.0003	650	10750	200	-0.0163	0.0569	-0.0088	2.17			
Packaged Steam Boilers	6.9617	-1.48	0.3161	1200	9400	40	2.5941	-4.2348	1.7224	2.2	1.000	0.00184	3.35E-06

Heat Exchanger Data

Exchanger Type	K ₁	K ₂	K ₃	C ₁	C ₂	C ₃	B ₁	B ₂	A _{min} (m2)	A _{max} (m2)	P _{max} (barg)
Double Pipe	3.3444	0.2745	-0.0472	13.1467	-12.6574	3.0705	1.74	1.55	1	10	300
40 barg < P < 100 barg				0.6072	-0.912	0.3327					
P < 40 barg				0	0	0					
Multiple Pipe	2.7652	0.7282	0.0783	13.1467	-12.6574	3.0705	1.74	1.55	10	100	300
40 barg < P < 100 barg				0.6072	-0.912	0.3327					
P < 40 barg				0	0	0					
Fixed tube, sheet, or U tut tubes only > 5 barg	4.3247	-0.303	0.1634	0.03881	-0.11272	0.08183	1.63	1.66	10.0	1000	140
Floating Head tubes only > 5barg	4.8306	-0.8509	0.3187	0.03881	-0.11272	0.08183	1.63	1.66	10.0	1000	140
Bayonet tubes only > 5 barg	4.2768	-0.0495	0.1431	0.03881	-0.11272	0.08183	1.63	1.66	10.0	1000	140
Kettle Reboiler tubes only > 5 barg	4.4646	-0.5277	0.3955	0.03881	-0.11272	0.08183	1.63	1.66	10.0	100	140
Scraped Wall 40 barg < P < 100 barg	3.7803	0.8569	0.0349	13.1467	-12.6574	3.0705	1.74	1.55	2.0	20	300
P < 40 barg				0.6072	-0.912	0.3327					
Teflon Tube	3.8062	0.8924	-0.1671	0	0	0	1.63	1.66	1.0	10	15
Air Cooler	4.0336	0.2341	0.0497	-0.125	0.15361	-0.02861	0.96	1.21	10	10000	100
Spiral Tube - shell and tub tube only	3.9912	0.0668	0.243	-0.4045	0.1859	0	1.74	1.55	1	100	400
Spiral Plate	4.6561	-0.2947	0.2207	0	0	0	0.96	1.21	1	100	19
Flat Plate	4.6656	-0.1557	0.1547	0	0	0	0.96	1.21	10	1000	19

Material Factors, F_M

Exchanger Type	Shell - CS Tube - CS	CS Cu	Cu Cu	CS SS	SS SS	CS Ni	Ni Ni	CS Ti	Ti Ti
Double Pipe	1.00	1.35	1.69	1.81	2.73	2.68	3.73	4.63	11.38
Multiple Pipe	1.00	1.35	1.69	1.81	2.73	2.68	3.73	4.63	11.38
Fixed tube, sheet, or U tut	1.00	1.35	1.69	1.81	2.73	2.68	3.73	4.63	11.38
Floating Head	1.00	1.35	1.69	1.81	2.73	2.68	3.73	4.63	11.38
Bayonet	1.00	1.35	1.69	1.81	2.73	2.68	3.73	4.63	11.38
Kettle Reboiler	1.00	1.35	1.69	1.81	2.73	2.68	3.73	4.63	11.38
Scraped Wall	1.00	1.35	1.69	1.81	2.73	2.68	3.73	4.63	11.38
Spiral Tube	1.00	1.35	1.69	1.81	2.73	2.68	3.73	4.63	11.38

Shell Material					
Type of Exchanger	CS	Cu	SS	Ni	Ti
Teflon Tube Exchanger	1.00	1.20	1.30	1.40	3.30

Material In Contact with Process Fluid					
Type of Exchanger	CS	Cu	SS	Ni	Ti
Spiral Plate	1.00	1.35	2.45	2.68	4.63
Flat Plate	1.00	1.35	2.45	2.68	4.63

Tube Material			
Type of Exchanger	CS	Al	SS
Air Cooler	1.00	1.42	2.93

Pump Data (including electric drives)

Pump Type	K ₁	K ₂	K ₃	C ₁	C ₂	C ₃	B ₁	B ₂	F _{m(C)}	F _{m(SS)}	F _{m(Cu)}	F _{m(SS)}	F _{m(Ni)}	F _{m(Ti)}	P _{max(bar)}	W _{min(kW)}	W _{max(kW)}
Centrifugal pump	3.3892	0.0536	0.1538	-0.3935	0.3957	-0.00226	1.89	1.35	1.0	1.6	NA	2.3	4.4	NA	100	1	300
Positive Displacement	3.4771	0.1350	0.14380	-0.24538	0.259016	-0.01363	1.89	1.35	1.0	1.4	1.3	2.7	4.7	10.7	100	1	100
Reciprocating pump	3.8696	0.3161	0.12200	-0.2454	0.2590	-0.0136	1.89	1.35	1.0	1.5	1.3	2.4	4.0	6.4	100	0.1	200

Tank Data

Tank Type	K ₁	K ₂	K ₃	B ₁	B ₂	V _{min(m³/s)}	V _{max(m³/s)}
Fixed Roof	4.8509	-0.3973	0.1445	1.10	0	90	30000
Floating Roof	5.9567	-0.7585	0.1749	1.10	0.00	1000	40000

Turbine Data

Turbine Type	K ₁	K ₂	K ₃	F _{m(C)}	F _{m(SS)}	F _{m(Cu)}	F _{m(SS)}	F _{m(Ni)}	F _{m(Ti)}	W _{min(kW)}	W _{max(kW)}
Axial	2.7051	1.4398	-0.1776	NA	3.5	NA	6.1	11.7	NA	100	4000
Radial	2.2476	1.4965	-0.1618	NA	3.5	NA	6.1	11.7	NA	100	1500

Vaporizer and Evaporator Data

Vaporizer Types	K ₁	K ₂	K ₃	A _{min(m²)}	A _{max(m²)}	P _{max(bar)}	C ₁	C ₂	C ₃
Forced Circulation	5.0238	0.3475	0.0703	5	1000	150	0.1578	-0.2992	0.1413
Falling Film	3.9119	0.8627	-0.0088	50	500	150	0.1578	-0.2992	0.1413
Agitated (Scraped Wall)	5	0.149	-0.0134	0.5	5	150	0.1578	-0.2992	0.1413
Short Tube	5.2366	-0.6572	0.35	10	100	150	0.1578	-0.2992	0.1413
Long Tube	4.642	0.3698	0.0025	100	10000	150	0.1578	-0.2992	0.1413

Vaporizer Types	K ₁	K ₂	K ₃	V _{min(m³)}	V _{max(m³)}	P _{max(bar)}	C ₁	C ₂	C ₃
Jacketed Vessel	3.8751	0.3328	0.1901	1	100	320	0.1578	-0.2992	0.1413
Internal Coil	4.038	0.09142	0.2766	1	100	320	0.1578	-0.2992	0.1413
Jacketed Vessel w/ Coil	4.038	0.09142	0.2766	1	100	320	0.1578	-0.2992	0.1413

Bare Module Factors, F_{BM}					
Evaporator Types	CS	Cu Alloy	SS	Ni Alloy	Ti
Forced Circulation	2.9	3.63	5.08	9.66	14.5
Falling Film	2.25	2.81	3.94	7.49	11.25
Agitated (Scraped Wall)	2.25	2.81	3.94	7.49	11.25
Short Tube	2.9	3.63	5.08	9.66	14.5
Long Tube	2.9	3.63	5.08	9.66	14.5

Bare Module Factors, F_{BM}										
Vaporizer Types	CS	Cu	SS Lined	SS Lined Ni	SS	SS Clad	Ni Alloy	Ni Alloy Clad	Ti	Ti Clad
Jacketed Vessel	2.7	3.4	4.7	4.9	4.8	3.8	9.1	5.9	13.7	9.5
Internal Coil	3.0	3.8	5.2	5.5	5.2	4.1	10.1	6.6	15.2	10.6
Jacketed Vessel w/ Coil	3.0	3.8	5.2	5.5	5.2	4.1	10.1	6.6	15.2	10.6

Vessel Data (including data for distillation towers and packed columns)

Vertical Vessels						Horizontal Vessels					
K ₁	K ₂	K ₃	V _{min}	V _{max}	P _{max(bar)}	K ₁	K ₂	K ₃	V _{min}	V _{max}	P _{max(bar)}
3.4974	0.4485	0.1074	0.3	520	3.5565	0.3776	0.0905	0.1	628	400	

Vessel B-Values

	B1	B2
Horizontal	1.49	1.52
Vertical	2.25	1.82

F_a

Tray Type	K ₁	K ₂	K ₃	A _{min(m²)}	A _{max(m²)}
Sieve	2.9949	0.4465	0.3961	0.07	12.3
Valve	3.3322	0.4838	0.3434	0.7	10.5
Demister	3.2353	0.4838	0.3434	0.7	10.5

Tower Packing

Materials of Construction	K ₁	K ₂	K ₃	V _{min(m³)}	V _{max(m³)}
Ceramic	3.0664	0.9744	0.0055	0.03	628
304 SS	3.2999	0.9744	0.0055	0.03	628
Plastic Saddle	2.4493	0.9744	0.0055	0.03	628

F_{BM}

MOC	Sieve	Valve	Demister
CS	1.0	1	
SS	1.8	1.83	1.0
Fluorocarbon			1.8
Ni-alloy	5.6	5.58	5.6

Materials of Construction

$F_{M,CS}$	1.0
$F_{M,SS clad}$	1.7
$F_{M,SS}$	3.1
$F_{M,Ni clad}$	3.6
$F_{M,Ni}$	7.1
$F_{M,Ti clad}$	4.7
$F_{M,Ti}$	9.4

Add Equipment

Unit Number 100

Edit Equipment

CEPCI 462.4

User Added Equipment

Storage Tanks	Tank Type	Volume (cubic meters)	Volume (gallons)	Purchased Equipment Cost	Bare Module Cost
Tk-101	Fixed Roof	30000		\$ 1,080,000	\$ 1,190,000
Tk-102	Fixed Roof	30000		\$ 1,080,000	\$ 1,190,000
Tk-103	Fixed Roof	30000		\$ 1,080,000	\$ 1,190,000
Tk-104	Fixed Roof	30000		\$ 1,080,000	\$ 1,190,000
Tk-105	Fixed Roof	30000		\$ 1,080,000	\$ 1,190,000
Tk-106	Fixed Roof	30000		\$ 1,080,000	\$ 1,190,000
Tk-107	Fixed Roof	30000		\$ 1,080,000	\$ 1,190,000
Tk-108	Fixed Roof	30000		\$ 1,080,000	\$ 1,190,000
Tk-109	Fixed Roof	30000		\$ 1,080,000	\$ 1,190,000
Tk-110	Fixed Roof	30000		\$ 1,080,000	\$ 1,190,000
Tk-111	Fixed Roof	30000		\$ 1,080,000	\$ 1,190,000
Tk-112	Fixed Roof	30000		\$ 1,080,000	\$ 1,190,000
Tk-113	Fixed Roof	30000		\$ 1,080,000	\$ 1,190,000
Tk-114	Fixed Roof	30000		\$ 1,080,000	\$ 1,190,000
Tk-115	Fixed Roof	30000		\$ 1,080,000	\$ 1,190,000
Tk-116	Fixed Roof	30000		\$ 1,080,000	\$ 1,190,000
Tk-117	Fixed Roof	30000		\$ 1,080,000	\$ 1,190,000
Tk-118	Fixed Roof	30000		\$ 1,080,000	\$ 1,190,000
Tk-119	Fixed Roof	30000		\$ 1,080,000	\$ 1,190,000
Tk-120	Fixed Roof	30000		\$ 1,080,000	\$ 1,190,000
Tk-121	Fixed Roof	30000		\$ 1,080,000	\$ 1,190,000
Tk-122	Fixed Roof	30000		\$ 1,080,000	\$ 1,190,000
Tk-123	Fixed Roof	30000		\$ 1,080,000	\$ 1,190,000
Tk-124	Fixed Roof	30000		\$ 1,080,000	\$ 1,190,000
Tk-125	Fixed Roof	30000		\$ 1,080,000	\$ 1,190,000
Tk-126	Fixed Roof	30000		\$ 1,080,000	\$ 1,190,000
Tk-127	Fixed Roof	30000		\$ 1,080,000	\$ 1,190,000
Tk-128	Fixed Roof	30000		\$ 1,080,000	\$ 1,190,000
Tk-129	Fixed Roof	30000		\$ 1,080,000	\$ 1,190,000
Tk-130	Fixed Roof	30000		\$ 1,080,000	\$ 1,190,000
Tk-131	Fixed Roof	30000		\$ 1,080,000	\$ 1,190,000
Tk-132	Fixed Roof	30000		\$ 1,080,000	\$ 1,190,000
Tk-133	Fixed Roof	30000		\$ 1,080,000	\$ 1,190,000
Tk-134	Fixed Roof	30000		\$ 1,080,000	\$ 1,190,000
Tk-135	Fixed Roof	30000		\$ 1,080,000	\$ 1,190,000
Tk-136	Fixed Roof	30000		\$ 1,080,000	\$ 1,190,000

User Added Equipment	Description	BMF ₀	Actual BMF	Purchased Equipment Cost	Bare Module Cost
Z-101	Solar Collector	1	1	\$ 3,710,000,000	\$ 3,710,000,000
Z-102	glass for reactor	1	1	\$ 62,000,000	\$ 62,000,000
Z-103	CCLC Price installed	1	1	\$ 4,277,600,000	\$ 4,277,600,000
Z-104	Supporting equipment	1	1	\$ 2,000,000,000	\$ 2,000,000,000

Name	Total Module Cost	Grass Roots Cost	Utility Used	Efficiency	Actual Usage	Annual Utility Cost
Tk-101	\$ 1,640,000	\$ 2,330,000	NA			
Tk-102	\$ 1,640,000	\$ 2,330,000	NA			
Tk-103	\$ 1,640,000	\$ 2,330,000	NA			
Tk-104	\$ 1,640,000	\$ 2,330,000	NA			
Tk-105	\$ 1,640,000	\$ 2,330,000	NA			
Tk-106	\$ 1,640,000	\$ 2,330,000	NA			
Tk-107	\$ 1,640,000	\$ 2,330,000	NA			
Tk-108	\$ 1,640,000	\$ 2,330,000	NA			
Tk-109	\$ 1,640,000	\$ 2,330,000	NA			
Tk-110	\$ 1,640,000	\$ 2,330,000	NA			
Tk-111	\$ 1,640,000	\$ 2,330,000	NA			
Tk-112	\$ 1,640,000	\$ 2,330,000	NA			
Tk-113	\$ 1,640,000	\$ 2,330,000	NA			
Tk-114	\$ 1,640,000	\$ 2,330,000	NA			
Tk-115	\$ 1,640,000	\$ 2,330,000	NA			
Tk-116	\$ 1,640,000	\$ 2,330,000	NA			
Tk-117	\$ 1,640,000	\$ 2,330,000	NA			
Tk-118	\$ 1,640,000	\$ 2,330,000	NA			
Tk-119	\$ 1,640,000	\$ 2,330,000	NA			
Tk-120	\$ 1,640,000	\$ 2,330,000	NA			
Tk-121	\$ 1,640,000	\$ 2,330,000	NA			
Tk-122	\$ 1,640,000	\$ 2,330,000	NA			
Tk-123	\$ 1,640,000	\$ 2,330,000	NA			
Tk-124	\$ 1,640,000	\$ 2,330,000	NA			
Tk-125	\$ 1,640,000	\$ 2,330,000	NA			
Tk-126	\$ 1,640,000	\$ 2,330,000	NA			
Tk-127	\$ 1,640,000	\$ 2,330,000	NA			
Tk-128	\$ 1,640,000	\$ 2,330,000	NA			
Tk-129	\$ 1,640,000	\$ 2,330,000	NA			
Tk-130	\$ 1,640,000	\$ 2,330,000	NA			
Tk-131	\$ 1,640,000	\$ 2,330,000	NA			
Tk-132	\$ 1,640,000	\$ 2,330,000	NA			
Tk-133	\$ 1,640,000	\$ 2,330,000	NA			
Tk-134	\$ 1,640,000	\$ 2,330,000	NA			
Tk-135	\$ 1,640,000	\$ 2,330,000	NA			
Tk-136	\$ 1,640,000	\$ 2,330,000	NA			
Z-101	\$ 5,099,000,000	\$ 9,977,500,000				
Z-102	\$ 85,200,000	\$ 121,300,000	Unspecified			
Z-103	\$ 4,277,600,000	\$ 4,277,600,000				
Z-104	\$ 2,748,800,000	\$ 3,913,500,000	Unspecified			
Totals	\$12,269,600,000	\$18,373,800,000				\$ -

Add Materials

<u>Material</u>	<u>Classification</u>	<u>Price (\$/ton)</u>	<u>Consumption (ton/h)</u>	<u>Material Costs (\$/y)</u>
Biomass	Product	\$ 4,371.070	147.62	\$ 5,652,454,416
Carbon Dioxide Credits	Product	\$ 5.000	266.55	\$ 11,674,890
water	Raw Material	\$ 0.985	60	\$ 517,716

- 1 Chemical Marketing Reporter for black iron oxide, synthetic, baged, truck loaded, free on board, warehouse value
- 2 based on values for fillers for rubber, plastic etc.
- 3 Based on 1998 value from Chem marketing reporter - freight equalized

Economic Options

Cost of Land	\$	100,000,000
Taxation Rate		42%
Annual Interest Rate		6.50%
Salvage Value	\$	1,837,380,000
Working Capital	\$	1,837,521,772
FCIL	\$	18,373,800,000
Total Module Factor		1.18
Grass Roots Factor		0.50

Economic Information Calculated From Given Information

Revenue From Sales	\$	5,664,129,306
C _{RM} (Raw Materials Costs)	\$	517,716
C _{UT} (Cost of Utilities)	\$	100,000
C _{WT} (Waste Treatment Costs)	\$	-
C _{OL} (Cost of Operating Labor)	\$	900,000

Factors Used in Calculation of Cost of Manufacturing (COM)

$$Comd = 0.18*FCIL + 2.76*COL + 1.21*(CUT + CWT + CRM)$$

Multiplying factor for FCIL	0.18
Multiplying factor for C _{OL}	2.76
Facotrs for C _{UT} , C _{WT} , and C _{RM}	1.21
COM _d	\$ 3,310,515,436

Factors Used in Calculation of Working Capital

$$Working\ Capital = A*C_{RM} + B*FCIL + C*C_{OL}$$

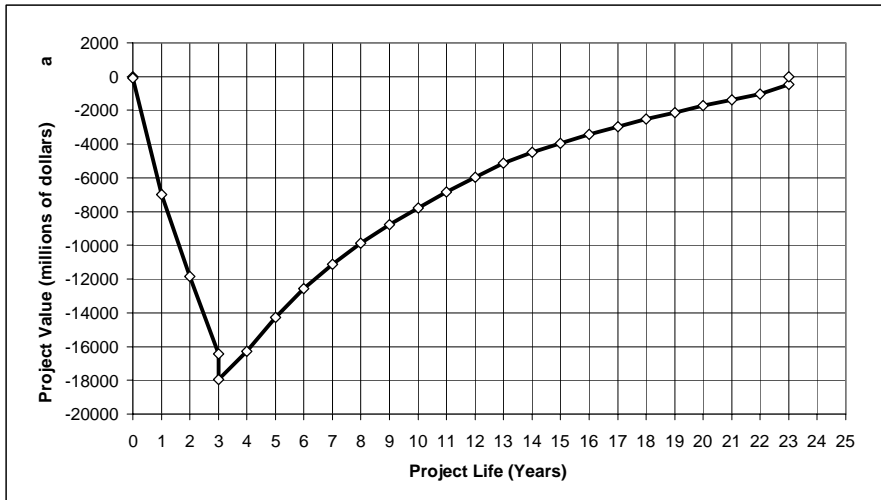
A	0.10
B	0.10
C	0.10

Project Life (Years after Startup)	20
------------------------------------	----

Construction period	3
---------------------	---

Distribution of Fixed Capital Investment (must sum to one)

End of year One	40%
End of year Two	30%
End of year Three	30%
End of year Four	
End of year Five	



Generate CFD

Discounted Profitability Criterion

Net Present Value (millions)	0.03
Discounted Cash Flow Rate of Return	6.50%
Discounted Payback Period (years)	17.3

Non-Discounted Profitability Criteria

Cumulative Cash Position (millions)	17710.80
Rate of Return on Investment	4.82%
Payback Period (years)	8.5

Year	Investment	d_k	$FCI_t - Sd_k$	R	COM_d	$(R - COM_d - d_k) * (1-t) + d_k$	Cash Flow (Non-discounted)	Cash Flow (discounted)	Cumulative Cash Flow (discounted)	Cumulative Cash Flow (Non-discounted)
0	0.00		18373.80				0.00	0.00	0.00	0.00
0	100.00		18373.80				(100.00)	(100.00)	(100.00)	(100.00)
1	7349.52		18373.80				(7349.52)	(6900.96)	(7000.96)	(7449.52)
2	5512.14		18373.80				(5512.14)	(4859.83)	(11860.79)	(12961.66)
3	5512.14		18373.80				(5512.14)	(4563.22)	(16424.01)	(18473.80)
3	1837.52		18373.80				(1837.52)	(1521.19)	(17945.20)	(20311.32)
4		1837.38	16536.42	5664.13	3310.52	2136.80	2136.80	1660.98	(16284.22)	(18174.53)
5		3307.28	13229.14	5664.13	3310.52	2754.16	2754.16	2010.21	(14274.01)	(15420.37)
6		2645.83	10583.31	5664.13	3310.52	2476.34	2476.34	1697.12	(12576.89)	(12944.03)
7		2112.99	8470.32	5664.13	3310.52	2252.55	2252.55	1449.53	(11127.36)	(10691.48)
8		1690.39	6779.93	5664.13	3310.52	2075.06	2075.06	1253.82	(9873.54)	(8616.42)
9		1359.66	5420.27	5664.13	3310.52	1936.15	1936.15	1098.48	(8775.06)	(6680.26)
10		1212.67	4207.60	5664.13	3310.52	1874.42	1874.42	998.55	(7776.51)	(4805.85)
11		1212.67	2994.93	5664.13	3310.52	1874.42	1874.42	937.61	(6838.90)	(2931.43)
12		1194.30	1800.63	5664.13	3310.52	1866.70	1866.70	876.76	(5962.15)	(1064.73)
13		1194.30	606.34	5664.13	3310.52	1866.70	1866.70	823.25	(5138.90)	801.97
14		606.34	-	5664.13	3310.52	1619.76	1619.76	670.74	(4468.16)	2421.73
15		-	-	5664.13	3310.52	1365.10	1365.10	530.79	(3937.37)	3786.83
16		-	-	5664.13	3310.52	1365.10	1365.10	498.39	(3438.98)	5151.92
17		-	-	5664.13	3310.52	1365.10	1365.10	467.97	(2971.01)	6517.02
18		-	-	5664.13	3310.52	1365.10	1365.10	439.41	(2531.60)	7882.11
19		-	-	5664.13	3310.52	1365.10	1365.10	412.59	(2119.01)	9247.21
20		-	-	5664.13	3310.52	1365.10	1365.10	387.41	(1731.60)	10612.31
21		-	-	5664.13	3310.52	1365.10	1365.10	363.77	(1367.83)	11977.40
22		-	-	5664.13	3310.52	1365.10	1365.10	341.56	(1026.27)	13342.50
23		-	-	5664.13	3310.52	2430.78	2430.78	571.09	(455.18)	15773.28
23		-	-	-	-	-	1937.52	455.20	0.03	17710.80

Probable Variation of Key Parameters over Plant Life

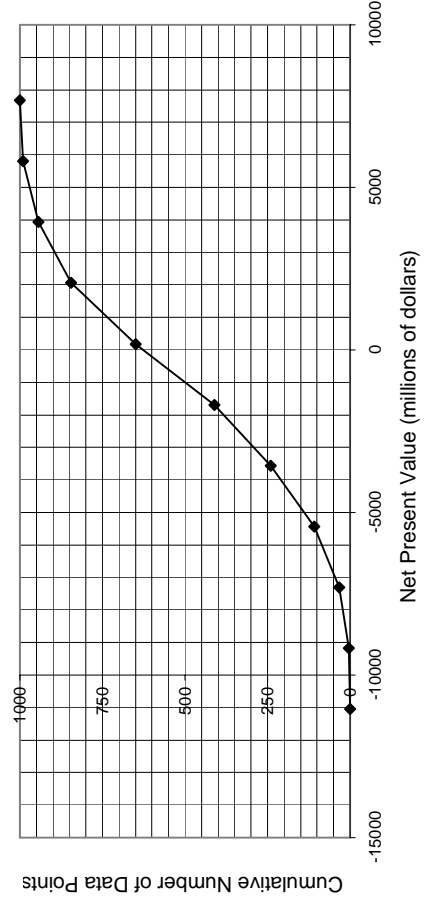
	<u>Lower Limit</u>	<u>Upper Limit</u>	<u>Base Value</u>
FCIL	-20%	30%	\$ 18,373,800,000
Price of Product	-10%	10%	\$ 5,664,129,306
Working Capital	-50%	10%	\$ 1,837,521,772
Income Tax Rate*	-20%	20%	42%
Interest Rate*	-10%	20%	6%
Raw Material Price	-10%	15%	\$ 517,716
Salvage Value	-80%	20%	\$ 1,837,380,000

* Please note that variations for percentages are a percent of a percent. For example, a 10% variance on a 12% interest rate would imply a 1.2% uncertainty

Run Economic Analysis

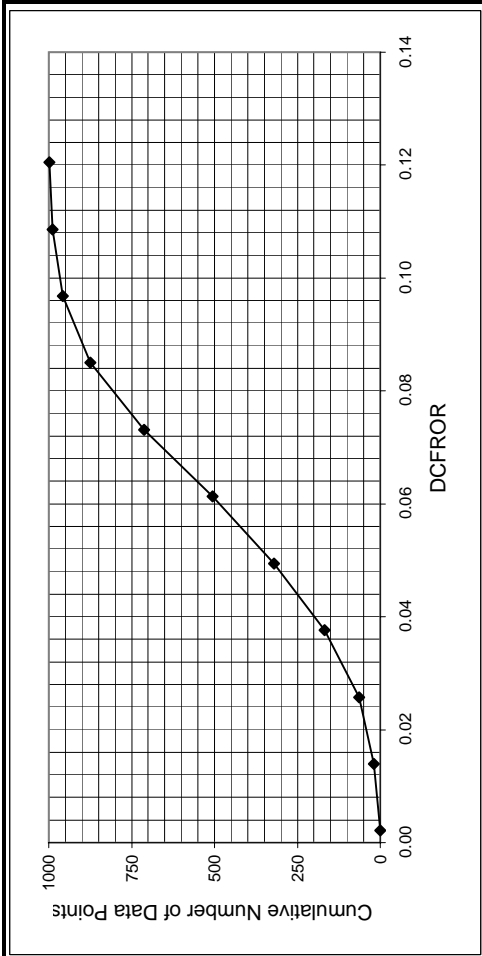
Net Present Value Data

Low NPV	-11038.4		
High NPV	7669.9		
<u>Bins</u>	<u>Upper Value</u>	<u># points/bin</u>	<u>Cumulative</u>
0	-11038.4	0	0
1	-9167.6	3	3
2	-7296.8	30	33
3	-5425.9	76	109
4	-3555.1	132	241
5	-1684.2	170	411
6	186.6	239	650
7	2057.4	194	844
8	3928.3	100	944
9	5799.1	46	990
10	7669.9	10	1000



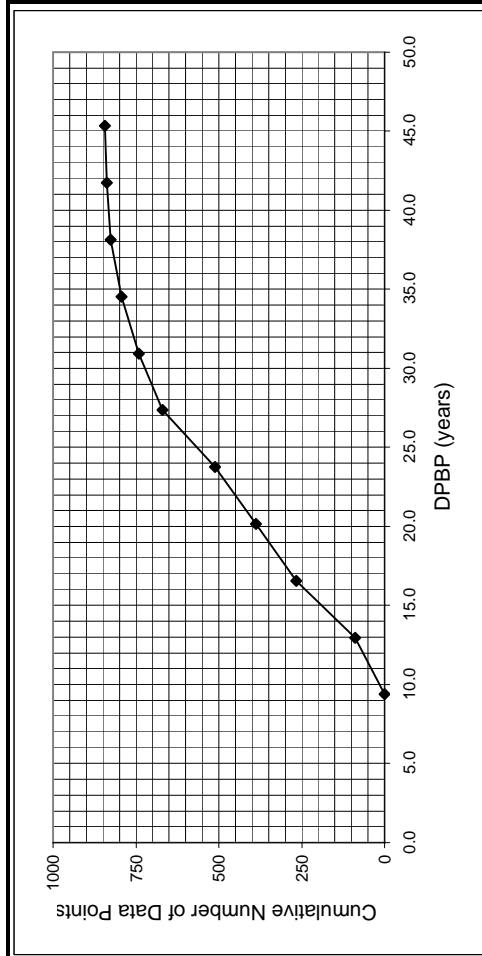
Discounted Cash Flow Rate of Return Data

Low DCFROR	0.00	Upper	#/bin	Cumulative
High DCFROR	0.12	0.00	0	0
Bins		0.01	19	19
		0.03	45	64
		0.04	104	168
		0.05	152	320
		0.06	186	506
		0.07	206	712
		0.08	163	875
		0.10	83	958
		0.11	30	988
		0.12	10	998



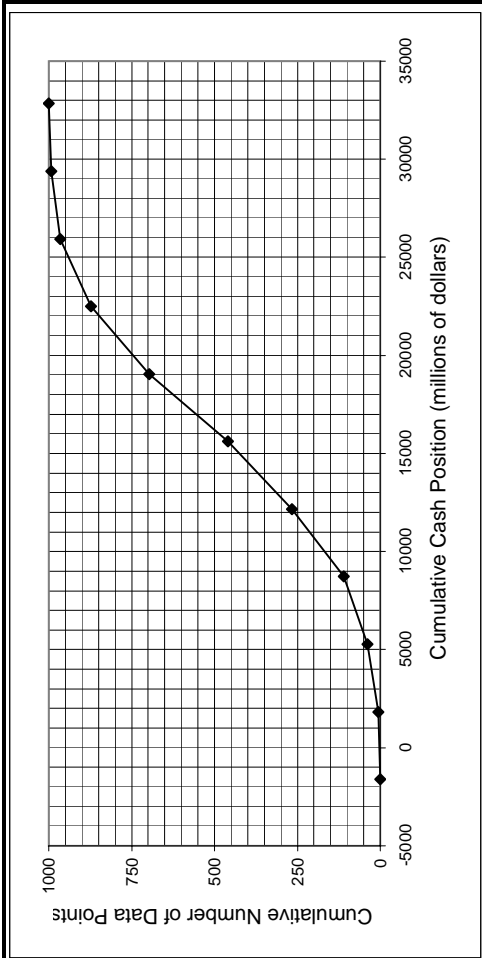
Discounted Payback Period Data

Low DPBP	9.4	Upper	#/bin	Cumulative
High DPBP	45.3	9.4	0	0
Bins		13.0	88	88
		16.6	178	266
		20.2	122	388
		23.8	124	512
		27.4	157	669
		31.0	72	741
		34.5	52	793
		38.1	34	827
		41.7	11	838
		45.3	5	843



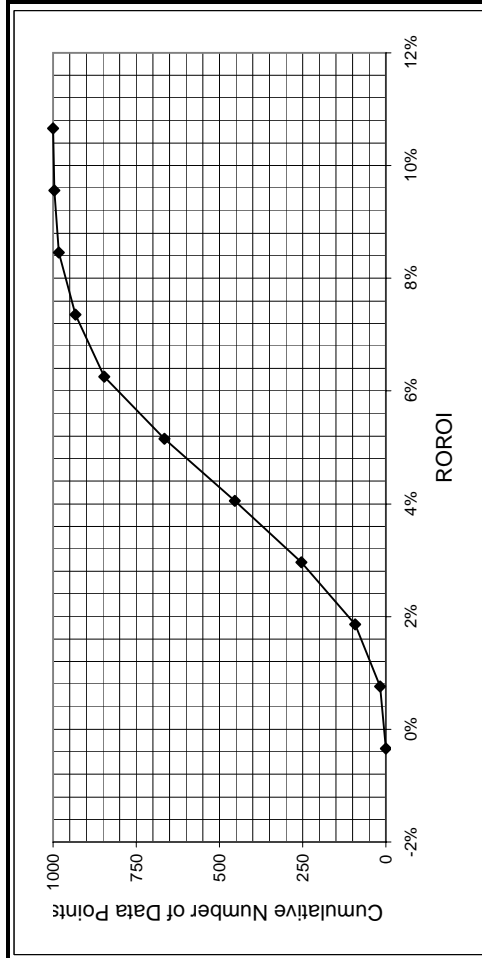
Cumulative Cash Position Data

Low CCP	-1612.15		
High CCP	32835.03		
<u>Bins</u>	<u>Upper Value</u>	<u># points/bin</u>	<u>Cumulative</u>
0	-1612.15	0	0
1	1832.57	6	6
2	5277.28	33	39
3	8722.00	71	110
4	12166.72	157	267
5	15611.44	193	460
6	19056.16	236	696
7	22500.87	176	872
8	25945.59	93	965
9	29390.31	28	993
10	32835.03	7	1000



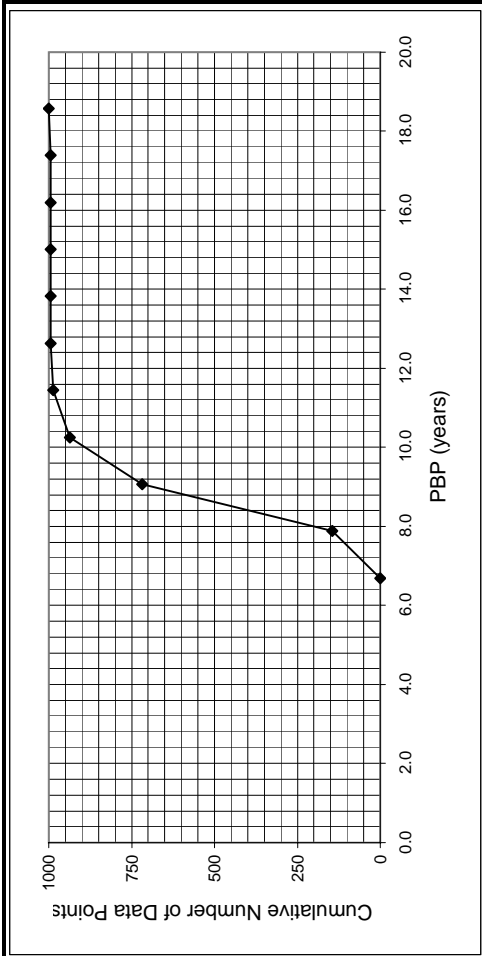
Rate of Return on Investment Data

Low RROI	0%		
High RROI	11%		
<u>Bins</u>	<u>Upper Value</u>	<u># points/bin</u>	<u>Cumulative</u>
0	0%	0	0
1	1%	18	18
2	2%	75	93
3	3%	160	253
4	4%	200	453
5	5%	213	666
6	6%	180	846
7	7%	87	933
8	8%	50	983
9	10%	13	996
10	11%	4	1000



Payback Period Data

Low DPBP	6.7	Upper	#/bin	Cumulative
High DPBP	18.6	6.7	0	0
		7.9	145	145
		9.1	573	718
		10.3	219	937
		11.4	49	986
		12.6	8	994
		13.8	0	994
		15.0	0	994
		16.2	0	994
		17.4	0	994
		18.6	6	1000



Hours per Operating Year	8760
---------------------------------	------

	<u>Cost (\$/GJ)</u>
Common Utilities	
Electricity (110V - 440V)	16.8
Cooling Water (30°C to 45°C)	0.354
Refrigerated Water (15°C to 25°C)	4.43
Steam from Boilers	
Low Pressure (5 barg, 160°C)	6.08
Medium Pressure (10 barg, 184°C)	6.87
High Pressure (41 barg, 254°C)	9.83
Fuels	
Fuel Oil (no. 2)	6.0
Natural Gas	6
Coal (FOB mine mouth)	1.07
Thermal Systems	
Moderately High (up to 330°C)	6.67
High (up to 400°C)	7
Very High (up to 600°C)	7.5
Refrigeration	
Moderately Low (5°C)	4.43
Low (-20°C)	7.89
Very low (-50°C)	13.11
Waste Disposal (solid and liquid)	
<u>Cost (\$/tonne)</u>	
Non-Hazardous	36
Hazardous	200

Cost of Steam used in Steam Drives	
	<u>Cost (\$/GJ)</u>
Steam used for steam-powered drives \$	9.83

Equipment Efficiencies	
Pump Efficiency	85%
Drive Efficiency	90%
Fan Efficiency	80%
Furnace Efficiency	90%
Turbine Efficiency	85%

Process Equipment	
Operators per shift per equipment	
Cost of Labor (per operator/year) \$	50,000

Update Preferences

Power Preference
kilowatts

Pressure Preference
barg

Heat Duty Preference
MJ/h

Length Preference
meters

Area Preference
square meters

Volume Preference
cubic meters

Gas Flow Preference
cubic meters/s

Cost Preference
\$/kg

Flowrate Preference
kg/h

Energy Price Preference
\$/Gigajoule

Compressor Data (without electric motors)

Compressor Type	K ₁	K ₂	K ₃	F _{BMCS}	F _{BMSS}	F _{BMNS}	W _{min} (kW)	W _{max} (kW)
Centrifugal	2.2891	1.3604	-0.1027	2.7	5.8	11.5	450	3000
Axial	2.2891	1.3604	-0.1027	3.8	8.0	15.9	450	3000
Rotary	5.0355	-1.8002	0.8253	2.4	5.0	9.9	18	950
Reciprocating	2.2891	1.3604	-0.1027	3.4	7.0	13.9	450	3000

Drive Data

Electric Drives	K ₁	K ₂	K ₃	F _{BM}	W _{min} (kW)	W _{max} (kW)
Explosion Proof	2.4604	1.4191	-0.1798	1.5	75	2600
Totally Enclosed	1.956	1.7142	-0.2282	1.5	75	2600
Open/Drip Proof	2.9508	1.0688	-0.1315	1.5	75	2600

Non-Electric Drives	K ₁	K ₂	K ₃	F _{BM}	W _{min} (kW)	W _{max} (kW)
Gas Turbine	-21.7702	13.2175	-1.5279	3.5	7500	23000
Steam Turbine	2.6259	1.4398	-0.1776	3.5	70	7500
Internal Combustion	2.7635	0.8574	-0.0098	2.0	10	10000

Fan Data (include electric motors)

Fan Type	K ₁	K ₂	K ₃	F _{BMCS}	F _{BM fiberglass}	F _{BMSS}	F _{BMNS}	Threshold	C ₁	C ₂	C ₃	V _{min} (m3/s)	V _{max} (m3/s)	P _{max} (barg)
Centrifugal Radial Fan	3.5391	-0.3533	0.4477	2.7	5.0	5.8	11.5	0.01	0.00	0.209	-0.033	1	100	0.16
Centrifugal Backward curv	3.3471	-0.0734	0.3090	2.7	5.0	5.8	11.5	0.01	0.00	0.209	-0.033	1	100	0.16
Axial Tube Fan	3.0414	-0.3375	0.4722	2.7	5.0	5.8	11.5	0.04	0.00	0.209	-0.033	1	100	0.16
Axial Vane Fan	3.1761	-0.1373	0.3414	2.7	5.0	5.8	11.5	0.04	0.00	0.209	-0.033	1	100	0.16

Fired Heater Data

Reactive Heaters	K ₁	K ₂	K ₃	Q _{min} (kW)	Q _{max} (kW)	P _{max} (barg)	C ₁	C ₂	C ₃	Bare Module Factor		
										CS	Alloy Steel	SS
Reformer Furnace	3.068	0.6597	0.0194	3000	100000	200	0.1405	-0.2698	0.1293	2.13	2.51	2.81
Pyrolysis Furnace	2.3859	0.9721	-0.0206	3000	100000	200	0.1017	-0.1957	0.09403	2.13	2.51	2.81

Non-reactive Heaters	K ₁	K ₂	K ₃	Q _{min} (kW)	Q _{max} (kW)	P _{max} (barg)	C ₁	C ₂	C ₃	Bare Module Factor		
										CS	Alloy Steel	SS
Process Heater	7.3488	-1.1666	0.2028	1000	100000	200	0.1347	-0.2368	0.1021	2.13	2.51	2.81

Thermal Fluid Heaters	K ₁	K ₂	K ₃	Q _{min} (kW)	Q _{max} (kW)	P _{max} (barg)	C ₁	C ₂	C ₃	F _{bm}	Steam Superheat Factor		
											F _{T1}	F _{T2}	F _{T3}
Hot Water	2.0829	0.9074	-0.0243	650	10750	200	-0.0163	0.0569	-0.0088	2.17			
Molten Salt, Mineral Oil,	1.1979	1.4782	-0.0958	650	10750	200	-0.0163	0.0569	-0.0088	2.17			
Diphenyl Based Oils	2.2628	0.8581	0.0003	650	10750	200	-0.0163	0.0569	-0.0088	2.17			
Packaged Steam Boilers	6.9617	-1.48	0.3161	1200	9400	40	2.5941	-4.2348	1.7224	2.2	1.000	0.00184	3.35E-06

Heat Exchanger Data

Exchanger Type	K ₁	K ₂	K ₃	C ₁	C ₂	C ₃	B ₁	B ₂	A _{min} (m2)	A _{max} (m2)	P _{max} (barg)
Double Pipe	3.3444	0.2745	-0.0472	13.1467	-12.6574	3.0705	1.74	1.55	1	10	300
40 barg < P < 100 barg				0.6072	-0.912	0.3327					
P < 40 barg				0	0	0					
Multiple Pipe	2.7652	0.7282	0.0783	13.1467	-12.6574	3.0705	1.74	1.55	10	100	300
40 barg < P < 100 barg				0.6072	-0.912	0.3327					
P < 40 barg				0	0	0					
Fixed tube, sheet, or U tut tubes only > 5 barg	4.3247	-0.303	0.1634	0.03881	-0.11272	0.08183	1.63	1.66	10.0	1000	140
Floating Head tubes only > 5barg	4.8306	-0.8509	0.3187	0.03881	-0.11272	0.08183	1.63	1.66	10.0	1000	140
Bayonet tubes only > 5 barg	4.2768	-0.0495	0.1431	0.03881	-0.11272	0.08183	1.63	1.66	10.0	1000	140
Kettle Reboiler tubes only > 5 barg	4.4646	-0.5277	0.3955	0.03881	-0.11272	0.08183	1.63	1.66	10.0	100	140
Scraped Wall 40 barg < P < 100 barg	3.7803	0.8569	0.0349	13.1467	-12.6574	3.0705	1.74	1.55	2.0	20	300
P < 40 barg				0.6072	-0.912	0.3327					
Teflon Tube	3.8062	0.8924	-0.1671	0	0	0	1.63	1.66	1.0	10	15
Air Cooler	4.0336	0.2341	0.0497	-0.125	0.15361	-0.02861	0.96	1.21	10	10000	100
Spiral Tube - shell and tub tube only	3.9912	0.0668	0.243	-0.4045	0.1859	0	1.74	1.55	1	100	400
Spiral Plate	4.6561	-0.2947	0.2207	0	0	0	0.96	1.21	1	100	19
Flat Plate	4.6656	-0.1557	0.1547	0	0	0	0.96	1.21	10	1000	19

Material Factors, F_M

Exchanger Type	Shell - CS	CS	Cu	CS	SS	CS	Ni	CS	Ti
	Tube - CS	Cu	Cu	SS	SS	Ni	Ni	Ti	Ti
Double Pipe	1.00	1.35	1.69	1.81	2.73	2.68	3.73	4.63	11.38
Multiple Pipe	1.00	1.35	1.69	1.81	2.73	2.68	3.73	4.63	11.38
Fixed tube, sheet, or U tut	1.00	1.35	1.69	1.81	2.73	2.68	3.73	4.63	11.38
Floating Head	1.00	1.35	1.69	1.81	2.73	2.68	3.73	4.63	11.38
Bayonet	1.00	1.35	1.69	1.81	2.73	2.68	3.73	4.63	11.38
Kettle Reboiler	1.00	1.35	1.69	1.81	2.73	2.68	3.73	4.63	11.38
Scraped Wall	1.00	1.35	1.69	1.81	2.73	2.68	3.73	4.63	11.38
Spiral Tube	1.00	1.35	1.69	1.81	2.73	2.68	3.73	4.63	11.38

Shell Material					
Type of Exchanger	CS	Cu	SS	Ni	Ti
Teflon Tube Exchanger	1.00	1.20	1.30	1.40	3.30

Material In Contact with Process Fluid					
Type of Exchanger	CS	Cu	SS	Ni	Ti
Spiral Plate	1.00	1.35	2.45	2.68	4.63
Flat Plate	1.00	1.35	2.45	2.68	4.63

Tube Material			
Type of Exchanger	CS	Al	SS
Air Cooler	1.00	1.42	2.93

Pump Data (including electric drives)

Pump Type	K ₁	K ₂	K ₃	C ₁	C ₂	C ₃	B ₁	B ₂	F _{m(C)}	F _{m(S)}	F _{m(Cu)}	F _{m(SS)}	F _{m(Ni)}	F _{m(Ti)}	P _{max(bar)}	W _{min(kW)}	W _{max(kW)}
Centrifugal pump	3.3892	0.0536	0.1538	-0.3935	0.3957	-0.00226	1.89	1.35	1.0	1.6	NA	2.3	4.4	NA	100	1	300
Positive Displacement	3.4771	0.1350	0.14380	-0.24538	0.259016	-0.01363	1.89	1.35	1.0	1.4	1.3	2.7	4.7	10.7	100	1	100
Reciprocating pump	3.8696	0.3161	0.12200	-0.2454	0.2590	-0.0136	1.89	1.35	1.0	1.5	1.3	2.4	4.0	6.4	100	0.1	200

Tank Data

Tank Type	K ₁	K ₂	K ₃	B ₁	B ₂	V _{min(m³/s)}	V _{max(m³/s)}
Fixed Roof	4.8509	-0.3973	0.1445	1.10	0	90	30000
Floating Roof	5.9567	-0.7585	0.1749	1.10	0.00	1000	40000

Turbine Data

Turbine Type	K ₁	K ₂	K ₃	F _{m(C)}	F _{m(S)}	F _{m(Cu)}	F _{m(SS)}	F _{m(Ni)}	F _{m(Ti)}	W _{min(kW)}	W _{max(kW)}
Axial	2.7051	1.4398	-0.1776	NA	3.5	NA	6.1	11.7	NA	100	4000
Radial	2.2476	1.4965	-0.1618	NA	3.5	NA	6.1	11.7	NA	100	1500

Vaporizer and Evaporator Data

Vaporizer Types	K ₁	K ₂	K ₃	A _{min(m²)}	A _{max(m²)}	P _{max(bar)}	C ₁	C ₂	C ₃
Forced Circulation	5.0238	0.3475	0.0703	5	1000	150	0.1578	-0.2992	0.1413
Falling Film	3.9119	0.8627	-0.0088	50	500	150	0.1578	-0.2992	0.1413
Agitated (Scraped Wall)	5	0.149	-0.0134	0.5	5	150	0.1578	-0.2992	0.1413
Short Tube	5.2366	-0.6572	0.35	10	100	150	0.1578	-0.2992	0.1413
Long Tube	4.642	0.3698	0.0025	100	10000	150	0.1578	-0.2992	0.1413

Vaporizer Types	K ₁	K ₂	K ₃	V _{min(m³)}	V _{max(m³)}	P _{max(bar)}	C ₁	C ₂	C ₃
Jacketed Vessel	3.8751	0.3328	0.1901	1	100	320	0.1578	-0.2992	0.1413
Internal Coil	4.038	0.09142	0.2766	1	100	320	0.1578	-0.2992	0.1413
Jacketed Vessel w/ Coil	4.038	0.09142	0.2766	1	100	320	0.1578	-0.2992	0.1413

Bare Module Factors, F_{BM}					
Vaporizer Types	CS	Cu Alloy	SS	Ni Alloy	Ti
Forced Circulation	2.9	3.63	5.08	9.66	14.5
Falling Film	2.25	2.81	3.94	7.49	11.25
Agitated (Scraped Wall)	2.25	2.81	3.94	7.49	11.25
Short Tube	2.9	3.63	5.08	9.66	14.5
Long Tube	2.9	3.63	5.08	9.66	14.5

Bare Module Factors, F_{BM}										
Vaporizer Types	CS	Cu	SS Lined	SS Lined Ni	SS	SS Clad	Ni Alloy	Ni Alloy Clad	Ti	Ti Clad
Jacketed Vessel	2.7	3.4	4.7	4.9	4.8	3.8	9.1	5.9	13.7	9.5
Internal Coil	3.0	3.8	5.2	5.5	5.2	4.1	10.1	6.6	15.2	10.6
Jacketed Vessel w/ Coil	3.0	3.8	5.2	5.5	5.2	4.1	10.1	6.6	15.2	10.6

Vessel Data (including data for distillation towers and packed columns)

Vertical Vessels						Horizontal Vessels					
K ₁	K ₂	K ₃	V _{min}	V _{max}	P _{max(bar)}	K ₁	K ₂	K ₃	V _{min}	V _{max}	P _{max(bar)}
3.4974	0.4485	0.1074	0.3	520	3.5565	0.3776	0.0905	0.1	628	400	

Vessel B-Values

	B1	B2
Horizontal	1.49	1.52
Vertical	2.25	1.82

F_a

Tray Type	K ₁	K ₂	K ₃	A _{min(m²)}	A _{max(m²)}
Sieve	2.9949	0.4465	0.3961	0.07	12.3
Valve	3.3322	0.4838	0.3434	0.7	10.5
Demister	3.2353	0.4838	0.3434	0.7	10.5

Tower Packing

Materials of Construction	K ₁	K ₂	K ₃	V _{min(m³)}	V _{max(m³)}
Ceramic	3.0664	0.9744	0.0055	0.03	628
304 SS	3.2999	0.9744	0.0055	0.03	628
Plastic Saddle	2.4493	0.9744	0.0055	0.03	628

F_{BM}

MOC	Sieve	Valve	Demister
CS	1.0	1	
SS	1.8	1.83	1.0
Fluorocarbon			1.8
Ni-alloy	5.6	5.58	5.6

Materials of Construction

$F_{M,CS}$	1.0
$F_{M,SS\ clad}$	1.7
$F_{M,SS}$	3.1
$F_{M,Ni\ clad}$	3.6
$F_{M,Ni}$	7.1
$F_{M,Ti\ clad}$	4.7
$F_{M,Ti}$	9.4

Add Equipment

Unit Number 100

Edit Equipment

CEPCI 462.4

User Added Equipment

Storage Tanks	Tank Type	Volume (cubic meters)	Volume (gallons)	Purchased Equipment Cost	Bare Module Cost
Tk-101	Fixed Roof	30000		\$ 1,080,000	\$ 1,190,000
Tk-102	Fixed Roof	30000		\$ 1,080,000	\$ 1,190,000
Tk-103	Fixed Roof	30000		\$ 1,080,000	\$ 1,190,000
Tk-104	Fixed Roof	30000		\$ 1,080,000	\$ 1,190,000
Tk-105	Fixed Roof	30000		\$ 1,080,000	\$ 1,190,000
Tk-106	Fixed Roof	30000		\$ 1,080,000	\$ 1,190,000
Tk-107	Fixed Roof	30000		\$ 1,080,000	\$ 1,190,000
Tk-108	Fixed Roof	30000		\$ 1,080,000	\$ 1,190,000
Tk-109	Fixed Roof	30000		\$ 1,080,000	\$ 1,190,000
Tk-110	Fixed Roof	30000		\$ 1,080,000	\$ 1,190,000
Tk-111	Fixed Roof	30000		\$ 1,080,000	\$ 1,190,000
Tk-112	Fixed Roof	30000		\$ 1,080,000	\$ 1,190,000
Tk-113	Fixed Roof	30000		\$ 1,080,000	\$ 1,190,000
Tk-114	Fixed Roof	30000		\$ 1,080,000	\$ 1,190,000
Tk-115	Fixed Roof	30000		\$ 1,080,000	\$ 1,190,000
Tk-116	Fixed Roof	30000		\$ 1,080,000	\$ 1,190,000
Tk-117	Fixed Roof	30000		\$ 1,080,000	\$ 1,190,000
Tk-118	Fixed Roof	30000		\$ 1,080,000	\$ 1,190,000
Tk-119	Fixed Roof	30000		\$ 1,080,000	\$ 1,190,000
Tk-120	Fixed Roof	30000		\$ 1,080,000	\$ 1,190,000
Tk-121	Fixed Roof	30000		\$ 1,080,000	\$ 1,190,000
Tk-122	Fixed Roof	30000		\$ 1,080,000	\$ 1,190,000
Tk-123	Fixed Roof	30000		\$ 1,080,000	\$ 1,190,000
Tk-124	Fixed Roof	30000		\$ 1,080,000	\$ 1,190,000
Tk-125	Fixed Roof	30000		\$ 1,080,000	\$ 1,190,000
Tk-126	Fixed Roof	30000		\$ 1,080,000	\$ 1,190,000
Tk-127	Fixed Roof	30000		\$ 1,080,000	\$ 1,190,000
Tk-128	Fixed Roof	30000		\$ 1,080,000	\$ 1,190,000
Tk-129	Fixed Roof	30000		\$ 1,080,000	\$ 1,190,000
Tk-130	Fixed Roof	30000		\$ 1,080,000	\$ 1,190,000
Tk-131	Fixed Roof	30000		\$ 1,080,000	\$ 1,190,000
Tk-132	Fixed Roof	30000		\$ 1,080,000	\$ 1,190,000
Tk-133	Fixed Roof	30000		\$ 1,080,000	\$ 1,190,000
Tk-134	Fixed Roof	30000		\$ 1,080,000	\$ 1,190,000
Tk-135	Fixed Roof	30000		\$ 1,080,000	\$ 1,190,000
Tk-136	Fixed Roof	30000		\$ 1,080,000	\$ 1,190,000

User Added Equipment	Description	BMF ₀	Actual BMF	Purchased Equipment Cost	Bare Module Cost
Z-101	Solar Collector	1	1	\$ 3,710,000,000	\$ 3,710,000,000
Z-102	glass for reactor	1	1	\$ 62,000,000	\$ 62,000,000
Z-103	CCLC Price installed	1	1	\$ 4,277,600,000	\$ 4,277,600,000
Z-104	Supporting equipment	1	1	\$ 2,000,000,000	\$ 2,000,000,000

Name	Total Module Cost	Grass Roots Cost	Utility Used	Efficiency	Actual Usage	Annual Utility Cost
Tk-101	\$ 1,640,000	\$ 2,330,000	NA			
Tk-102	\$ 1,640,000	\$ 2,330,000	NA			
Tk-103	\$ 1,640,000	\$ 2,330,000	NA			
Tk-104	\$ 1,640,000	\$ 2,330,000	NA			
Tk-105	\$ 1,640,000	\$ 2,330,000	NA			
Tk-106	\$ 1,640,000	\$ 2,330,000	NA			
Tk-107	\$ 1,640,000	\$ 2,330,000	NA			
Tk-108	\$ 1,640,000	\$ 2,330,000	NA			
Tk-109	\$ 1,640,000	\$ 2,330,000	NA			
Tk-110	\$ 1,640,000	\$ 2,330,000	NA			
Tk-111	\$ 1,640,000	\$ 2,330,000	NA			
Tk-112	\$ 1,640,000	\$ 2,330,000	NA			
Tk-113	\$ 1,640,000	\$ 2,330,000	NA			
Tk-114	\$ 1,640,000	\$ 2,330,000	NA			
Tk-115	\$ 1,640,000	\$ 2,330,000	NA			
Tk-116	\$ 1,640,000	\$ 2,330,000	NA			
Tk-117	\$ 1,640,000	\$ 2,330,000	NA			
Tk-118	\$ 1,640,000	\$ 2,330,000	NA			
Tk-119	\$ 1,640,000	\$ 2,330,000	NA			
Tk-120	\$ 1,640,000	\$ 2,330,000	NA			
Tk-121	\$ 1,640,000	\$ 2,330,000	NA			
Tk-122	\$ 1,640,000	\$ 2,330,000	NA			
Tk-123	\$ 1,640,000	\$ 2,330,000	NA			
Tk-124	\$ 1,640,000	\$ 2,330,000	NA			
Tk-125	\$ 1,640,000	\$ 2,330,000	NA			
Tk-126	\$ 1,640,000	\$ 2,330,000	NA			
Tk-127	\$ 1,640,000	\$ 2,330,000	NA			
Tk-128	\$ 1,640,000	\$ 2,330,000	NA			
Tk-129	\$ 1,640,000	\$ 2,330,000	NA			
Tk-130	\$ 1,640,000	\$ 2,330,000	NA			
Tk-131	\$ 1,640,000	\$ 2,330,000	NA			
Tk-132	\$ 1,640,000	\$ 2,330,000	NA			
Tk-133	\$ 1,640,000	\$ 2,330,000	NA			
Tk-134	\$ 1,640,000	\$ 2,330,000	NA			
Tk-135	\$ 1,640,000	\$ 2,330,000	NA			
Tk-136	\$ 1,640,000	\$ 2,330,000	NA			
Z-101	\$ 5,099,000,000	\$ 9,977,500,000				
Z-102	\$ 85,200,000	\$ 121,300,000	Unspecified			
Z-103	\$ 4,277,600,000	\$ 4,277,600,000				
Z-104	\$ 2,748,800,000	\$ 3,913,500,000	Unspecified			
Totals	\$12,269,600,000	\$18,373,800,000				\$ -

Add Materials

<u>Material</u>	<u>Classification</u>	<u>Price (\$/ton)</u>	<u>Consumption (ton/h)</u>	<u>Material Costs (\$/y)</u>
Biomass	Product	\$ 6,627.000	147.62	\$ 8,569,713,002
Carbon Dioxide Credits	Product	\$ 5.000	266.55	\$ 11,674,890
water	Raw Material	\$ 0.985	60	\$ 517,716

- 1 Chemical Marketing Reporter for black iron oxide, synthetic, baged, truck loaded, free on board, warehouse value
- 2 based on values for fillers for rubber, plastic etc.
- 3 Based on 1998 value from Chem marketing reporter - freight equalized

Economic Options

Cost of Land	\$	100,000,000
Taxation Rate		42%
Annual Interest Rate		6.50%
Salvage Value	\$	1,837,380,000
Working Capital	\$	1,837,521,772
FCIL	\$	18,373,800,000
Total Module Factor		1.18
Grass Roots Factor		0.50

Economic Information Calculated From Given Information

Revenue From Sales	\$	8,581,387,892
C _{RM} (Raw Materials Costs)	\$	517,716
C _{UT} (Cost of Utilities)	\$	100,000
C _{WT} (Waste Treatment Costs)	\$	-
C _{OL} (Cost of Operating Labor)	\$	900,000

Factors Used in Calculation of Cost of Manufacturing (COM)

$$Comd = 0.18*FCIL + 2.76*COL + 1.21*(CUT + CWT + CRM)$$

Multiplying factor for FCIL	0.18
Multiplying factor for C _{OL}	2.76
Facotrs for C _{UT} , C _{WT} , and C _{RM}	1.21
COM _d	\$ 3,310,515,436

Factors Used in Calculation of Working Capital

$$Working\ Capital = A*C_{RM} + B*FCIL + C*C_{OL}$$

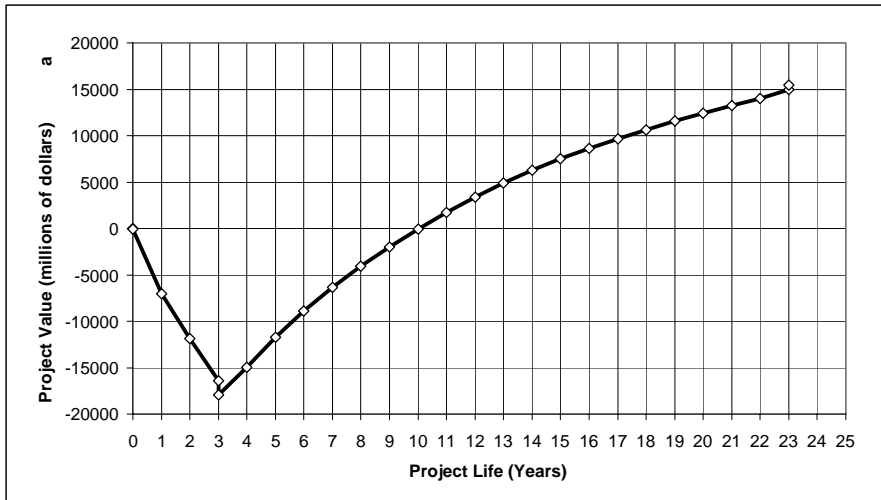
A	0.10
B	0.10
C	0.10

Project Life (Years after Startup)	20
------------------------------------	----

Construction period	3
---------------------	---

Distribution of Fixed Capital Investment (must sum to one)

End of year One	40%
End of year Two	30%
End of year Three	30%
End of year Four	
End of year Five	



Generate CFD

Discounted Profitability Criterion

Net Present Value (millions)	15433.97
Discounted Cash Flow Rate of Return	15.00%
Discounted Payback Period (years)	6.2

Non-Discounted Profitability Criteria

Cumulative Cash Position (millions)	51551.00
Rate of Return on Investment	14.03%
Payback Period (years)	4.5

Year	Investment	d_k	$FCI_L - Sd_k$	R	COM_d	$(R - COM_d - d_k) * (1-t) + d_k$	Cash Flow (Non-discounted)	Cash Flow (discounted)	Cumulative Cash Flow (discounted)	Cumulative Cash Flow (Non-discounted)
0	0.00		18373.80				0.00	0.00	0.00	0.00
0	100.00		18373.80				(100.00)	(100.00)	(100.00)	(100.00)
1	7349.52		18373.80				(7349.52)	(6900.96)	(7000.96)	(7449.52)
2	5512.14		18373.80				(5512.14)	(4859.83)	(11860.79)	(12961.66)
3	5512.14		18373.80				(5512.14)	(4563.22)	(16424.01)	(18473.80)
3	1837.52		18373.80				(1837.52)	(1521.19)	(17945.20)	(20311.32)
4		1837.38	16536.42	8581.39	3310.52	3828.81	3828.81	2976.22	(14968.98)	(16482.52)
5		3307.28	13229.14	8581.39	3310.52	4446.17	4446.17	3245.17	(11723.81)	(12036.35)
6		2645.83	10583.31	8581.39	3310.52	4168.35	4168.35	2856.71	(8867.09)	(7868.00)
7		2112.99	8470.32	8581.39	3310.52	3944.56	3944.56	2538.35	(6328.74)	(3923.44)
8		1690.39	6779.93	8581.39	3310.52	3767.07	3767.07	2276.18	(4052.56)	(156.37)
9		1359.66	5420.27	8581.39	3310.52	3628.16	3628.16	2058.45	(1994.11)	3471.80
10		1212.67	4207.60	8581.39	3310.52	3566.43	3566.43	1899.93	(94.18)	7038.22
11		1212.67	2994.93	8581.39	3310.52	3566.43	3566.43	1783.97	1689.79	10604.65
12		1194.30	1800.63	8581.39	3310.52	3558.71	3558.71	1671.47	3361.25	14163.36
13		1194.30	606.34	8581.39	3310.52	3558.71	3558.71	1569.45	4930.70	17722.07
14		606.34	-	8581.39	3310.52	3311.77	3311.77	1371.40	6302.11	21033.84
15		-	-	8581.39	3310.52	3057.11	3057.11	1188.68	7490.79	24090.95
16		-	-	8581.39	3310.52	3057.11	3057.11	1116.14	8606.93	27148.05
17		-	-	8581.39	3310.52	3057.11	3057.11	1048.01	9654.94	30205.16
18		-	-	8581.39	3310.52	3057.11	3057.11	984.05	10638.99	33262.26
19		-	-	8581.39	3310.52	3057.11	3057.11	923.99	11562.98	36319.37
20		-	-	8581.39	3310.52	3057.11	3057.11	867.60	12430.58	39376.48
21		-	-	8581.39	3310.52	3057.11	3057.11	814.65	13245.23	42433.58
22		-	-	8581.39	3310.52	3057.11	3057.11	764.93	14010.15	45490.69
23		-	-	8581.39	3310.52	4122.79	4122.79	968.61	14978.76	49613.48
23		-	-	-	-	-	1937.52	455.20	15433.97	51551.00

Probable Variation of Key Parameters over Plant Life

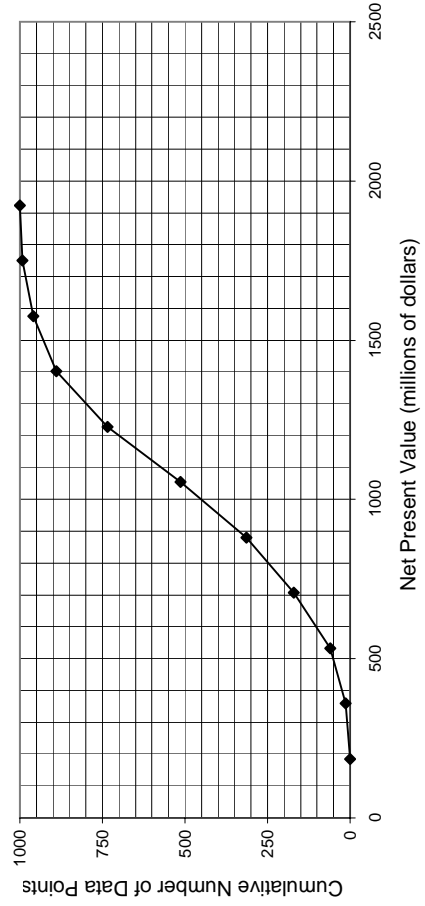
	<u>Lower Limit</u>	<u>Upper Limit</u>	<u>Base Value</u>
FCIL	-20%	30%	\$ 18,373,800,000
Price of Product	-10%	10%	\$ 8,581,387,892
Working Capital	-50%	10%	\$ 1,837,521,772
Income Tax Rate*	-20%	20%	42%
Interest Rate*	-10%	20%	6%
Raw Material Price	-10%	15%	\$ 517,716
Salvage Value	-80%	20%	\$ 1,837,380,000

* Please note that variations for percentages are a percent of a percent.
For example, a 10% variance on a 12% interest rate would imply a 1.2% uncertainty

Run Economic Analysis

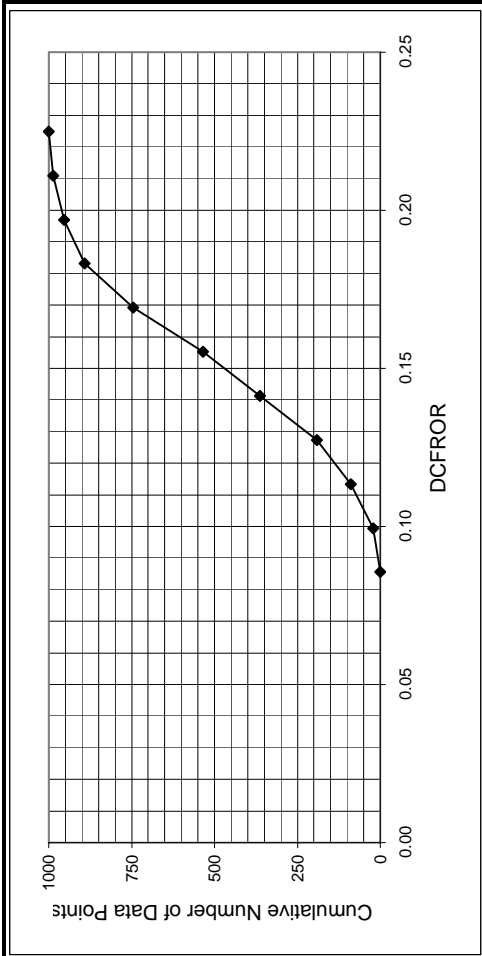
Net Present Value Data

Low NPV	185.3		
High NPV	1923.7		
<u>Bins</u>	<u>Upper Value</u>	<u># points/bin</u>	<u>Cumulative</u>
0	185.3	0	0
1	359.1	14	14
2	533.0	46	60
3	706.8	111	171
4	880.7	143	314
5	1054.5	199	513
6	1228.3	222	735
7	1402.2	154	889
8	1576.0	71	960
9	1749.8	33	993
10	1923.7	7	1000



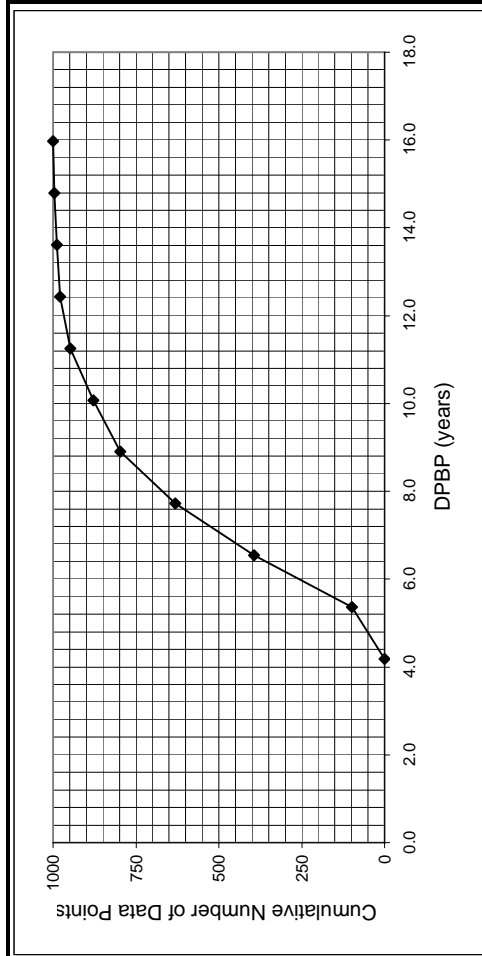
Discounted Cash Flow Rate of Return Data

Low DCFROR	0.09	Upper	#/bin	Cumulative
High DCFROR	0.22	0.09	0	0
		0.10	21	21
		0.11	68	89
		0.13	103	192
		0.14	171	363
		0.16	171	534
		0.17	211	745
		0.18	146	891
		0.20	62	953
		0.21	34	987
		0.22	13	1000



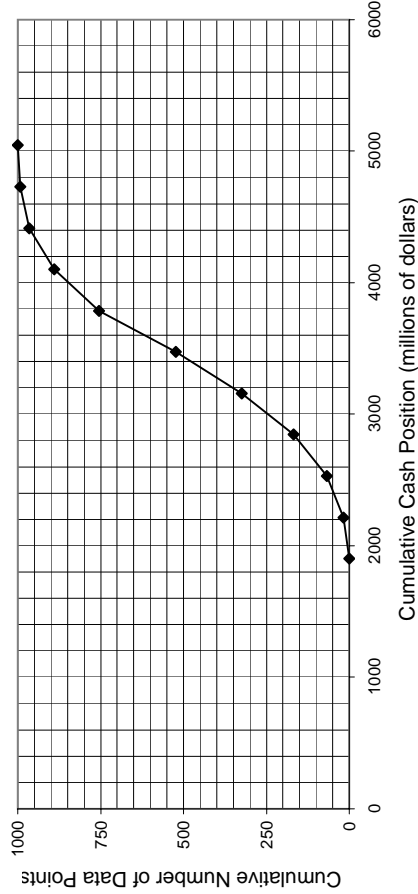
Discounted Payback Period Data

Low DPBP	4.2	Upper	#/bin	Cumulative
High DPBP	16.0	4.2	0	0
		5.4	98	98
		6.5	295	393
		7.7	239	632
		8.9	165	797
		10.1	81	878
		11.3	69	947
		12.4	31	978
		13.6	11	989
		14.8	8	997
		16.0	3	1000



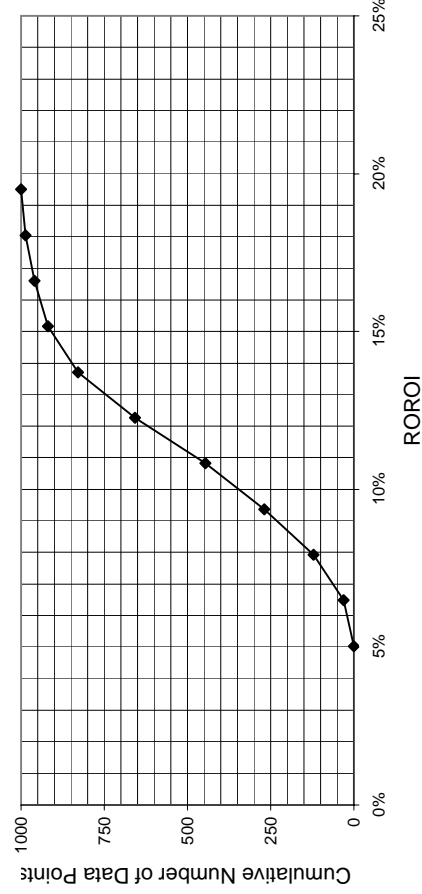
Cumulative Cash Position Data

Low CCP	1901.98		
High CCP	5044.08		
Bins	Upper Value	# points/bin	Cumulative
0	1901.98	0	0
1	2216.19	18	18
2	2530.40	49	67
3	2844.61	101	168
4	3158.82	156	324
5	3473.03	200	524
6	3787.24	230	754
7	4101.45	136	890
8	4415.66	75	965
9	4729.87	28	993
10	5044.08	7	1000



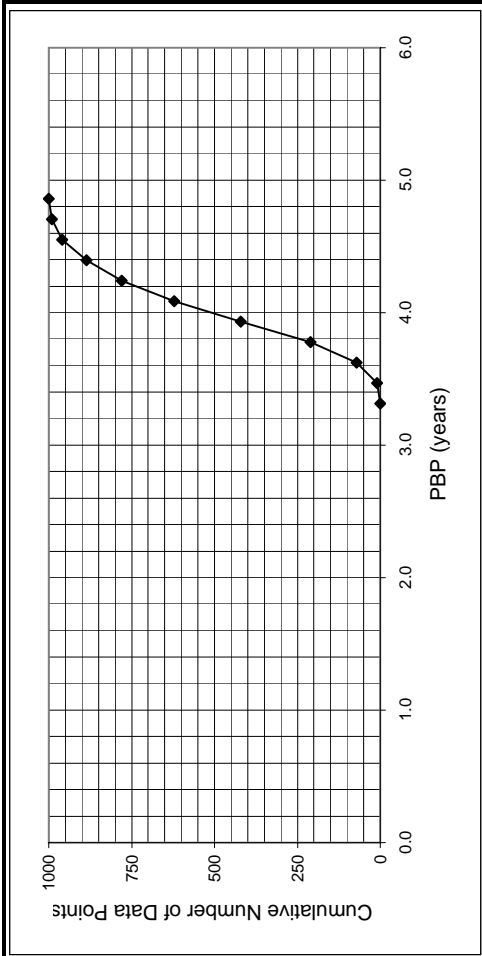
Rate of Return on Investment Data

Low ROROI	5%		
High ROROI	19%		
Bins	Upper Value	# points/bin	Cumulative
0	5%	0	0
1	6%	30	30
2	8%	91	121
3	9%	149	270
4	11%	177	447
5	12%	210	657
6	14%	171	828
7	15%	92	920
8	17%	40	960
9	18%	27	987
10	19%	13	1000



Payback Period Data

Low DPBP	3.3			
High DPBP	4.9			
<u>Bins</u>	<u>Upper</u>	<u>#/bin</u>	<u>Cumulative</u>	
0	3.3	0	0	
1	3.5	9	9	
2	3.6	63	72	
3	3.8	139	211	
4	3.9	209	420	
5	4.1	201	621	
6	4.2	158	779	
7	4.4	107	886	
8	4.5	73	959	
9	4.7	32	991	
10	4.9	9	1000	



Hours per Operating Year	8760
---------------------------------	------

	<u>Cost (\$/GJ)</u>
Common Utilities	
Electricity (110V - 440V)	16.8
Cooling Water (30°C to 45°C)	0.354
Refrigerated Water (15°C to 25°C)	4.43
Steam from Boilers	
Low Pressure (5 barg, 160°C)	6.08
Medium Pressure (10 barg, 184°C)	6.87
High Pressure (41 barg, 254°C)	9.83
Fuels	
Fuel Oil (no. 2)	6.0
Natural Gas	6
Coal (FOB mine mouth)	1.07
Thermal Systems	
Moderately High (up to 330°C)	6.67
High (up to 400°C)	7
Very High (up to 600°C)	7.5
Refrigeration	
Moderately Low (5°C)	4.43
Low (-20°C)	7.89
Very low (-50°C)	13.11
Waste Disposal (solid and liquid)	
<u>Cost (\$/tonne)</u>	
Non-Hazardous	36
Hazardous	200

Cost of Steam used in Steam Drives	
	<u>Cost (\$/GJ)</u>
Steam used for steam-powered drives \$	9.83

Equipment Efficiencies	
Pump Efficiency	85%
Drive Efficiency	90%
Fan Efficiency	80%
Furnace Efficiency	90%
Turbine Efficiency	85%

Process Equipment	
Operators per shift per equipment	
Cost of Labor (per operator/year) \$	50,000

Update Preferences

Power Preference
kilowatts

Pressure Preference
barg

Heat Duty Preference
MJ/h

Length Preference
meters

Area Preference
square meters

Volume Preference
cubic meters

Gas Flow Preference
cubic meters/s

Cost Preference
\$/kg

Flowrate Preference
kg/h

Energy Price Preference
\$/Gigajoule

Compressor Data (without electric motors)

Compressor Type	K ₁	K ₂	K ₃	F _{BMCS}	F _{BMSS}	F _{BMNS}	W _{min} (kW)	W _{max} (kW)
Centrifugal	2.2891	1.3604	-0.1027	2.7	5.8	11.5	450	3000
Axial	2.2891	1.3604	-0.1027	3.8	8.0	15.9	450	3000
Rotary	5.0355	-1.8002	0.8253	2.4	5.0	9.9	18	950
Reciprocating	2.2891	1.3604	-0.1027	3.4	7.0	13.9	450	3000

Drive Data

Electric Drives	K ₁	K ₂	K ₃	F _{BM}	W _{min} (kW)	W _{max} (kW)
Explosion Proof	2.4604	1.4191	-0.1798	1.5	75	2600
Totally Enclosed	1.956	1.7142	-0.2282	1.5	75	2600
Open/Drip Proof	2.9508	1.0688	-0.1315	1.5	75	2600

Non-Electric Drives	K ₁	K ₂	K ₃	F _{BM}	W _{min} (kW)	W _{max} (kW)
Gas Turbine	-21.7702	13.2175	-1.5279	3.5	7500	23000
Steam Turbine	2.6259	1.4398	-0.1776	3.5	70	7500
Internal Combustion	2.7635	0.8574	-0.0098	2.0	10	10000

Fan Data (include electric motors)

Fan Type	K ₁	K ₂	K ₃	F _{BMCS}	F _{BMFBerglass}	F _{BMSS}	F _{BMNS}	Threshold	C ₁	C ₂	C ₃	V _{min} (m3/s)	V _{max} (m3/s)	P _{max} (barg)
Centrifugal Radial Fan	3.5391	-0.3533	0.4477	2.7	5.0	5.8	11.5	0.01	0.00	0.209	-0.033	1	100	0.16
Centrifugal Backward curv	3.3471	-0.0734	0.3090	2.7	5.0	5.8	11.5	0.01	0.00	0.209	-0.033	1	100	0.16
Axial Tube Fan	3.0414	-0.3375	0.4722	2.7	5.0	5.8	11.5	0.04	0.00	0.209	-0.033	1	100	0.16
Axial Vane Fan	3.1761	-0.1373	0.3414	2.7	5.0	5.8	11.5	0.04	0.00	0.209	-0.033	1	100	0.16

Fired Heater Data

Reactive Heaters	K ₁	K ₂	K ₃	Q _{min} (kW)	Q _{max} (kW)	P _{max} (barg)	C ₁	C ₂	C ₃	Bare Module Factor		
										CS	Alloy Steel	SS
Reformer Furnace	3.068	0.6597	0.0194	3000	100000	200	0.1405	-0.2698	0.1293	2.13	2.51	2.81
Pyrolysis Furnace	2.3859	0.9721	-0.0206	3000	100000	200	0.1017	-0.1957	0.09403	2.13	2.51	2.81

Non-reactive Heaters	K ₁	K ₂	K ₃	Q _{min} (kW)	Q _{max} (kW)	P _{max} (barg)	C ₁	C ₂	C ₃	Bare Module Factor		
										CS	Alloy Steel	SS
Process Heater	7.3488	-1.1666	0.2028	1000	100000	200	0.1347	-0.2368	0.1021	2.13	2.51	2.81

Thermal Fluid Heaters	K ₁	K ₂	K ₃	Q _{min} (kW)	Q _{max} (kW)	P _{max} (barg)	C ₁	C ₂	C ₃	F _{bm}	Steam Superheat Factor		
											F _{T1}	F _{T2}	F _{T3}
Hot Water	2.0829	0.9074	-0.0243	650	10750	200	-0.0163	0.0569	-0.0088	2.17			
Molten Salt, Mineral Oil,	1.1979	1.4782	-0.0958	650	10750	200	-0.0163	0.0569	-0.0088	2.17			
Diphenyl Based Oils	2.2628	0.8581	0.0003	650	10750	200	-0.0163	0.0569	-0.0088	2.17			
Packaged Steam Boilers	6.9617	-1.48	0.3161	1200	9400	40	2.5941	-4.2348	1.7224	2.2	1.000	0.00184	3.35E-06

Heat Exchanger Data

Exchanger Type	K ₁	K ₂	K ₃	C ₁	C ₂	C ₃	B ₁	B ₂	A _{min} (m2)	A _{max} (m2)	P _{max} (barg)
Double Pipe	3.3444	0.2745	-0.0472	13.1467	-12.6574	3.0705	1.74	1.55	1	10	300
40 barg < P < 100 barg				0.6072	-0.912	0.3327					
P < 40 barg				0	0	0					
Multiple Pipe	2.7652	0.7282	0.0783	13.1467	-12.6574	3.0705	1.74	1.55	10	100	300
40 barg < P < 100 barg				0.6072	-0.912	0.3327					
P < 40 barg				0	0	0					
Fixed tube, sheet, or U tut tubes only > 5 barg	4.3247	-0.303	0.1634	0.03881	-0.11272	0.08183	1.63	1.66	10.0	1000	140
Floating Head tubes only > 5barg	4.8306	-0.8509	0.3187	0.03881	-0.11272	0.08183	1.63	1.66	10.0	1000	140
Bayonet tubes only > 5 barg	4.2768	-0.0495	0.1431	0.03881	-0.11272	0.08183	1.63	1.66	10.0	1000	140
Kettle Reboiler tubes only > 5 barg	4.4646	-0.5277	0.3955	0.03881	-0.11272	0.08183	1.63	1.66	10.0	100	140
Scraped Wall 40 barg < P < 100 barg	3.7803	0.8569	0.0349	13.1467	-12.6574	3.0705	1.74	1.55	2.0	20	300
P < 40 barg				0.6072	-0.912	0.3327					
Teflon Tube	3.8062	0.8924	-0.1671	0	0	0	1.63	1.66	1.0	10	15
Air Cooler	4.0336	0.2341	0.0497	-0.125	0.15361	-0.02861	0.96	1.21	10	10000	100
Spiral Tube - shell and tub tube only	3.9912	0.0668	0.243	-0.4045	0.1859	0	1.74	1.55	1	100	400
Spiral Plate	4.6561	-0.2947	0.2207	0	0	0	0.96	1.21	1	100	19
Flat Plate	4.6656	-0.1557	0.1547	0	0	0	0.96	1.21	10	1000	19

Material Factors, F_M

Exchanger Type	Shell - CS Tube - CS	CS Cu	Cu Cu	CS SS	SS SS	CS Ni	Ni Ni	CS Ti	Ti Ti
Double Pipe	1.00	1.35	1.69	1.81	2.73	2.68	3.73	4.63	11.38
Multiple Pipe	1.00	1.35	1.69	1.81	2.73	2.68	3.73	4.63	11.38
Fixed tube, sheet, or U tut	1.00	1.35	1.69	1.81	2.73	2.68	3.73	4.63	11.38
Floating Head	1.00	1.35	1.69	1.81	2.73	2.68	3.73	4.63	11.38
Bayonet	1.00	1.35	1.69	1.81	2.73	2.68	3.73	4.63	11.38
Kettle Reboiler	1.00	1.35	1.69	1.81	2.73	2.68	3.73	4.63	11.38
Scraped Wall	1.00	1.35	1.69	1.81	2.73	2.68	3.73	4.63	11.38
Spiral Tube	1.00	1.35	1.69	1.81	2.73	2.68	3.73	4.63	11.38

Shell Material					
Type of Exchanger	CS	Cu	SS	Ni	Ti
Teflon Tube Exchanger	1.00	1.20	1.30	1.40	3.30

Material In Contact with Process Fluid					
Type of Exchanger	CS	Cu	SS	Ni	Ti
Spiral Plate	1.00	1.35	2.45	2.68	4.63
Flat Plate	1.00	1.35	2.45	2.68	4.63

Tube Material			
Type of Exchanger	CS	Al	SS
Air Cooler	1.00	1.42	2.93

Pump Data (including electric drives)

Pump Type	K ₁	K ₂	K ₃	C ₁	C ₂	C ₃	B ₁	B ₂	F _{m(C)}	F _{m(SS)}	F _{m(Cu)}	F _{m(SS)}	F _{m(Ni)}	F _{m(Ti)}	P _{max(bar)}	W _{min(kW)}	W _{max(kW)}
Centrifugal pump	3.3892	0.0536	0.1538	-0.3935	0.3957	-0.00226	1.89	1.35	1.0	1.6	NA	2.3	4.4	NA	100	1	300
Positive Displacement	3.4771	0.1350	0.14380	-0.24538	0.259016	-0.01363	1.89	1.35	1.0	1.4	1.3	2.7	4.7	10.7	100	1	100
Reciprocating pump	3.8696	0.3161	0.12200	-0.2454	0.2590	-0.0136	1.89	1.35	1.0	1.5	1.3	2.4	4.0	6.4	100	0.1	200

Tank Data

Tank Type	K ₁	K ₂	K ₃	B ₁	B ₂	V _{min(m³/s)}	V _{max(m³/s)}
Fixed Roof	4.8509	-0.3973	0.1445	1.10	0	90	30000
Floating Roof	5.9567	-0.7585	0.1749	1.10	0.00	1000	40000

Turbine Data

Turbine Type	K ₁	K ₂	K ₃	F _{m(C)}	F _{m(SS)}	F _{m(Cu)}	F _{m(SS)}	F _{m(Ni)}	F _{m(Ti)}	W _{min(kW)}	W _{max(kW)}
Axial	2.7051	1.4398	-0.1776	NA	3.5	NA	6.1	11.7	NA	100	4000
Radial	2.2476	1.4965	-0.1618	NA	3.5	NA	6.1	11.7	NA	100	1500

Vaporizer and Evaporator Data

Vaporizer Types	K ₁	K ₂	K ₃	A _{min(m²)}	A _{max(m²)}	P _{max(bar)}	C ₁	C ₂	C ₃
Forced Circulation	5.0238	0.3475	0.0703	5	1000	150	0.1578	-0.2992	0.1413
Falling Film	3.9119	0.8627	-0.0088	50	500	150	0.1578	-0.2992	0.1413
Agitated (Scraped Wall)	5	0.149	-0.0134	0.5	5	150	0.1578	-0.2992	0.1413
Short Tube	5.2366	-0.6572	0.35	10	100	150	0.1578	-0.2992	0.1413
Long Tube	4.642	0.3698	0.0025	100	10000	150	0.1578	-0.2992	0.1413

Vaporizer Types	K ₁	K ₂	K ₃	V _{min(m³)}	V _{max(m³)}	P _{max(bar)}	C ₁	C ₂	C ₃
Jacketed Vessel	3.8751	0.3328	0.1901	1	100	320	0.1578	-0.2992	0.1413
Internal Coil	4.038	0.09142	0.2766	1	100	320	0.1578	-0.2992	0.1413
Jacketed Vessel w/ Coil	4.038	0.09142	0.2766	1	100	320	0.1578	-0.2992	0.1413

Bare Module Factors, F_{EM}					
Evaporator Types	CS	Cu Alloy	SS	Ni Alloy	Ti
Forced Circulation	2.9	3.63	5.08	9.66	14.5
Falling Film	2.25	2.81	3.94	7.49	11.25
Agitated (Scraped Wall)	2.25	2.81	3.94	7.49	11.25
Short Tube	2.9	3.63	5.08	9.66	14.5
Long Tube	2.9	3.63	5.08	9.66	14.5

Bare Module Factors, F_{EM}										
Vaporizer Types	CS	Cu	SS Lined	SS Lined Ni	SS	SS Clad	Ni Alloy	Ni Alloy Clad	Ti	Ti Clad
Jacketed Vessel	2.7	3.4	4.7	4.9	4.8	3.8	9.1	5.9	13.7	9.5
Internal Coil	3.0	3.8	5.2	5.5	5.2	4.1	10.1	6.6	15.2	10.6
Jacketed Vessel w/ Coil	3.0	3.8	5.2	5.5	5.2	4.1	10.1	6.6	15.2	10.6

Vessel Data (including data for distillation towers and packed columns)

Vertical Vessels						Horizontal Vessels					
K ₁	K ₂	K ₃	V _{min}	V _{max}	P _{max(bar)}	K ₁	K ₂	K ₃	V _{min}	V _{max}	P _{max(bar)}
3.4974	0.4485	0.1074	0.3	520	3.5565	0.3776	0.0905	0.1	628	400	

Vessel B-Values

	B1	B2
Horizontal	1.49	1.52
Vertical	2.25	1.82

F_a

Tray Type	K ₁	K ₂	K ₃	A _{min(m²)}	A _{max(m²)}
Sieve	2.9949	0.4465	0.3961	0.07	12.3
Valve	3.3322	0.4838	0.3434	0.7	10.5
Demister	3.2353	0.4838	0.3434	0.7	10.5

Tower Packing

Materials of Construction	K ₁	K ₂	K ₃	V _{min(m³)}	V _{max(m³)}
Ceramic	3.0664	0.9744	0.0055	0.03	628
304 SS	3.2999	0.9744	0.0055	0.03	628
Plastic Saddle	2.4493	0.9744	0.0055	0.03	628

F_{EM}

MOC	Sieve	Valve	Demister
CS	1.0	1	
SS	1.8	1.83	1.0
Fluorocarbon			1.8
Ni-alloy	5.6	5.58	5.6

Materials of Construction

$F_{M,CS}$	1.0
$F_{M,SS\ clad}$	1.7
$F_{M,SS}$	3.1
$F_{M,Ni\ clad}$	3.6
$F_{M,Ni}$	7.1
$F_{M,Ti\ clad}$	4.7
$F_{M,Ti}$	9.4

Add Equipment

Unit Number 100

Edit Equipment

CEPCI 462.4

User Added Equipment

Compressors	Compressor Type	Power (kilowatts)	# Spares	MOC	Purchased Equipment Cost	Bare Module Cost
C-101	Centrifugal	2190	2	Stainless Steel	\$ 1,700,000	\$ 9,780,000
C-102	Centrifugal	2080	2	Stainless Steel	\$ 1,640,000	\$ 9,440,000
C-103	Centrifugal	2960	1	Stainless Steel	\$ 1,380,000	\$ 7,960,000
C-104	Centrifugal	2700	1	Stainless Steel	\$ 1,300,000	\$ 7,500,000

Exchangers	Type of Exchanger	Shell Pressure (barg)	Tube Pressure (barg)	MOC	Area (square meters)	Purchased Equipment Cost	Bare Module Cost
E-101	Fixed, Sheet, or U-Tube	1	10.1	Stainless Steel / Carbon Steel	3200	\$ 309,000	\$ 1,440,000
E-102	Fixed, Sheet, or U-Tube	1	16.3	Stainless Steel / Stainless Steel	960	\$ 87,200	\$ 545,000
E-103	Fixed, Sheet, or U-Tube	1	26.4	Stainless Steel / Carbon Steel	378	\$ 49,600	\$ 235,000
E-104	Fixed, Sheet, or U-Tube	1	42.7	Stainless Steel / Carbon Steel	373	\$ 49,200	\$ 236,000

User Added Equipment	Description	BMF ₀	Actual BMF	Purchased Equipment Cost	Bare Module Cost
Z-101	Pipeline installed	1	1	\$ 20,000,000	\$ 20,000,000
Z-102	well cost	1	1	\$ 3,000,000	\$ 3,000,000
Z-103	CCL Cycle installed	1	1	\$ 40,000,000	\$ 40,000,000

Name	Total Module Cost	Grass Roots Cost	Utility Used	Efficiency	Actual Usage	Annual Utility Cost
C-101	\$ 13,400,000	\$ 16,200,000	NA			
C-102	\$ 13,000,000	\$ 15,600,000	NA			
C-103	\$ 10,940,000	\$ 13,100,000	NA			
C-104	\$ 10,300,000	\$ 12,400,000	NA			
E-101	\$ 1,984,000	\$ 2,580,000	Cooling Water		93300 MJ/h	\$ 290,000
E-102	\$ 750,000	\$ 917,000	Cooling Water		32200 MJ/h	\$ 100,000
E-103	\$ 323,000	\$ 418,000	Cooling Water		28500 MJ/h	\$ 88,000
E-104	\$ 324,000	\$ 418,000	Cooling Water		30600 MJ/h	\$ 95,000
Z-101	\$ 20,000,000	\$ 20,000,000	Unspecified			
Z-102	\$ 4,120,000	\$ 5,870,000	Unspecified			
Z-103	\$ 40,000,000	\$ 40,000,000	Unspecified			
Totals	\$ 115,100,000	\$ 127,500,000				\$ 573,000

Add Materials

<u>Material</u>	<u>Classification</u>	<u>Price (\$/kwh \$/ton)</u>	<u>Consumption (kW ton/h)</u>	<u>Material Costs (\$/y)</u>
Carbon Dioxide Credits	Product	\$ 5.000	589.28	\$ 25,810,464
Price hike	Product	\$ 0.00333	500000	\$ 14,602,920

- 1 Chemical Marketing Reporter for black iron oxide, synthetic, baged, truck loaded, free on board, warehouse value
- 2 based on values for fillers for rubber, plastic etc.
- 3 Based on 1998 value from Chem marketing reporter - freight equalized

Economic Options

Cost of Land \$	1,000,000
Taxation Rate	42%
Annual Interest Rate	6.50%
Salvage Value \$	12,750,000
Working Capital \$	12,820,000
FCIL \$	127,500,000
Total Module Factor	1.18
Grass Roots Factor	0.50

Economic Information Calculated From Given Information

Revenue From Sales \$	40,413,384
C _{RM} (Raw Materials Costs) \$	-
C _{UT} (Cost of Utilities) \$	573,000
C _{WT} (Waste Treatment Costs) \$	-
C _{OL} (Cost of Operating Labor) \$	700,000

Factors Used in Calculation of Cost of Manufacturing (COM)

Comd = 0.18*FCIL + 2.76*COL + 1.1*(CUT + CWT + CRM)

Multiplying factor for FCIL	0.18
Multiplying factor for C _{OL}	2.76
Facotrs for C _{UT} , C _{WT} , and C _{RM}	1.1
COM _d \$	25,512,300

Factors Used in Calculation of Working Capital

Working Capital = A*C_{RM} + B*FCIL + C*C_{OL}

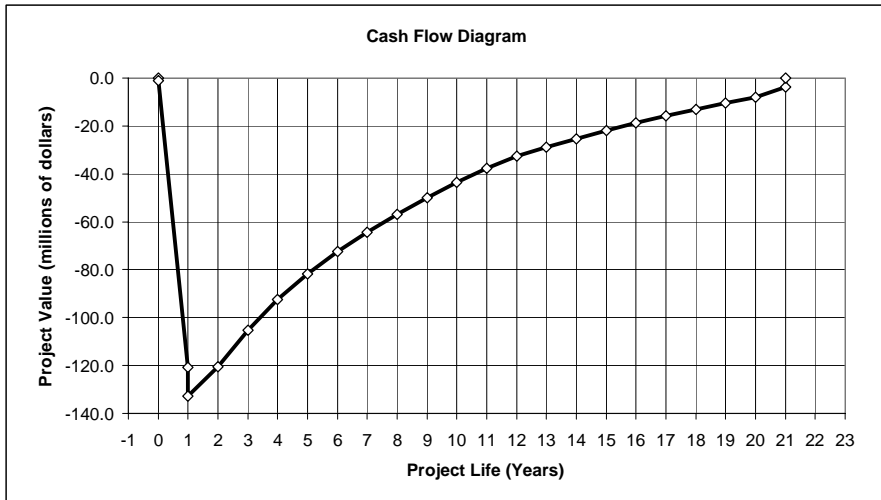
A	0.10
B	0.10
C	0.10

Project Life (Years after Startup)	20
------------------------------------	----

Construction period	1
---------------------	---

Distribution of Fixed Capital Investment (must sum to one)

End of year One	100%
End of year Two	
End of year Three	
End of year Four	
End of year Five	



Generate CFD

Discounted Profitability Criterion

Net Present Value (millions)	(0.00)
Discounted Cash Flow Rate of Return	6.50%
Discounted Payback Period (years)	17.0

Non-Discounted Profitability Criteria

Cumulative Cash Position (millions)	106.30
Rate of Return on Investment	4.17%
Payback Period (years)	9.1

Year	Investment	d_k	$FCI_t - Sd_k$	R	COM_d	$(R - COM_d - d_k) * (1-t) + d_k$	Cash Flow (Non-discounted)	Cash Flow (discounted)	Cumulative Cash Flow (discounted)	Cumulative Cash Flow (Non-discounted)
0	0.00		127.50				0.00	0.00	0.00	0.00
0	1.00		127.50				(1.00)	(1.00)	(1.00)	(1.00)
1	127.50		127.50				(127.50)	(119.72)	(120.72)	(128.50)
1	12.82		127.50				(12.82)	(12.04)	(132.76)	(141.32)
2		12.75	114.75	40.41	25.51	14.00	14.00	12.34	(120.41)	(127.32)
3		22.95	91.80	40.41	25.51	18.28	18.28	15.13	(105.28)	(109.04)
4		18.36	73.44	40.41	25.51	16.35	16.35	12.71	(92.57)	(92.69)
5		14.66	58.78	40.41	25.51	14.80	14.80	10.80	(81.77)	(77.89)
6		11.73	47.05	40.41	25.51	13.57	13.57	9.30	(72.47)	(64.32)
7		9.44	37.61	40.41	25.51	12.61	12.61	8.11	(64.35)	(51.71)
8		8.42	29.20	40.41	25.51	12.18	12.18	7.36	(57.00)	(39.53)
9		8.42	20.78	40.41	25.51	12.18	12.18	6.91	(50.09)	(27.36)
10		8.29	12.50	40.41	25.51	12.12	12.12	6.46	(43.63)	(15.23)
11		8.29	4.21	40.41	25.51	12.12	12.12	6.06	(37.57)	(3.11)
12		4.21	-	40.41	25.51	10.41	10.41	4.89	(32.68)	7.30
13		-	-	40.41	25.51	8.64	8.64	3.81	(28.86)	15.94
14		-	-	40.41	25.51	8.64	8.64	3.58	(25.29)	24.58
15		-	-	40.41	25.51	8.64	8.64	3.36	(21.92)	33.23
16		-	-	40.41	25.51	8.64	8.64	3.16	(18.77)	41.87
17		-	-	40.41	25.51	8.64	8.64	2.96	(15.81)	50.51
18		-	-	40.41	25.51	8.64	8.64	2.78	(13.02)	59.15
19		-	-	40.41	25.51	8.64	8.64	2.61	(10.41)	67.80
20		-	-	40.41	25.51	8.64	8.64	2.45	(7.96)	76.44
21		-	-	40.41	25.51	16.04	16.04	4.27	(3.69)	92.48
21		-	-	-	-	-	13.82	3.68	(0.00)	106.30

Probable Variation of Key Parameters over Plant Life

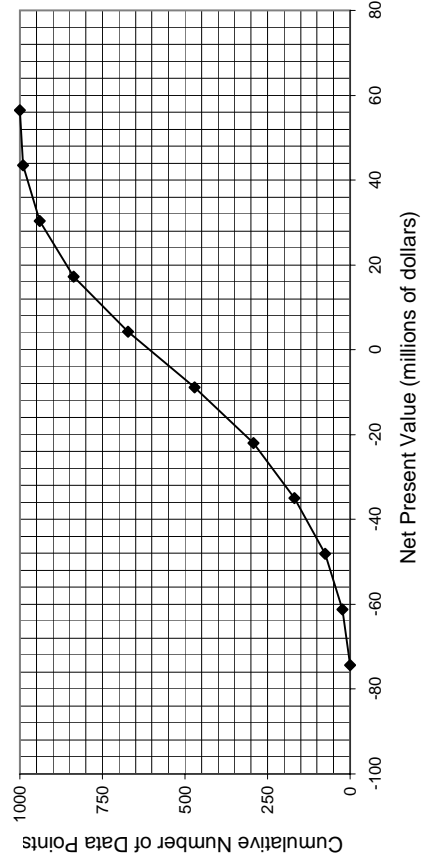
	<u>Lower Limit</u>	<u>Upper Limit</u>	<u>Base Value</u>
FCIL	-20%	30%	\$ 127,500,000
Price of Product	-10%	10%	\$ 40,413,384
Working Capital	-50%	20%	\$ 12,820,000
Income Tax Rate*	-20%	42%	6%
Interest Rate*	-10%	20%	15%
Raw Material Price	-10%	20%	-
Salvage Value	-80%	20%	\$ 12,750,000

* Please note that variations for percentages are a percent of a percent. For example, a 10% variance on a 12% interest rate would imply a 1.2% uncertainty

Run Economic Analysis

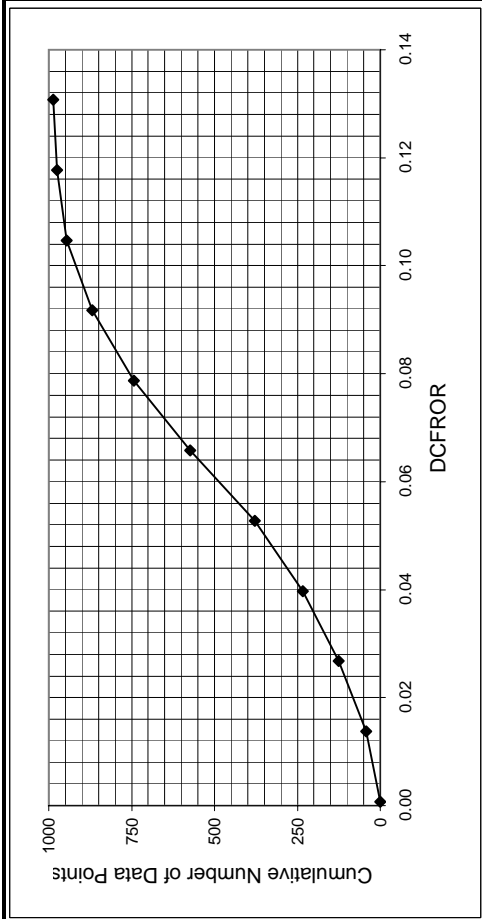
Net Present Value Data

Low NPV	-74.3		
High NPV	56.5		
<u>Bins</u>	<u>Upper Value</u>	<u># points/bin</u>	<u>Cumulative</u>
0	-74.3	0	0
1	-61.2	24	24
2	-48.1	51	75
3	-35.0	93	168
4	-22.0	125	293
5	-8.9	177	470
6	4.2	202	672
7	17.3	165	837
8	30.4	103	940
9	43.4	50	990
10	56.5	10	1000



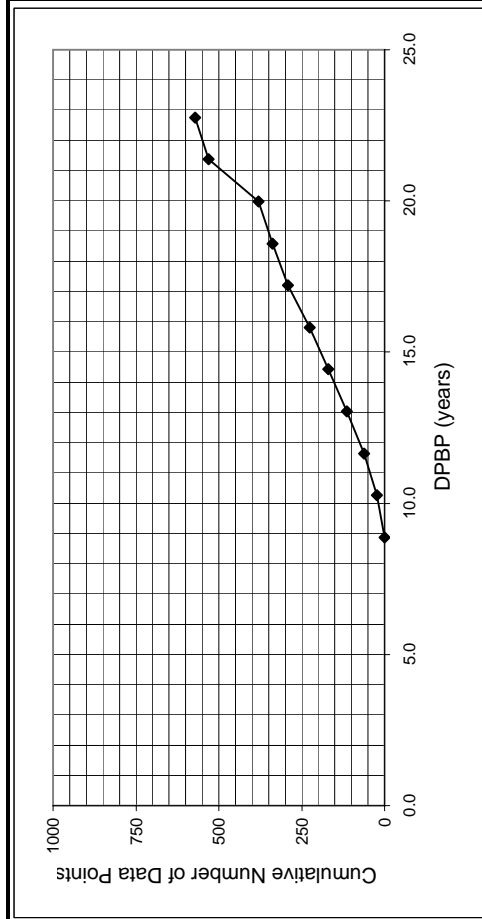
Discounted Cash Flow Rate of Return Data

Low DCFROR	0.00	Upper		#/bin		Cumulative	
High DCFROR	0.13	Lower		#/bin		Cumulative	
Bins	Upper	Lower	#/bin	Cumulative			
0	0.00		0	0			
1	0.01		42	42			
2	0.03		84	126			
3	0.04		108	234			
4	0.05		145	379			
5	0.07		195	574			
6	0.08		169	743			
7	0.09		125	868			
8	0.10		78	946			
9	0.12		29	975			
10	0.13		11	986			



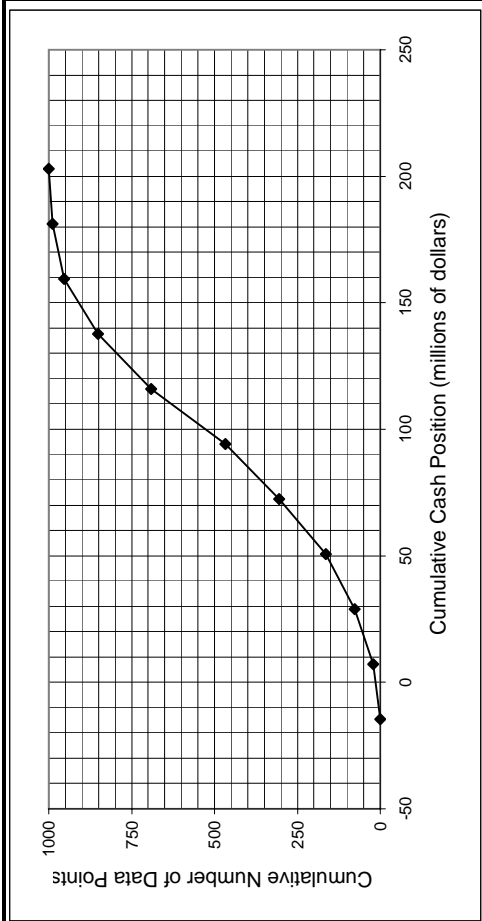
Discounted Payback Period Data

Low DPBP	8.9	Upper		#/bin		Cumulative	
High DPBP	22.8	Lower		#/bin		Cumulative	
Bins	Upper	Lower	#/bin	Cumulative			
0	8.9		0	0			
1	10.3		23	23			
2	11.7		38	61			
3	13.0		53	114			
4	14.4		55	169			
5	15.8		57	226			
6	17.2		65	291			
7	18.6		47	338			
8	20.0		42	380			
9	21.4		150	530			
10	22.8		42	572			



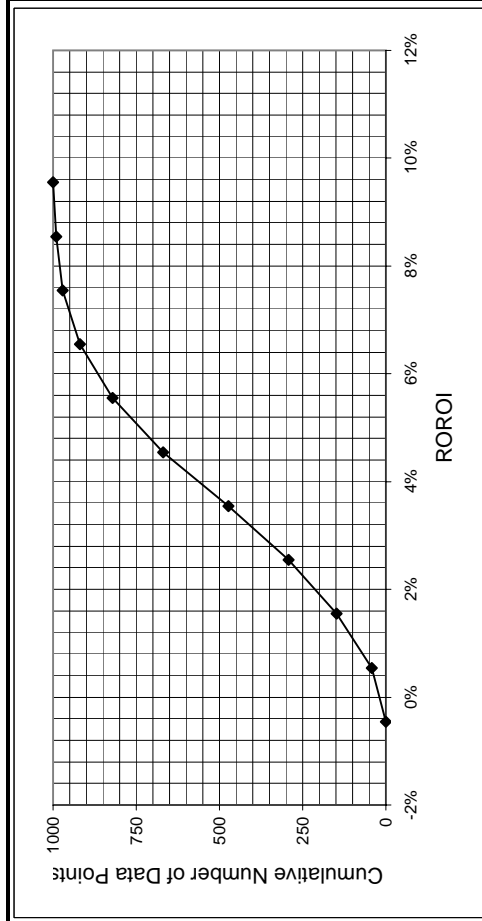
Cumulative Cash Position Data

Low CCP	-14.59		
High CCP	203.07		
Bins	Upper Value	# points/bin	Cumulative
0	-14.59	0	0
1	7.18	22	22
2	28.94	56	78
3	50.71	87	165
4	72.48	140	305
5	94.24	163	468
6	116.01	224	692
7	137.77	159	851
8	159.54	103	954
9	181.30	34	988
10	203.07	12	1000



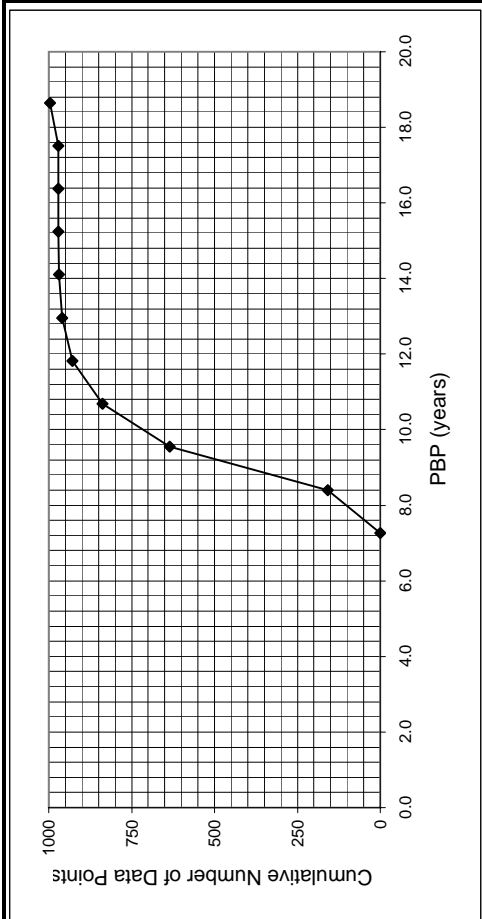
Rate of Return on Investment Data

Low RORO	0%		
High RORO	10%		
Bins	Upper Value	# points/bin	Cumulative
0	0%	0	0
1	1%	43	43
2	2%	105	148
3	3%	145	293
4	4%	180	473
5	5%	196	669
6	6%	152	821
7	7%	99	920
8	8%	52	972
9	9%	19	991
10	10%	9	1000



Payback Period Data

Low DPBP	7.3	Upper	#/bin	Cumulative
High DPBP	18.7	7.3	0	0
Bins		8.4	159	159
		9.5	476	635
		10.7	202	837
		11.8	92	929
		13.0	30	959
		14.1	11	970
		15.2	1	971
		16.4	0	971
		17.5	0	971
		18.7	26	997



Hours per Operating Year	8760
---------------------------------	------

	<u>Cost (\$/GJ)</u>
Common Utilities	
Electricity (110V - 440V)	16.8
Cooling Water (30°C to 45°C)	0.354
Refrigerated Water (15°C to 25°C)	4.43
Steam from Boilers	
Low Pressure (5 barg, 160°C)	6.08
Medium Pressure (10 barg, 184°C)	6.87
High Pressure (41 barg, 254°C)	9.83
Fuels	
Fuel Oil (no. 2)	6.0
Natural Gas	6
Coal (FOB mine mouth)	1.07
Thermal Systems	
Moderately High (up to 330°C)	6.67
High (up to 400°C)	7
Very High (up to 600°C)	7.5
Refrigeration	
Moderately Low (5°C)	4.43
Low (-20°C)	7.89
Very low (-50°C)	13.11
<u>Cost (\$/tonne)</u>	
Waste Disposal (solid and liquid)	
Non-Hazardous	36
Hazardous	200

Cost of Steam used in Steam Drives	
	<u>Cost (\$/GJ)</u>
Steam used for steam-powered drives \$	9.83

Equipment Efficiencies	
Pump Efficiency	85%
Drive Efficiency	90%
Fan Efficiency	80%
Furnace Efficiency	90%
Turbine Efficiency	85%

Process Equipment	
Operators per shift per equipment	
Cost of Labor (per operator/year) \$	50,000

Update Preferences

Power Preference
kilowatts

Pressure Preference
barg

Heat Duty Preference
MJ/h

Length Preference
meters

Area Preference
square meters

Volume Preference
cubic meters

Gas Flow Preference
cubic meters/s

Cost Preference
\$/kg

Flowrate Preference
kg/h

Energy Price Preference
\$/Gigajoule

Compressor Data (without electric motors)

Compressor Type	K ₁	K ₂	K ₃	F _{BMCS}	F _{BMSS}	F _{BMNS}	W _{min} (kW)	W _{max} (kW)
Centrifugal	2.2891	1.3604	-0.1027	2.7	5.8	11.5	450	3000
Axial	2.2891	1.3604	-0.1027	3.8	8.0	15.9	450	3000
Rotary	5.0355	-1.8002	0.8253	2.4	5.0	9.9	18	950
Reciprocating	2.2891	1.3604	-0.1027	3.4	7.0	13.9	450	3000

Drive Data

Electric Drives	K ₁	K ₂	K ₃	F _{BM}	W _{min} (kW)	W _{max} (kW)
Explosion Proof	2.4604	1.4191	-0.1798	1.5	75	2600
Totally Enclosed	1.956	1.7142	-0.2282	1.5	75	2600
Open/Drip Proof	2.9508	1.0688	-0.1315	1.5	75	2600

Non-Electric Drives	K ₁	K ₂	K ₃	F _{BM}	W _{min} (kW)	W _{max} (kW)
Gas Turbine	-21.7702	13.2175	-1.5279	3.5	7500	23000
Steam Turbine	2.6259	1.4398	-0.1776	3.5	70	7500
Internal Combustion	2.7635	0.8574	-0.0098	2.0	10	10000

Fan Data (include electric motors)

Fan Type	K ₁	K ₂	K ₃	F _{BMCS}	F _{BM fiberglass}	F _{BMSS}	F _{BMNS}	Threshold	C ₁	C ₂	C ₃	V _{min} (m3/s)	V _{max} (m3/s)	P _{max} (barg)
Centrifugal Radial Fan	3.5391	-0.3533	0.4477	2.7	5.0	5.8	11.5	0.01	0.00	0.209	-0.033	1	100	0.16
Centrifugal Backward curv	3.3471	-0.0734	0.3090	2.7	5.0	5.8	11.5	0.01	0.00	0.209	-0.033	1	100	0.16
Axial Tube Fan	3.0414	-0.3375	0.4722	2.7	5.0	5.8	11.5	0.04	0.00	0.209	-0.033	1	100	0.16
Axial Vane Fan	3.1761	-0.1373	0.3414	2.7	5.0	5.8	11.5	0.04	0.00	0.209	-0.033	1	100	0.16

Fired Heater Data

Reactive Heaters	K ₁	K ₂	K ₃	Q _{min} (kW)	Q _{max} (kW)	P _{max} (barg)	C ₁	C ₂	C ₃	Bare Module Factor		
										CS	Alloy Steel	SS
Reformer Furnace	3.068	0.6597	0.0194	3000	100000	200	0.1405	-0.2698	0.1293	2.13	2.51	2.81
Pyrolysis Furnace	2.3859	0.9721	-0.0206	3000	100000	200	0.1017	-0.1957	0.09403	2.13	2.51	2.81

Non-reactive Heaters	K ₁	K ₂	K ₃	Q _{min} (kW)	Q _{max} (kW)	P _{max} (barg)	C ₁	C ₂	C ₃	Bare Module Factor		
										CS	Alloy Steel	SS
Process Heater	7.3488	-1.1666	0.2028	1000	100000	200	0.1347	-0.2368	0.1021	2.13	2.51	2.81

Thermal Fluid Heaters	K ₁	K ₂	K ₃	Q _{min} (kW)	Q _{max} (kW)	P _{max} (barg)	C ₁	C ₂	C ₃	F _{bm}	Steam Superheat Factor		
											F _{T1}	F _{T2}	F _{T3}
Hot Water	2.0829	0.9074	-0.0243	650	10750	200	-0.0163	0.0569	-0.0088	2.17			
Molten Salt, Mineral Oil,	1.1979	1.4782	-0.0958	650	10750	200	-0.0163	0.0569	-0.0088	2.17			
Diphenyl Based Oils	2.2628	0.8581	0.0003	650	10750	200	-0.0163	0.0569	-0.0088	2.17			
Packaged Steam Boilers	6.9617	-1.48	0.3161	1200	9400	40	2.5941	-4.2348	1.7224	2.2	1.000	0.00184	3.35E-06

Heat Exchanger Data

Exchanger Type	K ₁	K ₂	K ₃	C ₁	C ₂	C ₃	B ₁	B ₂	A _{min} (m2)	A _{max} (m2)	P _{max} (barg)
Double Pipe	3.3444	0.2745	-0.0472	13.1467	-12.6574	3.0705	1.74	1.55	1	10	300
40 barg < P < 100 barg				0.6072	-0.912	0.3327					
P < 40 barg				0	0	0					
Multiple Pipe	2.7652	0.7282	0.0783	13.1467	-12.6574	3.0705	1.74	1.55	10	100	300
40 barg < P < 100 barg				0.6072	-0.912	0.3327					
P < 40 barg				0	0	0					
Fixed tube, sheet, or U tut tubes only > 5 barg	4.3247	-0.303	0.1634	0.03881	-0.11272	0.08183	1.63	1.66	10.0	1000	140
Floating Head tubes only > 5barg	4.8306	-0.8509	0.3187	0.03881	-0.11272	0.08183	1.63	1.66	10.0	1000	140
Bayonet tubes only > 5 barg	4.2768	-0.0495	0.1431	0.03881	-0.11272	0.08183	1.63	1.66	10.0	1000	140
Kettle Reboiler tubes only > 5 barg	4.4646	-0.5277	0.3955	0.03881	-0.11272	0.08183	1.63	1.66	10.0	100	140
Scraped Wall 40 barg < P < 100 barg	3.7803	0.8569	0.0349	13.1467	-12.6574	3.0705	1.74	1.55	2.0	20	300
P < 40 barg				0.6072	-0.912	0.3327					
Teflon Tube	3.8062	0.8924	-0.1671	0	0	0	1.63	1.66	1.0	10	15
Air Cooler	4.0336	0.2341	0.0497	-0.125	0.15361	-0.02861	0.96	1.21	10	10000	100
Spiral Tube - shell and tub tube only	3.9912	0.0668	0.243	-0.4045	0.1859	0	1.74	1.55	1	100	400
Spiral Plate	4.6561	-0.2947	0.2207	0	0	0	0.96	1.21	1	100	19
Flat Plate	4.6656	-0.1557	0.1547	0	0	0	0.96	1.21	10	1000	19

Material Factors, F_M

Exchanger Type	Shell - CS	CS	Cu	CS	SS	CS	Ni	CS	Ti
	Tube - CS	Cu	Cu	SS	SS	Ni	Ni	Ti	Ti
Double Pipe	1.00	1.35	1.69	1.81	2.73	2.68	3.73	4.63	11.38
Multiple Pipe	1.00	1.35	1.69	1.81	2.73	2.68	3.73	4.63	11.38
Fixed tube, sheet, or U tut	1.00	1.35	1.69	1.81	2.73	2.68	3.73	4.63	11.38
Floating Head	1.00	1.35	1.69	1.81	2.73	2.68	3.73	4.63	11.38
Bayonet	1.00	1.35	1.69	1.81	2.73	2.68	3.73	4.63	11.38
Kettle Reboiler	1.00	1.35	1.69	1.81	2.73	2.68	3.73	4.63	11.38
Scraped Wall	1.00	1.35	1.69	1.81	2.73	2.68	3.73	4.63	11.38
Spiral Tube	1.00	1.35	1.69	1.81	2.73	2.68	3.73	4.63	11.38

Shell Material					
Type of Exchanger	CS	Cu	SS	Ni	Ti
Teflon Tube Exchanger	1.00	1.20	1.30	1.40	3.30

Material In Contact with Process Fluid					
Type of Exchanger	CS	Cu	SS	Ni	Ti
Spiral Plate	1.00	1.35	2.45	2.68	4.63
Flat Plate	1.00	1.35	2.45	2.68	4.63

Tube Material			
Type of Exchanger	CS	Al	SS
Air Cooler	1.00	1.42	2.93

Pump Data (including electric drives)

Pump Type	K ₁	K ₂	K ₃	C ₁	C ₂	C ₃	B ₁	B ₂	F _{m(C)}	F _{m(S)}	F _{m(Cu)}	F _{m(SS)}	F _{m(Ni)}	F _{m(Ti)}	P _{max(bar)}	W _{min(kW)}	W _{max(kW)}
Centrifugal pump	3.3892	0.0536	0.1538	-0.3935	0.3957	-0.00226	1.89	1.35	1.0	1.6	NA	2.3	4.4	NA	100	1	300
Positive Displacement	3.4771	0.1350	0.14380	-0.24538	0.259016	-0.01363	1.89	1.35	1.0	1.4	1.3	2.7	4.7	10.7	100	1	100
Reciprocating pump	3.8696	0.3161	0.12200	-0.2454	0.2590	-0.0136	1.89	1.35	1.0	1.5	1.3	2.4	4.0	6.4	100	0.1	200

Tank Data

Tank Type	K ₁	K ₂	K ₃	B ₁	B ₂	V _{min(m³/s)}	V _{max(m³/s)}
Fixed Roof	4.8509	-0.3973	0.1445	1.10	0	90	30000
Floating Roof	5.9567	-0.7585	0.1749	1.10	0.00	1000	40000

Turbine Data

Turbine Type	K ₁	K ₂	K ₃	F _{m(C)}	F _{m(S)}	F _{m(Cu)}	F _{m(SS)}	F _{m(Ni)}	F _{m(Ti)}	W _{min(kW)}	W _{max(kW)}
Axial	2.7051	1.4398	-0.1776	NA	3.5	NA	6.1	11.7	NA	100	4000
Radial	2.2476	1.4965	-0.1618	NA	3.5	NA	6.1	11.7	NA	100	1500

Vaporizer and Evaporator Data

Vaporizer Types	K ₁	K ₂	K ₃	A _{min(m²)}	A _{max(m²)}	P _{max(bar)}	C ₁	C ₂	C ₃
Forced Circulation	5.0238	0.3475	0.0703	5	1000	150	0.1578	-0.2992	0.1413
Falling Film	3.9119	0.8627	-0.0088	50	500	150	0.1578	-0.2992	0.1413
Agitated (Scraped Wall)	5	0.149	-0.0134	0.5	5	150	0.1578	-0.2992	0.1413
Short Tube	5.2366	-0.6572	0.35	10	100	150	0.1578	-0.2992	0.1413
Long Tube	4.642	0.3698	0.0025	100	10000	150	0.1578	-0.2992	0.1413

Vaporizer Types	K ₁	K ₂	K ₃	V _{min(m³)}	V _{max(m³)}	P _{max(bar)}	C ₁	C ₂	C ₃
Jacketed Vessel	3.8751	0.3328	0.1901	1	100	320	0.1578	-0.2992	0.1413
Internal Coil	4.038	0.09142	0.2766	1	100	320	0.1578	-0.2992	0.1413
Jacketed Vessel w/ Coil	4.038	0.09142	0.2766	1	100	320	0.1578	-0.2992	0.1413

Bare Module Factors, F_{EM}					
Evaporator Types	CS	Cu Alloy	SS	Ni Alloy	Ti
Forced Circulation	2.9	3.63	5.08	9.66	14.5
Falling Film	2.25	2.81	3.94	7.49	11.25
Agitated (Scraped Wall)	2.25	2.81	3.94	7.49	11.25
Short Tube	2.9	3.63	5.08	9.66	14.5
Long Tube	2.9	3.63	5.08	9.66	14.5

Bare Module Factors, F_{EM}										
Vaporizer Types	CS	Cu	SS Lined	SS Lined Ni	SS	SS Clad	Ni Alloy	Ni Alloy Clad	Ti	Ti Clad
Jacketed Vessel	2.7	3.4	4.7	4.9	4.8	3.8	9.1	5.9	13.7	9.5
Internal Coil	3.0	3.8	5.2	5.5	5.2	4.1	10.1	6.6	15.2	10.6
Jacketed Vessel w/ Coil	3.0	3.8	5.2	5.5	5.2	4.1	10.1	6.6	15.2	10.6

Vessel Data (including data for distillation towers and packed columns)

Vertical Vessels						Horizontal Vessels					
K ₁	K ₂	K ₃	V _{min}	V _{max}	P _{max(bar)}	K ₁	K ₂	K ₃	V _{min}	V _{max}	P _{max(bar)}
3.4974	0.4485	0.1074	0.3	520	3.5565	0.3776	0.0905	0.1	628	400	

Vessel B-Values

	B1	B2
Horizontal	1.49	1.52
Vertical	2.25	1.82

F_a

Tray Type	K ₁	K ₂	K ₃	A _{min(m²)}	A _{max(m²)}
Sieve	2.9949	0.4465	0.3961	0.07	12.3
Valve	3.3322	0.4838	0.3434	0.7	10.5
Demister	3.2353	0.4838	0.3434	0.7	10.5

Tower Packing

Materials of Construction	K ₁	K ₂	K ₃	V _{min(m³)}	V _{max(m³)}
Ceramic	3.0664	0.9744	0.0055	0.03	628
304 SS	3.2999	0.9744	0.0055	0.03	628
Plastic Saddle	2.4493	0.9744	0.0055	0.03	628

F_{EM}

MOC	Sieve	Valve	Demister
CS	1.0	1	
SS	1.8	1.83	1.0
Fluorocarbon			1.8
Ni-alloy	5.6	5.58	5.6

Materials of Construction

$F_{M,CS}$	1.0
$F_{M,SS clad}$	1.7
$F_{M,SS}$	3.1
$F_{M,Ni clad}$	3.6
$F_{M,Ni}$	7.1
$F_{M,Ti clad}$	4.7
$F_{M,Ti}$	9.4

Add Equipment

Unit Number 100

Edit Equipment

CEPCI 462.4

User Added Equipment

Compressor s	Compressor Type	Power (kilowatts)	# Spares	MOC	Purchased Equipment Cost	Bare Module Cost
C-101	Centrifugal	2190	2	Stainless Steel	\$ 1,700,000	\$ 9,780,000
C-102	Centrifugal	2080	2	Stainless Steel	\$ 1,640,000	\$ 9,440,000
C-103	Centrifugal	2960	1	Stainless Steel	\$ 1,380,000	\$ 7,960,000
C-104	Centrifugal	2700	1	Stainless Steel	\$ 1,300,000	\$ 7,500,000

Exchangers	Type of Exchanger	Shell Pressure (barg)	Tube Pressure (barg)	MOC	Area (square meters)	Purchased Equipment Cost	Bare Module Cost
E-101	Fixed, Sheet, or U-Tube	1	10.1	Stainless Steel / Carbon Steel	3200	\$ 309,000	\$ 1,440,000
E-102	Fixed, Sheet, or U-Tube	1	16.4	Stainless Steel / Stainless Steel	960	\$ 87,200	\$ 546,000
E-103	Fixed, Sheet, or U-Tube	1	26.4	Stainless Steel / Carbon Steel	378	\$ 49,600	\$ 235,000
E-104	Fixed, Sheet, or U-Tube	1	42.7	Stainless Steel / Carbon Steel	373	\$ 49,200	\$ 236,000

User Added Equipment	Description	BMF ₀	Actual BMF	Purchased Equipment Cost	Bare Module Cost
Z-101	Pipeline installed	1	1	\$ 20,000,000	\$ 20,000,000
Z-102	well cost	1	1	\$ 3,000,000	\$ 3,000,000

Name	Total Module Cost	Grass Roots Cost	Utility Used	Efficiency	Actual Usage	Annual Utility Cost
C-101	\$ 13,400,000	\$ 16,200,000	NA			
C-102	\$ 13,000,000	\$ 15,600,000	NA			
C-103	\$ 10,940,000	\$ 13,100,000	NA			
C-104	\$ 10,310,000	\$ 12,400,000	NA			
E-101	\$ 1,984,000	\$ 2,580,000	Cooling Water		93300 MJ/h	\$ 290,000
E-102	\$ 749,806	\$ 917,000	Cooling Water		32200 MJ/h	\$ 100,000
E-103	\$ 323,000	\$ 418,000	Cooling Water		28500 MJ/h	\$ 88,000
E-104	\$ 324,000	\$ 418,000	Cooling Water		30600 MJ/h	\$ 95,000
Z-101	\$ 20,000,000	\$ 20,000,000	Unspecified			
Z-102	\$ 4,120,000	\$ 5,870,000	Unspecified			
Totals	\$ 75,200,000	\$ 87,500,000				\$ 573,000

Add Materials

<u>Material</u>	<u>Classification</u>	<u>Price (\$/kwh \$/ton)</u>	<u>Consumption (kW ton/h)</u>	<u>Material Costs (\$/y)</u>
Carbon Dioxide Credits	Product	\$ 5.000	589.28	\$ 25,810,464
Electrical consumption	Raw Material	\$ 0.030	24725.965	\$ 6,497,984
Price hike	Product	\$ 0.00228	500000	\$ 9,986,400

- 1 Chemical Marketing Reporter for black iron oxide, synthetic, baged, truck loaded, free on board, warehouse value
- 2 based on values for fillers for rubber, plastic etc.
- 3 Based on 1998 value from Chem marketing reporter - freight equalized

Economic Options

Cost of Land \$	1,000,000
Taxation Rate	42%
Annual Interest Rate	6.50%
Salvage Value \$	8,750,000
Working Capital \$	9,469,798
FCI _L \$	87,500,000
Total Module Factor	1.18
Grass Roots Factor	0.50

Economic Information Calculated From Given Information

Revenue From Sales \$	35,796,864
C _{RM} (Raw Materials Costs) \$	6,497,984
C _{UT} (Cost of Utilities) \$	573,000
C _{WT} (Waste Treatment Costs) \$	-
C _{OL} (Cost of Operating Labor) \$	700,000

Factors Used in Calculation of Cost of Manufacturing (COM)

$$Comd = 0.18*FCIL + 2.76*COL + 1.1*(CUT + CWT + CRM)$$

Multiplying factor for FCIL	0.18
Multiplying factor for C _{OL}	2.76
Facotrs for C _{UT} , C _{WT} , and C _{RM}	1.1
COM _d \$	25,460,082

Factors Used in Calculation of Working Capital

$$Working\ Capital = A*C_{RM} + B*FCI_L + C*C_{OL}$$

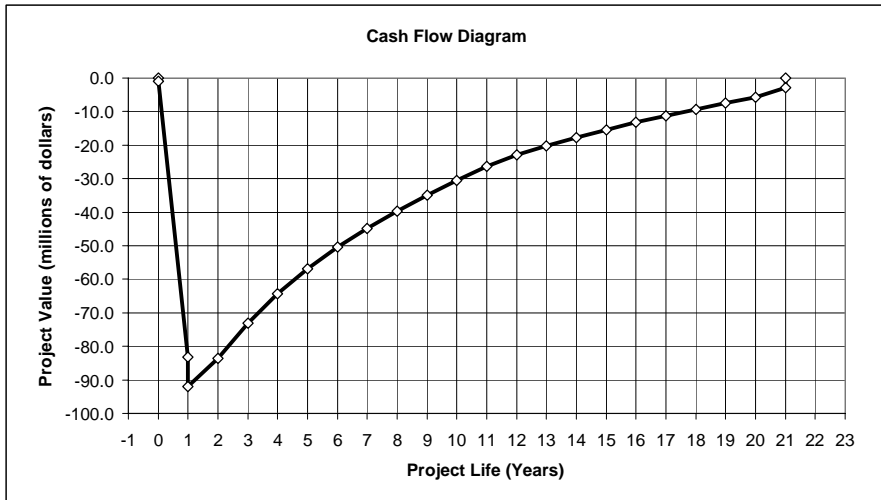
A	0.10
B	0.10
C	0.10

Project Life (Years after Startup)	20
------------------------------------	----

Construction period	1
---------------------	---

Distribution of Fixed Capital Investment (must sum to one)

End of year One	100%
End of year Two	
End of year Three	
End of year Four	
End of year Five	



Generate CFD

Discounted Profitability Criterion

Net Present Value (millions)	(0.02)
Discounted Cash Flow Rate of Return	6.30%
Discounted Payback Period (years)	17.3

Non-Discounted Profitability Criteria

Cumulative Cash Position (millions)	74.23
Rate of Return on Investment	4.24%
Payback Period (years)	9.2

Year	Investment	d_k	$FCI_t - Sd_k$	R	COM_d	$(R - COM_d - d_k) * (1-t) + d_k$	Cash Flow (Non-discounted)	Cash Flow (discounted)	Cumulative Cash Flow (discounted)	Cumulative Cash Flow (Non-discounted)
0	0.00		87.50				0.00	0.00	0.00	0.00
0	1.00		87.50				(1.00)	(1.00)	(1.00)	(1.00)
1	87.50		87.50				(87.50)	(82.16)	(83.16)	(88.50)
1	9.47		87.50				(9.47)	(8.89)	(92.05)	(97.97)
2		8.75	78.75	35.80	25.46	9.67	9.67	8.53	(83.53)	(88.30)
3		15.75	63.00	35.80	25.46	12.61	12.61	10.44	(73.09)	(75.69)
4		12.60	50.40	35.80	25.46	11.29	11.29	8.77	(64.31)	(64.40)
5		10.06	40.34	35.80	25.46	10.22	10.22	7.46	(56.85)	(54.18)
6		8.05	32.29	35.80	25.46	9.38	9.38	6.43	(50.43)	(44.80)
7		6.48	25.81	35.80	25.46	8.71	8.71	5.61	(44.82)	(36.09)
8		5.78	20.04	35.80	25.46	8.42	8.42	5.09	(39.73)	(27.67)
9		5.78	14.26	35.80	25.46	8.42	8.42	4.78	(34.95)	(19.25)
10		5.69	8.58	35.80	25.46	8.38	8.38	4.47	(30.49)	(10.86)
11		5.69	2.89	35.80	25.46	8.38	8.38	4.19	(26.29)	(2.48)
12		2.89	-	35.80	25.46	7.21	7.21	3.39	(22.91)	4.73
13		-	-	35.80	25.46	6.00	6.00	2.64	(20.26)	10.72
14		-	-	35.80	25.46	6.00	6.00	2.48	(17.78)	16.72
15		-	-	35.80	25.46	6.00	6.00	2.33	(15.45)	22.71
16		-	-	35.80	25.46	6.00	6.00	2.19	(13.26)	28.71
17		-	-	35.80	25.46	6.00	6.00	2.06	(11.20)	34.71
18		-	-	35.80	25.46	6.00	6.00	1.93	(9.27)	40.70
19		-	-	35.80	25.46	6.00	6.00	1.81	(7.46)	46.70
20		-	-	35.80	25.46	6.00	6.00	1.70	(5.76)	52.69
21		-	-	35.80	25.46	11.07	11.07	2.95	(2.81)	63.76
21		-	-	-	-	-	10.47	2.79	(0.02)	74.23

Probable Variation of Key Parameters over Plant Life

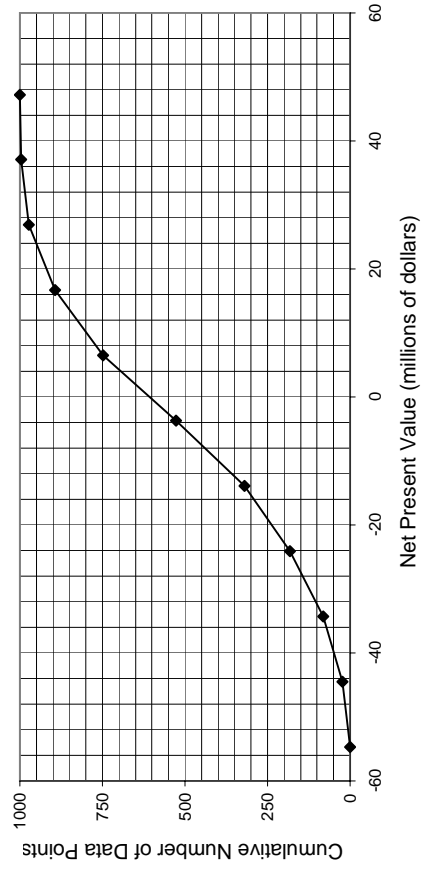
	<u>Lower Limit</u>	<u>Upper Limit</u>	<u>Base Value</u>
FCIL	-20%	30%	\$ 87,500,000
Price of Product	-10%	10%	\$ 35,796,864
Working Capital	-50%	10%	\$ 9,469,798
Income Tax Rate*	-20%	20%	42%
Interest Rate*	-10%	20%	6%
Raw Material Price	-10%	15%	\$ 6,497,984
Salvage Value	-80%	20%	\$ 8,750,000

* Please note that variations for percentages are a percent of a percent.
For example, a 10% variance on a 12% interest rate would imply a 1.2% uncertainty

Run Economic Analysis

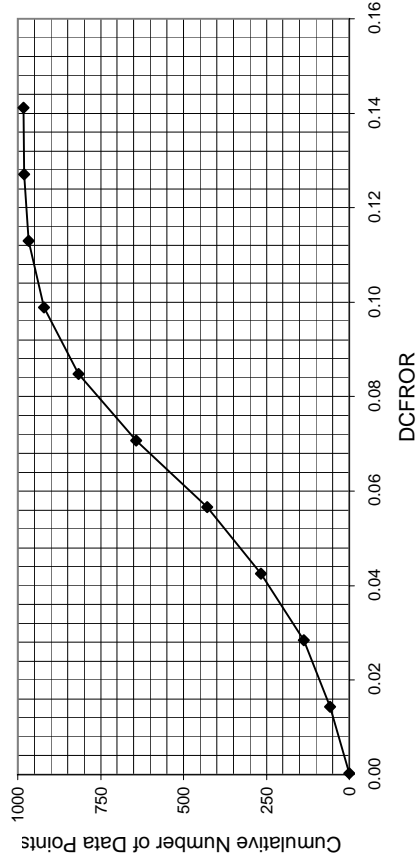
Net Present Value Data

Low NPV	-54.7		
High NPV	47.2		
<u>Bins</u>	<u>Upper Value</u>	<u># points/bin</u>	<u>Cumulative</u>
0	-54.7	0	0
1	-44.5	23	23
2	-34.3	59	82
3	-24.1	101	183
4	-13.9	136	319
5	-3.7	208	527
6	6.5	221	748
7	16.7	146	894
8	26.9	79	973
9	37.1	24	997
10	47.2	3	1000



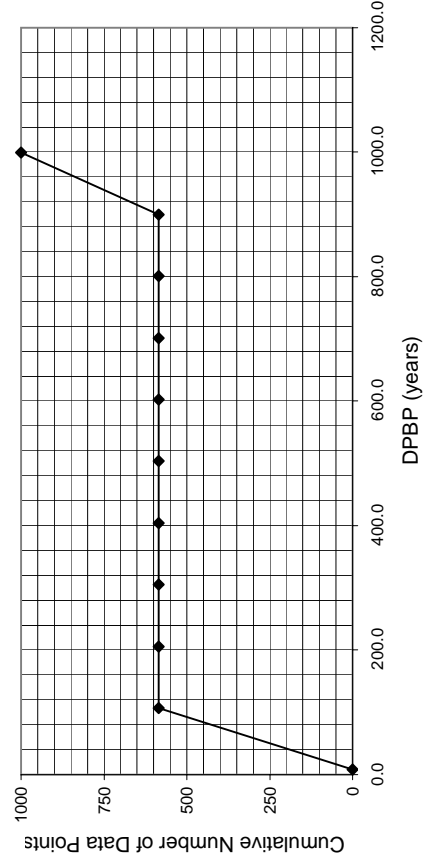
Discounted Cash Flow Rate of Return Data

Low DCFROR	0.00	Upper	#/bin	Cumulative
High DCFROR	0.14	0.00	0	0
Bins		0.01	58	58
		0.03	80	138
		0.04	128	266
		0.06	163	429
		0.07	214	643
		0.08	173	816
		0.10	105	921
		0.11	46	967
		0.13	13	980
		0.14	2	982



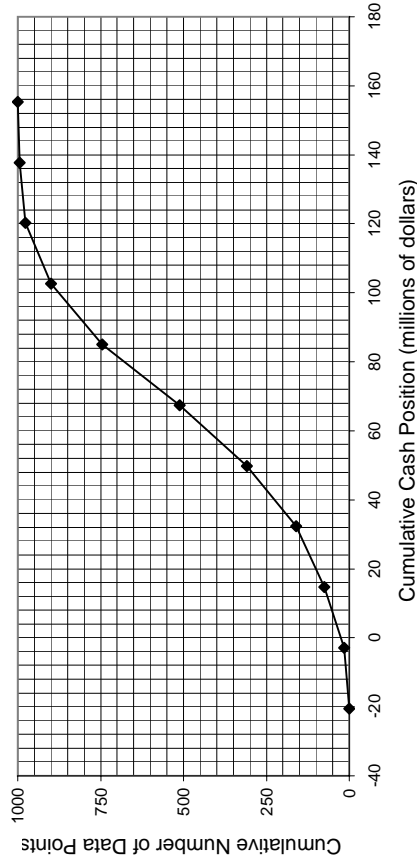
Discounted Payback Period Data

Low DPBP	7.9	Upper	#/bin	Cumulative
High DPBP	999.0	7.9	0	0
Bins		107.0	584	584
		206.1	0	584
		305.2	0	584
		404.3	0	584
		503.4	0	584
		602.6	0	584
		701.7	0	584
		800.8	0	584
		899.9	0	584
		999.0	416	1000



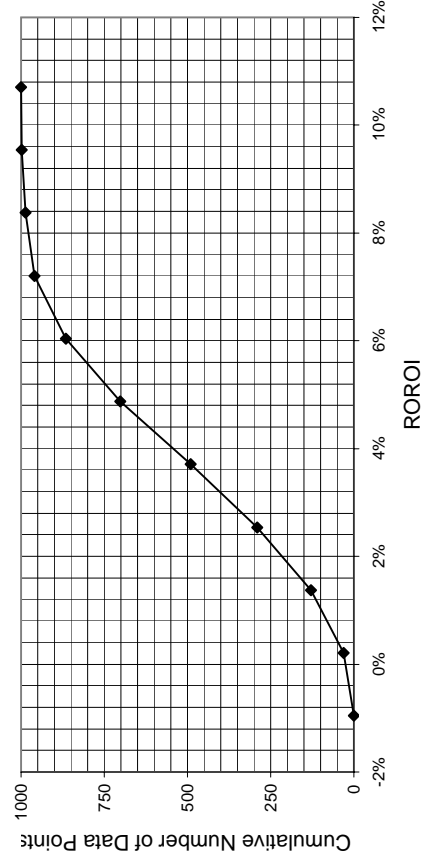
Cumulative Cash Position Data

Low CCP	-20.46		
High CCP	155.36		
<u>Bins</u>	<u>Upper Value</u>	<u># points/bin</u>	<u>Cumulative</u>
0	-20.46	0	0
1	-2.88	15	15
2	14.70	60	75
3	32.28	85	160
4	49.87	148	308
5	67.45	204	512
6	85.03	234	746
7	102.61	153	899
8	120.19	78	977
9	137.77	18	995
10	155.36	5	1000



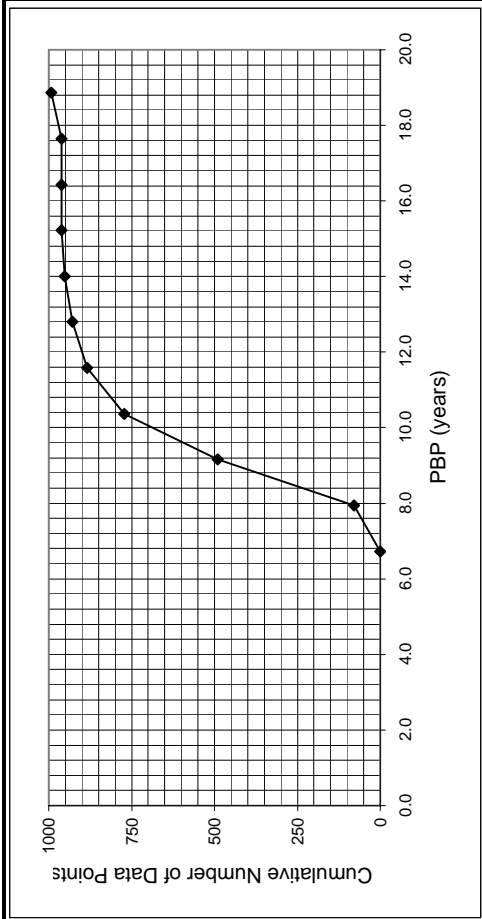
Rate of Return on Investment Data

Low RORO	-1%		
High RORO	11%		
<u>Bins</u>	<u>Upper Value</u>	<u># points/bin</u>	<u>Cumulative</u>
0	-1%	0	0
1	0%	31	31
2	1%	98	129
3	3%	161	290
4	4%	201	491
5	5%	211	702
6	6%	163	865
7	7%	94	959
8	8%	27	986
9	10%	12	998
10	11%	2	1000



Payback Period Data

Low DPBP	6.7	Upper	#/bin	Cumulative
High DPBP	18.9	6.7	0	0
Bins	0	7.9	80	80
	1	9.2	410	490
	2	10.4	282	772
	3	11.6	113	885
	4	12.8	43	928
	5	14.0	24	952
	6	15.2	9	961
	7	16.4	0	961
	8	17.6	0	961
	9	18.9	32	993
	10			



Hours per Operating Year	8760
---------------------------------	------

	<u>Cost (\$/GJ)</u>
Common Utilities	
Electricity (110V - 440V)	16.8
Cooling Water (30°C to 45°C)	0.354
Refrigerated Water (15°C to 25°C)	4.43
Steam from Boilers	
Low Pressure (5 barg, 160°C)	6.08
Medium Pressure (10 barg, 184°C)	6.87
High Pressure (41 barg, 254°C)	9.83
Fuels	
Fuel Oil (no. 2)	6.0
Natural Gas	6
Coal (FOB mine mouth)	1.07
Thermal Systems	
Moderately High (up to 330°C)	6.67
High (up to 400°C)	7
Very High (up to 600°C)	7.5
Refrigeration	
Moderately Low (5°C)	4.43
Low (-20°C)	7.89
Very low (-50°C)	13.11
Waste Disposal (solid and liquid)	
<u>Cost (\$/tonne)</u>	
Non-Hazardous	36
Hazardous	200

Cost of Steam used in Steam Drives	
	<u>Cost (\$/GJ)</u>
Steam used for steam-powered drives \$	9.83

Equipment Efficiencies	
Pump Efficiency	85%
Drive Efficiency	90%
Fan Efficiency	80%
Furnace Efficiency	90%
Turbine Efficiency	85%

Process Equipment	
Operators per shift per equipment	
Cost of Labor (per operator/year) \$	50,000

Update Preferences

Power Preference
kilowatts

Pressure Preference
barg

Heat Duty Preference
MJ/h

Length Preference
meters

Area Preference
square meters

Volume Preference
cubic meters

Gas Flow Preference
cubic meters/s

Cost Preference
\$/kg

Flowrate Preference
kg/h

Energy Price Preference
\$/Gigajoule

Compressor Data (without electric motors)

Compressor Type	K ₁	K ₂	K ₃	F _{BMCS}	F _{BMSS}	F _{BMNS}	W _{min} (kW)	W _{max} (kW)
Centrifugal	2.2891	1.3604	-0.1027	2.7	5.8	11.5	450	3000
Axial	2.2891	1.3604	-0.1027	3.8	8.0	15.9	450	3000
Rotary	5.0355	-1.8002	0.8253	2.4	5.0	9.9	18	950
Reciprocating	2.2891	1.3604	-0.1027	3.4	7.0	13.9	450	3000

Drive Data

Electric Drives	K ₁	K ₂	K ₃	F _{BM}	W _{min} (kW)	W _{max} (kW)
Explosion Proof	2.4604	1.4191	-0.1798	1.5	75	2600
Totally Enclosed	1.956	1.7142	-0.2282	1.5	75	2600
Open/Drip Proof	2.9508	1.0688	-0.1315	1.5	75	2600

Non-Electric Drives	K ₁	K ₂	K ₃	F _{BM}	W _{min} (kW)	W _{max} (kW)
Gas Turbine	-21.7702	13.2175	-1.5279	3.5	7500	23000
Steam Turbine	2.6259	1.4398	-0.1776	3.5	70	7500
Internal Combustion	2.7635	0.8574	-0.0098	2.0	10	10000

Fan Data (include electric motors)

Fan Type	K ₁	K ₂	K ₃	F _{BMCS}	F _{BM fiberglass}	F _{BMSS}	F _{BMNS}	Threshold	C ₁	C ₂	C ₃	V _{min} (m3/s)	V _{max} (m3/s)	P _{max} (barg)
Centrifugal Radial Fan	3.5391	-0.3533	0.4477	2.7	5.0	5.8	11.5	0.01	0.00	0.209	-0.033	1	100	0.16
Centrifugal Backward curv	3.3471	-0.0734	0.3090	2.7	5.0	5.8	11.5	0.01	0.00	0.209	-0.033	1	100	0.16
Axial Tube Fan	3.0414	-0.3375	0.4722	2.7	5.0	5.8	11.5	0.04	0.00	0.209	-0.033	1	100	0.16
Axial Vane Fan	3.1761	-0.1373	0.3414	2.7	5.0	5.8	11.5	0.04	0.00	0.209	-0.033	1	100	0.16

Fired Heater Data

Reactive Heaters	K ₁	K ₂	K ₃	Q _{min} (kW)	Q _{max} (kW)	P _{max} (barg)	C ₁	C ₂	C ₃	Bare Module Factor		
										CS	Alloy Steel	SS
Reformer Furnace	3.068	0.6597	0.0194	3000	100000	200	0.1405	-0.2698	0.1293	2.13	2.51	2.81
Pyrolysis Furnace	2.3859	0.9721	-0.0206	3000	100000	200	0.1017	-0.1957	0.09403	2.13	2.51	2.81

Non-reactive Heaters	K ₁	K ₂	K ₃	Q _{min} (kW)	Q _{max} (kW)	P _{max} (barg)	C ₁	C ₂	C ₃	Bare Module Factor		
										CS	Alloy Steel	SS
Process Heater	7.3488	-1.1666	0.2028	1000	100000	200	0.1347	-0.2368	0.1021	2.13	2.51	2.81

Thermal Fluid Heaters	K ₁	K ₂	K ₃	Q _{min} (kW)	Q _{max} (kW)	P _{max} (barg)	C ₁	C ₂	C ₃	F _{bm}	Steam Superheat Factor		
											F _{T1}	F _{T2}	F _{T3}
Hot Water	2.0829	0.9074	-0.0243	650	10750	200	-0.0163	0.0569	-0.0088	2.17			
Molten Salt, Mineral Oil,	1.1979	1.4782	-0.0958	650	10750	200	-0.0163	0.0569	-0.0088	2.17			
Diphenyl Based Oils	2.2628	0.8581	0.0003	650	10750	200	-0.0163	0.0569	-0.0088	2.17			
Packaged Steam Boilers	6.9617	-1.48	0.3161	1200	9400	40	2.5941	-4.2348	1.7224	2.2	1.000	0.00184	3.35E-06

Heat Exchanger Data

Exchanger Type	K ₁	K ₂	K ₃	C ₁	C ₂	C ₃	B ₁	B ₂	A _{min} (m2)	A _{max} (m2)	P _{max} (barg)
Double Pipe	3.3444	0.2745	-0.0472	13.1467	-12.6574	3.0705	1.74	1.55	1	10	300
40 barg < P < 100 barg				0.6072	-0.912	0.3327					
P < 40 barg				0	0	0					
Multiple Pipe	2.7652	0.7282	0.0783	13.1467	-12.6574	3.0705	1.74	1.55	10	100	300
40 barg < P < 100 barg				0.6072	-0.912	0.3327					
P < 40 barg				0	0	0					
Fixed tube, sheet, or U tube only > 5 barg	4.3247	-0.303	0.1634	0.03881	-0.11272	0.08183	1.63	1.66	10.0	1000	140
Floating Head tubes only > 5 barg	4.8306	-0.8509	0.3187	0.03881	-0.11272	0.08183	1.63	1.66	10.0	1000	140
Bayonet tubes only > 5 barg	4.2768	-0.0495	0.1431	0.03881	-0.11272	0.08183	1.63	1.66	10.0	1000	140
Kettle Reboiler tubes only > 5 barg	4.4646	-0.5277	0.3955	0.03881	-0.11272	0.08183	1.63	1.66	10.0	100	140
Scraped Wall 40 barg < P < 100 barg	3.7803	0.8569	0.0349	13.1467	-12.6574	3.0705	1.74	1.55	2.0	20	300
P < 40 barg				0.6072	-0.912	0.3327					
Teflon Tube	3.8062	0.8924	-0.1671	0	0	0	1.63	1.66	1.0	10	15
Air Cooler	4.0336	0.2341	0.0497	-0.125	0.15361	-0.02861	0.96	1.21	10	10000	100
Spiral Tube - shell and tube only	3.9912	0.0668	0.243	-0.4045	0.1859	0	1.74	1.55	1	100	400
Spiral Plate	4.6561	-0.2947	0.2207	0	0	0	0.96	1.21	1	100	19
Flat Plate	4.6656	-0.1557	0.1547	0	0	0	0.96	1.21	10	1000	19

Material Factors, F_M

Exchanger Type	Shell - CS	CS	Cu	CS	SS	CS	Ni	CS	Ti
	Tube - CS	Cu	Cu	SS	SS	Ni	Ni	Ti	Ti
Double Pipe	1.00	1.35	1.69	1.81	2.73	2.68	3.73	4.63	11.38
Multiple Pipe	1.00	1.35	1.69	1.81	2.73	2.68	3.73	4.63	11.38
Fixed tube, sheet, or U tut	1.00	1.35	1.69	1.81	2.73	2.68	3.73	4.63	11.38
Floating Head	1.00	1.35	1.69	1.81	2.73	2.68	3.73	4.63	11.38
Bayonet	1.00	1.35	1.69	1.81	2.73	2.68	3.73	4.63	11.38
Kettle Reboiler	1.00	1.35	1.69	1.81	2.73	2.68	3.73	4.63	11.38
Scraped Wall	1.00	1.35	1.69	1.81	2.73	2.68	3.73	4.63	11.38
Spiral Tube	1.00	1.35	1.69	1.81	2.73	2.68	3.73	4.63	11.38

Shell Material					
Type of Exchanger	CS	Cu	SS	Ni	Ti
Teflon Tube Exchanger	1.00	1.20	1.30	1.40	3.30

Material In Contact with Process Fluid					
Type of Exchanger	CS	Cu	SS	Ni	Ti
Spiral Plate	1.00	1.35	2.45	2.68	4.63
Flat Plate	1.00	1.35	2.45	2.68	4.63

Tube Material			
Type of Exchanger	CS	Al	SS
Air Cooler	1.00	1.42	2.93

Pump Data (including electric drives)

Pump Type	K ₁	K ₂	K ₃	C ₁	C ₂	C ₃	B ₁	B ₂	F _{m(C)}	F _{m(S)}	F _{m(Cu)}	F _{m(SS)}	F _{m(Ni)}	F _{m(Ti)}	P _{max(bar)}	W _{min(kW)}	W _{max(kW)}
Centrifugal pump	3.3892	0.0536	0.1538	-0.3935	0.3957	-0.00226	1.89	1.35	1.0	1.6	NA	2.3	4.4	NA	100	1	300
Positive Displacement	3.4771	0.1350	0.14380	-0.24538	0.259016	-0.01363	1.89	1.35	1.0	1.4	1.3	2.7	4.7	10.7	100	1	100
Reciprocating pump	3.8696	0.3161	0.12200	-0.2454	0.2590	-0.0136	1.89	1.35	1.0	1.5	1.3	2.4	4.0	6.4	100	0.1	200

Tank Data

Tank Type	K ₁	K ₂	K ₃	B ₁	B ₂	V _{min(m³/s)}	V _{max(m³/s)}
Fixed Roof	4.8509	-0.3973	0.1445	1.10	0	90	30000
Floating Roof	5.9567	-0.7585	0.1749	1.10	0.00	1000	40000

Turbine Data

Turbine Type	K ₁	K ₂	K ₃	F _{m(C)}	F _{m(S)}	F _{m(Cu)}	F _{m(SS)}	F _{m(Ni)}	F _{m(Ti)}	W _{min(kW)}	W _{max(kW)}
Axial	2.7051	1.4398	-0.1776	NA	3.5	NA	6.1	11.7	NA	100	4000
Radial	2.2476	1.4965	-0.1618	NA	3.5	NA	6.1	11.7	NA	100	1500

Vaporizer and Evaporator Data

Vaporizer Types	K ₁	K ₂	K ₃	A _{min(m²)}	A _{max(m²)}	P _{max(bar)}	C ₁	C ₂	C ₃
Forced Circulation	5.0238	0.3475	0.0703	5	1000	150	0.1578	-0.2992	0.1413
Falling Film	3.9119	0.8627	-0.0088	50	500	150	0.1578	-0.2992	0.1413
Agitated (Scraped Wall)	5	0.149	-0.0134	0.5	5	150	0.1578	-0.2992	0.1413
Short Tube	5.2366	-0.6572	0.35	10	100	150	0.1578	-0.2992	0.1413
Long Tube	4.642	0.3698	0.0025	100	10000	150	0.1578	-0.2992	0.1413

Vaporizer Types	K ₁	K ₂	K ₃	V _{min(m³)}	V _{max(m³)}	P _{max(bar)}	C ₁	C ₂	C ₃
Jacketed Vessel	3.8751	0.3328	0.1901	1	100	320	0.1578	-0.2992	0.1413
Internal Coil	4.038	0.09142	0.2766	1	100	320	0.1578	-0.2992	0.1413
Jacketed Vessel w/ Coil	4.038	0.09142	0.2766	1	100	320	0.1578	-0.2992	0.1413

Bare Module Factors, F_{BM}					
Vaporizer Types	CS	Cu Alloy	SS	Ni Alloy	Ti
Forced Circulation	2.9	3.63	5.08	9.66	14.5
Falling Film	2.25	2.81	3.94	7.49	11.25
Agitated (Scraped Wall)	2.25	2.81	3.94	7.49	11.25
Short Tube	2.9	3.63	5.08	9.66	14.5
Long Tube	2.9	3.63	5.08	9.66	14.5

Bare Module Factors, F_{BM}										
Vaporizer Types	CS	Cu	SS Lined	SS Lined Ni	SS	SS Clad	Ni Alloy	Ni Alloy Clad	Ti	Ti Clad
Jacketed Vessel	2.7	3.4	4.7	4.9	4.8	3.8	9.1	5.9	13.7	9.5
Internal Coil	3.0	3.8	5.2	5.5	5.2	4.1	10.1	6.6	15.2	10.6
Jacketed Vessel w/ Coil	3.0	3.8	5.2	5.5	5.2	4.1	10.1	6.6	15.2	10.6

Vessel Data (including data for distillation towers and packed columns)

Vertical Vessels						Horizontal Vessels					
K ₁	K ₂	K ₃	V _{min}	V _{max}	P _{max(bar)}	K ₁	K ₂	K ₃	V _{min}	V _{max}	P _{max(bar)}
3.4974	0.4485	0.1074	0.3	520	3.5565	0.3776	0.0905	0.1	628	400	

Vessel B-Values

	B1	B2
Horizontal	1.49	1.52
Vertical	2.25	1.82

F_a

Tray Type	K ₁	K ₂	K ₃	A _{min(m²)}	A _{max(m²)}
Sieve	2.9949	0.4465	0.3961	0.07	12.3
Valve	3.3322	0.4838	0.3434	0.7	10.5
Demister	3.2353	0.4838	0.3434	0.7	10.5

Tower Packing

Materials of Construction	K ₁	K ₂	K ₃	V _{min(m³)}	V _{max(m³)}
Ceramic	3.0664	0.9744	0.0055	0.03	628
304 SS	3.2999	0.9744	0.0055	0.03	628
Plastic Saddle	2.4493	0.9744	0.0055	0.03	628

F_{BM}

MOC	Sieve	Valve	Demister
CS	1.0	1	
SS	1.8	1.83	1.0
Fluorocarbon			1.8
Ni-alloy	5.6	5.58	5.6

Materials of Construction

$F_{M,CS}$	1.0
$F_{M,SS\ clad}$	1.7
$F_{M,SS}$	3.1
$F_{M,Ni\ clad}$	3.6
$F_{M,Ni}$	7.1
$F_{M,Ti\ clad}$	4.7
$F_{M,Ti}$	9.4

Add Equipment

Unit Number 100

Edit Equipment

CEPCI 462.4

User Added Equipment

Compressors	Compressor Type	Power (kilowatts)	# Spares	MOC	Purchased Equipment Cost	Bare Module Cost
C-101	Centrifugal	2190	2	Stainless Steel	\$ 1,700,000	\$ 9,780,000
C-102	Centrifugal	2080	2	Stainless Steel	\$ 1,640,000	\$ 9,440,000
C-103	Centrifugal	2960	1	Stainless Steel	\$ 1,380,000	\$ 7,960,000
C-104	Centrifugal	2700	1	Stainless Steel	\$ 1,300,000	\$ 7,500,000

Exchangers	Type of Exchanger	Shell Pressure (barg)	Tube Pressure (barg)	MOC	Area (square meters)	Purchased Equipment Cost	Bare Module Cost
E-101	Fixed, Sheet, or U-Tube	1	10.1	Stainless Steel / Carbon Steel	3200	\$ 309,000	\$ 1,440,000
E-102	Fixed, Sheet, or U-Tube	1	16.3	Stainless Steel / Stainless Steel	960	\$ 87,200	\$ 545,000
E-103	Fixed, Sheet, or U-Tube	1	26.4	Stainless Steel / Carbon Steel	378	\$ 49,600	\$ 235,000
E-104	Fixed, Sheet, or U-Tube	1	42.7	Stainless Steel / Carbon Steel	373	\$ 49,200	\$ 236,000

User Added Equipment	Description	BMF ₀	Actual BMF	Purchased Equipment Cost	Bare Module Cost
Z-101	Pipeline installed	1	1	\$ 20,000,000	\$ 20,000,000
Z-102	well cost	1	1	\$ 3,000,000	\$ 3,000,000

Name	Total Module Cost	Grass Roots Cost	Utility Used	Efficiency	Actual Usage	Annual Utility Cost
C-101	\$ 13,400,000	\$ 16,200,000	NA			
C-102	\$ 13,000,000	\$ 15,600,000	NA			
C-103	\$ 10,940,000	\$ 13,100,000	NA			
C-104	\$ 10,310,000	\$ 12,400,000	NA			
E-101	\$ 1,984,000	\$ 2,580,000	Cooling Water		93300 MJ/h	\$ 290,000
E-102	\$ 749,726	\$ 917,000	Cooling Water		32200 MJ/h	\$ 100,000
E-103	\$ 323,000	\$ 418,000	Cooling Water		28500 MJ/h	\$ 88,000
E-104	\$ 324,000	\$ 418,000	Cooling Water		30600 MJ/h	\$ 95,000
Z-101	\$ 20,000,000	\$ 20,000,000	Unspecified			
Z-102	\$ 4,120,000	\$ 5,870,000	Unspecified			
Totals	\$ 75,200,000	\$ 87,500,000				\$ 573,000

Add Materials

<u>Material</u>	<u>Classification</u>	<u>Price (\$/kwh \$/ton)</u>	<u>Consumption (kW ton/h)</u>	<u>Material Costs (\$/y)</u>
Carbon Dioxide Credits	Product	\$ 5.000	589.28	\$ 25,810,464
Electrical consumption	Raw Material	\$ 0.025	23724.9677	\$ 5,195,768
Price hike	Product	\$ 0.00205	476275.0323	\$ 8,544,603

- 1 Chemical Marketing Reporter for black iron oxide, synthetic, baged, truck loaded, free on board, warehouse value
- 2 based on values for fillers for rubber, plastic etc.
- 3 Based on 1998 value from Chem marketing reporter - freight equalized

Economic Options

Cost of Land \$	1,000,000
Taxation Rate	42%
Annual Interest Rate	6.50%
Salvage Value \$	8,750,000
Working Capital \$	9,339,577
FCI _L \$	87,500,000
Total Module Factor	1.18
Grass Roots Factor	0.50

Economic Information Calculated From Given Information

Revenue From Sales \$	34,355,067
C _{RM} (Raw Materials Costs) \$	5,195,768
C _{UT} (Cost of Utilities) \$	573,000
C _{WT} (Waste Treatment Costs) \$	-
C _{OL} (Cost of Operating Labor) \$	700,000

Factors Used in Calculation of Cost of Manufacturing (COM)

$$Comd = 0.18*FCIL + 2.76*COL + 1.1*(CUT + CWT + CRM)$$

Multiplying factor for FCIL	0.18
Multiplying factor for C _{OL}	2.76
Facotrs for C _{UT} , C _{WT} , and C _{RM}	1.1
COM _d \$	24,027,645

Factors Used in Calculation of Working Capital

$$Working\ Capital = A*C_{RM} + B*FCI_L + C*C_{OL}$$

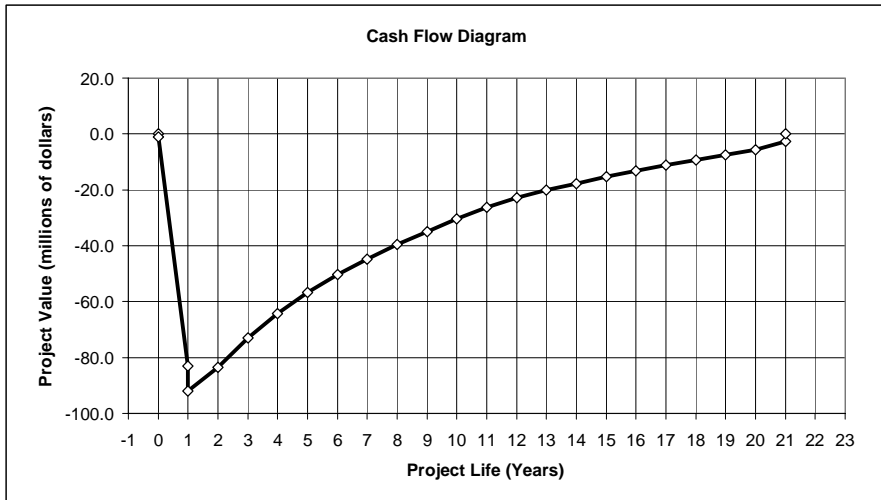
A	0.10
B	0.10
C	0.10

Project Life (Years after Startup)	20
------------------------------------	----

Construction period	1
---------------------	---

Distribution of Fixed Capital Investment (must sum to one)

End of year One	100%
End of year Two	
End of year Three	
End of year Four	
End of year Five	



Generate CFD

Discounted Profitability Criterion

Net Present Value (millions)	0.01
Discounted Cash Flow Rate of Return	6.50%
Discounted Payback Period (years)	16.7

Non-Discounted Profitability Criteria

Cumulative Cash Position (millions)	74.12
Rate of Return on Investment	4.24%
Payback Period (years)	9.1

Year	Investment	d_k	$FCI_t - Sd_k$	R	COM_d	$(R - COM_d - d_k) * (1-t) + d_k$	Cash Flow (Non-discounted)	Cash Flow (discounted)	Cumulative Cash Flow (discounted)	Cumulative Cash Flow (Non-discounted)
0	0.00		87.50				0.00	0.00	0.00	0.00
0	1.00		87.50				(1.00)	(1.00)	(1.00)	(1.00)
1	87.50		87.50				(87.50)	(82.16)	(83.16)	(88.50)
1	9.34		87.50				(9.34)	(8.77)	(91.93)	(97.84)
2		8.75	78.75	34.36	24.03	9.66	9.66	8.52	(83.41)	(88.17)
3		15.75	63.00	34.36	24.03	12.60	12.60	10.43	(72.97)	(75.57)
4		12.60	50.40	34.36	24.03	11.28	11.28	8.77	(64.20)	(64.29)
5		10.06	40.34	34.36	24.03	10.22	10.22	7.46	(56.75)	(64.07)
6		8.05	32.29	34.36	24.03	9.37	9.37	6.42	(50.32)	(44.70)
7		6.48	25.81	34.36	24.03	8.71	8.71	5.60	(44.72)	(35.99)
8		5.78	20.04	34.36	24.03	8.42	8.42	5.08	(39.64)	(27.58)
9		5.78	14.26	34.36	24.03	8.42	8.42	4.77	(34.86)	(19.16)
10		5.69	8.58	34.36	24.03	8.38	8.38	4.46	(30.40)	(10.78)
11		5.69	2.89	34.36	24.03	8.38	8.38	4.19	(26.21)	(2.40)
12		2.89	-	34.36	24.03	7.20	7.20	3.38	(22.82)	4.80
13		-	-	34.36	24.03	5.99	5.99	2.64	(20.18)	10.79
14		-	-	34.36	24.03	5.99	5.99	2.48	(17.70)	16.78
15		-	-	34.36	24.03	5.99	5.99	2.33	(15.37)	22.77
16		-	-	34.36	24.03	5.99	5.99	2.19	(13.19)	28.76
17		-	-	34.36	24.03	5.99	5.99	2.05	(11.13)	34.75
18		-	-	34.36	24.03	5.99	5.99	1.93	(9.20)	40.74
19		-	-	34.36	24.03	5.99	5.99	1.81	(7.39)	46.73
20		-	-	34.36	24.03	5.99	5.99	1.70	(5.69)	52.72
21		-	-	34.36	24.03	11.06	11.06	2.95	(2.74)	63.78
21		-	-	-	-	-	10.34	2.76	0.01	74.12

Probable Variation of Key Parameters over Plant Life

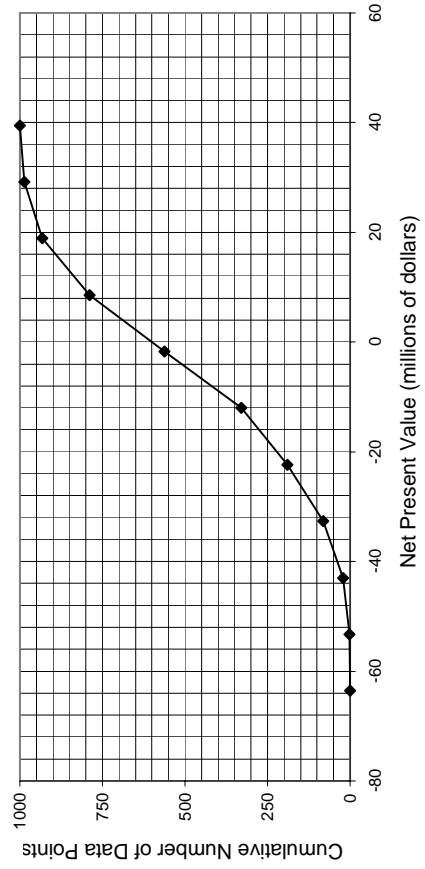
	<u>Lower Limit</u>	<u>Upper Limit</u>	<u>Base Value</u>
FCIL	-20%	30%	\$ 87,500,000
Price of Product	-10%	10%	\$ 34,355,067
Working Capital	-50%	10%	\$ 9,339,577
Income Tax Rate*	-20%	20%	42%
Interest Rate*	-10%	20%	6%
Raw Material Price	-10%	15%	\$ 5,195,768
Salvage Value	-80%	20%	\$ 8,750,000

* Please note that variations for percentages are a percent of a percent. For example, a 10% variance on a 12% interest rate would imply a 1.2% uncertainty

Run Economic Analysis

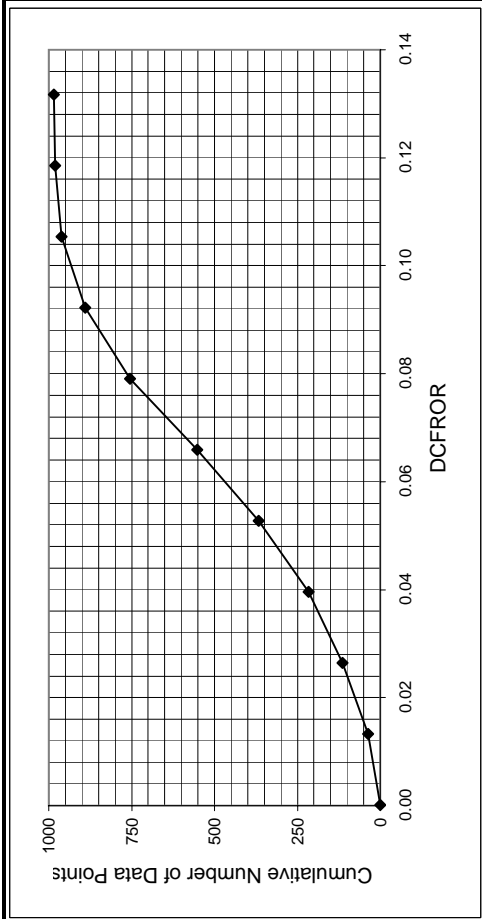
Net Present Value Data

Low NPV	-63.6		
High NPV	39.5		
<u>Bins</u>	<u>Upper Value</u>	<u># points/bin</u>	<u>Cumulative</u>
0	-63.6	0	0
1	-53.3	1	1
2	-43.0	20	21
3	-32.7	60	81
4	-22.3	108	189
5	-12.0	140	329
6	-1.7	233	562
7	8.6	226	788
8	18.9	145	933
9	29.2	54	987
10	39.5	13	1000



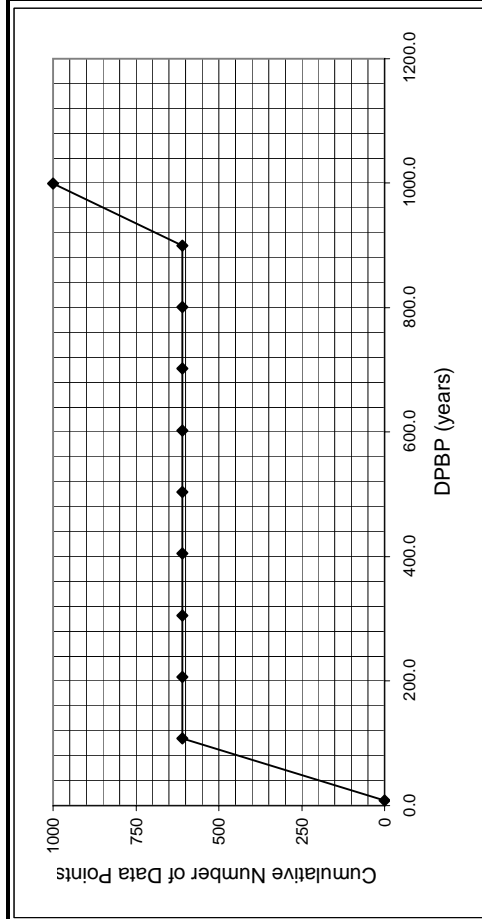
Discounted Cash Flow Rate of Return Data

Low DCFROR	0.00	Upper		#/bin		Cumulative	
High DCFROR	0.13	Lower		#/bin		Cumulative	
Bins	Upper	Lower	#/bin	Cumulative			
0	0.00		0	0			
1	0.01		37	37			
2	0.03		76	113			
3	0.04		104	217			
4	0.05		150	367			
5	0.07		186	553			
6	0.08		201	754			
7	0.09		136	890			
8	0.11		71	961			
9	0.12		19	980			
10	0.13		5	985			



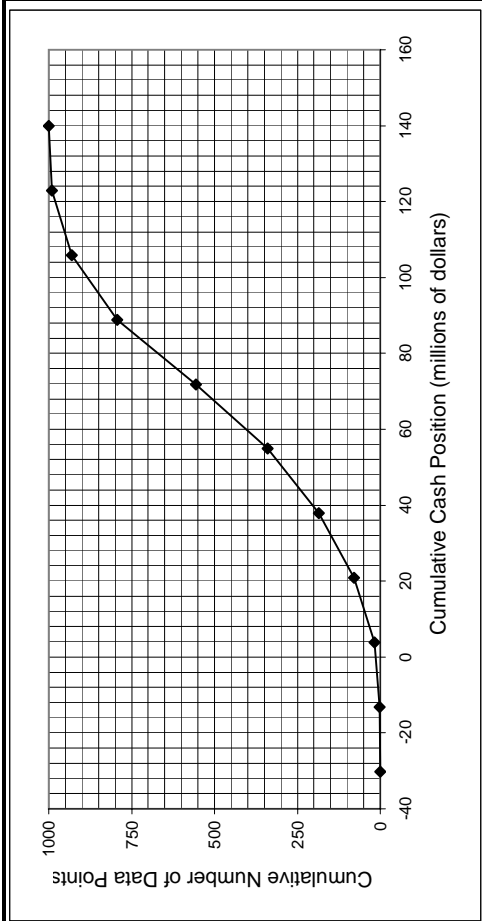
Discounted Payback Period Data

Low DPBP	8.5	Upper		#/bin		Cumulative	
High DPBP	999.0	Lower		#/bin		Cumulative	
Bins	Upper	Lower	#/bin	Cumulative			
0	8.5		0	0			
1	107.5		611	611			
2	206.6		0	611			
3	305.6		0	611			
4	404.7		0	611			
5	503.7		0	611			
6	602.8		0	611			
7	701.8		0	611			
8	800.9		0	611			
9	899.9		0	611			
10	999.0		389	1000			



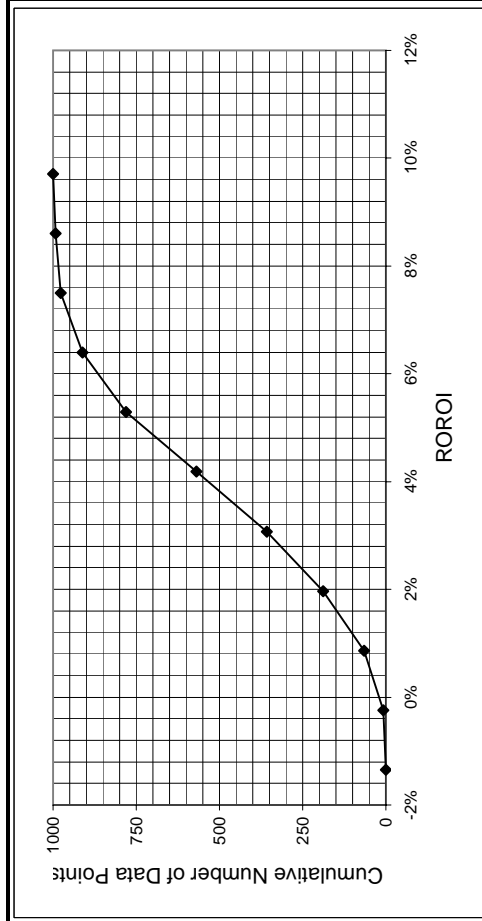
Cumulative Cash Position Data

Low CCP	-30.21		
High CCP	139.95		
Bins	Upper Value	# points/bin	Cumulative
0	-30.21	0	0
1	-13.19	1	1
2	3.82	16	17
3	20.84	63	80
4	37.86	106	186
5	54.87	154	340
6	71.89	216	556
7	88.91	237	793
8	105.92	138	931
9	122.94	59	990
10	139.95	10	1000



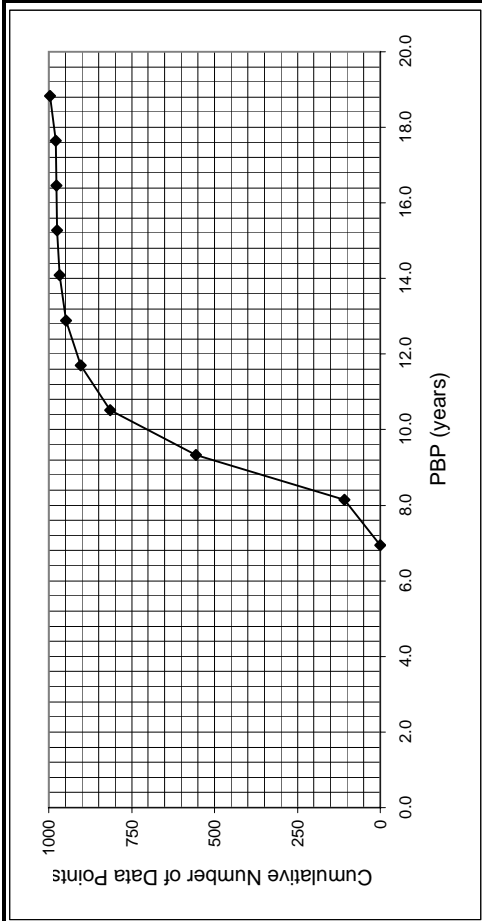
Rate of Return on Investment Data

Low RORI	-1%		
High RORI	10%		
Bins	Upper Value	# points/bin	Cumulative
0	-1%	0	0
1	0%	8	8
2	1%	57	65
3	2%	124	189
4	3%	169	358
5	4%	212	570
6	5%	211	781
7	6%	130	911
8	7%	66	977
9	9%	16	993
10	10%	7	1000



Payback Period Data

Low DPBP	6.9	Upper	#/bin	Cumulative
High DPBP	18.8	6.9	0	0
Bins		8.1	109	109
		9.3	447	556
		10.5	259	815
		11.7	88	903
		12.9	44	947
		14.1	21	968
		15.3	7	975
		16.5	1	976
		17.6	2	978
		18.8	19	997



Hours per Operating Year	8760
---------------------------------	------

	<u>Cost (\$/GJ)</u>
Common Utilities	
Electricity (110V - 440V)	16.8
Cooling Water (30°C to 45°C)	0.354
Refrigerated Water (15°C to 25°C)	4.43
Steam from Boilers	
Low Pressure (5 barg, 160°C)	6.08
Medium Pressure (10 barg, 184°C)	6.87
High Pressure (41 barg, 254°C)	9.83
Fuels	
Fuel Oil (no. 2)	6.0
Natural Gas	6
Coal (FOB mine mouth)	1.07
Thermal Systems	
Moderately High (up to 330°C)	6.67
High (up to 400°C)	7
Very High (up to 600°C)	7.5
Refrigeration	
Moderately Low (5°C)	4.43
Low (-20°C)	7.89
Very low (-50°C)	13.11
Waste Disposal (solid and liquid)	
<u>Cost (\$/tonne)</u>	
Non-Hazardous	36
Hazardous	200

Cost of Steam used in Steam Drives	
	<u>Cost (\$/GJ)</u>
Steam used for steam-powered drives \$	9.83

Equipment Efficiencies	
Pump Efficiency	85%
Drive Efficiency	90%
Fan Efficiency	80%
Furnace Efficiency	90%
Turbine Efficiency	85%

Process Equipment	
Operators per shift per equipment	
Cost of Labor (per operator/year) \$	50,000

Update Preferences

Power Preference
kilowatts

Pressure Preference
barg

Heat Duty Preference
MJ/h

Length Preference
meters

Area Preference
square meters

Volume Preference
cubic meters

Gas Flow Preference
cubic meters/s

Cost Preference
\$/kg

Flowrate Preference
kg/h

Energy Price Preference
\$/Gigajoule

Compressor Data (without electric motors)

Compressor Type	K ₁	K ₂	K ₃	F _{BMCS}	F _{BMSS}	F _{BMNS}	W _{min} (kW)	W _{max} (kW)
Centrifugal	2.2891	1.3604	-0.1027	2.7	5.8	11.5	450	3000
Axial	2.2891	1.3604	-0.1027	3.8	8.0	15.9	450	3000
Rotary	5.0355	-1.8002	0.8253	2.4	5.0	9.9	18	950
Reciprocating	2.2891	1.3604	-0.1027	3.4	7.0	13.9	450	3000

Drive Data

Electric Drives	K ₁	K ₂	K ₃	F _{BM}	W _{min} (kW)	W _{max} (kW)
Explosion Proof	2.4604	1.4191	-0.1798	1.5	75	2600
Totally Enclosed	1.956	1.7142	-0.2282	1.5	75	2600
Open/Drip Proof	2.9508	1.0688	-0.1315	1.5	75	2600

Non-Electric Drives	K ₁	K ₂	K ₃	F _{BM}	W _{min} (kW)	W _{max} (kW)
Gas Turbine	-21.7702	13.2175	-1.5279	3.5	7500	23000
Steam Turbine	2.6259	1.4398	-0.1776	3.5	70	7500
Internal Combustion	2.7635	0.8574	-0.0098	2.0	10	10000

Fan Data (include electric motors)

Fan Type	K ₁	K ₂	K ₃	F _{BMCS}	F _{BMFB}	F _{BMSS}	F _{BMNS}	Threshold	C ₁	C ₂	C ₃	V _{min} (m3/s)	V _{max} (m3/s)	P _{max} (barg)
Centrifugal Radial Fan	3.5391	-0.3533	0.4477	2.7	5.0	5.8	11.5	0.01	0.00	0.209	-0.033	1	100	0.16
Centrifugal Backward curv	3.3471	-0.0734	0.3090	2.7	5.0	5.8	11.5	0.01	0.00	0.209	-0.033	1	100	0.16
Axial Tube Fan	3.0414	-0.3375	0.4722	2.7	5.0	5.8	11.5	0.04	0.00	0.209	-0.033	1	100	0.16
Axial Vane Fan	3.1761	-0.1373	0.3414	2.7	5.0	5.8	11.5	0.04	0.00	0.209	-0.033	1	100	0.16

Fired Heater Data

Reactive Heaters	K ₁	K ₂	K ₃	Q _{min} (kW)	Q _{max} (kW)	P _{max} (barg)	C ₁	C ₂	C ₃	Bare Module Factor		
										CS	Alloy Steel	SS
Reformer Furnace	3.068	0.6597	0.0194	3000	100000	200	0.1405	-0.2698	0.1293	2.13	2.51	2.81
Pyrolysis Furnace	2.3859	0.9721	-0.0206	3000	100000	200	0.1017	-0.1957	0.09403	2.13	2.51	2.81

Non-reactive Heaters	K ₁	K ₂	K ₃	Q _{min} (kW)	Q _{max} (kW)	P _{max} (barg)	C ₁	C ₂	C ₃	Bare Module Factor		
										CS	Alloy Steel	SS
Process Heater	7.3488	-1.1666	0.2028	1000	100000	200	0.1347	-0.2368	0.1021	2.13	2.51	2.81

Thermal Fluid Heaters	K ₁	K ₂	K ₃	Q _{min} (kW)	Q _{max} (kW)	P _{max} (barg)	C ₁	C ₂	C ₃	F _{bm}	Steam Superheat Factor		
											F _{T1}	F _{T2}	F _{T3}
Hot Water	2.0829	0.9074	-0.0243	650	10750	200	-0.0163	0.0569	-0.0088	2.17			
Molten Salt, Mineral Oil,	1.1979	1.4782	-0.0958	650	10750	200	-0.0163	0.0569	-0.0088	2.17			
Diphenyl Based Oils	2.2628	0.8581	0.0003	650	10750	200	-0.0163	0.0569	-0.0088	2.17			
Packaged Steam Boilers	6.9617	-1.48	0.3161	1200	9400	40	2.5941	-4.2348	1.7224	2.2	1.000	0.00184	3.35E-06

Heat Exchanger Data

Exchanger Type	K ₁	K ₂	K ₃	C ₁	C ₂	C ₃	B ₁	B ₂	A _{min} (m2)	A _{max} (m2)	P _{max} (barg)
Double Pipe	3.3444	0.2745	-0.0472	13.1467	-12.6574	3.0705	1.74	1.55	1	10	300
40 barg < P < 100 barg				0.6072	-0.912	0.3327					
P < 40 barg				0	0	0					
Multiple Pipe	2.7652	0.7282	0.0783	13.1467	-12.6574	3.0705	1.74	1.55	10	100	300
40 barg < P < 100 barg				0.6072	-0.912	0.3327					
P < 40 barg				0	0	0					
Fixed tube, sheet, or U tut tubes only > 5 barg	4.3247	-0.303	0.1634	0.03881	-0.11272	0.08183	1.63	1.66	10.0	1000	140
Floating Head tubes only > 5barg	4.8306	-0.8509	0.3187	0.03881	-0.11272	0.08183	1.63	1.66	10.0	1000	140
Bayonet tubes only > 5 barg	4.2768	-0.0495	0.1431	0.03881	-0.11272	0.08183	1.63	1.66	10.0	1000	140
Kettle Reboiler tubes only > 5 barg	4.4646	-0.5277	0.3955	0.03881	-0.11272	0.08183	1.63	1.66	10.0	100	140
Scraped Wall 40 barg < P < 100 barg	3.7803	0.8569	0.0349	13.1467	-12.6574	3.0705	1.74	1.55	2.0	20	300
P < 40 barg				0.6072	-0.912	0.3327					
Teflon Tube	3.8062	0.8924	-0.1671	0	0	0	1.63	1.66	1.0	10	15
Air Cooler	4.0336	0.2341	0.0497	-0.125	0.15361	-0.02861	0.96	1.21	10	10000	100
Spiral Tube - shell and tub tube only	3.9912	0.0668	0.243	-0.4045	0.1859	0	1.74	1.55	1	100	400
Spiral Plate	4.6561	-0.2947	0.2207	0	0	0	0.96	1.21	1	100	19
Flat Plate	4.6656	-0.1557	0.1547	0	0	0	0.96	1.21	10	1000	19

Material Factors, F_M

Exchanger Type	Shell - CS	CS	Cu	CS	SS	CS	Ni	CS	Ti
	Tube - CS	Cu	Cu	SS	SS	Ni	Ni	Ti	Ti
Double Pipe	1.00	1.35	1.69	1.81	2.73	2.68	3.73	4.63	11.38
Multiple Pipe	1.00	1.35	1.69	1.81	2.73	2.68	3.73	4.63	11.38
Fixed tube, sheet, or U tut	1.00	1.35	1.69	1.81	2.73	2.68	3.73	4.63	11.38
Floating Head	1.00	1.35	1.69	1.81	2.73	2.68	3.73	4.63	11.38
Bayonet	1.00	1.35	1.69	1.81	2.73	2.68	3.73	4.63	11.38
Kettle Reboiler	1.00	1.35	1.69	1.81	2.73	2.68	3.73	4.63	11.38
Scraped Wall	1.00	1.35	1.69	1.81	2.73	2.68	3.73	4.63	11.38
Spiral Tube	1.00	1.35	1.69	1.81	2.73	2.68	3.73	4.63	11.38

Shell Material					
Type of Exchanger	CS	Cu	SS	Ni	Ti
Teflon Tube Exchanger	1.00	1.20	1.30	1.40	3.30

Material In Contact with Process Fluid					
Type of Exchanger	CS	Cu	SS	Ni	Ti
Spiral Plate	1.00	1.35	2.45	2.68	4.63
Flat Plate	1.00	1.35	2.45	2.68	4.63

Tube Material			
Type of Exchanger	CS	Al	SS
Air Cooler	1.00	1.42	2.93

Pump Data (including electric drives)

Pump Type	K ₁	K ₂	K ₃	C ₁	C ₂	C ₃	B ₁	B ₂	F _{m(C)}	F _{m(SS)}	F _{m(Cu)}	F _{m(SS)}	F _{m(Ni)}	F _{m(Ti)}	P _{max(bar)}	W _{min(kW)}	W _{max(kW)}
Centrifugal pump	3.3892	0.0536	0.1538	-0.3935	0.3957	-0.00226	1.89	1.35	1.0	1.6	NA	2.3	4.4	NA	100	1	300
Positive Displacement	3.4771	0.1350	0.14380	-0.24538	0.259016	-0.01363	1.89	1.35	1.0	1.4	1.3	2.7	4.7	10.7	100	1	100
Reciprocating pump	3.8696	0.3161	0.12200	-0.2454	0.2590	-0.0136	1.89	1.35	1.0	1.5	1.3	2.4	4.0	6.4	100	0.1	200

Tank Data

Tank Type	K ₁	K ₂	K ₃	B ₁	B ₂	V _{min(m³/s)}	V _{max(m³/s)}
Fixed Roof	4.8509	-0.3973	0.1445	1.10	0	90	30000
Floating Roof	5.9567	-0.7585	0.1749	1.10	0.00	1000	40000

Turbine Data

Turbine Type	K ₁	K ₂	K ₃	F _{m(C)}	F _{m(SS)}	F _{m(Cu)}	F _{m(SS)}	F _{m(Ni)}	F _{m(Ti)}	W _{min(kW)}	W _{max(kW)}
Axial	2.7051	1.4398	-0.1776	NA	3.5	NA	6.1	11.7	NA	100	4000
Radial	2.2476	1.4965	-0.1618	NA	3.5	NA	6.1	11.7	NA	100	1500

Vaporizer and Evaporator Data

Vaporizer Types	K ₁	K ₂	K ₃	A _{min(m²)}	A _{max(m²)}	P _{max(bar)}	C ₁	C ₂	C ₃
Forced Circulation	5.0238	0.3475	0.0703	5	1000	150	0.1578	-0.2992	0.1413
Falling Film	3.9119	0.8627	-0.0088	50	500	150	0.1578	-0.2992	0.1413
Agitated (Scraped Wall)	5	0.149	-0.0134	0.5	5	150	0.1578	-0.2992	0.1413
Short Tube	5.2366	-0.6572	0.35	10	100	150	0.1578	-0.2992	0.1413
Long Tube	4.642	0.3698	0.0025	100	10000	150	0.1578	-0.2992	0.1413

Vaporizer Types	K ₁	K ₂	K ₃	V _{min(m³)}	V _{max(m³)}	P _{max(bar)}	C ₁	C ₂	C ₃
Jacketed Vessel	3.8751	0.3328	0.1901	1	100	320	0.1578	-0.2992	0.1413
Internal Coil	4.038	0.09142	0.2766	1	100	320	0.1578	-0.2992	0.1413
Jacketed Vessel w/ Coil	4.038	0.09142	0.2766	1	100	320	0.1578	-0.2992	0.1413

Bare Module Factors, F_{BM}					
Vaporizer Types	CS	Cu Alloy	SS	Ni Alloy	Ti
Forced Circulation	2.9	3.63	5.08	9.66	14.5
Falling Film	2.25	2.81	3.94	7.49	11.25
Agitated (Scraped Wall)	2.25	2.81	3.94	7.49	11.25
Short Tube	2.9	3.63	5.08	9.66	14.5
Long Tube	2.9	3.63	5.08	9.66	14.5

Bare Module Factors, F_{BM}										
Vaporizer Types	CS	Cu	SS Lined	SS Lined Ni	SS	SS Clad	Ni Alloy	Ni Alloy Clad	Ti	Ti Clad
Jacketed Vessel	2.7	3.4	4.7	4.9	4.8	3.8	9.1	5.9	13.7	9.5
Internal Coil	3.0	3.8	5.2	5.5	5.2	4.1	10.1	6.6	15.2	10.6
Jacketed Vessel w/ Coil	3.0	3.8	5.2	5.5	5.2	4.1	10.1	6.6	15.2	10.6

Vessel Data (including data for distillation towers and packed columns)

Vertical Vessels						Horizontal Vessels					
K ₁	K ₂	K ₃	V _{min}	V _{max}	P _{max(bar)}	K ₁	K ₂	K ₃	V _{min}	V _{max}	P _{max(bar)}
3.4974	0.4485	0.1074	0.3	520	3.5565	0.3776	0.0905	0.1	628	400	

Vessel B-Values

	B1	B2
Horizontal	1.49	1.52
Vertical	2.25	1.82

F_a

Tray Type	K ₁	K ₂	K ₃	A _{min(m²)}	A _{max(m²)}
Sieve	2.9949	0.4465	0.3961	0.07	12.3
Valve	3.3322	0.4838	0.3434	0.7	10.5
Demister	3.2353	0.4838	0.3434	0.7	10.5

Tower Packing

Materials of Construction	K ₁	K ₂	K ₃	V _{min(m³)}	V _{max(m³)}
Ceramic	3.0664	0.9744	0.0055	0.03	628
304 SS	3.2999	0.9744	0.0055	0.03	628
Plastic Saddle	2.4493	0.9744	0.0055	0.03	628

F_{BM}

MOC	Sieve	Valve	Demister
CS	1.0	1	
SS	1.8	1.83	1.0
Fluorocarbon			1.8
Ni-alloy	5.6	5.58	5.6

Materials of Construction

$F_{M,CS}$	1.0
$F_{M,SS\ clad}$	1.7
$F_{M,SS}$	3.1
$F_{M,Ni\ clad}$	3.6
$F_{M,Ni}$	7.1
$F_{M,Ti\ clad}$	4.7
$F_{M,Ti}$	9.4

Appendix E

Solubility Trapping Calculations and Modeling

Equations of state utilize expanded relations between pressure, volume, and temperature (PVT) to distribute phase tendency in an ideal formulation. The Peng-Robinson EOS [1] may be expressed as,

$$P = \frac{RT}{V-b} - \frac{a\alpha(T)}{V(V+b)+b(V-b)}, \quad (1)$$

with universal gas constant, R, system temperature, T, and pressure, P, molar volume of the mixture, V, and for the PVT relations [1] $a = 0.45724R^2T_c^2 / P_c$ and $b = 0.07780RT_c / P_c$, representing the PVT behavior of the components in a thermodynamic system for the critical temperature, T_c , and pressure, P_c , of each component to be considered. The interaction between these two parameters may be expressed, ideally, by a mixing relation (binary mixing rules) between them.

These mixing rules may be expressed for a two component system as [e.g. 3],

$$\begin{aligned} a_{mix} &= \sum_{i=1}^2 \sum_{j=1}^2 y_i y_j a_{ij} \\ b_{mix} &= \sum_{i=1}^2 y_i b_i \end{aligned}, \quad (2)$$

for the mole fraction of component ij, y_{ij} , and the PVT relations, a and b, of each component ij. The *attractive parameter*, $\alpha(T)$, provides additional temperature dependence and may be expressed as [3],

$$\ln \alpha = m(1-T_r) + n(1-T_r)^2, \quad (3)$$

for the reduced temperature, $T_r = T / T_c$, and binary system parameters, m and n, such as those provided by Aznar and Telles [4].

Expansion of Eq. (4) yields,

$$\ln \hat{\phi}_i = \frac{PV}{RT} - 1 - \ln \left(\frac{P(V-b_{mix})}{RT} \right) + \frac{a_{mix}}{2\sqrt{2}b_{mix}RT} \ln \left(\frac{V + (1-\sqrt{2}b_{mix})}{V + (1+\sqrt{2}b_{mix})} \right), \quad (4)$$

for the fugacity coefficient, ϕ . Volume may be determined as the roots of Eq. (4), where the minimum root always necessitates the liquid phase and the opposite holds for the gaseous phase. Utilizing an EOS to determine the fugacity coefficient of each component in the CO₂-H₂O binary system then lends to the formulation of a solubility relation utilizing some form of Henry's constant. The general procedure for such a determination begins by equating the fugacity of each component between its liquid and vapor phases, $f_i^v = f_i^l$, where, $f_i = \phi_{i(T,P)} y_i P$, for fugacity coefficient, ϕ , and mole fraction, y_i . A commonly utilized Henry's constant solubility relation is the Krichevsky-Kasarnovsky (KK) equation [5],

$$\ln \left(\frac{f_{CO_2}}{x_{CO_2}} \right) = \ln H_{CO_2}^* + \frac{v_{CO_2}^{-\infty}}{RT} P, \quad (5)$$

which assumes infinite dilution of, in the current binary case, CO₂ in the liquid water phase and water in the pure CO₂ phase, and that utilizes a reference Henry's constant, $H_{CO_2}^*$, and the molar volume at infinite dilution, $v_{CO_2}^{-\infty}$.

Empirical relations for $H_{CO_2}^*$ and $v_{CO_2}^{-\infty}$ are provided in [5], while a correction for the density of CO₂ saturated brine density was utilized as outlined in Garcia [6]. Determining the phase tendency of CO₂ at any given set of state parameters may be accomplished, following determination of gas and liquid phase volumes as the roots of Eq. (4), by examining the structure of a P-V-T diagram (Figure 1). Phase transition will occur when the work done to cross from

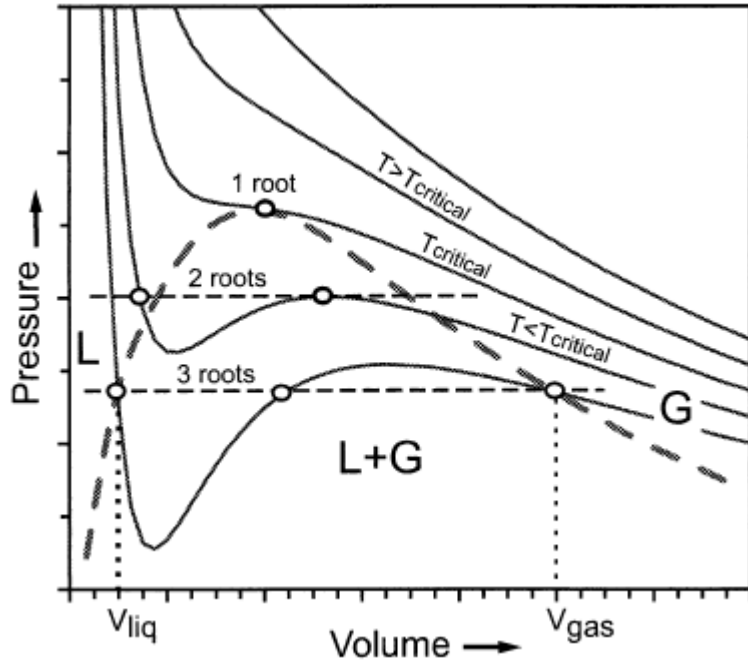


Figure 1: PVT relationship predicted by PR EOS or similar EOS (from Spycher *et al.* [2]).

V_{gas} to V_{liq} is the same along the straight path (tie-line) as for the curved isotherm. The definition of work, $w = \int PdV$, may be integrated to achieve, $w_1 = P(V_{gas} - V_{liq})$, for the straight line work, while Eq. (1) may be integrated from V_{gas} to V_{liq} to obtain w_2 . If $(w_2 - w_1) > 0$, then V is taken as the maximum root of Eq. (1), while the opposite indicates use of the minimum root. Should the two work paths achieve equality, then the phases are stable and either volume will provide the correct answer. A similar procedure was followed in Spycher *et al.* [2] by use of the Reidlich-Kwong EOS. A Matlab coding sequence was developed to carry out these analyses, and is available on request from the authors.

REFERENCES

1. Peng, D.Y. and D.B. Robinson, A new two-constant equation of state. *Industrial Engineering Chemical Fundamentals*, 1976. 15: p. 59-64.
2. Spycher, N., K. Pruess, and J. Ennis-King, CO₂-H₂O mixtures in the geological sequestration of CO₂. I. Assessment and calculation of mutual solubilities from 12 to 100 degrees C and up to 600 bar. *Geochimica Et Cosmochimica Acta*, 2003. 67(16): p. 3015-3031.
3. Melhem, G.A., A modified Peng-Robinson equation of state. *Fluid Phase Equilibria*, 1989. 47: p. 189-237.
4. Aznar, M. and A.S. Telles, A data bank of parameters for the attractive coefficient of the Peng-Robinson equation of state. *Brazilian Journal of Chemical Engineering*, 1997. 14(1).
5. Enick, R. and S.M. Klara, CO₂ solubility in water and brine under reservoir conditions. *Chemical Engineering Communications*, 1990. 90: p. 23-33.
6. Garcia, J.E., *Density of aqueous solutions of CO₂*, in *Report LBNL-49023*. 2001, Lawrence Berkeley National Laboratory. p. 8.

Appendix F

Mineral Trapping Calculations

As stated before, the equation that governs the rate of mineral dissolution and precipitation is given by:

$$r_m = -\text{sgn} \left[\log \left(\frac{Q_m}{K_m} \right) \right] k_m A_m \left[\left(\frac{Q_m}{K_m} \right)^\mu - 1 \right]^\eta, \quad (1)$$

where m is the mineral index, r_m is the dissolution/precipitation rate (positive values indicate dissolution and negative values precipitation), A_m is the specific reactive surface area per kg H_2O , k_m is the rate constant (moles per unit mineral surface area and unit time) which is temperature dependent, K_m is the equilibrium constant for mineral water reaction written for one mole of mineral m , Q_m is the ion activity product, the parameters μ and η are two positive numbers normally determined by experiment and are usually but not always taken equal to unity (as in the present work). The expression “ $\text{sgn} [\log (Q/K)]$ ” ensures that the correct sign is enforced when the exponents μ and η are not equal to one.

The temperature dependence of the reaction rates is expressed by the following Arrhenius equation:

$$k = k_{25} \exp \left[\frac{-E_a}{R} \left(\frac{1}{T} - \frac{1}{298.15} \right) \right], \quad (2)$$

where E_a is the activation energy, k_{25} is the rate constant at 25 °C, R is the gas constant and T is the absolute temperature.

The activity of aqueous species is the product of the activity coefficient and the molar concentration. The activity coefficients of aqueous species are determined with the help of the extended Debye Huckel relationship which is given by:

$$\log(\gamma_j) = -\frac{A_\gamma z_j^2 I^{0.5}}{\Lambda} + \log(1 + 0.01801053m^*) - [\omega_j b_{\text{NaCl}} + b_{\text{Na}^+, \text{Cl}^-} - 0.19(|z_j| - 1)]I, \quad (3)$$

where,

$$\Lambda = 1 + a B_\gamma \bar{I}^{-1/2}, \quad (4)$$

$$\omega_j = \eta \frac{z_j^2}{r_{e,j}}. \quad (5)$$

where the subscript j refers to each ion, γ is the activity coefficient of the ion, a , $b_{\text{Na}^+, \text{Cl}^-}$, b_{NaCl} , A_γ and B_γ are the Debye Huckel parameters, z is the ion electric charge, I is taken as the true ionic strength of the solution, ω is the Born coefficient, η is a constant equal to 1.66027 (Å cal/mol), and $r_{e,j}$ is the ion effective ionic radius.

For calculating the activity coefficient of CO₂, gaseous and aqueous CO₂ are assumed to be in equilibrium and the mass-action law is applied which is:

$$K\Gamma P = \gamma C \quad (6)$$

where K is the equilibrium constant, Γ is the gaseous CO₂ fugacity coefficient, P is the partial pressure (bar), γ is the aqueous CO₂ activity coefficient and C is the aqueous concentration (mol/kg H₂O). The equilibrium constant, K, at different temperatures can be derived from the following expression,

$$\log K = b_1 \ln T + b_2 + b_3 T + \frac{b_4}{T} + \frac{b_5}{T^2} \quad (7)$$

where the values of the coefficients b₁, b₂, b₃, b₄ and b₅ are obtained from the EQ3/6 database. Assuming that H₂O and CO₂ are real gases forming an ideal mixture, the fugacity coefficients are calculated from:

$$\ln \Gamma = \left(\frac{a}{T^2} + \frac{b}{T} + c \right) P + \left(\frac{d}{T^2} + \frac{e}{T} + f \right) \frac{P^2}{2} \quad (8)$$

where P is the total gas pressure, T is the absolute temperature, and a,b,c,d,e and f are constants determined from literature.

For low ionic strength solutions the CO₂(aq) activity coefficient can be taken to be 1. For high ionic strength NaCl solution, γ should be corrected to take into account the salting out effect. The following expression is used:

$$\ln \gamma = \left(C + FT + \frac{G}{T} \right) I - \left(E + HT \right) \left(\frac{I}{I+1} \right), \quad (9)$$

where T is the absolute temperature, I is the ionic strength (or NaCl molality), C, F, G, E and H are constants determined from geochemical database EQ3/6. Here the ionic strength I is defined by:

$$I = \frac{1}{2} \sum_i c_i z_i^2, \quad (10)$$

where the summation is over all aqueous species and c_i and z_i are concentration (mol/kg H₂O) and electrical charge of species i.

The precipitation of various minerals was determined and the amount of CO₂ that can be sequestered was estimated to be roughly 1.6 kg/m³ of the medium.

Appendix G

Stream Property Table for Compression Modeling

Stream Number	100	101	102	103	104	105	106	107	108
Temperature C	100	45	45	88.9	88.9	88.9	88.9	88.9	88.9
Pressure bar	10.133	10.133	10.133	69.5	69.5	69.5	69.402	69.402	69.276
Vapor Frac	0.982	0.883	1	1	1	1	1	1	1
Mole Flow kmol/hr	14994.16	14994.16	13245.248	13141.248	6570.624	6570.624	6570.624	5256.499	5256.499
Mass Flow kg/hr	594184.531	594184.531	561873.939	559887.729	279943.864	279943.864	279943.864	223955.091	223955.091
Volume Flow cum/hr	43701.821	33127.26	33089.33	4665.06	2332.53	2332.53	2336.513	1869.211	1873.33
Enthalpy MMkcal/hr	-1230.737	-1253.454	-1133.82	-1128.087	-564.043	-564.043	-564.038	-451.23	-451.225
Mass Flow kg/hr									
CO2	528960.828	528960.828	527611.938	527422.808	263711.404	263711.404	263711.404	210969.123	210969.123
H2O	33497.612	33497.612	2554.009	759.391	379.696	379.696	379.696	303.757	303.757
N2	27918.234	27918.234	27903.412	27901.392	13950.696	13950.696	13950.696	11160.557	11160.557
OXYGEN	3807.857	3807.857	3804.579	3804.137	1902.068	1902.068	1902.068	1521.655	1521.655
Mass Frac									
CO2	0.89	0.89	0.939	0.942	0.942	0.942	0.942	0.942	0.942
H2O	0.056	0.056	0.005	0.001	0.001	0.001	0.001	0.001	0.001
N2	0.047	0.047	0.05	0.05	0.05	0.05	0.05	0.05	0.05
OXYGEN	0.006	0.006	0.007	0.007	0.007	0.007	0.007	0.007	0.007
Mole Flow kmol/hr									
CO2	12019.16	12019.16	11988.51	11984.213	5992.106	5992.106	5992.106	4793.685	4793.685
H2O	1859.4	1859.4	141.769	42.153	21.076	21.076	21.076	16.861	16.861
N2	996.6	996.6	996.071	995.999	497.999	497.999	497.999	398.4	398.4
CO									
PROPANE									
OXYGEN	119	119	118.898	118.884	59.442	59.442	59.442	47.553	47.553
Mole Frac									
CO2	0.802	0.802	0.905	0.912	0.912	0.912	0.912	0.912	0.912
H2O	0.124	0.124	0.011	0.003	0.003	0.003	0.003	0.003	0.003
N2	0.066	0.066	0.075	0.076	0.076	0.076	0.076	0.076	0.076
OXYGEN	0.008	0.008	0.009	0.009	0.009	0.009	0.009	0.009	0.009

Stream Number	109	110	111	112	113	114	115	116	117
Temperature C	88.9	88.9	88.9	88.9	88.9	88.9	88.9	88.9	88.9
Pressure bar	69.276	69.204	69.204	69.172	69.172	69.163	69.402	69.276	69.204
Vapor Frac	1	1	1	1	1	1	1	1	1
Mole Flow kmol/hr	3942.374	3942.374	2628.25	2628.25	1314.125	1314.125	1314.125	1314.125	1314.125
Mass Flow kg/hr	167966.319	167966.319	111977.546	111977.546	55988.773	55988.773	55988.773	55988.773	55988.773
Volume Flow cum/hr	1404.998	1406.757	937.838	938.369	469.184	469.253	467.303	468.333	468.919
Enthalpy MMkcal/hr	-338.419	-338.416	-225.611	-225.61	-112.805	-112.805	-112.808	-112.806	-112.805
Mass Flow kg/hr									
CO2	158226.843	158226.843	105484.562	105484.562	52742.281	52742.281	52742.281	52742.281	52742.281
H2O	227.817	227.817	151.878	151.878	75.939	75.939	75.939	75.939	75.939
N2	8370.418	8370.418	5580.278	5580.278	2790.139	2790.139	2790.139	2790.139	2790.139
OXYGEN	1141.241	1141.241	760.827	760.827	380.414	380.414	380.414	380.414	380.414
Mass Frac									
CO2	0.942	0.942	0.942	0.942	0.942	0.942	0.942	0.942	0.942
H2O	0.001	0.001	0.001	0.001	0.001	0.001	0.001	0.001	0.001
N2	0.05	0.05	0.05	0.05	0.05	0.05	0.05	0.05	0.05
OXYGEN	0.007	0.007	0.007	0.007	0.007	0.007	0.007	0.007	0.007
Mole Flow kmol/hr									
CO2	3595.264	3595.264	2396.843	2396.843	1198.421	1198.421	1198.421	1198.421	1198.421
H2O	12.646	12.646	8.431	8.431	4.215	4.215	4.215	4.215	4.215
N2	298.8	298.8	199.2	199.2	99.6	99.6	99.6	99.6	99.6
CO									
PROPANE									
OXYGEN	35.665	35.665	23.777	23.777	11.888	11.888	11.888	11.888	11.888
Mole Frac									
CO2	0.912	0.912	0.912	0.912	0.912	0.912	0.912	0.912	0.912
H2O	0.003	0.003	0.003	0.003	0.003	0.003	0.003	0.003	0.003
N2	0.076	0.076	0.076	0.076	0.076	0.076	0.076	0.076	0.076
OXYGEN	0.009	0.009	0.009	0.009	0.009	0.009	0.009	0.009	0.009

Stream Number	118	119	120	121	122	123	124	125	126	127
Temperature C	88.9	40	40	40	40	40	45	40	40	40
Pressure bar	69.172	81.617	81.455	81.363	81.321	81.31	10.133	16.398	26.537	42.946
Vapor Frac	1	1	1	1	1	1	0	0	0	0
Mole Flow kmol/hr	1314.125	1314.125	1314.125	1314.125	1314.125	1314.125	1748.912	70.743	22.151	11.106
Mass Flow kg/hr	55988.773	55988.773	55988.773	55988.773	55988.773	55988.773	32310.592	1332.333	428.926	224.952
Volume Flow cum/hr	469.184	238.015	238.961	239.499	239.742	239.805	37.965	1.538	0.485	0.246
Enthalpy MMkcal/hr	-112.805	-114.053	-114.049	-114.046	-114.045	-114.045	-119.634	-4.872	-1.538	-0.781
Mass Flow kg/hr										
CO2	52742.281	52742.281	52742.281	52742.281	52742.281	52742.281	1348.889	97.203	50.169	41.758
H2O	75.939	75.939	75.939	75.939	75.939	75.939	30943.602	1233.893	378.103	182.622
N2	2790.139	2790.139	2790.139	2790.139	2790.139	2790.139	14.822	1.013	0.536	0.471
OXYGEN	380.414	380.414	380.414	380.414	380.414	380.414	3.278	0.224	0.117	0.101
Mass Frac										
CO2	0.942	0.942	0.942	0.942	0.942	0.942	0.042	0.073	0.117	0.186
H2O	0.001	0.001	0.001	0.001	0.001	0.001	0.958	0.926	0.882	0.812
N2	0.05	0.05	0.05	0.05	0.05	0.05	459 PPM	760 PPM	0.001	0.002
OXYGEN	0.007	0.007	0.007	0.007	0.007	0.007	101 PPM	168 PPM	273 PPM	448 PPM
Mole Flow kmol/hr										
CO2	1198.421	1198.421	1198.421	1198.421	1198.421	1198.421	30.65	2.209	1.14	0.949
H2O	4.215	4.215	4.215	4.215	4.215	4.215	1717.631	68.491	20.988	10.137
N2	99.6	99.6	99.6	99.6	99.6	99.6	0.529	0.036	0.019	0.017
CO										
PROPANE										
OXYGEN	11.888	11.888	11.888	11.888	11.888	11.888	0.102	0.007	0.004	0.003
Mole Frac										
CO2	0.912	0.912	0.912	0.912	0.912	0.912	0.018	0.031	0.051	0.085
H2O	0.003	0.003	0.003	0.003	0.003	0.003	0.982	0.968	0.948	0.913
N2	0.076	0.076	0.076	0.076	0.076	0.076	303 PPM	511 PPM	864 PPM	0.002
OXYGEN	0.009	0.009	0.009	0.009	0.009	0.009	59 PPM	99 PPM	166 PPM	284 PPM

Stream Number	128	129
Temperature C	35	92.1
Pressure bar	1.013	1.013
Vapor Frac	0	0
Mole Flow kmol/hr	22203.374	22203.374
Mass Flow kg/hr	400000	400000
Volume Flow cum/hr	475.63	497.042
Enthalpy MMkcal/hr	-1512.165	-1489.449
Mass Flow kg/hr		
CO2		
H2O	400000	400000
N2		
OXYGEN		
Mass Frac		
CO2		
H2O	1	1
N2		
OXYGEN		
Mole Flow kmol/hr		
CO2		
H2O	22203.374	22203.374
N2		
CO		
PROPANE		
OXYGEN		
Mole Frac		
CO2		
H2O	1	1
N2		
OXYGEN		